

TECHNISCHE UNIVERSITÄT MÜNCHEN
Lehrstuhl für Energiesysteme

Reaction Kinetics of Solid Fuels during Entrained Flow Gasification

Dipl.-Ing. Univ. Alexander Tremel

Vollständiger Abdruck der von der Fakultät für Maschinenwesen
der Technischen Universität München zur Erlangung des akademischen Grades eines

Doktor-Ingenieurs

genehmigten Dissertation.

Vorsitzender: Univ.-Prof. Dr.-Ing. habil. Boris Lohmann
Prüfer der Dissertation: 1. Univ.-Prof. Dr.-Ing. habil. Hartmut Spliethoff
2. Univ.-Prof. Dr.-Ing. Thomas Kolb,
Karlsruher Institut für Technologie

Die Dissertation wurde am 30.11.2011 bei der Technischen Universität München eingereicht und durch die Fakultät für Maschinenwesen am 24.10.2012 angenommen.

Preface

Die vorliegende Dissertation entstand während meiner Tätigkeit als wissenschaftlicher Mitarbeiter am Lehrstuhl für Energiesysteme der Technischen Universität München. Mein herzlichster Dank gilt meinem Doktorvater Prof. Hartmut Spliethoff für die sehr guten Rahmenbedingungen zur Promotion und für die Freiheit bei der wissenschaftlichen Arbeit. Herrn Prof. Thomas Kolb danke ich für die Übernahme des Koreferats.

Der Aufbau und der Betrieb der Versuchsanlagen waren nur durch die Rahmenbedingungen des Verbundforschungsvorhabens HotVeGas (Projektnummer 0327773A) möglich. Ich danke dem Bundesministerium für Wirtschaft und Technologie und den beteiligten Industriepartnern für die finanzielle Unterstützung.

Ein ganz besonderer Dank gilt den Kolleginnen und Kollegen am Lehrstuhl für die freundliche Atmosphäre, die ständige Hilfsbereitschaft und die menschliche Unterstützung. Ohne die Freude an der Arbeit ist eine kreative wissenschaftliche Tätigkeit nicht möglich. Besonders bedanken möchte ich mich bei Thomas Haselsteiner für die menschliche, fachliche sowie technische Unterstützung beim Aufbau des Druckflugstromreaktors. In sehr guter Erinnerung wird mir die allgäuerische-fränkische Bürogemeinschaft mit Richard Aumann bleiben, der immer ein offenes Ohr für meine Probleme hatte. Stellvertretend für alle anderen möchte ich Jan-Peter Bohn, Christoph Wieland, Günter Zapf und Valentin Becher nennen, mit denen ich immer gerne zusammengearbeitet habe.

Weiterhin danke ich dem Sekretariat, dem Laborteam und der Werkstatt für die tatkräftige Unterstützung bei der Verwaltung und bei technischen Belangen. Hervorheben möchte ich dabei Andrea Hartung und Stefan Schirmel, die beide mit ihrem Einsatz und ihrem Fachwissen das experimentelle Arbeiten vorangetrieben haben.

Ohne die Unterstützung von Studenten wäre die Durchführung mancher Arbeiten nicht möglich gewesen. Ich möchte mich bei insgesamt ca. 30 Studentinnen und Studenten bedanken, die mich im Rahmen von Studienarbeiten oder als studentische Hilfskräfte unterstützt haben. Stellvertretend für alle möchte ich hier Andreas Baumgartner, Maximilian Blume, Michael Herrmann, Nikola Fink, Stefan Pleintinger, Martin Voit, Stephan Fromm, Jefferson Ferronato und Koenraad Beckers nennen.

From October to December 2009, I spent two month at the Commonwealth Scientific and Industrial Research Organisation (CSIRO) in Brisbane, Australia. I like to thank Dr. David Harris and Dr. Daniel Roberts for the kind invitation, the research cooperation, and the opportunity to work on such a high research level.

Mein größter Dank gilt meinen Eltern, die mir erst das Studium ermöglichten, mir stets ein Rückhalt waren und mich während der Promotionszeit bestärkt haben. Zuletzt danke ich noch Tina, die während der gesamten Promotionszeit immer für mich da war.

Klosterlangheim, im August 2011

A theory is something nobody believes, except the person who made it. An experiment is something everybody believes, except the person who made it.

Albert Einstein, 1879-1955

This dissertation is a combination of theoretical and experimental work.

Abstract

Despite the application of entrained flow gasification on larger scales, the reaction rates in the hot conversion zone are almost unknown. But the knowledge of the rates of the gasification reactions at high temperature and high pressure is crucial for the detailed design and optimisation of these gasifiers. This dissertation provides measurements of fuel conversion under operation conditions relevant to industrial gasifiers and aims at the transfer of the data to larger scale applications.

A novel pilot-scale research reactor is developed that enables the study of gasification reactions at high temperature, high pressure and under entrained flow conditions. The Pressurised High Temperature Entrained Flow Reactor (PiTER) is operated at up to 1600°C and 4.0 MPa in pyrolysis and gasification experiments. The data set is extended by measurements in an atmospheric entrained flow reactor and a pressurised wire mesh reactor. Devolatilisation and gasification behaviour of a wide range of fuels is analysed including anthracite, bituminous coal, lignite, biocoal (from hydrothermal carbonisation), and biomass; however, Rhenish lignite is used in most of the experiments. The pyrolysis data enable the validation of a simple first order reaction model that describes the influence of pressure, temperature, and residence time on volatile yield.

Char samples collected from the three reactors are analysed using laboratory procedures and bench-scale setups. Specific char surface area is measured by CO₂ adsorption at 273 K, and is found to be significantly influenced by char conversion, reaction temperature, and devolatilisation pressure. The surface data are described by an extension of the Random Pore Model. Intrinsic char reactivity is measured in a pressurised thermogravimetric analyser and the influence of reactant partial pressure and temperature on the char-CO₂ and char-H₂O reaction is studied. The intrinsic reaction rate is described by nth order and Langmuir-Hinshelwood type equations. In the thermogravimetric analysis it is observed that the reactivity of char strongly depends on devolatilisation conditions. At higher temperature and longer time scales the char reactivity declines due to thermal deactivation. Standard char reactivity is measured in an atmospheric thermogravimetric analyser at 375°C to 400°C and in an oxygen containing atmosphere. The loss of reactivity can be described by a thermal deactivation model.

As the influence of mass transport limitations on char conversion at high temperature cannot be measured directly, an effectiveness factor approach is derived to describe pore diffusion. A Sherwood Number correlation is used to account for boundary layer diffusion. The mass transport limitation models are combined with the submodels for devolatilisation, intrinsic reactivity, specific surface area evolution, and thermal char deactivation. The PiTER is modelled as a one-dimensional plug flow reactor, and a good correlation between experimental data and model predictions is achieved. The only adjustable parameter is the average pore diameter in the pore diffusion submodel. The model prediction is best for

an average pore size of 47 Å which is in the expected range as char conversion occurs in micro and mesopores.

In order to transfer the data to technical applications, the model framework is used to design and optimise industrial scale entrained flow gasifiers. A 500 MW entrained flow gasifier operated at 2.5 MPa is modelled for the conversion of Rhenish lignite. The axial temperature profile and gas concentrations within the reaction zone are predicted, and the influence of gasifier volume and operation parameters on cold gas efficiency (CGE) and fuel conversion is analysed. The optimum oxygen to fuel stoichiometry leads to a cold gas efficiency of 79.7 %. However, a stoichiometry above the optimum might be required to achieve a higher fuel conversion and to adjust the gasifier outlet temperature to meet slag requirements. Simple empirical reaction rate models that are directly derived from the entrained flow experiments are used to evaluate larger scale entrained flow gasification of other fuels. The use of Lusatian lignite results in a comparable gasifier performance. The maximum CGE of the bituminous coal in a 500 MW gasifier is 82.5 %, but a larger gasifier size compared to the lignite gasifier is required. Also, the addition of steam to the burner is considered to reduce the flame temperature. The entrained flow gasification of biocoal is simulated for a thermal fuel input of 10 MW and for an operation pressure of 0.5 MPa. If the gasifier is operated above the ash melting temperature, a maximum cold gas efficiency of 78.9 % is achieved. The potential operation of the gasifier in a non-slugging mode improves the efficiency up to 82.0 %.

The experience obtained during collecting the measurement sets and the theoretical background of the model development are then used to derive a test procedure for the evaluation of entrained flow reaction behaviour of unknown (coals, residuals) and alternative (biomass, waste) solid fuels. The test procedure consists of a limited number of measurements and leads to a comprehensive data set that enables the accurate prediction of fuel conversion in larger scale entrained flow gasifiers. This will enable significantly enhanced gasifier performance in the future.

Keywords: Gasification; Reaction Kinetics; Entrained Flow; Coal; Biomass; Experimental; Modelling

Kurzfassung

Trotz der verbreiteten Anwendung der Flugstromvergasung im industriellen Maßstab ist die Reaktionsgeschwindigkeit fester Brennstoffe in der heißen Reaktionszone nahezu unbekannt. Allerdings ist die Kenntnis der Vergasungsgeschwindigkeit bei hohen Temperaturen und hohen Drücken sehr wichtig für die detaillierte Auslegung und Optimierung dieser Reaktoren. Die Dissertation stellt daher experimentelle Daten für Umsetzungsgeschwindigkeiten unter großtechnisch relevanten Prozessbedingungen zur Verfügung und zielt darauf ab, diese Daten auf industrielle Flugstromvergaser zu übertragen.

Für die Messung von Reaktionsraten fester Brennstoffe bei hohen Temperaturen und hohen Drücken wurde ein Druckflugstromreaktor (Pressurised High Temperature Entrained Flow Reactor PiTER) im Technikumsmaßstab entwickelt, aufgebaut und in Betrieb genommen. Pyrolyse- und Vergasungsversuche wurden bei bis zu 1600°C und bis zu 4,0 MPa durchgeführt. Die Daten wurden durch einen zweiten atmosphärischen Flugstromreaktor und einen Druckdrahtnetzreaktor ergänzt. Um ein großes Brennstoffband abzudecken, wurden Versuche mit Anthrazit, Steinkohle, Braunkohle, Biokohle und Biomasse durchgeführt, wobei der Schwerpunkt der Messungen auf der Umsetzung einer Rheinischen Braunkohle lag. Durch die Pyrolyseversuche in allen drei Reaktoren wird ein einfaches Modell (Arrhenius Ansatz erster Ordnung) validiert, das die Flüchtigenfreisetzung beschreibt.

Zudem wurden aus allen Reaktoren Koksproben entnommen, die dann im Labor weiter untersucht wurden. Da die spezifische Koksoberfläche ein wichtiger Parameter für die heterogenen Koks-Gas-Reaktionen ist, wurde die Oberfläche der porösen Kokspartikel mittel CO₂-Adsorption bei 273 K bestimmt. Dabei wird ein Zusammenhang von spezifischer Oberfläche und den Reaktionsbedingungen bei der Flüchtigenfreisetzung deutlich.

Im Flugstromprozess bei hohen Temperaturen wird die Umsetzungsgeschwindigkeit von Koks durch kombinierte Diffusions- und Reaktionsvorgänge bestimmt. Bei geringeren Temperaturen kann die Oberflächenreaktion (intrinsische Reaktion) durch thermogravimetrische Analyse in Abwesenheit der Diffusionslimitierung gemessen werden. In einer Druckthermowaage wurde daher der Einfluss der Temperatur und des Partialdrucks der Reaktanden CO₂ und H₂O auf die intrinsische Reaktionsrate bestimmt und durch Reaktionsgleichungen n-ter Ordnung und Langmuir-Hinshelwood-Gleichungen ausgedrückt.

Bei der Analyse verschiedener Koksproben wurde eine thermische Deaktivierung festgestellt, wenn der Koks einer höheren Temperatur oder einer längeren Zeit bei hoher Temperatur ausgesetzt war. Für die Quantifizierung dieses Effekts wurde die Reaktionsgeschwindigkeit von Koksproben in einer Thermowaage bei standardisierten Bedingungen (375°C bis 400°C, oxidierende Atmosphäre) gemessen. Für die Beschreibung des Reaktivitätsverlusts wird ein Deaktivierungsmodell entwickelt und mittels der Messdaten validiert.

Da Diffusionsprozesse bei der Koksvergasung nicht direkt gemessen werden können, wird der Katalysatornutzungsgrad in Analogie zur heterogenen Katalyse verwendet. Dadurch

kann die intrinsische Reaktion und die Porendiffusion im Kokspartikel kombiniert werden und es ist eine Berechnung der Umsetzungsgeschwindigkeit auch bei hohen Temperaturen möglich. Für die Beschreibung der Filmdiffusion, die bei sehr hohen Temperaturen eine Rolle spielen kann, wird zusätzlich eine Korrelation basierend auf der Sherwood-Zahl verwendet. Die Kombination der beiden Diffusionsmodelle mit den Ansätzen für Pyrolyse, für intrinsische Reaktivität, für die Entwicklung der Koksoberfläche und für die thermische Koksdeaktivierung erlaubt schließlich die ganzheitliche Beschreibung der Umsetzungsgeschwindigkeit fester Brennstoffe in Flugstromreaktoren. Die Modellansätze werden in eine numerische Simulation integriert, die den PiTER als eindimensionalen Reaktor (Propfenströmung) abbildet. Der einzige unbekannte Modellparameter, der nicht aus experimentellen Daten abgeleitet werden kann, ist der mittlere Porendurchmesser des Kokes. Eine gute Übereinstimmung von Modell und Vergasungsexperimenten von Rheinischer Braunkohle wird für einen mittleren Porendurchmesser von 47 Å erreicht, was im erwarteten Größenbereich liegt, da die Koksumsetzung in Mikro- und Mesoporen stattfindet.

Um die experimentellen Daten auf den industriellen Maßstab zu übertragen, wird die Modellstruktur für die Auslegung und Optimierung realer Vergaser verwendet. Die Reaktoren werden wiederum durch eine eindimensionale Propfenströmung beschrieben. Für die Vergasung von Rheinischer Braunkohle wird ein Flugstromreaktor mit einer thermischen Leistung von 500 MW bei einem Druck von 2,5 MPa modelliert. Dabei wird das axiale Temperaturprofil und die Gaskonzentrationen innerhalb der Reaktionszone simuliert und der Einfluss von Reaktorgröße und Betriebsparametern auf den Kaltgaswirkungsgrad und die Brennstoffumsetzung analysiert. Die Simulation ergibt eine optimale Stöchiometrie, bei der ein Kaltgaswirkungsgrad von 79,7 % erreicht wird, wobei allerdings mögliche Temperaturgrenzen für den Schlackefluss nicht berücksichtigt werden.

Da für die anderen Brennstoffe die gesamte Modellstruktur nicht validiert werden kann, werden einfache empirische Reaktionsgleichungen direkt aus den Flugstromversuchen abgeleitet. Für die Lausitzer Braunkohle wird damit ein ähnliches Vergasungsverhalten simuliert und der maximale Kaltgaswirkungsgrad liegt bei 78,7 %. Der Kaltgaswirkungsgrad für den Einsatz von Steinkohle im 500 MW Vergaser liegt bei 82,5 %, allerdings muss der Vergaser größer dimensioniert werden und die Zugabe von Wasserdampf scheint notwendig. Die Flugstromvergasung von Biokohle wird in einem 10 MW Vergaser bei einem Druck von 0,5 MPa modelliert. Wird der Vergaser oberhalb der Ascheschmelztemperatur von Biokohle betrieben, ist ein maximaler Kaltgaswirkungsgrad von 78,9 % möglich. Alternativ wird der Vergaser bei einer niedrigeren Temperatur betrieben, was das Ascheschmelzen vermeidet und gleichzeitig den Kaltgaswirkungsgrad auf 82,0 % erhöht.

Abschließend wird die Erfahrung aus den Pyrolyse- und Vergasungsversuchen und der Modellentwicklung verwendet, um ein experimentelles Testverfahren vorzuschlagen, das die Analyse des Reaktionsverhaltens von unbekanntem und alternativen Festbrennstoffen ermöglicht. Das Testverfahren besteht aus einer beschränkten Anzahl von Messungen in verschiedenen Versuchsanlagen und führt zu einem abgeschlossenen Datensatz, der die Vorhersage der Brennstoffumsetzung in großtechnischen Flugstromreaktoren erlaubt.

Schlagwörter: Vergasung; Reaktionskinetik; Flugstrom; Kohle; Biomasse; experimentelle Untersuchung; Modellierung

Contents

Preface	I
Abstract	III
Kurzfassung	V
Abbreviations and Nomenclature	XI
1 Introduction and Background Information	1
1.1 The Development of Our Energy System	1
1.2 Gasification as a Tool for Future Sustainable Energy Utilisation	2
1.3 Outline of the Dissertation	4
2 Fundamentals	7
2.1 The Gasification Process of Solid Fuels	7
2.1.1 Devolatilisation	7
2.1.2 Heterogeneous Gasification Reactions	9
2.1.3 Homogeneous Gas Reactions	12
2.1.4 Reaction Rates of Singular Processes	13
2.1.5 Definition of Reaction Rate	15
2.2 Experimental Methods for the Investigation of Solid Fuel Gasification	16
2.2.1 Flow Reactors	16
2.2.2 Thermogravimetric Analysers	18
2.2.3 Wire Mesh Reactors	20
2.2.4 Fluidised and Fixed Bed Reactors	21
2.2.5 Laboratory Procedures for Fuel and Char Characterisation	22
3 Literature Review on Gasification Kinetics	27
3.1 Volatile Yield and Char Properties after Devolatilisation	28
3.1.1 Effect of Thermal History on Volatile Yield and Char Properties	28
3.1.2 Effect of Pressure on Volatile Yield and Char Properties	38
3.1.3 Effect of Gas Atmosphere on Volatile Yield and Char Properties	42
3.2 Influences on the Heterogeneous Char Conversion	43
3.2.1 Influence of Operation Parameters on the Intrinsic Reaction Rate	43
3.2.2 Measurements of Reaction Rates at Higher Temperature	49
3.3 Summary of the Literature Review and Research Demand	54
3.4 Aims and Research Strategy of the Dissertation	58

4	Theoretical Development and Selection of Gasification Models for Solid Fuels	61
4.1	Selection of a Pyrolysis Model	61
4.1.1	Overview of Pyrolysis Models from Literature	61
4.1.2	Development of a Pyrolysis Model Based on Experimental Data	63
4.2	Development and Selection of Char Conversion Models	67
4.2.1	Notation and Definition of Char Reactivity	67
4.2.2	Simple Model Approach for the Observed Reaction Rate	68
4.2.3	Submodels for Intrinsic Char Reactivity under Regime I Conditions	69
4.2.4	Submodel for the Variation of Reaction Rate with Conversion	74
4.2.5	Submodel for the Influence of Thermal Deactivation	76
4.2.6	Submodel for Pore Diffusion	82
4.2.7	Submodel for Boundary Layer Diffusion	92
4.2.8	Submodel for Particle Size and Density	93
4.2.9	State of the Art in CFD Modelling of Entrained Flow Gasifiers	96
5	Experimental Techniques, Procedures, and Results	99
5.1	Fuel and Reference Char Preparation	99
5.1.1	Procedure for Processing Coal and Biomass	99
5.1.2	Production of Reference Char	100
5.2	Methods used in the Laboratory Analysis	101
5.2.1	Proximate and Ultimate Analysis	101
5.2.2	Char Surface Measurement	102
5.2.3	Measurement of Particle Size Distribution	102
5.2.4	Particle Density Measurement	102
5.3	Experimental Facilities and Procedures	103
5.3.1	Pressurised High Temperature Entrained Flow Reactor	103
5.3.2	Baby High Temperature Entrained Flow Reactor	113
5.3.3	Pressurised Wire Mesh Reactor	116
5.3.4	Pressurised Thermogravimetric Analyser	119
5.3.5	Atmospheric Thermogravimetric Analyser	124
5.4	Experimental Results	126
5.4.1	Results from the Entrained Flow Reactors	126
5.4.2	Results from the Wire Mesh Reactor	154
5.4.3	Results from the Pressurised Thermogravimetric Analysis	156
5.4.4	Results from the Atmospheric Thermogravimetric Analysis	164
6	Validation of Pyrolysis Models for Entrained Flow Gasification	169
6.1	Volatile Yield as a Function of Pressure and Temperature	169
6.2	Analysis of the Devolatilisation Kinetics	171
7	Validation of the Char Conversion Models for Entrained Flow Gasification	175
7.1	Validation of the Char Gasification Submodels	175
7.1.1	Validation of the Intrinsic Reactivity Submodels	176
7.1.2	Validation of the Surface Area Submodel	184
7.1.3	Validation of the Thermal Deactivation Submodels	188

7.2	Validation of the Model Framework by Using Entrained Flow Data	191
7.2.1	Validation of the Simple Empirical Char Gasification Model	193
7.2.2	Validation of the Comprehensive Model Framework	198
8	Simulation of Industrial Scale Entrained Flow Gasifiers	203
8.1	Description of the Simulation Approach	203
8.1.1	Gasifier Geometry and Boundary Conditions	203
8.1.2	Calculation of Reaction Rate, Temperature, and Gas Composition	204
8.1.3	Limitations of the Simulation	205
8.2	Simulation of a 500 MW Entrained Flow Gasifier for Lignite R	206
8.2.1	Design of the Lignite R Gasifier	206
8.2.2	Optimisation of the Lignite R Gasifier	210
8.3	Fuel Specific Adaption of Gasifier Layout and Operation	213
8.4	Analysis of the Reaction Regime in Entrained Flow Gasifiers	217
9	Development of a Fuel Test Procedure for Entrained Flow Gasification	221
9.1	Entrained Flow Gasification Experiments	222
9.2	Pyrolysis Experiments	223
9.2.1	Entrained Flow Pyrolysis Experiments	224
9.2.2	Pyrolysis Experiments in the Wire Mesh Reactor	225
9.3	Char Analysis	226
9.3.1	Char Specific Surface Area Evolution during Conversion	226
9.3.2	Quantification of Thermal Char Deactivation	226
9.3.3	Measurement of Intrinsic Char Reactivity	227
10	Summary, Conclusions, and Recommendations	231
10.1	Summary of the Dissertation	231
10.1.1	Data Set for Fuel Conversion under Entrained Flow Conditions . .	231
10.1.2	Model Development for Entrained Flow Gasification	232
10.1.3	Layout and Optimisation of Larger Scale Entrained Flow Gasifiers .	233
10.1.4	The Reaction Regime during Entrained Flow Gasification	234
10.1.5	Development of a Test Procedure for Solid Fuels	235
10.2	Recommendations for Future Work	235
10.2.1	Recommendations for Future Experimental Work	235
10.2.2	Recommendations for Future Model and Simulation Approaches . .	236
	Bibliography	239
	Appendices	253
A	Calculation of Conversion - Ash Tracer Method	253
B	Error Calculation	255
C	Calculation of Chemical Equilibrium	259

Abbreviations

ASA	active surface area
ASTM	American Society for Testing and Materials
ATGA	Atmospheric Thermogravimetric Analyser
BabiTER	Baby High Temperature Entrained Flow Reactor
bit.	bituminous coal
CCS	carbon capture and storage
CFD	Computational Fluid Dynamics
CGE	cold gas efficiency
CPD	Chemical Percolation Depolymerisation model
CSIRO	Commonwealth Scientific and Industrial Research Organisation
DAE	distributed activation energy
DFT	density functional theory
DR	Dubinin-Radushkevich
DRK	Dubinin-Radushkevich-Kaganer
EF	entrained flow
EFR	entrained flow reactor
FG-DVC	Functional Group - Depolymerisation Vaporisation Crosslinking model
FT	Fischer Tropsch
GC	gas chromatography
GSP	Gaskombinat Schwarze Pumpe
HRTEM	high-resolution transmission electron microscopy
HTC	hydrothermal carbonisation
IEA	International Energy Agency
i.d.	inner diameter
IGCC	Integrated Gasification Combined Cycle
LH	Langmuir-Hinshelwood
LHHW	Langmuir-Hinshelwood-Hougen-Watson
LHV	lower heating value
NDIR	non-dispersive infrared
NMR	nuclear magnetic resonance

NSC	Nagle and Strickland-Constable
OECD	Organisation of Economic Co-operation and Development
PDTF	pressurised drop tube furnace
PLC	programmable logic controller
PiTER	Pressurised High Temperature Entrained Flow Reactor
PRETA	Pressurised Thermogravimetric Analyser
PTGA	pressurised thermogravimetric analyser
PWMR	Pressurised Wire Mesh Reactor
RPM	Random Pore Model
RSA	reactive surface area
SFOR	single first order reaction
SNG	synthetic natural gas
TGA	thermogravimetric analyser
TSA	total surface area
TUM	Technische Universität München
XRD	X-ray diffraction
YSZ	yttria stabilised zirconia

Nomenclature

A	constant parameter ratio of the pre-exponential factors in the simple annealing model
A_{max}	ratio of the pre-exponential factors in the comprehensive annealing model
A_V	pre-exponential factor in the pyrolysis model [1/s]
a	constant ash content
a_i	replacement character in the Level 2 intrinsic model
B	constant parameter
b	constant parameter
C_{daf}	carbon content
c	gas concentration [g/m^3], [mol/m^3] volatile yield constant
c_V	volatiles concentration within a fuel particle
D_{eff}	effective diffusivity [m^2/s]
D_K	Knudsen diffusivity [m^2/s]
D_M	molecular diffusivity [m^2/s]
ΔH	enthalpy of reaction [kJ/mol]
Δh_V	enthalpy of vapourisation [kJ/kg]
d	particle diameter [m]
d_{pore}	pore diameter [m]
E	energy particle entrainment
E_A	activation energy [kJ/mol]
E_a	activation energy [kJ/mol]
$E_{A,F}$	activation energy in the comprehensive annealing model [kJ/mol]
$E_{A,V}$	activation energy in the single first order pyrolysis model [kJ/mol]
F_0	pre-exponential factor in the comprehensive annealing model [1/s]
f	fraction of fresh sites
G_i	replacement character in the Level 3 intrinsic model
H_i	replacement character in the Level 2 intrinsic model
I_i	replacement character in the Level 3 intrinsic model

J	flux [$g/(m^2 \cdot s)$], [$mol/(m^2 \cdot s)$]
K	adsorption constant
k	kinetic constant
k_0	pre-exponential factor [$g/(m^2s)$], [$g/(m^2sPa^n)$], [$g/(m^2sPa)$]
L	characteristic length [m]
M	molecular weight [g/mol]
m	mass [g] total pressure reaction order
N	gravimetric stoichiometric coefficient
n	reaction order
p	pressure [Pa]
q	heat flux [W/m^2]
R	ideal gas constant [$8.314J/(mol \cdot K)$] particle radius [m]
R_{max}	maximum char reactivity [$1/s$]
Re	Reynolds Number
r	particle radius coordinate reaction rate [$1/s$], [$g/(m^2s)$]
r_{stand}	standard reactivity [$g/(g \cdot s)$]
S	specific surface area [m^2/g], [m^2/m^3]
S_p	particle outer surface area [m^2]
Sc	Schmidt Number
Sh	Sherwood Number
Sw	Swelling ratio
s	surface fraction
T	temperature [K], [$^{\circ}C$]
T_{HT}	annealing temperature [K]
t	time [s]
t_{HT}	annealing time [s]
u	uncertainty
V_p	particle volume [m^3]
v	particle free fall velocity [m/s]
W_i	replacement character in the Level 3 intrinsic model
X	total conversion of volatiles
x	char conversion
Y_v	volatile yield

Greek Symbols

α	constant parameter
β	constant parameter
	mass transfer coefficient in the particle boundary layer [m/s]
Δ	difference
ϵ	porosity
ϕ	Thiele modulus
γ	number of active sites required for the adsorption of one gas molecule
η	effectiveness factor
ν	stoichiometric coefficient of a reaction
Θ	surface coverage
	temperature parameter in the volatile yield model
ϑ	temperature constant in the volatile yield model
P	pressure parameter in the volatile yield model
ρ	pressure constant in the volatile yield model
	density [g/m^3]
σ	standard deviation
	binary power constant of the Lennard Jones Potential
τ	tortuosity factor
	residence time [s]
Ω	collision integral in binary diffusion
ω	adjustable parameter in the simple thermal annealing model
ξ	reaction coordinate
Ψ	constant parameter in the Random Pore Model

Subscripts

0	initial; reference; mean
<i>An</i>	annealing
<i>app</i>	apparent
<i>bulk</i>	in the bulk phase
<i>Deact</i>	deactivated
<i>daf</i>	on a dry ash free basis
<i>des</i>	desorption
<i>dry</i>	on a dry basis

<i>ex</i>	at the external particle surface
<i>Fresh</i>	fresh
<i>final</i>	final
<i>g</i>	on a mass basis
<i>gas</i>	gas
<i>gen</i>	general
<i>HR</i>	at constant heating rate
<i>i</i>	replacement character
∞	infinity
<i>ini</i>	initial
<i>int</i>	internal
<i>intr</i>	intrinsic
<i>j</i>	replacement character
<i>L1</i>	Level 1 of the intrinsic model
<i>L2</i>	Level 2 of the intrinsic model
<i>L3</i>	Level 3 of the intrinsic model
<i>max</i>	maximum
<i>min</i>	minimum
<i>N</i>	under normal conditions
<i>norm</i>	normalised
<i>obs</i>	observed
<i>particle</i>	particle
<i>Pl</i>	plate
<i>S</i>	at the outer particle surface
<i>set</i>	setpoint
<i>sph</i>	spherical geometry
<i>T</i>	temperature
<i>t</i>	total
<i>V</i>	volatile
<i>v</i>	on a volume basis
<i>Z</i>	subscript in the NSC model

Chapter 1

Introduction and Background Information

1.1 The Development of Our Energy System

As the development of the world's economy speeds up, a fundamental discrepancy arises that threatens the well-being of our society. The United Nations predict a growth of the world's population from currently 7 billion people up to 9.3 billion by the middle of this century [UN2011]. Simultaneously, the legitimate pursuit of economic wealth in developing countries leads to an increase in energy consumption. Due to the economic upturn in non-OECD countries and the slight growth in OECD countries, the worldwide energy consumption per capita is predicted to increase from 2010 to 2030 by 20 % [Ito2007]. The rise of the world's population and energy consumption per capita will significantly boost the world's total energy demand.

Today's energy supply is based on fossil fuels. In 2009, 81 % of the world's total primary energy came from fossil fuels [IEA2010] that account for almost all CO₂ emissions worldwide.

The current strong dependence on fossil fuels and the predicted upsurge of the worldwide energy consumption are contradictory to essential goals for the future sustainable development. Developed and emerging countries agree that a secure and affordable energy supply for everybody is a basic need for the well-being of our society. An increase in energy consumption is inevitable to improve the standard of living especially in poorer regions. Due to the dependence on fossil fuels, the declining availability of resources, and the pick-up in demand, a rise in energy prices seems to be unavoidable.

On the other hand, the need for a reduction of CO₂ emissions additionally complicates the situation. The 450 Scenario of the International Energy Agency (IEA) sets out an energy pathway consistent with the goal of limiting the rise of average global temperature to 2°C [IEA2010b]. In this scenario, the stabilisation of the concentration of global greenhouse gases at 450 ppm CO₂-equivalent is achieved. But the world energy outlook to 2035 predicts that fossil fuels will remain the dominant energy source [IEA2010b]. Carbon capture and storage (CCS) plays an important role in reducing the emissions in the power sector. The 450 Scenario requires that by 2035, power generation from coal plants fitted with CCS will exceed generation from coal plants not equipped with this technology [IEA2010b]. At the same time, the share of nuclear power in the total energy mix increases by about 50 % over current levels, which is an ambitious target. Renewable-based generation will increase

the most and will reach more than 45 % of global generation. The range of outcomes in the model is largest for important energy sources like coal, nuclear power and non-hydro renewables which indicate uncertainties in the prediction. Despite the uncertainties, the need for a change of our energy system is made clear.

The support and the implementation of new technologies are required to achieve the ambitious goals. Future energy generation and conversion technologies have to increase the energy efficiency of conversion processes, reduce the energy demand, and decrease energy related emissions. Energy efficiency will contribute to reduce the CO₂ emissions. But the need for massive CO₂ reductions can only be tackled by two pathways: carbon capture and renewable energy technologies. Major reductions of CO₂ emissions from fossil fuels are only achieved by separating CO₂ and either storing it in geological formations or using it as a raw material for synthetic products. Renewable energy sources are essential as their CO₂ emissions are far below fossil fuels. However, in their current stage of development they are generally more expensive than fossil resources. As renewable sources like wind and solar are fluctuating sources, storage technologies are required to balance variations and make power production more reliable. Both the currently higher costs and the fluctuations are contradictory to a secure and affordable energy supply.

To change our energy system, major advances in the field of fossil and renewable energy sources are essential. The implementation of carbon capture and renewable energy technologies is dependent on local and regional aspects like the availability of fossil and renewable energy carriers, the support or opposition of local populations, and the economic possibilities. The potentials and specific advantages and disadvantages of new technologies are not known a priori. As the change of our energy system has to proceed at a high pace, enormous research and development efforts are required to adapt state of the art systems and to develop new ideas. Research on the basic level should be independent of political and social constraints and should address all possibilities of future energy carriers. The outcomes of the research activities in combination with social and economic considerations will guide the way to the implementation of new technologies and the changes necessary in our energy system.

1.2 Gasification as a Tool for Future Sustainable Energy Utilisation

One of the technologies that can contribute to the reduction of CO₂ emissions of fossil fuels and can enable the implementation of renewable energy sources is gasification. Solid fuels like coal and biomass are converted to a gas that can be used in chemical syntheses and power production (gas turbine applications, fuel cells, etc.).

In an Integrated Gasification Combined Cycle (IGCC) solid fuels are first converted in a pressurised gasifier to generate a product gas with high concentrations of carbon monoxide (CO) and hydrogen (H₂). The gas is then converted to power in a gas turbine combined cycle. The combination of a gas and a steam turbine allows the utilisation of combustion heat over a wide range of temperature which is thermodynamically preferable to conventional combustion systems. As a result, an IGCC offers a high electrical efficiency up to

51.5 % [Goettlicher1999, Higman2003].

By using the gasification technology, the power plant is operated on solid fuels like coal. Compared with natural gas, coal is available around the world and the resources are distributed across several countries and continents. Price increases and uncertain supplies that are expected for natural gas due to regional and political issues are unlikely for coal. For example, in Germany coal (lignite) resources are predicted to last for more than 200 years [Cramer2010] enabling a secure and independent energy supply for the next decades. If carbon capture will be an environmentally and economically favoured requirement, the CO after the gasification is converted to CO₂ by water steam addition in a shift reactor. This leads to a gaseous mixture of H₂ and CO₂. The high pressure and high concentration of CO₂ in the mixture allow a very efficient separation in a scrubbing column or in a membrane process. CO₂ can then be stored or used as raw material in chemical syntheses. The resulting pure H₂ is used for power production in the combined cycle and the only emission is pure water.

Today large scale power plants are operated on coal. Due to the high conversion temperature of the gasifier in an IGCC, different solid fuels (for example also low quality coals and biomass) can be used. This fuel flexibility allows the input of low quality coals and alternative fuels which can increase the economic efficiency of the IGCC. Furthermore, the co-utilisation or full scale biomass applications are feasible. Further technological developments are required in the pre-treatment and feeding equipment for biomass, but biomass has already been used on a larger scale [Dongen2006]. The fuel flexibility of a gasifier enables the change from fossil fuels (coal) to renewable energy sources (biomass) within the lifetime of a power plant.

The flexibility of an IGCC can further be increased by the implementation of chemical synthesis. In parallel to the combined cycle, the product gas from the gasifier can be fed to a reactor where synthetic fuels (e.g. FT¹, SNG²) or chemical raw materials (e.g. methanol, ammonia) are produced. Furthermore, heat that is produced in the process steps can be used for heating or industrial applications. The overall system is then referred to as a polygeneration plant and can adapt its output to the current demand of synthetic products, heat and power.

If a major task of the power plant is balancing the fluctuating supplies from renewable energy sources, the gasifier can be decoupled from the power production unit by chemical storage. The product gas can be stored directly or can be first converted to a gaseous (e.g. H₂, SNG) or liquid fuel (e.g. methanol, FT). The gasification island that has high investment costs is then operated at full load which considerably improves the economic efficiency. Power is produced in gas turbine combined cycles that are fuelled by the storage and are operated only when electricity is required. Due to their lower specific investment costs, combined cycles can be economically operated at a low number of annual full load hours. The number and capacity of the combined cycles per gasifier depend on the range of fluctuations that have to be balanced. The operation of a full flexible gasification power plant enables the progressing integration of fluctuating renewables like wind and solar and also the complete change to renewables if the gasifier is operated on biomass.

¹Fischer Tropsch fuel is a liquid fuel similar to diesel

²Synthetic Natural Gas can be produced in a methanation reactor

In larger scale gasification projects like IGCCs, entrained flow gasifiers are the dominant technology. According to the US Department of Energy, from 2005 to 2011 94 % (82 out of 87) of all registered gasification projects worldwide (in operation and planned) are based on entrained flow gasification [DOE2010]. Due to its high throughput, its relative simple design and its reliability, the entrained flow gasifier is also expected to be the dominant technology in the future.

The state of knowledge in gasification technologies is clearly at a lower level when compared with combustion processes - especially gas combustion [Spliethoff2010b]. A primary parameter for the design and optimisation of entrained flow gasifiers is the reactivity of fuel particles under operation conditions. The gasifiers are operated at high pressures from 2.0 MPa to 7.0 MPa and high temperatures of at least 1400°C [Higman2003], but the conversion rates of different solid fuels are almost unknown. If a gasifier is designed for a single fuel or a range of fuels, it is required to know the reaction time to achieve complete conversion. This reaction time specifies dimensions of the gasifier and determines the maximum throughput. The reaction rate is also influenced by operation conditions. Therefore, it is required that one knows the effects of operation conditions like temperature and pressure on the conversion rate to enable a prediction of optimum reaction conditions. If an existing gasifier should be operated on an alternative fuel, it is important to have information about the reaction behaviour of the new fuel. This knowledge will identify fuel related difficulties and will improve the operation strategy of the gasifier as the required adjustments are known in advance.

The focus of this dissertation is the evaluation of the reaction behaviour of solid fuels under entrained flow operation conditions. Based on experimental data at high temperature and high pressure, the reactivity of different fuels is analysed and mathematical models are developed that describe the conversion rate. The dissertation aims to contribute to the design and optimisation of existing and innovative entrained flow gasifiers and to the application of different coals, alternative fuels, and biomass in high temperature processes.

1.3 Outline of the Dissertation

After the short introduction in this first chapter, the second chapter focuses on fundamentals and basic considerations of the gasification process. In Chapter 3, the literature on gasification kinetics is reviewed and parameters that influence the reaction rate are discussed. The motivation and contribution of the dissertation are also outlined. In Chapter 4, the current status of high temperature reaction modelling is summarised and a set of mathematical formulations is derived that allows a quantification of the influences of fuel properties and gasifier operation parameters.

The primary contribution of the dissertation is the design, construction and commissioning of four experimental setups that allow the investigation of gasification reactions at high temperature and high pressure. The layout of the facilities, the experimental procedure, and the results of several measurement sets are summarised in Chapter 5. The experiments include gasification data of biomass, lignite and hard coal that enable the validation of model equations and the derivation of model parameters. The data are used to validate entrained flow pyrolysis models in Chapter 6 and char conversion models in Chapter 7.

Different submodels are combined to depict the reaction behaviour of a range of fuels at high temperature, high heating rate and pressure.

As the experimental data are measured at conditions relevant to larger scale entrained flow gasifiers and the model equations can be applied in numerical simulations, a model of an industrial scale gasifier is presented in Chapter 8. The influence of reactor geometry and operation parameters on gasifier performance is analysed. Entrained flow gasifiers in different scales are designed for lignite, bituminous coal and biocoal. In Chapter 9, the experience from the experiments and the requirements from the model development and gasifier simulation are used to develop a fuel test procedure that analyses fuel specific reaction behaviour at high temperature and high pressure. The experimental test procedure enables the efficient derivation of the model parameters and the transfer of fuel conversion to an industrial scale.

Finally, in Chapter 10 the main findings are summarised and recommendations for further research in this field are given.

Chapter 2

Fundamentals on Solid Fuel Gasification

2.1 The Gasification Process of Solid Fuels

When coal or biomass particles enter the hot reaction zone of a gasifier, several co-current and subsequent reactions occur. Basically, the reactions can be classified in three conversion steps:

- Devolatilisation
- Combustion of devolatilisation products (volatiles and partially char)
- Gasification of char particles by heterogeneous reactions

The reaction scheme is shown in Figure 2.1. After the fuel particles enter the reaction zone, the devolatilisation occurs and porous char particles and volatiles (light gases, tar compounds) are generated. Volatiles and partially char (depending on volatile yield and stoichiometry) are combusted by oxygen in exothermic reactions that provide the thermal energy for particle heat-up and the subsequent endothermic gasification reactions. The main products from combustion are CO_2 and H_2O . Depending on stoichiometry also CO and H_2 may be generated. The char particles are further converted in heterogeneous gasification reactions by CO_2 and H_2O . The gasification products CO and H_2 may inhibit the reaction. Several properties of the char particles (e.g. size, density, porosity) can continuously change during reaction and the mineral matter content of the char particles increases during the consumption of solid organic matter. As the particle density decreases, fragmentation may occur during the conversion and smaller particles are generated. Finally, the char particles are converted to ash particles. Depending on temperature and ash properties, the mineral matter is melted and a liquid slag is formed. During all heterogeneous gas-solid reactions, mineral matter components (e.g. alkali and earth alkali metals) can promote the reaction rate by catalysis.

The next sections will focus on the different reaction steps in more detail.

2.1.1 Devolatilisation

The devolatilisation of volatile matter from solid fuels is the first process in thermal conversion. The term *pyrolysis* is often used as a synonym for devolatilisation, but pyrolysis precisely means devolatilisation in an inert gas atmosphere [Smith1994].

The understanding of devolatilisation processes is important because of their influence on

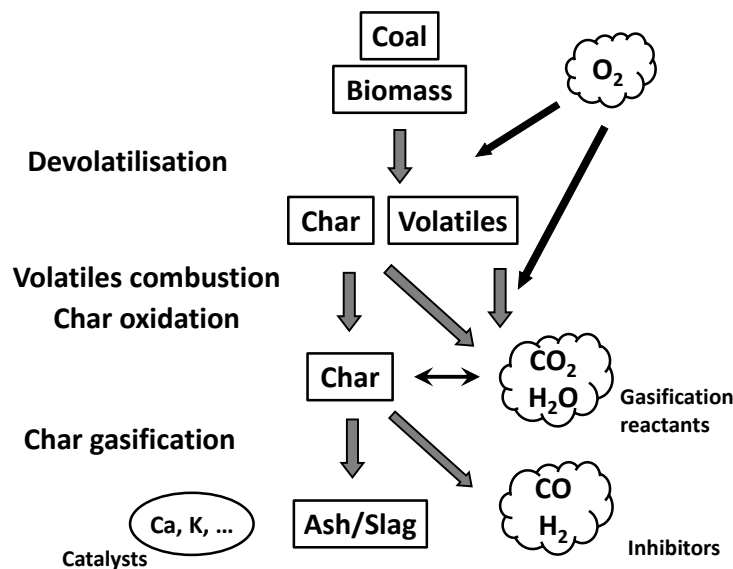


Figure 2.1: Basic reaction scheme in an autothermal gasification process

the subsequent conversion process [Solomon1993]. The volatile yield and volatiles composition influence the burner operation as they control ignition, temperature, and stability of the flame. Fuels of different rank show wide variations in devolatilisation behaviour because of different extents of coalification [Smith1994]. Biomass has a significantly higher volatile matter content than coal [Spliethoff2010]. On a dry basis, the volatile matter content of biomass is approximately 70 wt% to 80 wt%. The volatile yields are very similar for lignites, sub-bituminous, and high-volatile bituminous coals (about 50 wt%), but diminish for coals of higher rank [Smith1994]. Despite the consistence in total volatile yield, the proportions of light gases and tars that are generated during devolatilisation vary widely with coal rank and also between coals of similar rank. Smith [Smith1994] summarises product composition after devolatilisation: high gas yields and low tar yields are measured for low-rank coals; high-volatile bituminous coals exhibit moderate gas yields and high tar yields; and high-rank coals exhibit low gas yields and also moderate or low tar yields. The proportions of low-molecular weight gases and pyrolytic liquid (bio-oil/tar) after the pyrolysis of biomass depend on numerous factors including operation conditions and fuel properties [DiBlasi2008].

Different processes occur within a fuel particle during heat-up. These processes depend on many factors such as peak temperature, heating rate, pressure, particle size, and coal type [Smith1994]. The cracking of organic compounds begins at temperatures above 300°C [Spliethoff2010]. In low rank coals, oxygen-bearing functional groups form cross links that lead to a highly aromatic network [Alonso2001]. Coals of medium rank that have reduced their oxygen content during coalification exhibit thermoplastic behaviour and melt like non-Newtonian fluids during heat-up. Fluidity usually occurs in coals with a carbon content of 81 % to 92 %, but is also dependent on hydrogen and oxygen content and heating rate [Smith1994]. The formation of a metaplast during coal devolatilisation is interpreted by an analogy to the steam distillation of petroleum [Niksa2003]. The release of light gases from the original three-dimensional coal structure is compared with the bubbling of steam through a barrel of crude oil. Material with high molecular weight remains in

the coal metaplast and condenses into char if the temperature exceeds a threshold value. This theory is integrated into three comprehensive devolatilisation models that are briefly explained in Chapter 4. The analogy is able to describe the influences of heating rate, temperature, and pressure during devolatilisation. More information about the basic processes during devolatilisation can be found in several review papers (e.g. [Niksa2003, Yu2007]) and books (e.g. [Smith1994, Spliethoff2010]).

2.1.2 Heterogeneous Gasification Reactions

In the devolatilisation stage, char is generated that is further converted in heterogeneous reactions. As char properties influence these reactions, it is important to understand typical char properties such as composition, pore structure, morphology, and surface area [Roberts2000]. It is hardly possible to describe char properties in general terms, as almost all of the parameters are dependent on the conditions under which the char was made [Roberts2000]. The reactivity of char depends on total surface area, the number of reactive sites per unit surface area, and the local gaseous reactant concentration [Laurendeau1978]. Consequently, char reactivity depends on three important characteristics of the sample [Laurendeau1978]:

1. Chemical structure: the chemical structure of the char surface provides active sites (dislocations, crystalline edges, and heterocyclic centres).
2. Mineral matter: inorganic constituents promote catalytic activity and create further dislocations (not the total amount of mineral matter is important, but the nature, distribution, and chemical form [Li2007]).
3. Physical char structure: the pore structure determines the total surface area accessible for reaction; it influences diffusion and therefore the local gas concentration within the char particle.

The conversion of a char particle is then a series of reaction and diffusion processes that can be separated in seven singular reaction steps [Baerns2002]:

- Transport of the reactant gas molecule to the outer surface of the char particle
- Diffusion within a char pore
- Adsorption on the char surface
- Chemical reaction on the char surface
- Desorption of the product(s) from the char surface
- Diffusion within the char pores to the outer char surface
- Transport from the char surface to the bulk gas phase

In this sequence of reaction steps, one or more can be identified as the rate-determining steps, i.e. the slowest step and therefore the step that controls the rate of the overall process. In practical applications generally a combination of several steps has a controlling influence. For a given coal char, the degree of limitation by chemical reaction or diffusion is mainly a function of reaction temperature. The dependence of the reaction rate

on temperature is usually shown as an Arrhenius plot of reactivity (logarithmic) versus temperature (inverse), as shown in Figure 2.2. The relation between chemical reaction and mass transport limitation is classified in three regimes. The chemical reaction is a strong function of temperature (typically exponentially). In Regime I at low temperature the chemical reaction rate at the char surface is very slow and determines the overall reaction rate. The gas concentration is uniform within the char particle and the bulk gas phase. With increasing temperature the chemical reaction rate increases exponentially and becomes comparable to the pore diffusion rate within the particle. As the reactant is consumed at the inner particle surface, a concentration gradient develops within the char particle. Under ideal Regime II conditions, the reactant concentration is equal to the bulk concentration at the outer particle surface and zero at the particle centre. Under Regime II conditions the reaction rate is influenced by the chemical reaction rate and the pore diffusion rate. When the temperature is increased further, the chemical reaction is very fast and reactants are consumed at the outer particle surface before reaching the pore system. The overall rate is controlled by the mass transfer between bulk phase and particle outer surface and a concentration gradient is formed in the boundary layer. As diffusion processes are only slightly influenced by temperature, the slope of the curve approaches zero. There are two transition zones (between Regime I and II and between Regime II and III) where the overall rate is influenced by a combination of the adjoining regimes. In fact, in real gasification systems a combination of chemical reaction and both internal and external mass transfer limitations are likely. The surface reaction as well as diffusion phenomena have to be considered.

The transition temperature from Regime I to Regime II conditions is dependent on char properties and reaction conditions. Table 2.1 summarises qualitatively the effects of char properties and operation conditions on the transition temperature to Regime II conditions. When continuously increasing the temperature in an experiment, the reaction rate

Table 2.1: Qualitative influence of char properties and operation conditions on the transition temperature to Regime II conditions

	Parameter	Transition Temperature
Char Properties	Particle Size ↑	↓
	Porosity ↑	↑
	Pore Size ↑	↑
	Intrinsic Reactivity ↑	↓
	Inner Surface Area ↑	↓
Operation Parameters	Reactant Partial Pressure ↑	↓
	Total Pressure ^a ↑	↓ ^b

^aVariation of total pressure at a constant partial pressure of reactants

^bMolecular gas diffusivity decreases at higher total pressure

increases. The transition to Regime II conditions is typically observed by a decreasing temperature influence, i.e. the slope in the Arrhenius plot (see Figure 2.2) decreases. As with entrained flow gasification the reaction regimes of other thermal char conversion processes are not known a priori. The reaction regimes that are typically expected in pul-

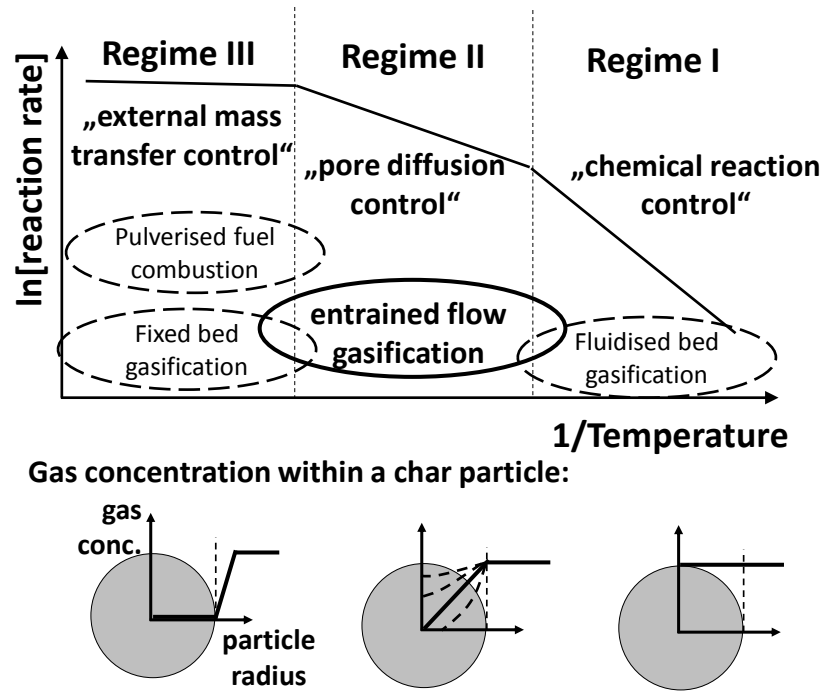


Figure 2.2: Influence of temperature on gasification rate (Arrhenius plot) and gas concentration gradients within a porous char particle

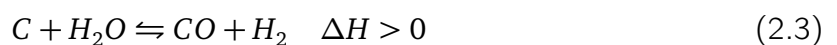
verised fuel combustion, fluidised bed gasification, and fixed bed gasification are also shown in Figure 2.2. Due to the fast chemical reaction rate of char combustion at high temperature, pulverised fuel combustion (pfc) is limited by mass transport limitations (Regime II and III)¹. The reaction temperature during fluidised bed gasification is significantly lower and char conversion is expected to occur under Regime I conditions (at least for small and medium sized particles). In fixed bed gasifiers usually larger particle sizes are used. As the diffusion pathways within the particles are long, internal and external mass transfer is expected to play an important role.

In autothermal reactors that are operated with oxygen, heterogeneous combustion and gasification occur. In an allothermal gasifier, heat is transferred to the reactor instead of oxygen and only gasification reactions occur. The main reactions in gasifiers are:

The heterogeneous combustion reaction:



The heterogeneous gasification reactions:



¹Theoretically, a limitation by chemical reaction is possible at a very small particle size.

²Depending on reaction conditions, the primary product might be CO at the char surface. In excess of oxygen CO₂ is formed in the gas phase.

Furthermore, the methanation of carbon is possible:



As the reactions with free oxygen are all essentially complete under gasification conditions, only the reactions 2.2, 2.3, and 2.4 need to be considered in the thermodynamic determination of product gas composition [Higman2003].

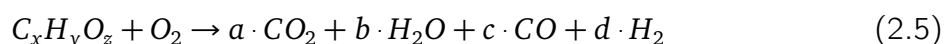
All practical fuels (coal and biomass) contain other chemical elements in addition to carbon. These are mainly oxygen, hydrogen, nitrogen, and sulphur, but almost any other element of the periodic table can also be present. These elements are released during devolatilisation and during the heterogeneous char reactions. Oxygen and hydrogen are converted to main gas elements and contribute in the reactions 2.2, 2.3, and 2.4. Under gasification conditions, sulphur is converted to H_2S and COS , and the nitrogen to N_2 , NH_3 , and HCN . However, the quantities of sulphur, nitrogen, and other trace elements are sufficiently small that their effect on the main reactions and on the product gas composition is negligible [Higman2003].

Trace elements significantly influence slag properties and determine the amount and composition of minor gases in the product gas. Their concentrations have to be considered in the determination of slagging behaviour and the analysis of corrosion issues in downstream applications. The focus of this dissertation is on the carbon, hydrogen, and oxygen chemistry during gasification. Trace elements are not considered in the further analysis.

2.1.3 Homogeneous Gas Reactions

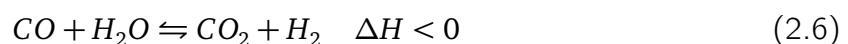
Homogeneous reactions are reactions that include only reactants and products in the same phase. In gasification, these are reactions in the gas phase.

The volatiles that are released during devolatilisation are combusted and a gaseous mixture of CO_2 , H_2O , CO , and H_2 is produced depending on the stoichiometry. In gasifiers that are operated above $850^\circ C$ reaction rates are sufficiently high so that the complex network of volatiles reactions does not need to be considered in detail and the determination of gas composition can be based on chemical equilibrium [Higman2003]. The conversion of volatiles is then described by a simple equation:

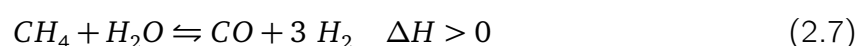


The reactions of the main components in the gas phase can be reduced to two homogeneous reactions [Higman2003]:

water gas shift reaction:



and steam methane reforming reaction:



Due to the endothermic character of Reaction 2.7, the equilibrium at high temperature is completely on the right side. In high temperature entrained flow reactors the concentration of CH_4 approaches zero and the gas phase equilibrium can be described in good approximation only by the water gas shift reaction (Reaction 2.6).

2.1.4 Reaction Rates of Singular Processes

It is generally observed that devolatilisation and homogeneous gas reactions are several orders of magnitude faster than the heterogeneous char reactions. However, experimental data on the rate of devolatilisation at conditions relevant to industrial entrained flow gasifiers are rare. For example, Yeasmin et al. [Yeasmin1999] measured pyrolysis yield of pulverised coal at medium temperature (600°C to 1000°C) in a flow reactor. They observed that the yield approaches a constant value at a residence time of about 2 s. At very high temperature ($>1500^\circ\text{C}$) the devolatilisation is completed even below 100 ms as shown by Kobayashi et al. [Kobayashi1977] in pyrolysis experiments with lignite and bituminous coal. As several factors like heating rate, maximum temperature, and particle size influence the devolatilisation rate, the precise description of the rates is not always possible. In Table 2.2 some more literature data about devolatilisation time scales are shown.

It is obvious from the data that operation conditions (e.g. temperature) and coal properties (e.g. particle size) have an influence on the rate of devolatilisation. Pyrolysis (including particle heat-up) occurs in a time interval of some ten to hundreds of milliseconds mainly depending on temperature. At low temperature ($< 1000^\circ\text{C}$) the pyrolysis process extends to time scales above one second. However, in entrained flow systems temperatures are usually higher and devolatilisation is completed after less than one hundred milliseconds. Although not much kinetic data on volatiles combustion are available, it is clearly established that these homogeneous reactions are much faster than the heterogeneous char gasification reactions [Higman2003].

Compared with fast devolatilisation and volatiles combustion, the heterogeneous char reactions are much slower. The rate of each reaction is depending on the reaction conditions. However, at identical conditions a direct comparison of the CO_2 and the H_2O reactions to combustion and methanation is possible. Table 2.3 shows literature data that compare directly the rates of heterogeneous reactions.

Char combustion is several orders of magnitudes faster than gasification by CO_2 and H_2O . Therefore, oxygen is consumed instantly and the combustion reaction (2.1) does not limit the overall conversion rate. In contrast, the methanation (Reaction 2.4) is very slow and does only marginally contribute to char conversion. After the consumption of oxygen, the char conversion rate is limited by CO_2 and H_2O gasification. The rates of both reactions are similar, at least at the operation conditions and for the char properties shown here.

Similar to volatiles combustion, the other homogeneous reactions are very fast. The local gas composition in the reactor at high temperature can be described by chemical equilibrium [Liu2004]. Homogeneous reactions do not determine the overall reaction rate.

In the sequence of all reactions, the heterogeneous char reactions with CO_2 and H_2O are

Table 2.2: A direct comparison of time scales for pyrolysis under entrained flow conditions (Fuel data and operation conditions are summarised. After the time scale indicated the pyrolysis reaction is complete and volatile yield did not change with increasing residence time. As the data are measured in drop-tube or entrained flow reactors, the time scales include the initial particle heating.)

Reference	Fuel	Volatile matter dry wt%	Particle Size μm	p MPa	T $^{\circ}\text{C}$	Time scale
						ms
[Manton2004]	Newlands (AUS)	28.5				140
	Ebenezer (AUS)	40.6				240
	Blair Athol (AUS)	22.1	75-106	1.0	1627	170
	Tatong (CHN)	28.3				250
	Taiheiyō (JPN)	37.1				220
[Kobayashi1977]					1273	>100
					1467	50
	Pittsburgh #8	41.6	37-44	0.1	1667	25
					1827	25
[Kobayashi1977]					1273	160
					1467	70
	Montana	41.9	37-44	0.1	1667	40
					1827	30
[Yeasmin1999]				0.1	1000	1000
		51.2	37-53	0.5	1000	1300
	Yallourn			1.0	1000	1500

Table 2.3: A direct comparison of the rates of heterogeneous reactions in char combustion or gasification taken from literature. The rates of each experimental study are normalised by the reaction rate of the char-CO₂ reaction.

	[Laurendeau1978] carbon	[Harris1991] pet coke brown		[Roberts2003] bit.	[Kajitani2002] bit. bit.	
Reactant	527°C 0.1 atm	800°C 0.2 atm		800°C 15 atm	1050°C 0.1 MPa	1400°C 0.5 MPa
O ₂	10 ⁵	0.9 · 10 ⁵	10 ⁴	5 · 10 ⁵	5000	
CO ₂	1	1	1	1	1	1
H ₂ O	3	0.2	2	3-15		10
H ₂	3 · 10 ⁻³					

the slowest step. Fundamental knowledge of the rates of these reactions is important to

- design gasification reactors,
- choose suitable fuels (coal and biomass) for gasification,
- develop mathematical models for gasification reactions, and
- implement high temperature gasification models in numerical simulation approaches.

After the heterogeneous gasification reactions, the devolatilisation process is the slowest reaction. However, devolatilisation is at least one magnitude faster than char gasification. The detailed description of devolatilisation certainly improves the prediction of the overall gasification rate, but is not required for the determination of the residence time for complete conversion in an entrained flow gasifier. The homogeneous reactions are much faster and the assumption of chemical equilibrium for these reactions (volatiles combustion, homogeneous gas reactions) is a good approximation when considering the whole gasification process.

2.1.5 Definition of Reaction Rate

The reaction rate of fuel gasification is described by several terms that have already been used in this chapter and will further be used. In the following these terms are summarised and are briefly explained:

Kinetics The term *kinetics* is an umbrella term for time dependent processes in science in engineering. Chemical kinetics is the study of the rates of a chemical reaction. In this dissertation, the term kinetics describes the time dependent conversion of solid fuels and covers all stages of gasification. If the term is further specified - for instance, kinetics of char conversion - the single reaction step is focused on. Per se, the term kinetics is not limited to a specific reaction mechanism or reaction regime and can be seen as an overall expression.

Reaction rate Similar to kinetics, reaction rate is a general term that is neither limited to a specific product/educt (e.g. fuel, char) nor to a reaction regime. Furthermore, the term *observed reaction rate* is also frequently used if the reaction regime is not specified.

Intrinsic If the term *intrinsic* is used, the reaction at the char surface is described. A limitation by mass transport (Regimes II and III) is not considered. As intrinsic reaction rates can only be observed under chemical control (Regime I conditions), the term *chemical reaction rate* is frequently used as a synonym.

Char reactivity is used as a material property of a char sample. However, it is not defined generally in quantitative terms. If two fuels are compared according their char reactivity, this can be done in all reaction regimes. If the term *intrinsic reactivity* is used only the char reactivity under Regime I conditions is considered.

In summary, the terms kinetics, reaction rate, and reactivity can be used when the reaction mechanism is not known and/or the reaction regime is not specified, i.e. if there is a combination of mass transport limitation and chemical reaction at the char surface. If only the reaction at the char surface is described, the terms *intrinsic* and *chemical* are used.

2.2 Experimental Methods for the Investigation of Solid Fuel Gasification

The gasification reactions of solid fuels are analysed in different experimental setups that operate under various conditions and are available on different scales. The functional principle, the advantages, but also limitations of several experimental setups are described in this section.

2.2.1 Flow Reactors

Flow reactors are the experimental facilities most relevant to industrial scale entrained flow gasifiers. Fuel particles are added to a gas stream and the reactions occur in the two-phase flow. The reaction zone is usually a tube that is heated. Prior to the particle addition, the gas flow can be preheated. Alternatively, gas and particles enter the reaction tube at ambient temperature and the heating occurs within the tube.

Depending on the ratio between gas and particle velocity, the reactors are referred to as drop-tube or entrained flow reactors. In drop-tube reactors the gas flow rate is slow and the particle velocity is influenced by gravity. Residence time is dependent on the vertical distance and the free fall velocity of the particles. Entrained flow reactors are operated at a higher gas flow rate and particles are entrained in the gas stream. The particle residence time is adjusted by the gas flow rate and the vertical distance from injection to particle sampling.

Most of the flow reactors are operated at ambient pressure, but there are also some

facilities that are designed for higher pressures. The operation temperature is usually very high and the reaction time is short as reaction conditions relevant to industrial scale entrained flow gasifiers are imitated. Most of the facilities that are described in literature are operated in a range from 900°C to 1400°C. The scale of the facility is mainly dependent on the length of the reaction tube and the experimental rigs are constructed from laboratory to pilot scale³.

The advantages of flow reactors are:

- Flow reactors can be operated at high temperature and high pressure and therefore enable conditions relevant to industrial scale facilities.
- Due to the injection of fuel particles into a hot gas stream, high heating rates are achieved that are similar to industrial scale gasifiers.
- The operation in a differential and integral mode is possible. In a differential mode the fuel flow rate is small compared to the gas flow rate and gas concentrations do not change along the reaction tube. In this configuration, the rates of single reactions (char-CO₂ or char-H₂O) are analysed. In the integral mode the fuel flow rate is larger and the gas concentrations are significantly influenced by fuel conversion. The integral mode is used to approach the change of gas atmosphere along the reaction pathway in a larger scale entrained flow gasifier. In an experimental flow reactor the integral mode is achieved by applying a defined stoichiometry between fuel and gas. These experiments are performed with a certain amount of oxygen in the gas flow. As devolatilisation, homogeneous and heterogeneous reactions occur simultaneously in the reaction zone, the gas concentrations continuously change. Therefore, the environment in a larger scale entrained flow reactor is imitated. By collecting char and gas samples after a defined residence time, reaction rates can be derived that are relevant to industrial gasifiers.
- The residence time can be adjusted in the range of milliseconds to seconds depending on the gas flow rate and vertical reaction length. The particle injection enables a defined start of reaction and the reaction is terminated by a fast quench in a sampling probe.

Disadvantages and limitations of flow reactors are:

- The initial thermal history of particles during heat-up is not known exactly and can only be derived by calculations. Heating rates given in literature range from 10⁴ K/s to 10⁶ K/s. When particles are injected into the hot reaction zone, the heat-up is dependent on the local flow profile and the thermal history is affected by turbulence and gas mixing. This limitation particularly influences devolatilisation experiments as the residence time is in the order of a few hundred milliseconds and the accurate particle temperature is required for the determination of devolatilisation kinetics. For the evaluation of gasification reactions, a high heating rate is required to simulate char properties relevant to industrial gasifiers. The exact knowledge of the thermal history during heat-up is not required.

³The term pilot scale describes installations that are between the laboratory or bench scale and the full industrial scale.

- The average gas residence time is adjusted by the gas flow rate and the vertical reaction length. However, the particle residence time may deviate due to the flow profile in the reaction tube, due to devolatilisation reactions that increase the amount of gas, and due to the free fall velocity of the particles. Despite the good adjustability of the gas residence time, an uncertainty of the particle residence time remains.
- Industrial operation conditions can only be applied in pressurised entrained flow reactors that are operated at high temperature and are equipped with a reaction tube that allows residence times in the seconds range. For the design and installation of these facilities a high construction effort and high investment costs are required. These reactors have to be built in the pilot-scale.
- At a larger scale the operation, revision, and inspection of flow reactors is time consuming. Small conceptual changes require a high expenditure in terms of time and personnel.

Despite their limitations, flow reactors - especially entrained flow reactors - are the only experimental facilities that can enable reaction conditions similar to industrial scale entrained flow gasifiers. For the evaluation of reaction rates at very high temperatures, especially under Regime II or III conditions, experimental data from entrained flow reactors are required.

2.2.2 Thermogravimetric Analysers

In entrained flow gasifiers, single particles are entrained in a gas stream and mass transport limitations occur in the char pore structure and boundary layer. In the absence of these limitations, i.e. at low temperature, thermogravimetric analysers are widely used for the measurement of gasification rates. Char is placed in a ceramic crucible or a metal mesh and is then put onto the sample holder. The sample holder is situated in an oven where a defined temperature can be adjusted. A defined gas atmosphere is feasible and experiments can be carried out in pure gases as well as in gas mixtures. If the weighing unit is enclosed in a pressure vessel, experiments above ambient pressure are feasible.

As the char particles form a fixed bed in the crucible or the mesh, the configuration is different from entrained flow gasifiers. The low experimental temperature of usually 700°C to 1000°C ensures that the intrinsic reactions at the char surface are slow compared with the diffusion in the fixed bed and within the pore structure of the char. The reaction rate in a thermogravimetric analyser is usually calculated by the weight change of the sample. Additionally, the monitoring of the gas atmosphere is possible and the reaction process can be analysed in more detail.

The advantages of thermogravimetric analysers (TGAs) are:

- TGAs can be operated at precisely defined conditions in terms of temperature, gas atmosphere, and pressure. A variation of operation conditions over wide ranges is possible.
- TGAs are commercially available for operation conditions required to analyse char gasification, i.e. temperatures of up to 1000°C and pressures of up to 10.0 MPa.

- Experiments are relatively easy to perform. It is possible to carry out several series of experiments in a limited time.
- No extraordinary expenditures in terms of time and personnel are required to modify the experimental facility or change spare parts.

But, thermogravimetric analysers have also disadvantages and limitations arise:

- Char gasification experiments in TGAs are limited to Regime I conditions. An increase in temperature would accelerate the chemical reaction and reactant gas would be consumed faster than it could be transported to the char surface by diffusion. A concentration gradient would develop within the fixed bed. As the diffusion paths within the fixed bed are much longer than within single particles, the concentration gradient will mainly occur in the fixed bed. As a result, there is a significant difference between the adjusted gas concentrations in the TGA and the true gas concentration at the particle surface. The fixed bed diffusion could be avoided by the use of fewer, but larger particles. In this case, the diffusion paths within the particles would increase and again an interaction of mass transport limitations and intrinsic reaction would occur. In both cases, kinetic data at high temperature is not derived under defined conditions.
- The particle size used in thermogravimetric analysers is usually larger than in entrained flow systems to avoid any removal of particles by the gas stream. The loss of particles during the experiments would be incorrectly interpreted as fuel conversion.
- The heating rate of TGAs is usually limited to 20-30 K/min. If the TGA is the only experimental facility, pyrolysis has to be carried out at a low heating rate to produce char. As the devolatilisation conditions influence char reactivity, the measurements from the TGA are not relevant to industrial scale applications where higher heating rates are achieved. To analyse char gasification in a TGA, a second experimental facility is required to produce char samples at higher heating rate.
To increase the heating rate in a TGA, a drop-in method can be applied in some systems. The fuel sample is attached to a chain and is lowered into the hot zone. With this configuration the fuel is heated to TGA temperature in a few seconds. However, the heating rate is still significantly lower than in entrained flow systems and the recondensation of volatiles on the char surface is likely as volatiles are released within a fuel fixed bed.
- TGAs are limited to the differential mode. The simultaneous occurrence of devolatilisation, homogeneous and heterogeneous reactions cannot be analysed.

TGAs allow measurements of char gasification under well defined conditions. But it is not possible to derive intrinsic gasification rates from TGA measurements that are not made under Regime I conditions and these measurements cannot be directly transferred to entrained flow conditions. The devolatilisation experiments can only be carried out at a low heating rate and their transferability to industrial scale gasifiers is doubtful.

2.2.3 Wire Mesh Reactors

Wire mesh reactors typically consist of a metal mesh that is clamped between two electrodes. The fuel sample is in the milligram range and is put on top of this mesh or between two mesh layers. The mesh area is small with an edge length of only a few centimetres. When applying a voltage between the electrodes, the mesh acts as a resistance heater and its temperature increases. The temperature of the mesh material is measured by a pyrometer or a thermocouple with a good contact to the mesh. Defined heating rates and temperature profiles are enabled by a feedback control system that calculates the electrode voltage by comparing mesh temperature to setpoint temperature.

The maximum heating rate depends on the control speed and the measurement delay of pyrometer or thermocouple. A typical heating rate that is reported in literature is 1000 K/s. The maximum temperature depends on the mesh material. Stainless steel meshes are mainly used that allow a maximum temperature of about 1000°C. Higher temperatures (~1600°C) are reported for molybdenum or noble metal meshes. The use of graphite strips instead of metal meshes enables temperatures above 2000°C.

If the electrodes are situated within a pressure vessel, experiments at increased pressure are feasible. The atmosphere around the mesh is adjustable and experiments are carried out in an inert atmosphere as well as in reactive atmospheres. The mesh can be purged by a constant gas flow that removes reaction products and ensures a defined gas atmosphere. The fuel conversion is measured by weighing the sample before and after the experiment or by monitoring the gas concentrations of products in the off-gas of the reactor.

The advantages of wire mesh reactors are:

- The experimental setup enables a high heating rate of the sample. Temperature and pressure are in the range of industrial scale systems. The gas atmosphere is very flexible and pyrolysis as well as gasification experiments are feasible.
- Wire mesh reactors are bench-scale rigs that have low investment costs. They are not commercially available, but the design and the assembly are possible in a limited time frame. The development of a very fast feedback control system is challenging, but feasible with state of the art hard and software.
- Due to the relatively simple setup, the change of the sample is fast and a large number of experiments can be done. If using stainless steel meshes which are relatively inexpensive, the operational costs of a wire mesh reactor are low.

Wire mesh reactors also have disadvantages and limitations:

- The minimum fuel particle size depends on the mesh width. If the particles are too small, they may get lost during the experiment and falsify the results in the weighing procedure. Stainless steel meshes are supplied in a very small mesh width, but alternative materials (e.g. molybdenum) with a mesh width <100 μm are usually not available on the market. On the other hand, if the mesh width is too small or gas tight metal/carbon sheets are used, the purge gas cannot pass through the sample. In this case, volatiles or product gases are not removed.
- The heating rate of the mesh is controlled. As there might not always be a good contact between the fuel sample and the mesh, the sample temperature can deviate

from the mesh temperature. The true heating rate of the sample can be lower than the setpoint heating rate of the mesh. Although high heating rates are achieved, these are still lower than in flow reactors where single particles can be injected into a hot gas stream.

Furthermore, an inhomogeneous temperature distribution across the mesh might occur, as there might be local differences in mesh electrical conductivity and the fuel sample might affect the local temperature.

- The sample weight in wire mesh reactors is very low (in the range of 5 mg to 20 mg). This enables a good contact of each fuel particle to the mesh and prevents the mutual interference of particles. However, the small sample size leads to a relatively high measurement error in the weighing procedure because small weighing errors are interpreted as fuel conversion.

Although some limitations exist, wire mesh reactors are an excellent tool to perform bench-scale experiments under operation conditions relevant to larger scale industrial gasifiers. The high heating rate and the pressurised operation enable the production of char that should be comparable to char from flow reactors and industrial facilities. When wire mesh reactors are operated with a reactive gas atmosphere, the overall fuel reaction can be studied. However, at higher temperatures mass transport limitations within the char particles might arise. As the particle size is typically larger than in entrained flow applications and as the gas flow field around the particles deviates, these reaction rates cannot simply be transferred to industrial scale conditions. As larger particles and lower temperatures are also used in fluidised bed applications, it should be possible to transfer wire mesh results directly to fluidised bed gasifiers.

2.2.4 Fluidised and Fixed Bed Reactors

Gasification reactions are also analysed in fluidised and fixed bed reactors. As the temporal resolution of these reactors is low, devolatilisation is usually not considered and only char gasification experiments are carried out.

In fluidised bed reactors a char sample is added to the hot bed material and the reaction rate is analysed by the measurement of product gas concentrations in the off-gas. The composition of the gas that is used for bed fluidisation is variable and the reaction rate can be analysed dependent on gas concentrations.

Fixed beds consist of only the char sample or a matrix of inert bed material and char. The reaction rate is also measured by gas analysis and the feed gas atmosphere is variable.

The maximum temperature is limited by the melting temperature of the bed material and the ash melting temperature of the fuel. Depending on the mineral composition of bed material and ash, the formation of eutectics is possible. This effect decreases further the operation temperature as agglomerations might occur. Both reactor types can be operated at pressure.

Advantages of fluidised and fixed bed reactors are:

- In fluidised bed reactors, a homogeneous temperature distribution exists. By the injection of fuel particles into the fluidised bed, relatively high heating rates can be

achieved. Char is then produced in-situ and char gasification reactions are observed by gas analysis.

- The reactors can be built in bench-scale which causes low expenditures in terms of personnel and investment costs.
- If the focus is on the analysis of reaction rates for larger scale fluidised or fixed bed reactors, the reaction conditions in the bench-scale rigs can be adjusted to match expected operation conditions in the larger scale. Temperature, pressure, gas flow rates, bed material, and fluidisation state can be chosen identical to the larger application.

Especially in terms of the analysis of reaction rates for entrained flow gasifiers, fluidised and fixed bed reactors have disadvantages and limitations:

- In both reactors, the required particle size is relatively large and rather in the millimetre range. Smaller particles are carried away by the gas flow and are removed from the reaction zone.
- In fluidised bed reactors, char can be generated at a high heating rate by the injection of fuel particles. As these particles have to be larger than in entrained flow applications, heat and mass transfer limitations are likely within the particles and the heating rate is slower and the temperature is initially lower in the particle centre.
- An interaction with the bed material is possible. The bed material can be catalytically active and can increase the reaction rate.
- Especially in fixed bed reactors, temperature and concentration gradients might occur. The gas concentration and temperature at the char surface is then dependent on the reactor configuration and operation conditions. The derivation of independent reaction rates is not possible.

Fluidised and fixed bed reactors are good tools to analyse gasification reactions for larger scale systems that use the same reactor type. As the boundary conditions are different in entrained flow gasifiers, fluidised and fixed bed reactors are not the best choices to analyse entrained flow reaction behaviour.

2.2.5 Laboratory Procedures for Fuel and Char Characterisation

The best method to quantify the reaction rate of char is the measurement of kinetic data under realistic entrained flow operation conditions, i.e. in an entrained flow reactor. However, gasification experiments in these facilities are limited. Data from entrained flow reactors are not easy to interpret as the operation conditions are not always defined and the reaction rate measured is affected by the interaction of surface reaction and diffusion. The data can be used for the development of a rather empirical kinetic model. However, the extrapolation of the data to operation conditions differing from the experimental ones (e.g. higher or lower temperature, variant pressure, different gas concentrations) can be very erroneous.

A mathematical description of the reaction behaviour should not only be based on an

empirical evaluation, but should rather be based on physical and chemical principles. For the development of a mechanistic gasification model and the understanding of reaction processes in more detail, the char properties and the changes of these properties during conversion need to be studied.

There are different methods to characterise char properties. Thermogravimetric analysis at low temperature can be used to assess char reactivity under defined reaction conditions. The porous structure of char can be characterised by its surface area and density.

2.2.5.1 Measurement of Standard Char Reactivity at Low Temperature

TGA experiments are performed at low temperature where the overall reaction rate is in chemical control and free from diffusion limitations. Usually, the rate of the intrinsic char reaction is measured by a variation of temperature, pressure, and gas atmosphere. In contrast to this procedure, the objective of a TGA experiment can also be the measurement of a *standard reaction rate* that can be used to compare different chars in terms of their reactivity applying only one experiment for each char. It is not the purpose of these experiments to derive kinetic data of a char sample by a variation of operation conditions. Several authors characterize the reactivity of chars at a temperature of 400°C to 500°C in air at atmospheric pressure (e.g. [Zhuo2000, Cai1996]). Others [Fermoso2009] use a self defined standard method at higher temperature with CO₂ and H₂O. A defined amount of char is placed in the TGA and the weight loss during oxidation is recorded. The rate of weight loss is used as a parameter to characterize char reactivity.

These TGA experiments enable defined operation conditions and the char reactivity can be compared quantitatively. The standard TGA measurements are used to evaluate the influences of char treatment conditions (temperature, pressure, etc.) on the reactivity. Furthermore, effects of fuel type and origin are analysed. However, it is unknown if the quantitative or even qualitative differences in char reactivity are still valid at the operation conditions of entrained flow reactors. As the TGA measurements at low temperature are easy to perform, they can help to understand the factors that influence conversion behaviour.

2.2.5.2 Characterisation of Chars by Specific Surface Area

Another method for the assessment of char reactivity is the measurement of the specific surface area. Reaction rates depend on the surface area available for reaction and are higher for higher-surface-area chars [Smith1994].

Pore sizes in chars are classified into three pore sizes ranges: micropores with radii less than 1 nm (10 Å), mesopores with radii from 1 nm to 20 nm, and macropores with a pore size larger than 20 nm. In coal chars most of the surface area is found in the micropores [Smith1994]. After devolatilisation, the surface area and particle porosity of char are larger compared with the parent fuel. This can be explained by [White1991]: the removal of molecules or volatile hydrocarbons from micropores and small mesopores; the creation of new pores during the restructuring process involved in devolatilisation; and the opening up of pores by oxidation that were previously blocked.

There are several definitions for surface area that are used for the characterisation of a

char:

Total surface area (TSA) The total internal and external surface of char is measured. Surface chemistry and structure are not evaluated.

Active surface area (ASA) The ASA measurement aims at the determination of active sites like edges and defects on the surface. Reactions are likely occurring at these defects. The ASA is most commonly measured by a low-temperature chemisorption method with oxygen [Smith1994]. However, it is not clear if the active sites at low temperature are also reactive during high temperature gasification.

Reactive surface area (RSA) A further approximation of the real gasification process is the measurement of RSA. Temperature-programmed desorption techniques are used that involve adsorption of oxygen followed by desorption of CO and CO₂. RSA is believed to access active sites that are also reactive at gasification conditions [Smith1994]. However, the sites on the char surface that are active during the high temperature reaction cannot be directly identified. Therefore, the RSA does not need to correlate to surface activity at higher temperature.

The definition and measurement of ASA and RSA need different experimental procedures. In principle, also the definition of further specific surface area parameters is possible.

Due to the uncertainties in the determination and interpretation of ASA and RSA, total surface areas are most widely measured and used for coal and char characterisation. Furthermore, the ratio ASA/TSA is often constant over a wide range of conversion, thus the TSA can be more conveniently used to analyse char behaviour [Feng2003b].

The measurement of specific surface area can be based on different methods. Of those, NMR spin-relaxation, mercury porosimetry, and helium pycnometry are measurement procedures that are seldom applied for the determination of char surface area. More information about these methods can be found elsewhere (e.g. [Smith1994]).

In contrast, gas adsorption measurements are frequently used to study surface properties. A char sample is placed in a gas tight cell and a vacuum is applied. When increasing the pressure in the cell, the temperature is held constant and the amount of gas that is taken up by the sample is measured. Gas molecules penetrate into the char structure and adsorb at the inner surface. The adsorbed gas volume is directly dependent on the surface availability. At lower pressure the gas molecules adsorb in smaller pores. By increasing the pressure, the adsorption occurs in continuously larger pores. From the resulting gas adsorption isotherm, the surface area and the pore size/volume distribution can be derived using mathematical methods.

Gas type, temperature, and analysis method are varied in gas adsorption measurements. Nitrogen adsorption is carried out at 77 K (the boiling point at atmospheric pressure). Due to the low temperature, and therefore the low mobility of the gas molecules, the small micropores of char cannot be readily accessed. Thus, nitrogen adsorption does not correctly characterise the total surface area of coal and char that are highly microporous [Smith1994]. Nitrogen isotherms are typically interpreted using the Brunauer-Emmett-Teller (BET) equation that assumes a monolayer of molecules onto the surface. Despite the uncertainties in the micropore range, the N₂-BET analysis is widely used for char characterisation. As N₂ adsorption preferentially occurs in the mesopores, some information about the mesopore structure is derived [Smith1994].

Carbon dioxide adsorption is usually measured at higher temperature (195 K to 298 K). Since the temperature is much higher than for nitrogen adsorption, and since the CO₂ molecule is slightly smaller, its mobility is higher compared to nitrogen. CO₂ can assess the micropore structure [Smith1994]. Hence, CO₂ is used to measure surface area and pore volume in the micropore range. Different theories have been developed that allow an analysis of adsorption isotherms. The most common procedures are based on the Dubinin-Radushkevich equation (DR) and the Density Functional Theory (DFT). In both procedures, the measured adsorption isotherm is compared with a theoretical model and the surface area is then a result of fitting experimental data and theory. The mathematical development of both theories can be found elsewhere (e.g. [Lowell2006]).

Smith et al. [Smith1994] summarised the literature on coal and char surface area measured by N₂ and CO₂ adsorption. The CO₂ surface area of coal is 20 to 200 times, of char 2 to 3 times larger than the corresponding N₂ surface area. White et al. [White1991] measured surface area of chars produced in a flat flame burner. They showed that most of the surface area is in micropores with radii less than 1.5 nm, while 85 % of the pore volume is contained in mesopores. During char formation, changes are more significant for N₂ surface areas than for CO₂ surface areas. This might be caused by the enlargement of the mesopore network due to the evaporation of volatiles. The changes in the micropore network are rather small.

Therefore, CO₂ adsorption should be used when the focus of the measurement is on the specific surface area of chars. N₂ adsorption is the best method to evaluate the pore volume.

Besides N₂ and CO₂, also other gases are used for surface area and pore size measurements. Jagiello et al. [Jagiello2004] measured adsorption isotherms of N₂, Ar, CO₂, and H₂ on activated carbons and analysed the data using the DFT method. They compared pore size distributions obtained from the adsorption experiments with each gas. Both results with N₂ (77 K) and Ar (77 K) agree with CO₂ adsorption at 273 K in the range of small micropores. If using H₂, the pore size range can be extended to lower diameters. However, this seems not to be required as char has mainly a microporous surface. Jagiello et al. [Jagiello2004] conclude that in this case the analysis can be performed at higher temperature (273 K), which enables a faster analysis and - more importantly - a greater confidence because the measured adsorption isotherms are in equilibrium at higher temperature.

2.2.5.3 Char Density Measurement

If char is converted under Regime II conditions, the reaction rate is partially determined by mass transport within the pore structure. A high char porosity can be an indicator of a low gas diffusion resistance and therefore a higher reactivity. Chars that have a low density are expected to have a high porosity. The definition and measurement of char density are not straightforward. Due to the porous structure of char and the small particle size, the definition of several densities is possible:

- Solid density
- Particle density

- Bulk density

Solid density is generally measured by helium pycnometry. The technique is described in the literature (e.g. [Shields1985]). A char sample of known weight is placed in a cell, vacuum is applied, and the cell is purged with helium. Then the helium pressure is increased to a fixed value above ambient. When the pressure is stable, a valve is opened and the cell is connected to an additional volume of known size. From the two volumes and the pressure decrease after opening, the volume of the sample can be calculated. As He atoms are small and hardly interact with the char surface, He penetrates into all pores of the char sample. Hence, the density measured is the density of the solid organic and mineral matrix. A good estimation for solid density is the density of graphite (2.27 g/cm³ [Fedoseev1986]). However, char samples are less dense than graphite [Smith1994].

Particle density includes the internal pore structure of the char. For highly porous char particles, the particle density is significantly lower than the solid density. The agglomeration of particles including inter and intra particle voids is characterised by bulk density. It is measured by filling up a sample cell of known volume and measuring the char mass. The bulk density is measured as weight per volume.

By assuming a constant bed porosity, the particle density can be determined from bulk density. The bed porosity is dependent on particle diameter, size distribution, particle shape, and roughness. Usually, a constant value of bed porosity is applied to calculate the particle density. White et al. [White1991] assumed a value of 0.45 for char particles produced in a flat flame burner at 1200°C. Ma [Ma2006] obtained bulk density data for a variety of coals and chars and found that a constant packing factor of 0.42 is adequate to describe the packing of particles in the size range 5 μm 200 μm .

As the relation between particle and bulk density seems to be almost constant, both densities are an indicator for particle porosity. Chars with a high porosity (low density) are expected to be reactive under Regime II conditions.

In summary, several experimental facilities (flow reactors, thermogravimetric analysers, wire mesh reactors, fluidised and fixed beds) can be used to approach char reactivity under entrained flow conditions. Furthermore, char properties that are measured in laboratory (standard reactivity, surface area, and density) can also be used as an indicator for char reactivity at higher temperatures.

Chapter 3

Literature Review about the Influence of Operation Parameters on Gasification Kinetics

The operation conditions of a gasification system influence the rates of solid fuel conversion. For a fuel of given type and given particle size distribution, the most important operation parameters are the reaction temperature, the particle heating rate, the operation pressure and the gas atmosphere within the gasifier. The pressure is roughly constant along the conversion path of the gasifier but is dependent on the gasification technology. The particle heating rate is dependent on the gasifier type and the feeding system. Temperature and gas atmosphere change during conversion. For a detailed understanding of the gasification mechanism, it is important to evaluate the influence of these parameters on the rate of conversion.

The best possible kinetic gasification model includes all parameters that possibly have an effect on fuel conversion and quantifies their specific influence. The influence of these parameters can be separated in two reaction steps:

- Devolatilisation: effect of thermal history (heating rate, peak temperature, time at temperature), pressure, and gas atmosphere on the amount and the properties of char,
- Char gasification: effect of thermal history, pressure (partial/total), gas concentrations (CO_2 , CO , H_2O , H_2), and progress in char conversion on the heterogeneous char reactions.

This short itemisation already lists an abundance of influencing factors. Separating the single parameters leads to around 20 factors that could be implemented in a kinetic model. The non-linear influence of most of the parameters increases the complexity. Therefore, simplifications and abstractions are required to develop usable kinetic gasification models. A good model should include the most significant influencing factors and should quantify the effects of these parameters on the gasification rate.

The following literature review summarises the effect of different parameters. Investigations that analyse the influence of one or more parameters on volatile yield, on char structure, and on the heterogeneous reaction rate are presented and the importance of these parameters is evaluated.

3.1 Volatile Yield and Char Properties after Devolatilisation

The process parameters during devolatilisation influence the volatile and char yield of a fuel particle, but also the composition of volatiles and the structure and reactivity of the remaining char. As volatiles are converted to the adequate equilibrium gas composition instantly at high temperature, the detailed composition of volatiles (tars and gases) is rather unimportant for the overall kinetic evaluation. However, the amount and structure of char are important parameters for the subsequent heterogeneous gasification reactions.

3.1.1 Effect of Thermal History on Volatile Yield and Char Properties

The thermal history of a fuel particle can be described in a simple way by heating rate, peak temperature, and time-at-temperature.

Effect of Thermal History on Volatile Yield Most of the experiments that measure volatile yield are not carried out under entrained flow conditions where volatiles can leave the particle surface and where the interaction with other particles is low. The recondensation of volatiles onto the char surface is not likely under entrained flow conditions. However, the recondensation is likely to occur in the standard test procedure for the proximate analysis because volatiles (especially tar compounds) remain in the vicinity of the char¹. The volatile matter content from the proximate analysis is expected to underestimate volatile yield under industrial scale conditions.

Several authors report on the effect of temperature on volatile yield. Cai et al. [Cai1996] analysed the volatile yield of five coals by rapid heating in a WMR. The reactor was operated with purge gas, and the recondensation of volatiles was prevented. For all coals the volatile yield increased slowly but steadily with temperature. Figure 3.1 shows the volatile yield of Pittsburgh No.8 bituminous coal in helium at a heating rate of 1000 K/s and under atmospheric pressure. The volatile yield achieved with the standard procedure is 41.7 %.

Kobayashi et al. [Kobayashi1977] measured the volatile yield after pyrolysis in an atmospheric laminar flow furnace operated with argon. For both a lignite and a bituminous coal (Pittsburgh No.8) the volatile yield increased significantly with temperature from about 30 wt% (daf) at 987°C and 20 ms to 63 wt% (daf) at 1827°C and 25 ms (Figure 3.2). The ASTM proximate volatile test resulted in a yield of 46 wt% for both coals.

The effect of peak temperature on the char yield of lignocellulosic fuels is summarised in a recent review paper [DiBlasi2009]. Although the particle sizes (mm to cm) and temperatures (<727°C) reviewed are far from entrained flow gasification, the trend of a decreasing char yield with increasing temperature can be observed in Figure 3.3. For the fast pyrolysis of biomass, char yields are 8 % to 28 % and for a slower pyrolysis 20 % to 40 %. Char is a product of both primary and secondary reactions, but the quantitative understanding of the char generation process of biomass is very limited [DiBlasi2009]. A volatile yield

¹In the standard procedure a fuel sample is heated to 900°C and held for several minutes in an inert gas atmosphere. Volatiles can adsorb on the char surface even at high temperature or condense when the char sample is cooled.

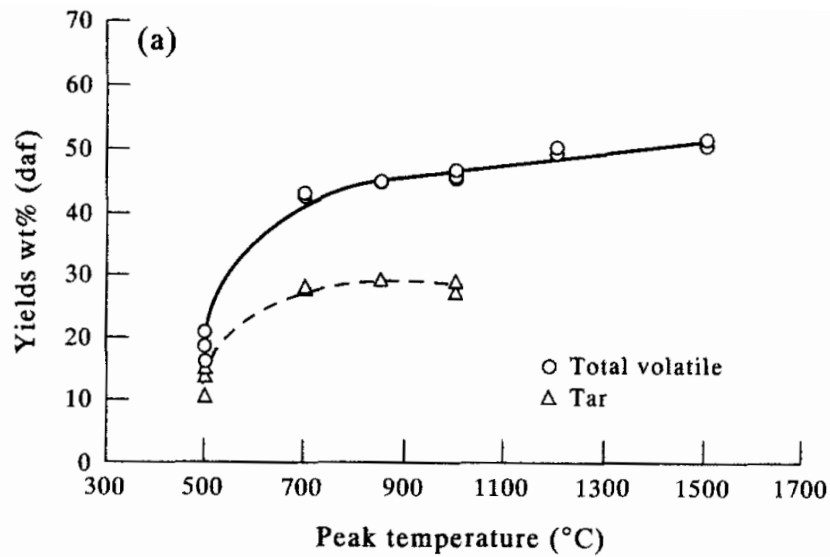


Figure 3.1: Volatile and tar yield of a bituminous coal (Pittsburgh No.8) in a WMR (heating rate 1000 K/s; helium atmosphere; atmospheric pressure; 2 s holding time) [Cai1996]

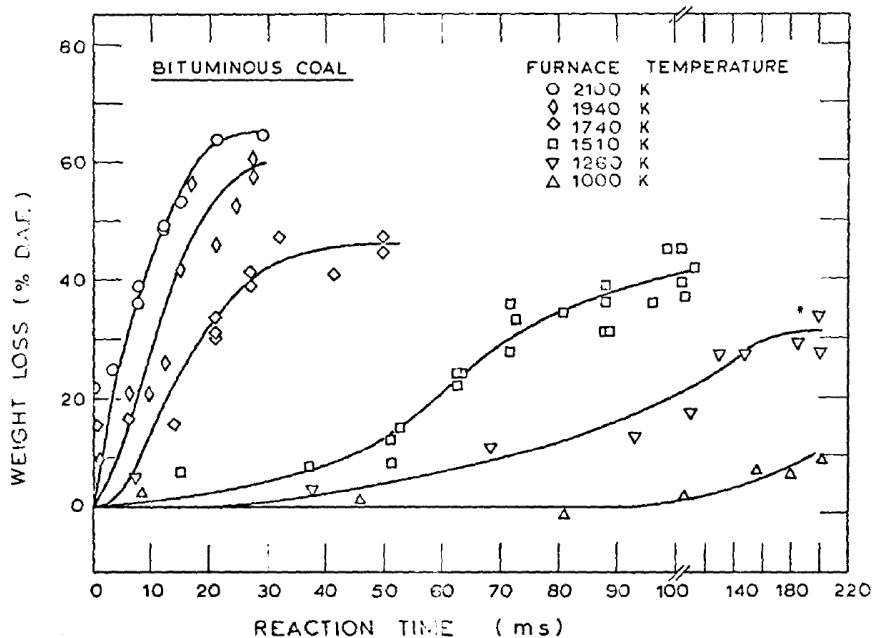


Figure 3.2: Volatile yield of Pittsburgh No.8 bituminous coal after pyrolysis in an atmospheric laminar flow reactor (heating rate 10,000 to 200,000 K/s; Argon atmosphere) [Kobayashi1977]

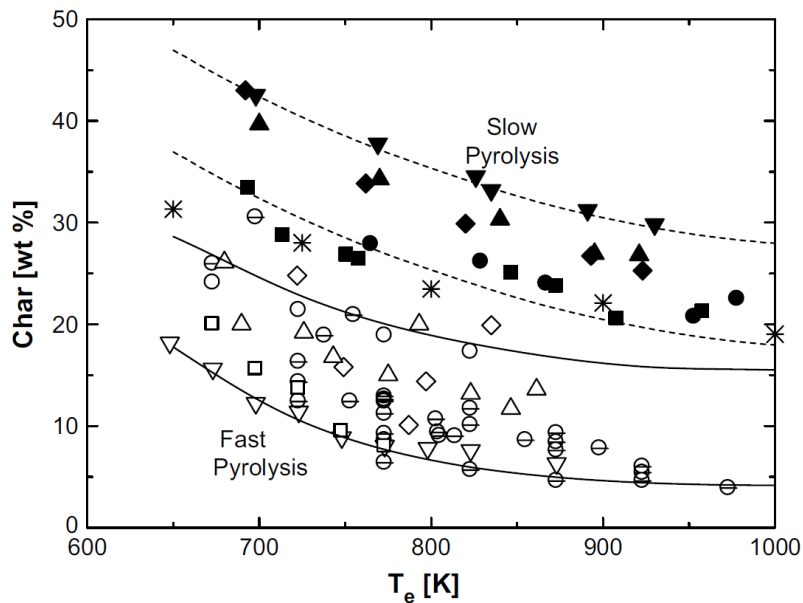


Figure 3.3: Char yield (wf) from fluidised bed pyrolysis of hardwood and softwood. Different symbols denote different authors. Slow pyrolysis (closed symbols) was achieved by using thick (40 mm) cylinders of wood. Data reviewed by [DiBlasi2009]

in excess of the standard proximate analysis and the trend of an increase in total volatile yield with peak temperature during devolatilisation are also confirmed by other authors (e.g. [Weeda1990, Hindmarsh1995, Yeasmin1999, Simone2009]).

In contrast, in one study [Brix2010] a decrease in volatile yield with increasing temperature was found. Brix et al. measured devolatilisation of El Cerrejon bituminous coal in an atmospheric entrained flow reactor. The volatile yield in CO_2 at higher temperatures (1300°C /1400°C) was slightly lower than at 1000°C to 1200°C. The authors assume that the drop is caused by a low residence time used for sampling at the highest temperatures. Furthermore, an ash evaporation effect might play a role because the volatile yield was calculated by an ash tracer method. The volatile yield at a temperature above 1000°C was always higher than in the standard proximate analysis.

The data so far are derived by experiments at high heating rates comparable to industrial entrained flow systems. But the effect of heating rate and the effect of peak temperature cannot always be analysed separately. Two studies try to analyse the effect of heating rate separately: Anthony et al. [Anthony1976] analysed experimental results from tube furnaces and wire mesh reactors and found that the total volatile yield increases around 11 % for a bituminous coal when the heating rate is increased from 1 K/s to 1000 K/s. Hindmarsh et al. [Hindmarsh1995] found an increase in volatile yield from 43.4 wt% to 53.3 wt% when increasing the heating rate in an atmospheric WMR from 2 K/s to 5000 K/s.

Yu et al. [Yu2007] reviewed the effect of heating rate on volatile yield. They propose that a high heating rate results in a more extensive thermal fragmentation of the molecular structure of coal and some of the fixed carbon is carried to the gas phase. Other possible reasons for the influence of heating rate that are considered in literature are similar: A higher volatile yield can be caused by fine char particles transported to the gas phase [Kimber1967]. At a higher heating rate also an increase in tar yield was measured

that indicates the presence of different reaction mechanisms depending on heating rate [Hindmarsh1995].

To quantify the increase in volatile yield, Yu et al. [Yu2007] define a factor Q that is the ratio of the yield of volatile matter during devolatilisation to the volatile matter content measured in the standard proximate analysis. Q is 1.3 to 1.5 for weakly swelling coals and 1.4 to above 1.8 for highly swelling coals in entrained flow applications. The effect is strongest for medium rank coals (bituminous coals). However, some experimental data in literature also show Q factors below 1 at high heating rates likely caused by incomplete pyrolysis [Yu2007].

In summary, the influence of temperature and heating rate is measured in some experimental studies, but devolatilisation reactions at high heating rate and high temperature are not understood completely. As the increase in volatile yield is dependent on the fuel properties and operation conditions, experimental data from facilities that enable high heating rates and high temperatures are required to describe variations of the volatile yield.

Effect of Thermal History on Char Structure and Reactivity An important factor after the devolatilisation is the reactivity of the remaining char. The temperature and the heating rate during devolatilisation also influence the conversion rate of the char produced. A high temperature during devolatilisation or the initial stages of char conversion can lead to a decrease in reactivity. In some experimental studies coals or chars were thermally treated using different temperature profiles and different peak temperatures were applied. This is typically done in an inert gas atmosphere to exclude the effects of char conversion. After the heat treatment, char reactivity is measured under low-temperature conditions that vary between the experimental studies. In most of the experimental studies, the reactivity in an oxygen containing atmosphere is measured at 400°C to 500°C in a TGA and is then related to the heat treatment severity of the char. The reactivity usually decreases with increasing peak temperature or time at temperature. This effect is described by the terms *thermal annealing* or *thermal deactivation*.

Zhuo et al. [Zhuo2000] produced chars from Daw mill bituminous coal at high heating rates and at a peak temperature of 1000°C in a wire mesh and a fluidised bed reactor. They analysed the reactivity of the char in an atmospheric TGA at a temperature of 500°C in air. The holding time at the peak temperature of 1000°C was a very important parameter. If a char was at high temperature for longer time scales, the reactivity decreased rapidly. Compared with the reactivity of char that was only heated up (0 s holding time), the reactivity may decrease to less than one third during the first 10 s at peak temperature. An atmospheric TGA for char reactivity measurements in air was also used by Cai et al. [Cai1996]. Chars from four different coals were prepared in a wire mesh reactor at a heating rate of 1000 K/s and a holding time of 2 s in helium. The TGA reactivity was found to significantly decrease with increasing pyrolysis temperature. The char reactivity after a heat treatment at 1500°C was up to 50 times lower than after a treatment at 700°C. The data is in agreement with data of Hindmarsh et al. [Hindmarsh1995] who reported a decrease in reactivity by a factor of 20 when increasing the peak temperature in wire mesh

experiments from 700°C to 1500°C (heating rate 1000 K/s, atmospheric pressure). In a similar study, Beeley et al. [Beeley1996] measured a decline of char reactivity by a factor of 30 to 50 between 1000°C and 1800°C in only 2 s of heat treatment in a wire mesh reactor. Structural characterisation by high-resolution transmission electron microscopy (HRTEM) proved that an increase in crystalline order occurred with increasing heat treatment temperature.

An even more significant loss of reactivity is reported by Shim et al. [Shim2000]. Chars were first prepared from different coals at 700°C (1h in He). Then a char sample was placed between two thin graphite sheets that are held at the ends by brass electrodes - a setup similar to a wire mesh reactor. After the heat treatment, the reactivity of the chars was measured by non-isothermal thermogravimetric analysis (7°C/min to 950°C in air). The heat treatment caused an enormous loss of reactivity. For example, Beulah lignite showed a loss of 4.5 orders of magnitude between 700°C and 2500°C. A general observation was that chars that initially have a high reactivity show a higher propensity for annealing, although there were exceptions to this trend. In a set of experiments the residence time was varied and also the reactivity of chars derived from a flame-supported entrained flow reactor (high heating rate, residence time approx. 10 ms) was measured. Although annealing was observed to be a strictly time dependent phenomenon, the reactivity was much more sensitive to peak temperature than to residence time [Shim2000]. In agreement with the earlier study of Beeley et al. [Beeley1996], a higher degree of structural ordering was observed by HRTEM after annealing.

Fermoso et al. [Fermoso2009] prepared wood char in an atmospheric drop tube furnace in an O₂/N₂ atmosphere at 1000°C and 1400°C. The char reactivity was measured in a PTGA in CO₂ at 0.1 MPa and 1.0 MPa. The char produced at 1400°C was found to be less reactive than the 1000°C char. The activation energy for the C-CO₂ reaction was also found to be dependent on pyrolysis temperature.

A meaningful set of experimental data about time dependent annealing is presented by Feng et al. [Feng2003]. The loss of reactivity in an entrained flow reactor during pyrolysis was measured. The data set of Cerrejon coal is shown in Figure 3.4. The reactivity of char that was collected at a defined residence time was analysed in a non-isothermal TGA procedure (20°C/min, air). The reactivity was compared with a reference char that was pyrolysed at 700°C for 1 s. The diagram shows the combined effects of temperature and residence time on thermal annealing. Char reactivity decreases initially fast and slowly afterwards. The reactivity at a long residence time decreased to one tenth from 700°C to 1475°C.

Senneca, Salatino and co-workers [Senneca1997, Salatino1999] used a slightly different experimental approach to study the combined effects of temperature and time on the thermal deactivation of chars. Char samples were prepared from a bituminous coal by the combined use of thermogravimetric analysers (slow heating rate, medium temperature) and a heated-strip reactor (high heating rate, high temperature). The common metal mesh in a wire mesh reactor was replaced by a pyrolytic carbon strip that was thermally stabilised and was used at up to 2000°C. Due to the closed strip, volatiles could not be removed by a gas flow and a potential influence of secondary volatiles reactions (recondensation/adsorption) could not be omitted. However, with both experimental setups a

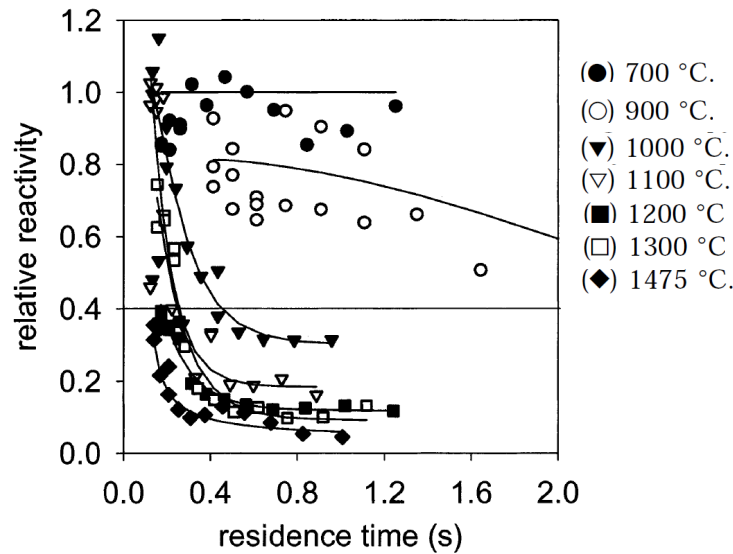


Figure 3.4: Reactivity of Cerrejon coal char after pyrolysis in an entrained flow reactor at the Technical University of Denmark [Feng2003]

wide range of time-temperature histories could be applied, ranging from 900°C to 2000°C and from 0.2 s to 300 min. To focus on the gasification reactivity, the reaction rate of the char after the heat treatment was measured in CO₂ at 900°C to 1200°C in an atmospheric TGA. The higher temperatures might be too high to exclude mass transport limitations in the TGA and the reaction rate measured could be lower than the intrinsic reactivity under Regime I conditions. However, the data set of Salatino et al. [Salatino1999] is the only one known that systematically analyses the effects of thermal annealing on gasification reactivity in CO₂. When the reactivity data were fitted to an Arrhenius type rate equation, annealing significantly affected the pre-exponential factor, but the apparent activation energy turned out to be only barely dependent on the time-temperature history of the coal sample. Salatino et al. [Salatino1999] then used a kinetic model to describe the effects of pyrolysis temperature and heating time and achieved a good correlation with experimental data. The model is described later in Section 4.2.5.

In a later publication Senneca et al. [Senneca2007] measured the weight loss of a char sample in an oxygen containing atmosphere, compared it with CO and CO₂ gas concentrations in the off gas, and measured a discrepancy in reaction rate calculated from both measurements. As the weight loss was lower in the initial stages of reaction, they assumed oxygen adsorption to be the reason and could then correlate the weight data and gas analysis well. Chars that were prepared under severe heat treatment conditions (>1400°C) from a South African bituminous coal showed negligible oxygen uptake compared with low-temperature chars. As the oxygen uptake is likely to occur at active sites that are reduced at high temperature, Senneca et al. established a close correlation between extent and accessibility of active sites and the combustion reactivity. Active sites that adsorb oxygen at low temperature are likely also involved in the char conversion at higher temperature.

Besides the peak temperature, also the heating rate is an important parameter for the char reactivity. Several authors report on the increase in reactivity of char when pyrolysed at

higher heating rate [Hindmarsh1995, Cai1996, Zhuo2000, Matsumoto2009, Simone2009, DiBlasi2009]. Zhuo et al. [Zhuo2000] varied the heating rate in a wire mesh reactor during pyrolysis of Daw Mill bituminous coal and then measured the combustion reactivity at 500°C in a TGA. The results are shown in Figure 3.5. For a short time at temperature (only heat-up, 0 s holding time) the reactivity significantly increases with increasing heating rate. For longer holding times (>10 s) the effect of heating rate diminishes. Similar analyses were performed earlier at Imperial College [Cai1996]. For rapidly heated chars in a wire mesh reactor, the combustion reactivity (TGA, air, 500°C) was found to increase with increasing heating rates up to 1000 K/s. At higher heating rates up to 5000 K/s the effect levelled off. The measurements are in agreement with wire mesh experiments of Hindmarsh et al. [Hindmarsh1995]. They measured an increase in combustion reactivity (TGA, air, 500°C) by a factor of 4 when increasing the heating rate from 2 K/s to 5000 K/s. Most of the increase in reactivity occurred from 2 K/s to 50 K/s and the effect levelled off between 1000 K/s and 5000 K/s. These results suggest that it may not be required to achieve higher heating rates than 1000 K/s in order to measure realistic values for char reactivity. The data indicate that a heating rate of 1000 K/s to the final temperature is suitable to imitate entrained flow conditions.

In summary, some data sets exist that analyse the effects of heating rate, peak temperature, and time at temperature. But, in an experimental setup it is not possible to separate these three influencing factors. When a fuel sample is heated slowly, the overall time at temperature is longer than at a high heating rate. Therefore, the effects of heating rate can partially be influenced and overlaid by effects of a prolonged time at temperature. The decrease in char reactivity with time that is reported in literature also leads to a decrease in reactivity at low heating rates.

The general trend in the literature data is a decrease in reactivity with increasing heat treatment severity. However, exceptions to this general claim have been reported. In some studies annealed chars show a maximum in reactivity in a curve of oxidation rate as a function of pyrolysis temperature [Suuberg1991].

However, in the majority of the experimental studies, the loss of reactivity with increasing pyrolysis temperature and time at temperature, and the increase in reactivity with increasing heating rate are observed. The reasons for the deactivation or activation are on the microscopic level and are connected to char structure and surface activity. With higher temperature either the specific surface area or the concentration of active sites per specific surface area (intrinsic reactivity) decreases. These two effects cannot be separated in TGA standard reactivity measurements. Additionally, specific surface area measurements are required. Kinoshita [Kinoshita1988] reviewed the variation of surface area of different types of carbons with heat treatment temperature. Data of BET surfaces are shown in Figure 3.6. Some carbons first show a maximum in surface area at around 1000°C. But the general trend is a decrease in surface area at higher temperature.

Roberts and Harris [Roberts2003] have shown that rapid heating affects primarily the structure and surface area of the char, and the intrinsic reactivity of the char is less affected. They produced char at high heating rate in a pressurised entrained flow reactor (PEFR) and at low heating rate (10 K/min) in a horizontal tube furnace (HTF). Both reactors were operated at 1100°C. The reactivity was measured in a PTGA in CO₂, H₂O,

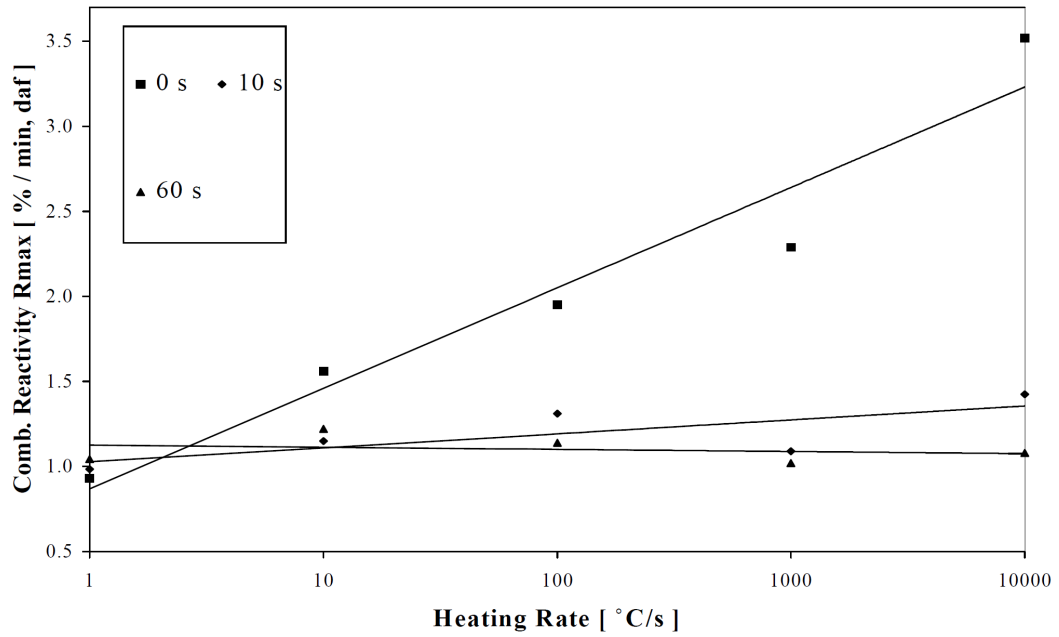


Figure 3.5: Effect of heating rate and time at 1000°C final temperature (WMR, helium atmosphere, atmospheric pressure) on the combustion reactivity (measured in a TGA in air at 500°C) of Daw Mill bituminous coal char [Zhuo2000]

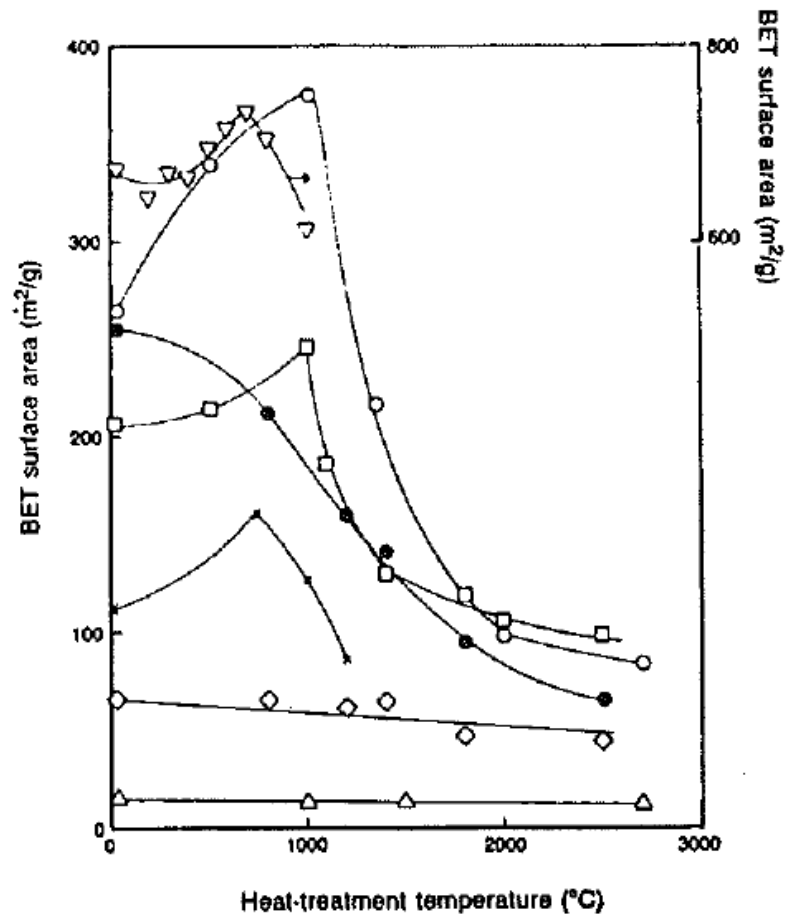


Figure 3.6: Variation of the BET surface area of different carbon blacks with heat treatment temperature [Kinoshita1988]

and O₂ atmospheres. The measured reaction rates of the PEFR chars (high heating rate, residence time not indicated) were almost 30 times higher than those for the HTF chars (low heating rate, 3 h holding time). After a normalisation with micropore surface area (CO₂-DR) the intrinsic reaction rates differed by less than a factor of 2. The data indicate that the main contributing factor to the large difference in measured reaction rate is the difference in surface area, but also intrinsic reactivity declines. At higher heating rate surface area significantly increases. The observations are in agreement with data from Cai et al. [Cai1996]. They prepared char at various heating rates in a wire mesh reactor and observed a higher porosity (micro and mesopores) and a higher surface area with increasing heating rate. Both resulted in higher reactivities in the TGA experiments.

The loss of specific surface area is found to be one reason for the decrease in reactivity. The causes for the loss of reactivity at high temperature or long time at temperature are discussed in literature and further possible explanations are:

- A massive loss of active sites with increasing temperature [Suuberg1991]. This might be due to the desorption of functional groups or the loss of hydrogen and oxygen atoms [Cai1996].
- Ordering of the carbon structure (graphitisation) at high temperature [Suuberg1991, Cai1996, Russell1999, Liu2000], indicated in Figure 3.7
- Loss, changes in the nature, and changes in the distribution of catalytically active mineral matter at high temperature [Weeda1990, Suuberg1991]
- Annealing process without a mechanistic explanation [Liu2000, Zhuo2000]

So far, only the chemical reactivity of the char surface and the surface area available in the absence of mass transport limitations are considered. The structure and pore size of char do not influence the reactivity under Regime I conditions. But under entrained flow conditions, i.e. in Regime II, the conversion rate is also influenced by pore diffusion, and char structure and pore size are important factors. Only a few studies are known that analyse the influence of thermal history on the char structure.

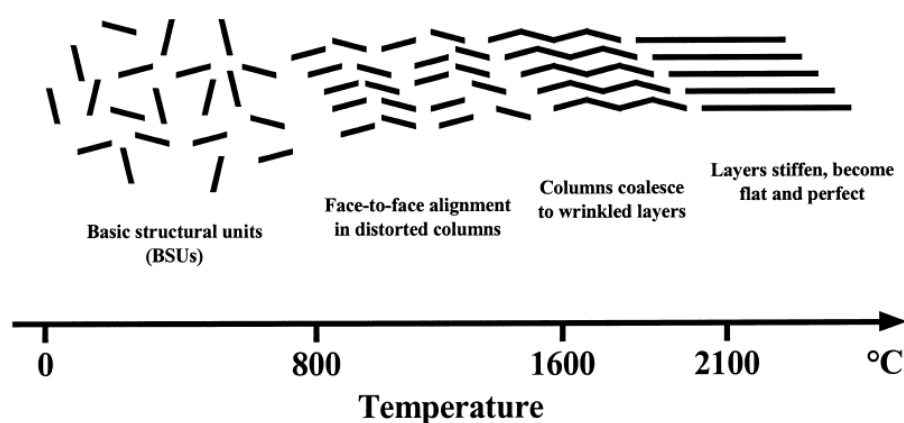


Figure 3.7: The four stages of texture improvement leading to crystalline order within chars [Russell1999]. Texture is not only a function of temperature, but also of time at temperature.

Alonso et al. [Alonso2001b] observed an enhanced porosity when chars were produced at 1300°C compared to 1000°C in a flat flame burner. There were only small differences between the 1000°C and 1300°C chars for two high volatile coals, but the 1300°C char of a low volatile coal was characterised by the presence of extremely thin walls that surround elongated pores. In a second study they extended the number of coals [Alonso2001c]. They conclude that the pyrolysis behaviour of the 10 coals used is rather complex and difficult to systematise. Optical microscopy images showed that some coals increased their porosity at 1300°C but for most of the coals there is no significant difference in structure. Alonso et al. [Alonso2001c] also measured CO₂-DR surface area of the 1000°C and 1300°C chars. 4 out of 10 coals decreased their surface area from 1000°C to 1300°C. The reduction could only partially be described by the plastic properties of the coals during heat-up. The formation of a very fluid metaplast at higher temperature could lead to the annihilation of the microporous structure, thus lowering surface area. As also coals with no plastic properties showed lower surface area at 1300°C, the authors supposed a different mechanism.

Rosenberg et al. [Rosenberg1996] compared the morphology of char sampled from various laboratory-scale reactors (drop-tube furnace, entrained flow reactor, muffle furnace) and from a full-scale pulverised combustion boiler. The temperature ranged from 800°C to 1500°C. The low-temperature chars of a Colombian coal were richer in the thin-walled morphotypes with high porosity, while the high-temperature chars were dominated by thicker-walled types with small bubbles. The chars produced in the muffle furnace were significantly different from all other chars as they were richer in dense char types and were more like coke than combustion chars. In general, chars that were produced in high temperature laboratory scale flow reactors showed high similarity to those found in the flame zone of a pulverised coal combustion boiler. The results of Rosenberg et al. [Rosenberg1996] suggest that a threshold temperature of ~1300°C is required to produce chars in flow reactors that are comparable with full-scale boiler chars. The morphology of chars produced at ~1150°C or lower is significantly different.

The results from the two research teams are contradictory, as higher porosity is measured at higher temperature [Alonso2001b, Alonso2001c] and at lower temperature [Rosenberg1996], respectively. Both studies show that it is difficult to measure the effect of temperature on char structure and that there is no clear trend.

Yu et al. [Yu2007] reviewed the structure of chars during devolatilisation. During heat-up, two physical coal properties are important: viscosity and coal pore structure. Both govern the rate of mass transport during pyrolysis and further determine the volatile yield and resulting char structure. The char structure evaluation is illustrated by the metaplast theory that assumes a two-step mechanism for the thermal decomposition of coal upon heating. In the first step the coal particle is transformed to a metaplast state. The thermoplastic properties of the metaplast are complicated functions of coal properties (e.g. rank and petrographic compositions) as well as pyrolysis conditions. Some coals develop significant fluidity and may behave like a Newtonian fluid. During this plastic state cross-linking reactions occur that determine the structure of the resulting char. Heating rate and temperature have a crucial impact on the coal fluidity during the metaplast stage and therefore also on the char structure. At an increased temperature the char morphology

changes to structures with larger central pores and network voids, and the microporosity of the char decreases [Yu2007]. Char preparation at high heating rates leads to a higher porosity (micro and mesopores) and higher internal surface area, resulting in higher reactivities [Cai1996].

Although there are several experimental studies, the effect of thermal history on char structure is not understood. Impacts are strongly fuel dependent. A complex interaction of temperature, heating rate and fuel petrography is expected. Similarly, the microscopic processes during annealing are not understood completely and are probably strongly dependent on the parent fuel. Therefore, it is currently only possible to assess char structure evolution and thermal deactivation of a fuel on the basis of experimental data.

3.1.2 Effect of Pressure on Volatile Yield and Char Properties

In contrast to pulverised coal combustion boilers, entrained flow gasifiers are usually operated at an increased pressure. Hence, it is important to evaluate the influence of pressure during devolatilisation.

Effect of Pressure on Volatile Yield The effect of total pressure on volatile yield during devolatilisation is analysed in several investigations and with different experimental setups [Cai1993, Sun1997, Lim1997, Ouyang1998, Yeasmin1999, Zhuo2000, Manton2004] and there are older and recent reviews available [Anthony1976, Wall2002, Yu2007]. All references report on a decrease in volatile yield with increasing pressure.

Exemplary, some of the data on the effect of pressure on volatile yield are summarised in Figure 3.8, and references and operation conditions are given in Table 3.1. Messenböck et al. [Messenboeck1999] measured the volatile yield of Daw Mill bituminous coal as a function of pressure in a wire mesh reactor. They observed a continuous decrease in volatile yield with increasing pressure from 0.1 MPa to 3.0 MPa. The holding time had no significant effect on the data.

Yeasmin et al. [Yeasmin1999] varied the operation pressure during entrained flow experiments from 0.1 MPa to 1.0 MPa at a temperature of 600°C, 800°C, and 1000°C in a nitrogen atmosphere. At a residence time of about 1 s and at 1000°C the volatile yield of Victorian brown coal was reduced from 80 wt% at atmospheric pressure to 70 wt% at 1.0 MPa. Suuberg et al. [Suuberg1978, Suuberg1979] pyrolysed a lignite and a bituminous coal in a pressurised wire mesh reactor. The pressure was varied up to 6.9 MPa in a helium atmosphere at variable heating rates and at a peak temperature of up to 1100°C. The pressure had little effect on the volatile yield of the lignite. In contrast, for the bituminous coal the increase in pressure resulted in more char, possibly due to the occurrence of secondary tar reactions.

The influence of pressure on volatile yield and mechanistic explanations are summarised in a recent review [Wall2002]:

- With increasing pressure tar is repolymerised and cracked more significantly, resulting in increased yields of char and light gases.

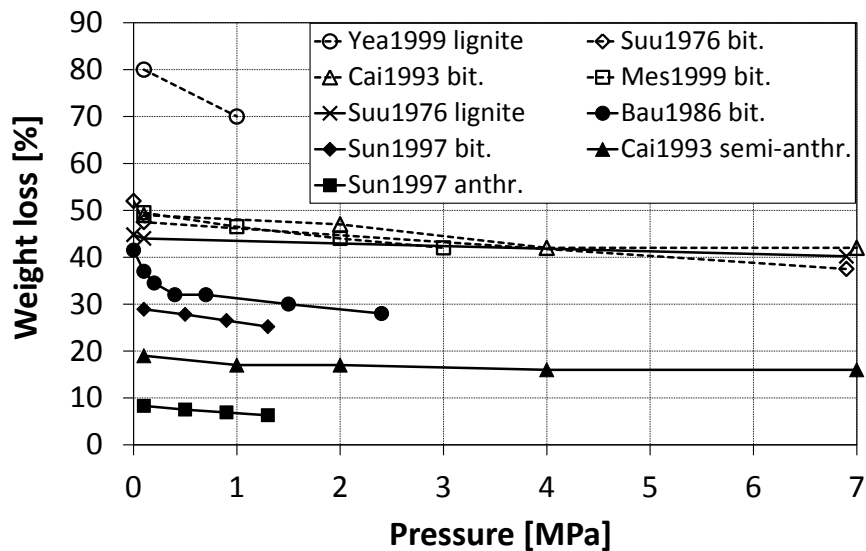


Figure 3.8: Summary of literature data about the effect of pressure on the weight loss (=volatile yield) of different solid fuels

Table 3.1: Database for the determination of volatile yield as a function of pressure

Reference	Reactor	Heating rate [K/s]	T_{max} [°C]	Gas
Sun1997 [Sun1997]	TGA	0.3	900	N ₂
Cai1993 [Cai1993]	WMR	1000	700	He
Mes1999 [Messenboeck1999]	WMR	1000	1000	He
Bau1986 [Bautista1986]	WMR	1000	750	He
Yea1999 [Yeasmin1999]	EFR		1000	N ₂
Suu1976 [Suuberg1978]	WMR	1000	1000	He

- The reduction of total volatile yield appears to be most significant for bituminous coals, but less pronounced for lignites.
- The pressure effect is more pronounced at higher temperatures.
- The effect of pressure levels off at high pressures.

As the pressure effect is dependent on the parent fuel and the pressure range, no general quantitative description is possible. In the data in Figure 3.8, the volatile yield is reduced by 0.3 wt% to 11 wt% per MPa. At low pressure the gradient is generally more pronounced.

Effect of Pressure on Char Reactivity and Morphology The operation pressure during devolatilisation affects char structure and reactivity, but there is disagreement in the open literature on the mechanistic explanation and quantification of the pressure influence. Whereas many authors [Sha1990, Messenboeck2000, Zhuo2000, Cetin2005, Zeng2005] report a decrease in observed reactivity with increasing pyrolysis pressure, also an increase in reactivity is found in some references [Benfell2000, Roberts2003]. Lim et al. [Lim1997] reported no effect of pyrolysis pressure on char combustion reactivity in the range 0.1 MPa to 3 MPa.

Some authors measured specific surface areas of their chars and related the pressure effect

to the intrinsic reactivity. In the following, some literature data are collected and the main findings are summarised in Table 3.2.

Cetin et al. [Cetin2005] analysed the effect of pyrolysis pressure (PWMP, 0.1 MPa to 2.0 MPa) on the CO₂ gasification of biomass (radiata pine) in a TGA at 850°C. The mass specific observed reaction rate decreased by a factor of about 3 from 0.1 MPa to 2.0 MPa pyrolysis pressure. The specific surface area of the chars after pyrolysis was determined by CO₂ adsorption (Dubinin-Radushkevich-Kaganer(DRK)-method). There was only a 10 % difference between the 0.1 MPa and the 2.0 MPa chars that could not explain the large difference in observed reactivity. The authors conclude that the pyrolysis pressure has an effect on the intrinsic reactivity of chars. Additionally, the graphitisation of chars was measured by XRD analysis. After a normalisation of the observed reactivity by specific surface area and a graphitisation factor, the pressure effect diminished. Therefore, the loss of reactivity with increasing pyrolysis pressure was attributed to an enhanced graphitisation at higher pressures.

Sha et al. [Sha1990] observed that the reactivities of coal chars obtained by pyrolysis at elevated pressure tend to decrease with increasing pressure. They prepared char from a Chinese lignite in a tube furnace at 900°C in N₂ and measured the gasification rate in CO₂ and H₂O in a PTGA at up to 900°C. A change in pore structure with increasing pyrolysis pressure was assumed to be the reason for the decrease in reactivity at higher pressure.

Other references report no influence of the pyrolysis pressure on the intrinsic reactivity. Benfell et al. [Benfell2000] investigated the effect of pyrolysis pressure on the combustion reactivity of two Eastern Australian coals. Chars were produced in a drop tube reactor (1300°C) at 0.5 MPa, 1.0 MPa, and 1.5 MPa. The reactivity was measured in a PTGA at 1.5 MPa in a 50%/50% O₂/N₂ atmosphere at 375°C. The char surface area after pyrolysis was measured by CO₂ adsorption (DR method). At higher pressure more char with a cenospherical structure is generated. However, only a few char samples showed an increase in observed reactivity with pyrolysis pressure and the overall trend was not consistent. Normalisation of the observed reactivity by the specific surface area resulted in no systematic effect of the pyrolysis pressure on intrinsic reactivity.

Roberts et al. [Roberts2003] prepared chars from three different coals in the Pressurised Entrained Flow Reactor (PEFR) at 1100°C and at 0.5 MPa, 1.0 MPa, and 1.5 MPa. Reaction rates in CO₂, H₂O, and O₂ were measured in a PTGA. Chars from two coals generally showed an increase in reactivity with increasing pyrolysis pressure in CO₂ and H₂O. One coal char tended to have decreasing reaction rates with increasing pyrolysis pressure. In an O₂ atmosphere the effects were less obvious. However, after a normalisation of the rates with surface area (CO₂-DR) the data showed little variation with pyrolysis pressure. The intrinsic reactivity was not considerably affected by the pyrolysis pressure. The authors conclude that the pyrolysis pressure affects the microporosity of chars, but there is little indication that the chemical properties of the char surface are dependent on pyrolysis pressure.

Zeng et al. [Zeng2005] produced Pittsburgh No. 8 bituminous coal chars in a pressurised flat flame burner at 1300°C and from 0.1 MPa to 1.5 MPa. The combustion reactivity was measured in a PTGA at the respective char preparation pressure and at an oxygen partial pressure of 0.032 MPa. Specific char surface area was measured by the N₂-BET method.

The mass specific observed reaction rate decreased with increasing pyrolysis pressure, but the intrinsic reactivity remained almost constant independently of pyrolysis pressure. In conclusion, the influences of pressure on the char reactivity during devolatilisation are not clear and they seem to be dependent on the parent fuel and on the specific operation conditions. Most of the studies that are found in literature agree that the intrinsic reactivity is not affected by devolatilisation pressure. The pressure has only an effect on char structure and surface area. When an influence of pyrolysis pressure on observed reaction rate in a TGA is reported, the variation is about a factor of 1.5 to 1.8 in the pressure range from 0.1 MPa to 3 MPa [Messenboeck2000, Zhuo2000], and therefore much less than the effects of temperature, heating rate, and time at temperature.




The influences of devolatilisation pressure on char structure and morphology are reported

Table 3.2: Literature review on the effect of pyrolysis pressure on observed char reactivity, surface area, and intrinsic reactivity

		Fuel type or C content (wt % daf)	Effect of pyrolysis pressure (↑) on		
			Observed reactivity	Surface area	Intrinsic reactivity
Cetin et al.	[Cetin2005]	biomass	↓	→	↓
Sha et al.	[Sha1990]	lignite	↓		
Benfell et al.	[Benfell2000]	76.0	→	→	→
		82.0	→	→	→
Roberts et al.	[Roberts2003]	82.0	↓	↓	→
		82.9	↑	↑	→
		76.0	↑	↑	→
Zeng et al.	[Zeng2005]	Pittsburgh No.8	↓	↓	→

in a systematic analysis of the University of Newcastle and CSIRO [Bailey1990, Liu1999, Wu2000, Benfell2000, Liu2000b, Yu2007]. Chars are classified into three groups that are shown in Figure 3.9. The classification relies on image processing techniques and structural parameters (wall thickness, shape, diameter, porosity) are required. The formation of different types of char structures is associated with the thermoplastic behaviour during devolatilisation [Yu2007]. During heat-up, solid fuels first form a metaplast and then char structure is generated in a second step. The effects of temperature and heating rate within this metaplast state have already been discussed. Devolatilisation pressure has also an influence and determines the char structure to some extent. Wu et al. [Wu2000] generated char from an Australian bituminous coal in two drop tube furnaces at a temperature of 1300°C and pressures from 0.1 MPa to 1.5 MPa. The char particle size increased with system pressure which is shown by the particle swelling ratio that was 1.1 at 0.1 MPa and continuously increased to 1.6 at 1.5 MPa. At high pressure the majority of the particles were classified into Group I as they had large internal voids and thin walls. Char generated at higher pressures had also a higher internal and surface porosity.

The general trend of the formation of highly porous chars at high devolatilisation pressure is confirmed by other research groups [Khan1986, Lee1991, Matsuoka2005]. Lee et al. [Lee1991] observed a maximum in swelling. They studied the pyrolysis behaviour of a

	Group I	Group II	Group III
Two-dimensional schematic representation			
Porosity (%)	>65%	Variable, 40%–60%	<40%
Wall thickness (μm)	<5	>5	>5
Shape	Spherical-sub spherical	Subspherical	Angular
Typical swelling ratio	>1.3	<1.0	<0.9
Typical residual mass ratio	0.1 ~ 0.5	0.1 ~ 0.5	1.0

Note: Residual char masses, compared to group III, are also presented (from subbituminous to medium volatile bituminous coals combusted at 1 atm).

Figure 3.9: Char classification system, including typical swelling ratios relative to the average particle diameter of the parent fuel [Benfell2000]

bituminous coal in entrained flow furnaces at pressures from 0.1 MPa to 3.8 MPa. At low pressure insignificant swelling occurred. At 0.8 MPa the swelling was most extensive and large blow holes were observed on the particle surface. A further increase in pressure reduced the swelling ratio.

Due to the interactions of fuel petrography, fluidity and devolatilisation pressure, particle swelling properties cannot be derived from fuel properties. Also swelling behaviour at elevated pressure could not be predicted from data taken at atmospheric pressure [Khan1986, Lee1991].

Matsuoka et al. [Matsuoka2005] measured reactivities of porous and dense chars in a TGA at 900°C in a CO₂ atmosphere. Chars were produced from a Shenmu coal that showed no swelling at atmospheric pressure. However, at a higher pyrolysis pressure a small portion of porous chars was produced due to swelling. The observed reactivity of both char types was initially equal, but the porous chars were less reactive at higher conversion. As the authors did not calculate intrinsic reactivity, it is not clear if the char structure or the surface activity has the major influence.

In conclusion, the system pressure has an influence on char structure. The influence is dependent on coal properties, especially on the fluidity during heat-up. The general trend is the production of more porous chars at higher pressure. The devolatilisation pressure seems not to have an influence on the intrinsic reactivity (Table 3.2), but on the surface area and on the reaction rate during char gasification under Regime II conditions when pore diffusion effects occur. To analyse char reaction relevant to entrained flow gasifiers the chars should be produced at increased pressure and the operation conditions should be imitated in such a way that they are close to industrial scale gasification conditions.

3.1.3 Effect of Gas Atmosphere on Volatile Yield and Char Properties

Studies on the effect of operation parameters on volatile yield and char properties are usually carried out in an inert gas atmosphere, i.e. in nitrogen, argon, or helium. An inert gas

is chosen not to affect the devolatilisation process by the overlaying gasification reactions. When the effect of a reactive gas atmosphere on devolatilisation is analysed, the heterogeneous char reactions can hardly be excluded. On the one hand, at low temperature the rates of the heterogeneous reactions are slow, but experiments at low temperature are not representative for entrained flow gasification. On the other hand, the heterogeneous reactions are fast at high temperature and therefore influence the pyrolysis result.

Only a few references report on an effect of a reactive gas atmosphere during pyrolysis. A recent review paper [Yu2007] concludes that hydrogen has an effect on the volatile yield. The condensation of polynuclear aromatic compounds produces hydrogen during the pyrolysis process within a coal particle. This hydrogen instantly cracks other heavier compounds and produces tars and lighter gases, but is also carried away from the particle interior and surface by diffusion and convection processes. An excess of hydrogen in the gas phase during the pyrolysis phase enhances the production of tars and light hydrocarbons and increases the total volatile yield [Yu2007].

Brix et al. [Brix2010] investigated the devolatilisation of El Cerrejon coal in an entrained flow reactor at residence times around 200 ms. Experiments in CO₂ and N₂ at 1300°C and 1400°C showed no difference in volatile yield. This suggests that there is no pronounced effect of CO₂ on volatile yield. Specific surface area measurements (N₂-BET) showed no significant difference indicating that there is also no influence of CO₂ on the char properties.

Despite the potential effect of hydrogen reported in literature [Yu2007], the gas atmosphere during devolatilisation seems not to have a significant influence on the volatile yield and char properties of the resulting char. However, more experimental studies are required to underpin this assumption.

3.2 Influences on the Heterogeneous Char Conversion

The products of the devolatilisation process are gaseous volatiles and solid char that both react further in homogeneous and heterogeneous reactions. At high temperature the gaseous volatiles react very fast towards their equilibrium composition, i.e. a gaseous mixture of the main components CO₂, CO, H₂O, H₂, and N₂. Trace element behaviour is not considered in this literature review. The reactions of char with these gases determine the further conversion of the solid fuel. The heterogeneous reactions are influenced by several process parameters that are evaluated regarding their impact on the reaction rate.

3.2.1 Influence of Operation Parameters on the Intrinsic Reaction Rate

The heterogeneous reactions occur on the surface of porous char particles. In this first section, the influences of operation parameters on this chemical surface reaction without any limitations by mass transport are evaluated. It is assumed that the bulk gas concentrations equal the local gas concentrations throughout the particle.

The reaction rate is usually described by different model equations that contain expressions for the quantitative description of the influence of several operation parameters.

First, different basic model equations are shown and literature data of model parameters are summarised. Then the influence of single operation parameters is discussed.

Many researchers use n th order Arrhenius equations of the following type to quantify the effect of temperature T and reactant gas partial pressure p_i on the reaction rate:

$$r = k_0 \cdot \exp \left[\frac{-E_A}{R \cdot T} \right] \cdot p_i^n \quad (3.1)$$

where the activation energy E_A quantifies the temperature influence and the exponent n quantifies the effect of partial pressure. The unit of the rate r depends on the measurement and modelling approach and r can be defined on a mass basis $[g / (g \cdot s)]$, on a char surface area basis $[g / (m^2 \cdot s)]$, or on a char particle volume basis $[g / (m^3 \cdot s)]$. Other definitions are also found in literature.

In order to express the char surface saturation at higher partial pressure and to consider inhibition by product gases, Langmuir-Hinshelwood (LH) type equations² are used. These more complicated equations represent high pressure TGA experiments more accurately. The saturation of reactant gas i at the char surface is implemented by an equation of the type

$$r = \frac{k_i \cdot p_i}{1 + K_i \cdot p_i} \quad (3.2)$$

where both k_i and K_i have Arrhenius form and contain the activation energies $E_{A,k,i}$ and $E_{A,K,i}$. If the adsorption of product gas j is considered the equation is extended to

$$r = \frac{k_i \cdot p_i}{1 + K_i \cdot p_i + K_j \cdot p_j} \quad (3.3)$$

where again k_i , K_i , and K_j have Arrhenius form with the corresponding activation energies $E_{A,k,i}$, $E_{A,K,i}$, and $E_{A,K,j}$.

The pre-exponential factors in all Arrhenius type expressions dependent on the units assumed for the reaction rate and for pressure (or gas concentration), the basis (mass, volume, or surface area specific), and further possible extensions of the model equations. Therefore, their quantity cannot be compared directly and differences in the pre-exponential factors are not discussed here.

The Tables 3.3 and 3.4 summarise published data of the char-CO₂ and char-H₂O gasification rate. Activation energies are given for the model equations used by the authors. With the information about activation energies and pressure exponents, the influences of temperature and reactant partial pressure are discussed in more detail.

3.2.1.1 Effect of Temperature on the Intrinsic Char Gasification Rate

The activation energy E_A is a measure for the temperature influence. Reactions with a high E_A are strongly affected by temperature; a low activation energy indicates a weak influence of temperature.

Under Regime I conditions, the reaction rate is usually measured in TGA experiments due to their controlled experimental conditions. Despite similar reaction conditions in the TGAs

²More information about gasification models and sophisticated model equations are given in Section 4.2.3.

Table 3.3: Literature review about activation energies and pressure exponents of the CO₂-char gasification reaction under Regime I conditions using different types of model equations

Reference	Fuel type	Char preparation	E_A kJ/mol	n_{CO_2}	E_{A,K,CO_2} kJ/mol	E_{A,K,CO_2} kJ/mol	$E_{A,K,CO}$ kJ/mol
[Muehlen1985]	bit. coal	not given			153	-23	-48
[Osafune1988]	different rank	1000°C	175-195	0			
[Hampartsoumian1993]	coal A	flat flame burner			187	-28	-138
	coal B	flat flame burner			178	-30	-150
	coal C	flat flame burner			171	-20	-148
[Salatino1998]	subbit. coal	fixed bed 900°C	213	0.74			
[Ye1998]	low-rank coal	not given	91	0			
[Roberts2000]	bit. coal	tube furnace 1100°C	209-220	0-0.7			
	semi-anthr.		223-250	0-0.7			
[Ollero2003]	olive residue	tube furnace 900°C	133	0.37-0.43	60	-107	-129
[Cetin2005]	pine	WMR 950°C	238	0.48	163	-56	-246
	eucalyptus	WMR 950°C	233	0.39			
	bagasse	WMR 950°C	198	1			
[Park2007]	coal char	flow reactor 1400°C	149-223	0.4-0.7			
[Fermoso2009]	wood	flow reactor 1000°C	166-184	0.33-0.35	100-131	172-220	
		flow reactor 1400°C	145-246	0.33-0.35			

Table 3.4: Literature review about activation energies and pressure exponents of the H₂O-char gasification reaction under Regime I conditions using different types of model equations

Reference	Char type	Char preparation	E_A kJ/mol	η_{H_2O} —	E_{A,K,H_2O} kJ/mol	E_{A,K,H_2O} kJ/mol	E_{A,K,H_2} kJ/mol
[Riede1975]	graphite		68	1			
[Jensen1975]	bit. coal	solvent refining	83	1			
[Schmal1982]	subbit.	in TGA	165	0			
[Muehlen1985]	bit. coal	not given			154	30	-209
[Weeda1993]	bit.	flow reactor			209	25	-114
[Peng1995]	lignite		80-85	0			
	subbit.	TGA	57-61	0	18	-67	
	bit. coal		37-57	0			
[Hansen1997]	wheat straw	flow reactor 900°C			149	-108	-118
[Ye1998]	low-rank coal	not given	131	0			
[Barrio2000]	birch		237	0.57	214	-59	11
	beech	TGA 600°C	211	0.51	199	-26	-79
[Roberts2003]	bit. coal	tube furnace 1100°C	227-231	0.4-0.5			
	semi-anthr.		221-235	0.4-0.5			

and similar fuels, there is a large range of activation energies reported in literature. In nth order rate equations, the activation energy ranges from 133 kJ/mol to 250 kJ/mol for the char-CO₂ reaction, and from 37 kJ/mol to 237 kJ/mol for the char-H₂O reaction. All authors assume that the reactions occur under Regime I conditions and are not influenced by mass transport limitations. A possible explanation for very low activation energies are catalytic effects. Mineral matter within the char structure could act as a catalyst and reduce the activation energy. Mass transport limitations within the char particles or in the outer boundary layer would also reduce the observed activation energy. This phenomena is shown in the Arrhenius plot in Figure 2.2 and is described in Chapter 2.1.2. Despite the assumptions of the authors, activation energies at the lower end were probably measured in experiments that are influenced by mass transport limitations.

The parent fuel and the char production conditions have also an influence on the activation energy as both affect the char reactivity. This has already been discussed in Section 3.1. A general trend of these influences is not seen. As an example Fermoso et al. [Fermoso2009] measured the activation energy (char-CO₂ reaction) of two wood chars that were prepared at 1000°C and 1400°C, respectively. The ranges of activation energies overlap and a significant difference could not be observed.

The value of the activation energy seems to be strongly dependent on parent fuel, char preparation conditions, but also on the experimental setup and the measurement procedure. Activation energies that were measured in the absence of mass transport limitations are expected at the upper end of the ranges that are reported in literature, i.e. around 200 kJ/mol or above.

The exact knowledge of activation energy is very important as only small variations cause large deviations between the reaction rates. For example, an increase in the activation energy from 200 kJ/mol to 210 kJ/mol (=5 %) at a temperature of 800°C lowers the reaction rate by 71 %. When mass transport limitations are involved at higher temperature, the influence of the activation energy is less pronounced. However, the activation energy is probably the most important parameter in a modelling approach for char gasification.

3.2.1.2 Effect of Reactant Gas Concentration on the Intrinsic Char Gasification Rate

The gas concentration is usually measured in units of mol/cm³ or g/cm³ and denotes the amount of a gas species per volume. In most engineering applications and rate equations the gas concentrations are described by partial pressures.

In the nth order rate equation, the effect of reactant gas partial pressure is described by the reaction order n_i . Low values of n_i denote that a change of partial pressure does only slightly influence the reaction rate. If n_i becomes larger, variations of the reactant gas pressure change the reaction rate more significantly. Values of n_i in the Tables 3.3 and 3.4 range from 0 to 1, both for CO₂ and H₂O.

The change of the reaction order with reactant gas partial pressure is modelled by a LH approach. At a low reactant partial pressure (if $K_i \cdot p_i < < 1$), the reaction order approaches unity. At high partial pressure (if $K_i \cdot p_i > > 1$), the reaction order approaches zero and a further increase in partial pressure does not accelerate the reaction rate.

In the nth order rate equation, the reaction order has an exponential influence on the

reaction rate. However, small uncertainties do not lead to large variations of the rate. For example, an increase in the reaction order from 0.5 to 0.525 (= 5 %) at a pressure of 0.5 MPa lowers the reaction rate only by 2 %.

At higher pressure, TGA measurements over wide ranges of partial pressures are rather predicted by LH rate equations than by nth order approaches [Roberts2000]. The activation energies for the adsorption constants K_{CO_2} and K_{H_2O} in the Tables 3.3 and 3.4 are in the majority of cases negative. The reduction of reaction rate by reactant adsorption is less pronounced at higher temperature. Assuming an activation energy of -30 kJ/mol, the influence of reactant adsorption is reduced by 70 % if the temperature is increased from 800°C (TGA experiments) to 1400°C (entrained flow conditions). It is therefore expected that model equations without the implementation of reactant gas adsorption can predict gasification rates at higher temperatures.

So far, the reactions of char with CO_2 and H_2O are considered separately. In the mechanistic explanations for both reactions, the oxide complexes have nominally the same composition [Liu2004b]:



When assuming a common oxide complex $C(O)$ for both reactions, different asymptotic limits for H_2O and CO_2 gasification at very high pressure cannot be modelled. Therefore, Liu and Niksa [Liu2004b] assumed different but coexisting surface oxides. The CO_2 and H_2O reactions occur simultaneously at different active sites and the reaction rate in a mixture of both gases is the sum of the individual rates.

Roberts and Harris [Roberts2007] analysed char gasification in mixtures of CO_2 and H_2O . They showed experimentally in a TGA that the rate of reaction in a mixture of CO_2 and H_2O is not the sum of the two pure-gas reaction rates. Experimental data at 850°C to 900°C showed that the presence of CO_2 inhibits the faster char- H_2O reaction. Moreover, the surface area (CO_2 -DR) that develops during the H_2O reaction was larger than during the CO_2 reaction. When comparing observed and intrinsic rates in water steam, it was observed that both are reduced after the addition of CO_2 . The authors conclude that both gases compete for the same active sites. They derived an equation to describe the inhibition of the H_2O reaction by CO_2 and to calculate reaction rates in mixtures of both gases [Roberts2007]:

$$\rho_{mixture} = \rho_{CO_2} + \rho_{H_2O} \cdot \left(1 - \frac{K_{CO_2} \cdot p_{CO_2}}{1 + K_{CO_2} \cdot p_{CO_2}} \right) \quad (3.6)$$

where ρ is the observed reaction rate, and K_{CO_2} is the adsorption constant in a LH rate equation. The knowledge of this constant and the rates in pure gases allow the calculation of reaction rate in mixtures of CO_2 and H_2O . The observed reaction rates of the pure gases are calculated from the intrinsic rates and the total surface area.

As the activation energy of the adsorption constant K_{CO_2} is in the majority of cases negative (see Table 3.3), the parameter K_{CO_2} decreases at higher temperature. According to Equation 3.6, the reaction rate in a mixture approaches the sum of the single reaction rates

at higher temperature. It is therefore expected, that the reaction rate under entrained flow conditions can be described by the sum of the rates of CO₂ and H₂O gasification.

3.2.1.3 Effect of Product Gases on the Intrinsic Reaction Rate

In a lot of studies an effect of the product gas concentration on the intrinsic reaction rate is measured (e.g. [Muehlen1985, Weeda1993, Barrio2000, Cetin2005]). This influence is assumed to be due to the adsorption of product gases like CO and H₂ at active sites on the char surface. Except one, all activation energies for CO and H₂ adsorption in the Tables 3.3 and 3.4 are negative. The activation energies are significant lower than for reactant gas adsorption making the effect of product gases at higher temperature less important. When assuming an activation energy of -100 kJ/mol the effect of product gas adsorption is reduced by 98 % if the temperature is increase from 800°C (TGA experiments) to 1400°C (entrained flow conditions).

3.2.1.4 Influence of Total Pressure on the Intrinsic Reaction Rate

So far, only the influences of gas concentrations and partial pressures are discussed. A further important parameter in reactivity studies is the total gas pressure. Only four studies are found that analyse the influence of total pressure on the reaction rate. Cetin et al. [Cetin2005] analysed the effect of total pressure on the CO₂ gasification of wood char in a TGA. The char pyrolysis pressure and the gasification pressure were identical. They measured an effect of total pressure on reaction rate, but assigned this to the effect of pyrolysis pressure on the intrinsic char reactivity. The total pressure had no influence on the intrinsic char gasification rate.

Goyal et al. [Goyal1989] analysed the effect of steam partial and total pressure on the reaction rate of a bituminous coal char. They detected small differences, but the variations were within the experimental uncertainty.

In a detailed study, Roberts et al. [Roberts2000c] measured reaction rates in CO₂, H₂O, and O₂ at a constant reactant pressure of 0.5 MPa and at different total pressures (0.5 MPa to 3 MPa) in a PTGA. They tested all three reactions with chars from three different coals and found no systematic effect of the total pressure. The authors conclude that the total pressure influences can be seen if diffusion effects are involved, but they have little to do with the intrinsic reactions.

Park and Ahn [Park2007] measured the effect of total pressure on the char-CO₂ reaction in a TGA. Minor variations in the reaction rates of three different coal chars were found, but the deviations were small.

The total pressure seems not to have an influence on the intrinsic reaction rate under Regime I conditions, but might be an important parameter if diffusion effects play a role.

3.2.2 Literature Review on the Measurements of Reaction Rates at Higher Temperature

The data presented so far are measured under Regime I conditions where the overall reaction rate is determined by the chemical reaction at the char surface and mass transfer

limitations are excluded.

As outlined in Section 2.2.2, thermogravimetric analysers that are used for Regime I conditions are not suitable to measure gasification rates under Regime II conditions. Data relevant to entrained flow gasifiers can only be measured in more complex systems where single particles are observed in a realistic gas flow regime. Drop tube furnaces and entrained flow reactors are used to measure high temperature gasification rates. However, only a few data sets are available that investigate the char gasification behaviour under operation conditions relevant to industrial scale entrained flow gasifiers. The reaction rate is either measured in an integral approach with oxygen being the reactant or in a differential approach with a constant gas atmosphere along the conversion path. Both methods have been applied in literature and the following research groups measured char conversion rates at high temperature and pressure using flow reactors.

Ahn et al. [Ahn2001] investigated the gasification rate of an Indonesian sub-bituminous coal-char with CO₂ using a pressurised drop tube furnace (PDTF) at the Korea Electric Power Research Institute. Char was first produced in nitrogen at atmospheric pressure, 1400°C, and 600 ms, and then sieved to a particle size of 45 μm to 64 μm. Gasification rates were measured from 900°C to 1400°C and at 1.0 MPa reactor pressure. From 900°C to 1000°C the activation energy was determined to be 144 kJ/mol. At higher temperature the activation energy decreased to 71.5 kJ/mol as shown in Figure 3.10 which indicates the occurrence of mass transport limitations. The transition from Regime I to Regime II conditions occurred between 1000°C and 1100°C. Furthermore, the authors varied the total pressure from 0.5 MPa to 1.5 MPa at a constant CO₂ partial pressure of 0.2 MPa and found a significant influence of the total system pressure. The reaction rate in the experiments could be modelled by a total pressure order of -0.65. When varying the CO₂ partial pressure, a reaction order of 0.4 was found.

At the Central Research Institute of Electric Power Industry (CRIEPI), Japan, a pressurised drop tube furnace (PDTF) has been installed to analyse the gasification rate of coal char [Kajitani2002, Kajitani2006]. The facility was operated at up to 1500°C and at up to 2 MPa. The PDTF is not equipped with a gas preheater that heats the reactant gas to reaction temperature. Therefore, the temperature in the initial stages of conversion might be lower than the setpoint temperature. The dimensions of the reactor, the experimental procedure, and the calculation of conversion are not described in the publications. Experiments were carried out with char that was produced in an atmospheric drop tube reactor at 1400°C in nitrogen and at a residence time of about 3 s. Two different coals were used that have an average particle diameter of 26 μm and 39 μm, respectively. The char feed rate was 10 g/h to 40 g/h. The reaction rates of char in CO₂ and H₂O were measured at different temperatures and gaseous partial pressures. The char residence time was assumed to be equal to the average gas residence time. The main kinetic data are shown in Figure 3.11.

The approximate transition temperatures between Regime I and II conditions are indicated by the flattening out of the curves in the Arrhenius plot at higher temperature. For steam gasification of the NL coal char the transition temperature is 1300°C to 1400°C, whereas it is 1200°C for CO₂ gasification. For the S coal char no transition in CO₂ is observed up to 1200°C. Although the reactivity of the steam gasification is about a factor 6 to 7 higher

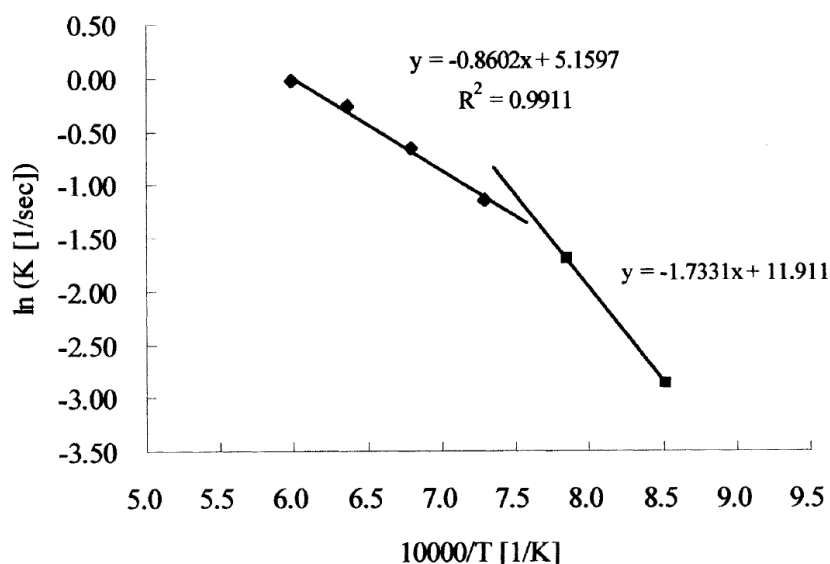


Figure 3.10: Arrhenius plot using experimental data for the char- CO_2 reaction in a pressurised drop tube furnace at the Korea Electric Power Research Institute [Ahn2001]

than for the CO_2 gasification, it is not discussed in the publication why CO_2 gasification is more influenced by mass transport limitations. For the NL coal char, the oxygen reaction rates in a TGA at atmospheric pressure are shown. Due to the higher reactivity of the combustion reaction and the mass transport limitation in the char fixed bed, diffusion limitations occur at a temperature of approx. 500°C . The Regime II conditions are also indicated by the apparent activation energy. In the TGA experiments the activation energy of the NL test char is 283 kJ/mol and decreases to 163 kJ/mol in the PDTF.

Matsumoto et al. [Matsumoto2009] measured reactions rates of biomass char with CO_2 and H_2O in a pressurised drop tube furnace at the Nagasaki Research and Development Center, Japan. The PDTF was operated at a total pressure of 0.4 MPa and at temperatures from 900°C to 1300°C . The partial pressures of CO_2 and H_2O were in the range 0.025 MPa to 0.3 MPa . Chars of four different biomass types were produced in a pilot scale entrained flow gasifier that was operated with steam and oxygen at 900°C to 1000°C . The measured activation energies were 136 kJ/mol for the H_2O reaction and 94 kJ/mol for the CO_2 gasification. The reaction order was 0.20 to 0.22 independent of the gasifying agent. The authors derived nth order rate equations to model the reaction rates in the temperature range 900°C to 1300°C .

Hodge et al. [Hodge2009] used the pressurised entrained flow reactor (PEFR) at the Commonwealth Scientific and Industrial Research Organisation (CSIRO) in Brisbane, Australia to measure high temperature char- CO_2 reaction rates. They operated the PEFR at high pressure (2 MPa) and at high temperature (1000°C to 1400°C). Three different coal samples were used and char was generated in-situ by adding small amounts of oxygen to the reaction gas to burn the volatiles. The activation energies measured at 0.5 MPa CO_2 partial pressure and a total pressure of 2 MPa were 78 kJ/mol to 156 kJ/mol . These were considerably lower than the activation energies of 242 kJ/mol to 281 kJ/mol that were measured for extracted chars under Regime I conditions in a TGA and a fixed bed reactor. The authors [Hodge2010] further analysed char morphology and related particle shape to diffusion limitations under Regime II conditions. The transition temperature from Regime

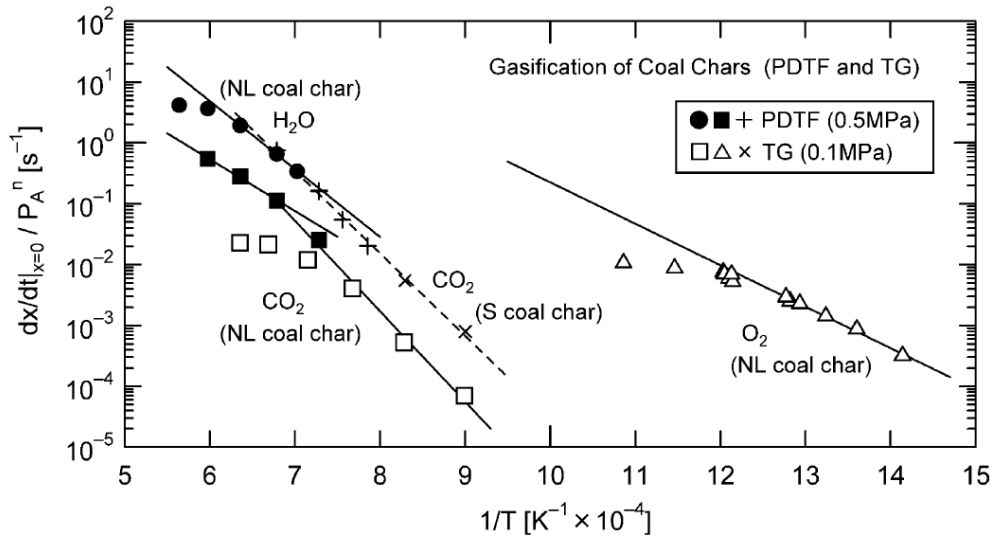


Figure 3.11: Arrhenius plots of gasification rates in PDTF and PTGA experiments at the Central Research Institute of Electric Power Industry, Japan [Kajitani2002]

I to Regime II occurred around 1000°C to 1100°C dependent on char morphology. So far, only differential gasification methods are presented that analyse the reaction rate of a single char-gas reaction. These investigations usually use drop tube reactors that do not allow the adjustment of a stoichiometry between fuel and gas phase. This can only be done in entrained flow reactors where back-mixing effects do not occur and fuel can be converted using a defined stoichiometry. The experiment is then called integral because numerous reactions occur simultaneously and consecutively.

Only one study is found that investigates solid fuel conversion under controlled conditions in an integral gasifier where the complex reaction network of a high pressure and high temperature entrained flow gasifier is imitated. Harris et al. [Harris2006] initially used the PEFR at CSIRO to analyse the integral gasification behaviour of a set of Australian coals. The reactor was operated from 1100°C to 1500°C and at a total pressure of 2 MPa. A gas mixture of 2.5 % O₂ in N₂ was used and the stoichiometry was controlled by a coal feed rate between 1 kg/h and 5 kg/h. Char samples were collected by an oil-cooled sampling probe after residence times from 0.5 s to 2.8 s. The coal conversion was calculated from measured gas composition and known gas and coal feed rates. The influence of residence time on carbon conversion for different coals at an ideal stoichiometry is shown in Figure 3.12. The carbon conversion increases at higher residence time and the conversion is strongly dependent on parent coal. Reaction rates were not calculated from the conversion profiles in this publication; therefore, influences of temperature and mass transport limitations were not discussed.

Another experimental approach is an integral gasification experiment in tube reactors with a high fuel mass flow rate (e.g. [Brown1988, Crnomarkovic2007]). These reactors are designed to simulate industrial scale entrained flow reactors on a laboratory or pilot scale. The reaction zone is heated by the autothermal gasification reaction and the temperature cannot be controlled independently, but is influenced and therefore adjusted by the fuel to oxygen stoichiometry. Experiments over a wide range of temperatures are not possible. As a major part of the gas is generated in the gasification reactions, the residence time of

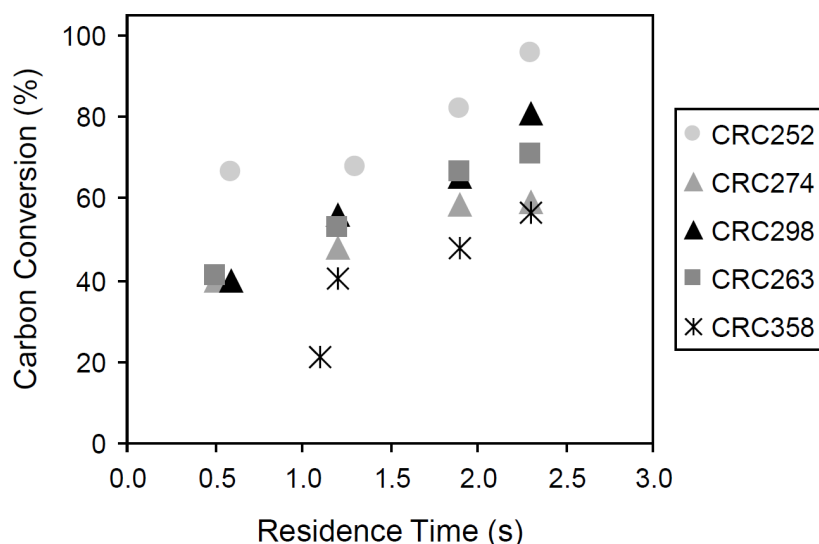


Figure 3.12: Carbon conversion versus residence time for integral gasification experiments at 1400°C and at a total pressure of 2 MPa using the pressurised entrained flow reactor at CSIRO [Harris2006]

particles is dependent on conversion and cannot be measured. Usually gas concentrations along the reactor axis are measured in these facilities and the influences of stoichiometry and parent fuel are analysed. As a lot of operation parameters (e.g. temperature, residence time, and gas composition) cannot be influenced or are not known, it is hardly possible to derive kinetic data from these experiments. Furthermore, the results cannot easily be extrapolated to an industrial scale as for example heat losses and flow profiles are different on a smaller scale. However, these experiments are an excellent opportunity to validate reaction models. Advanced mathematical methods like CFD can be used to calculate the expected reactions, heat and mass balances, and flow profiles within the reactor and compare the results to experimental data.

Other experimental gasification studies are carried out at high temperatures, but in atmospheric reactors. Lee et al. [Lee1996] used a drop tube reactor to measure the effects of reaction temperature, oxygen and steam addition, and residence time on the conversion of four different coal samples. The temperature was varied from 1000°C to 1500°C. All data are given as a function of axial reactor position. As the particle residence time is not known kinetic data cannot be derived. Couhert et al. [Couhert2009] converted torrefied wood in an entrained flow reactor at 1400°C in an atmosphere containing 20 vol% steam in N₂. They achieved high conversions but did not analyse fuel or char reaction rate. At the Karlsruhe Institute of Technology (KIT) an atmospheric pilot-scale entrained flow gasifier is installed [Santo2007, Kolb2009] and research work on the design of a pressurised entrained flow gasifier for biomass has been shown [Jakobs2011]. The research is focused on the gasification of biomass-based slurries at temperatures from 1200°C to 1500°C. An air assisted internal mixing atomizer for the injection of biomass slurries has been developed and glycol has been used as a model substance [Mancini2011]. As char samples are not collected during the operation, the char properties are not analysed. Because the focus of the experiments is not on the gasification kinetics, the conversion rates of fuel and char

are not given and kinetic models are not derived.

The measurement of high temperature reaction rates of the char-CO₂ reaction in a fluidised bed is described by Liu et al. [Liu2006, Liu2006b]. Coal was injected into an atmospheric fluidised bed made from alumina particles and heated up to 1600°C. The reaction rate is then measured by the CO concentration in the off-gas. The Arrhenius plots of the initial reaction rate of 7 different coals are shown in Figure 3.13. All curves show a strong decrease in the activation energy at higher temperature; for one coal even a negative activation energy is measured. The authors related the severity of the decrease in the activation energy to the ash fusion temperature. Furthermore, the specific surface area (N₂ adsorption, calculation method not given) and the particle porosity of two coals after pyrolysis at 1200°C and 1500°C were measured. The surface area and porosity decreased for the coal with the lower ash fusion temperature and both parameters increased for the coal with the higher ash fusion temperature. This observation was also confirmed by electron microscopy. The accumulation of ash and a smooth surface were detected on images of the coal char with the lower ash fusion temperature. The authors theoretically estimated external mass transfer limitations and concluded that these can be neglected even at the highest temperatures despite of the large particle size of 194 μm. Internal mass transfer limitations (pore diffusion) were not considered by the authors, but are expected to strongly influence the reaction rate at high temperature. However, the experimental data [Liu2006] showed that ash related aspects can also contribute to high temperature entrained flow kinetics. Despite the experimental approach it is questionable whether a fluidised bed should be used above the ash melting temperature.

In summary, the state of knowledge of high temperature gasification reactions is very low. There are only a few experimental studies that measure reaction rates at high temperature in flow reactors, analyse the effects of mass transport limitations, and aim at the development of reaction rate models for entrained flow gasification. Pore and boundary layer diffusion are important phenomena at higher temperature, but more experimental data are required to analyse their significance.

3.3 Summary of the Literature Review and Definition of the Research Demand

The parameters that are discussed in the literature review are summarised in this section and the research demand is derived. Furthermore, the importance of these parameters is outlined and suggestions for their implementation in a gasification model are given.

The influencing parameters during **devolatilisation** are

- **Volatile yield** after pyrolysis/devolatilisation is dependent on the operation conditions. With increasing **temperature and heating rate** higher volatile yields are reported and the amount of remaining char decreases. The increase in volatile yield is dependent on the parent fuel. The magnitude of the temperature effect has been analysed for several fuels. Heating rate has an influence, but the reasons and impacts are only vaguely known and further experimental activities are required.

A comprehensive model should describe the effect of temperature on volatile yield

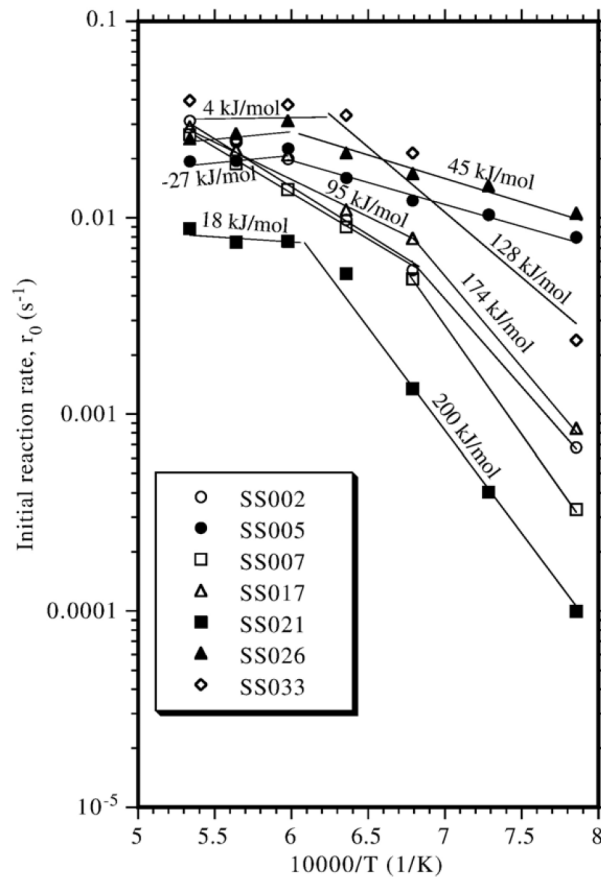


Figure 3.13: Arrhenius plot of the initial reaction rate during CO₂ gasification in a fluidised bed from 1000°C to 1600°C [Liu2006]

and should be based on experimental data derived at high heating rate.

- **Char reactivity** increases at higher **heating rate** during devolatilisation. As most of the increase occurs at up to 50 K/s and the effect levels off between 1000 K/s and 5000 K/s, a minimum heating rate of 1000 K/s in an experiment is required to produce realistic chars.
- There is no clear trend in the literature data indicating the influence of **thermal history** during devolatilisation on **char structure and morphology**. Some studies that are found are contradictory. However, Rosenberg et al. [Rosenberg1996] observed that char samples of different coals produced at temperature above ~1300°C in flow reactors have a morphotype composition very similar to chars from the flame zone of pulverised coal boilers. The composition of chars produced at ~1150°C is significantly different. It is therefore assumed that chars from high temperature flow reactors are similar to chars produced in industrial scale entrained flow gasifiers. Chars that are produced at a heating rate of minimum 1000 K/s and a temperature of minimum 1300°C are comparable to chars produced in large-scale burner facilities. As the amount of gasification data at these conditions is very limited, further experimental data sets from flow reactors are required.
For the evaluation of a gasification model experimental data should be used that are derived from chars that are produced at high temperature and heating rate.

- The effects of **thermal history** on **char reactivity** are significant, but the quantitative importance of these effects is not well understood. With increasing pyrolysis/devolatilisation temperature a considerable loss of reactivity is observed. At longer time scales the reactivity decreases significantly, even in the range of a few seconds. A high heating rate seems to result in a high reactivity. However, it is not easy to distinguish the effects of heating rate and time at temperature as a lower heating rate will always lead to an increased time at temperature in the experiment. Mainly chars derived from wire mesh reactors are analysed. No data set is known that systematically analysis reactivity of char from a high temperature entrained flow facility that is operated above 1100°C.
As the effect of thermal history on char reactivity is considerable, a submodel for thermal annealing should be included to describe char conversion rates. Influences of temperature and time at temperature should be considered and experimental data at high heating rate are required.
- With increasing **pressure**, the **volatile yield** declines. The reduction of volatile yield is strongly dependent on the parent fuel. The effect of pressure is mainly analysed in wire mesh reactors, and most data are collected below 1100°C.
An increased pressure reduces volatile yield on average by 2 to 3 wt% per MPa, but there are strong deviations and the pressure effect needs to be evaluated for every fuel. A comprehensive model should include the dependence of volatile yield on operation pressure. Fuel specific data have to be measured in wire mesh or flow reactors.
- The devolatilisation **pressure** also has an influence on **char structure**. The general trend is the production of more porous chars at a higher system pressure. But there is disagreement in the open literature about the effect of pyrolysis pressure on the observed **char reactivity**. However, after a normalisation with char specific surface area, most of the studies report no significant influence of pressure on the intrinsic reactivity. The pressure is assumed to influence char structure and surface accessibility, but not the chemical activity of the char surface.
In comparison to the effects of temperature, time at temperature, and heating rate, the pressure effect on the intrinsic reactivity is very small. However, as pressure influences char structure, an effect under Regime II conditions is likely. Char structure determines the diffusion properties of gases and contributes to the overall reaction rate. Chars that are converted at high temperature should also be produced at the relevant system pressure to generate a realistic char structure.
- The influence of a reactive **gas atmosphere** on **volatile yield and char properties** after devolatilisation is hardly measurable since heterogeneous gasification reactions occur simultaneously in an experimental setup. In most of the studies an influence of reactive gas atmosphere is not observed. If an influence is detected, it is small and not significant in comparison to the effects of thermal history and pressure.

As several parameters have an influence on the char structure and reactivity and the general trend and magnitude of these influences is not always clear in the literature, char that is used for the analysis of gasification reactions should be produced under operation

conditions that imitate the burner zone of an entrained flow gasifier as closely as possible. These are a high heating rate (minimum 1000 K/s), a high temperature (minimum $\sim 1300^{\circ}\text{C}$), and increased pressure (close to the industrial operation pressure).

After the devolatilisation the resulting char is converted in **heterogeneous reactions**. Several parameters have an influence on the reaction rate of char gasification under Regime I conditions:

- The quantitative influence of **temperature** is considered by the activation energy. As activation energies reported in literature vary widely dependent on the measurement procedure, on parent fuel, and on the char preparation conditions, general trends are not obvious.
It is very important to implement the influence of temperature in a model equation. Due to its exponential influence, only small variations of temperature cause large deviations of the reaction rate. For reliable model predictions, it is required to measure the activation energy of char produced under conditions relevant to entrained flow gasification.
- The influence of **reactant partial pressure** is accounted for by the reaction order. In the literature, the reaction orders are between 0 and 1 for both CO_2 and H_2O gasification and also for different model equations. The reaction order also has an exponential influence, but small uncertainties in the reaction order do not strongly influence the reaction rates.
LH rate equations represent TGA measurements over a wide range of reactant partial pressures. In literature, usually negative activation energies are reported for the adsorption of reactant gases. The effect of the reactant adsorption is therefore less important at higher temperature.
- In most gasification models it is assumed that the rate of char reaction is the sum of the single char-gas reactions. However, it has been shown that the reaction rate in a mixture of CO_2 and H_2O is not the sum of the two pure gas reaction rates [Roberts2007] because CO_2 inhibits the steam reaction. The effect has been quantified and it is important under TGA conditions, but it is less important at higher temperatures. Future experimental activities should analyse this effect also at higher temperature.
- **Product gas inhibition** is analysed in different experimental studies and a significant influence in TGA experiments is found. The activation energies of the inhibition are - with the exception of one study - negative around -100 kJ/mol . Therefore, the effect of product gas inhibition is less important at higher temperature. However, a measurement set at high temperature and high pressure is required to meaningfully evaluate the effect of product gas inhibition under entrained flow conditions.

Experimental data of reaction rates above 1000°C are rare. Only 4 datasets are known that analyse the rate of the char- CO_2 or char- H_2O reaction in pressurised flow reactors. The transition temperature from Regime I to Regime II is measured to be 1000°C to 1400°C , and generally a decrease in activation energy is observed at higher temperature. As this

transition is dependent on several parameters like intrinsic reactivity, particle diameter, and porosity, a general specification is not possible. Integral gasification experiments are only carried out by Harris et al. [Harris2006]. They measured coal conversion at 2 MPa and at temperatures of up to 1500°C. An experimental investigation [Liu2004] in a fluidised bed at high temperature showed that also ash melting can decrease the reaction rate at higher temperature.

The state of knowledge of gasification reactions at high temperature and high pressure is low. Worldwide, only a few experimental setups have been developed that enable the investigation of reaction rates under entrained flow conditions. Pressurised flow reactors were operated at up to 2.0 MPa ([Kajitani2006, Harris2006]) and at temperatures of up to 1500°C ([Kajitani2006, Harris2006]). As industrial gasifiers are operated at even more extreme conditions, future investigations should aim at the extension of the database and should try to measure gasification reaction above 2.0 MPa and above 1500°C.

3.4 Aims and Research Strategy of the Dissertation

In the literature review, the state of knowledge of high temperature and high pressure reaction kinetics in entrained flow gasifiers is summarised. From this overview the need for research for future investigations is identified. This dissertation aims at the extension of the data range at higher temperatures and pressures, wants to contribute to the understanding of entrained flow reaction rates, and wants to improve the transferability of laboratory and pilot scale data to the industrial application. The particular contributions and research goals are:

- As there are only a few data sets in literature that analyse reaction behaviour of solid fuels at temperatures above 1000°C, more experiments at conditions relevant to full scale entrained flow gasifiers are required to enable a basic understanding of the reaction mechanisms. A low number of data points is available at up to 1500°C and up to 2.0 MPa. The dissertation aims at the extension of the experimental range and the provision of **gasification data measured at high temperature and high pressure**.
- Most of the studies published in literature present reaction data that have been measured in one specific experimental facility and under very limited reaction conditions. To understand the reaction mechanism and to extrapolate reaction kinetics to wider ranges of operation conditions, the experimental analysis should be conducted in **several test facilities**. In this dissertation several experimental procedures are applied ranging from laboratory analysis to bench-scale (wire mesh reactor, atmospheric entrained flow reactor, and pressurised thermogravimetric analysis) and pilot-scale (pressurised entrained flow reactor) facilities in order to characterise the reaction behaviour of solid fuels under various conditions.

A comprehensive analysis of a fuel in different experimental facilities and over wide ranges of operation conditions has not been found in literature. The dissertation aims at the provision of a comprehensive data set of a single fuel derived in several experimental setups and under wide ranges of operation conditions.

- In literature studies the influence of a large number of parameters on the devolatilisation and char gasification is discussed. Usually, these influencing factors are analysed separately and mathematical formulations that quantify the influence of one parameter are developed. Most of the studies do not combine various effects and no gasification model is found in the open literature that is based on experimental data and quantitatively describes all parameters relevant to entrained flow gasification kinetics. In this dissertation first the most important parameters are evaluated and their quantitative influence is measured. Then a **detailed kinetic model** is developed that describes the influences of the most important parameters on devolatilisation and heterogeneous char gasification.
- A major objective of the analysis of gasification rates is the transfer of basic knowledge and research to the industrial level. The dissertation presents a way to transfer lab scale data in combination with measurements in a pilot scale entrained flow reactor to the industrial scale and to enable the **design and optimisation of industrial scale entrained flow gasifiers** based on kinetic data.
- Almost all studies in literature strictly separate the analysis of coal reaction behaviour from the experimental analysis of biomass or biomass derived fuels. This is mainly because the funding sources and research motivations are completely different. However, the basic structure and basic reaction behaviour of fossil and renewable solid fuels are identical and the same experimental procedures and analysis methods can be applied. Therefore, this dissertation includes the whole range of **solid fuels ranging from biomass to coal** and tries to link the reaction behaviour.

Chapter 4

Theoretical Development and Selection of Gasification Models for Solid Fuels

The qualitative influences of important parameters on devolatilisation and char conversion have been discussed in the literature review. To evaluate the reaction behaviour of different fuels, to understand the reaction mechanism, and to derive procedures for the application of these fuels in industrial scale gasifiers, the quantitative influences of fuel properties and operation parameters have to be described. Mathematical formulations that are partially based on chemical and physical principles but also on empirical observations are used to quantify the reaction behaviour. In this chapter, these models are discussed separately for pyrolysis and char gasification. First, in each section the literature on modelling is briefly reviewed and then a suitable model approach is derived.

4.1 Selection of a Pyrolysis Model

4.1.1 Overview of Pyrolysis Models from Literature

There is a great variation in the complexity of devolatilisation models. Any sophisticated pyrolysis model has to address the effects of temperature, heating rate, and pressure on volatile yield. In a recent review paper, Niksa et al. [Niksa2003] summarised the development of mechanistic interpretations of the pyrolysis reactions. The first interpretation put forward is called classical devolatilisation theory. It addresses the pressure effects by the implementation of the recondensation of tar compounds. Furthermore, transport mechanisms of volatiles are considered. Several of these classical models can predict the volatile yield over a wide range of pressures, but none has implemented heating rate effects, coal quality impacts, and particle size dependence [Niksa2003].

Based on the classical theory, further devolatilisation models and formulations have been developed [Smith1994]. The three comprehensive models are the FLASHCHAIN model [Niksa1995, Niksa2003], the Functional Group - Depolymerisation Vaporisation Crosslinking (FG-DVC) model [Solomon1991], and the Chemical Percolation Depolymerisation (CPD) model [Jupudi2009].

FLASHCHAIN This model invokes an analogy between coal devolatilisation and the steam distillation of petroleum [Niksa2003]. When steam is injected in crude oil, the lightest fractions pass into the vapour and are transported to the surface. Matter with a high

molecular weight remains in the liquid phase and condenses into coke if the temperature is higher than a certain threshold value. During coal devolatilisation, light non-condensable volatiles play the role of steam. Tar is produced and char is formed by crosslinking among heavier fragments. The influence of thermal history, pressure, and particle size is interpreted by different mechanisms. The model predicts the gas and the tar yield, gas compositions, and the molecular weight distribution of tar compounds. The only sample-specific input is the proximate and ultimate analysis of the coal [Liu2004c].

Functional Group - Depolymerisation Vaporisation Crosslinking model FG-DVC is a general pyrolysis model that combines a functional group (FG) model for gas evolution and a statistical depolymerisation, vaporisation, and crosslinking (DVC) model for tar formation [Solomon1991]. Gases evolve from coal, char, and tar. At low temperature CO_2 and at medium temperature CH_4 are generated. Tar production is described by the decomposition and condensation of a macromolecular network and the molecular weight distribution of the fragments can be predicted.

Chemical Percolation Depolymerisation model In the CPD model the devolatilisation behaviour of coals at high heating rate is described [Jupudi2009]. Based on the chemical structure of the coal, the overall char, tar, and light gas yields are predicted. In contrast to the other two more general models, the CPD model takes only coal structure coefficients based on NMR measurements as inputs without any adjustable constants.

Here, only a short overview of the sophisticated devolatilisation models is given. Further information about the models can be found in the references.

In contrast to the heterogeneous reactions, devolatilisation is very fast and a detailed mechanistic understanding is not necessarily required to analyse the rates of solid fuel conversion. Furthermore, the comprehensive models predict primary gas and tar composition that are only short-living intermediates in any high-temperature, entrained flow process [Niksa2003]. Therefore, it is not necessary to build a comprehensive devolatilisation mechanism into numerical or other engineering calculations for the overall gasifier simulation. For these calculations, a simple approach that predicts the rate of devolatilisation and volatile yield as a function of operation parameters is sufficient. Simpler expressions are the single first-order reaction, the two competing reactions, or the distributed activation energy models [Niksa2003].

Single first-order reaction model A simple expression that describes pyrolysis is a single first-order reaction (SFOR) model:

$$\frac{dY_V(t)}{dt} = A_V \cdot \exp\left[\frac{E_{A,V}}{R \cdot T}\right] \cdot (Y_{V,\infty} - Y_V(t)) \quad (4.1)$$

where Y_V is the instantaneous volatile yield, $Y_{V,\infty}$ is the final volatile yield, A_V is a frequency factor, and $E_{A,V}$ is the activation energy. The parameters are adjustable and their magnitudes have no mechanistic significance [Niksa2003].

Two competing reactions or multi-step models The SFOR model is extended to two or more reaction equations. The most mechanisms apply parallel reactions for the decomposition of volatile fractions of pseudo-components [DiBlasi2008]. An activation energy is assigned to each reaction which allows a more precise prediction of experimental data.

Distributed activation energy (DAE) model During pyrolysis several different reactions occur in parallel or consecutively. The assumption of a single activation energy in the SFOR model or a limited number of activation energies in the multi-step models is a substantial simplification. In DAE models an infinite number of irreversible first-order parallel reactions that have different activation energies is assumed [Sonobe2008]. The difference in activation energies is represented by a distribution function. A standard deviation is applied to the activation energy and effects of temperature and heating rate can be predicted in more detail.

The modelling of pyrolysis reactions is described only briefly. More information and further model equations are found in excellent reviews about devolatilisation kinetics of solid fuels (e.g. [Kobayashi1977, Niksa2003, DiBlasi2008]).

4.1.2 Development of a Pyrolysis Model Based on Experimental Data

In the short literature review about pyrolysis modelling several concepts are introduced that require a huge amount of experimental data and comprehensive analysis procedures. The more complex a model, the more parameters have to be adjusted and the more experimental data or further information are required. Hence, it is not always desired to develop and apply a detailed pyrolysis model. In the following, a pyrolysis model is presented that enables a stepwise integration of experimental data.

4.1.2.1 Volatile Yield after Devolatilisation

The simplest approach is a one stage model that only predicts volatile yield under entrained flow conditions. It is assumed that volatile yield Y_V is constant and independent of the thermal history and pressure of the fuel particles.

$$Y_V = c \quad (4.2)$$

c is a constant that is determined at high heating rate in a high temperature entrained flow experiment or a wire mesh reactor. Only one parameter has to be derived from experimental data. Pyrolysis occurs in one time step that is typically in the range of less than hundred milliseconds.

However, the operation parameters (thermal history, pressure, etc.) have an influence on volatile yield. Dependent on parent fuel and the range of operation parameters, these effects are considerable and the assumption of a constant volatile yield is inaccurate. Therefore, Equation 4.2 is extended by taking into account the effects of pressure and temperature.

Influence of Temperature on Volatile Yield Temperature has a positive effect on volatile yield. In literature, a progressing devolatilisation is observed when the temperature is increased - at low temperature in TGA experiments as well as at high temperature in entrained flow experiments. An empirical approach to model this behaviour is the assumption of a temperature-dependent linear decrease in the volatiles concentration in the solid fuel:

$$\frac{dc_V}{dT} = -\vartheta \cdot c_V \quad (4.3)$$

where c_V is the concentration of volatiles within the solid fuel and ϑ is an adjustable parameter that expresses the severity of the temperature effect. This equation is integrated and solved for c_V

$$\int_{c_{V,T_{min}}}^{c_V} \frac{dc_V}{c_V} = -\vartheta \int_{T_{min}}^T dT \quad (4.4)$$

$$\ln \frac{c_V}{c_{V,T_{min}}} = -\vartheta (T - T_{min}) \quad (4.5)$$

$$c_V = c_{V,T_{min}} \cdot \exp [(-\vartheta (T - T_{min}))] \quad (4.6)$$

where $c_{V,T_{min}}$ is the volatile concentration at the lowest temperature measured.

By using Equation 4.6 the total conversion of volatiles $X(T)$ in the temperature range T_{min} to T is calculated

$$X(T) = \frac{c_{V,T_{min}} - c_V}{c_{V,T_{min}}} = 1 - \exp [-\vartheta (T - T_{min})] \quad (4.7)$$

The total conversion of volatiles in a given temperature interval can also be expressed by volatile yield:

$$X(T) = \frac{Y_V(T) - Y_{V,T_{min}}}{Y_{V,T_{max}} - Y_{V,T_{min}}} \quad (4.8)$$

The combination of Equations 4.7 and Equation 4.8 results in a function that gives volatile yield dependent on temperature:

$$Y_V(T) = Y_{V,T_{min}} + (Y_{V,T_{max}} - Y_{V,T_{min}}) \cdot (1 - \exp [-\vartheta (T - T_{min})]) \quad (4.9)$$

This equation is derived on the empirical assumption of a linear temperature dependence of volatiles concentration within the fuel structure. ϑ is an adjustable parameter. Due to its empirical background, Equation 4.9 is valid in the temperature interval T_{min} to T_{max} where experimental data of minimum and maximum volatile yield are available.

Furthermore, it is possible to adjust the model to an arbitrary temperature range within the experimental temperature range. For example, T_{min} is changed to a setpoint temperature T_{set} .

$$Y_V(T) = Y_{V,T_{set}} + (Y_{V,T_{max}} - Y_{V,T_{set}}) \cdot (1 - \exp [-\vartheta (T - T_{set})]) \quad (4.10)$$

The model can still be fitted to the full experimental data range from T_{min} to T_{max} and is valid there. The adjustable parameter ϑ slightly changes depending on the choice of T_{set} .

Influence of Pressure on Volatile Yield Besides temperature, also total pressure has an influence on volatile yield in a pyrolysis experiment. With increasing pressure more volatiles remain in the char structure and the volatile yield decreases. The modelling of the pressure effect is based on an analogy to vapour pressure calculations. The change of vapour pressure of a substance with temperature is described by the Clausius-Clapeyron-Equation [Atkins1996]:

$$\frac{d \ln p}{dT} = \frac{\Delta h_V}{R \cdot T^2} \quad (4.11)$$

where p is the saturation vapour pressure, Δh_V is the enthalpy of vaporisation at the temperature T .

To derive a functional correlation of vapour pressure and temperature, Equation 4.11¹ is integrated. In the simplest way, the enthalpy of vaporisation is independent of temperature and the integration leads to

$$\ln (p/p_0) = A - \frac{B}{T} \quad (4.12)$$

The two species dependent constants A and B are derived from experimental vapour pressure data.

The vapour pressure curve describes a positive correlation between pressure and temperature, i.e. at a higher temperature the vapour pressure increases. Volatile yield and pressure have a negative correlation. Therefore, T is substituted by $1/Y_V$ which results in

$$\ln (p/p_0) = A - B \cdot Y_V (p) \quad (4.13)$$

$$Y_V (p) = \frac{1}{B} (A - \ln (p/p_0)) = A/B - \frac{\ln (p/p_0)}{B} \quad (4.14)$$

where $p_0 = p_{set}$ is a setpoint pressure, and A and B are constants. For $p = p_{set}$,

$$A/B = Y_{V,p_{set}} \quad (4.15)$$

and the pressure dependence of volatile yield is expressed as follows

$$Y_V (p) = Y_{V,p_{set}} - \frac{\ln (p/p_{set})}{\rho} \quad (4.16)$$

where ρ is the only adjustable parameter. $Y_{V,p_{set}}$ is derived from an experiment at the setpoint pressure p_{set} .

Equation 4.16 can also be derived by assuming an indirect proportionality between dY_V/dp and p .

Combination of the Effects of Pressure and Temperature on Volatile Yield As volatile yield is dependent on pressure and temperature, both Equation 4.10 and Equation 4.16 are combined. It is assumed that both functionalities are independent from each

¹If a correlation between Δh_V and T is assumed, the integration results in more complex formulations (e.g. the Kirchhoff Equation [Gmehling1992]).

other. First, the functions are normalised to volatile yield at T_{set} and p_{set} .

$$\Theta = \frac{Y_V(T)}{Y_{V,T_{set}}} = \frac{Y_{V,T_{set}} + (Y_{V,T_{max}} - Y_{V,T_{set}}) \cdot (1 - \exp[-\vartheta(T - T_{set})])}{Y_{V,T_{set}}} \quad (4.17)$$

$$P = \frac{Y_V(p)}{Y_{V,p_{set}}} = \frac{Y_{V,p_{set}} - \frac{\ln p/p_{set}}{\rho}}{Y_{V,p_{set}}} \quad (4.18)$$

P and Θ describe the deviations of volatile yield from the common data point. In one set of experiments the influence of pressure and in another set of experiments the influence of temperature is measured. Both sets should intersect in one common measurement point $(p_i, T_k) = (p_{set}, T_{set})$ as shown in Figure 4.1. If there is no common data point, an intersection has to be calculated from the single models. The volatile yield at the common data point $Y_{V,p_{set},T_{set}}$ is the starting point for the combined model. The influences of pressure and temperature on volatile yield are then described as

$$Y_V(p, T) = Y_{V,p_{set},T_{set}} \cdot \Theta \cdot P \quad (4.19)$$

4.1.2.2 Modelling the Kinetics of Devolatilisation

So far, the total volatile yield is predicted as a function of operation pressure and final operation temperature and any variations with time are not considered. If the influence of operation parameters on the devolatilisation rate is modelled, a more complex approach is necessary. The dynamic approach can be based on the single first-order reaction (SFOR) model (Equation 4.1). The devolatilisation rates are dependent on temperature. Input parameters are the pre-exponential factor A_V , the activation energy $E_{A,V}$, and the final volatile yield at long time scales. This final volatile yield is expressed as a function of operation pressure and final pyrolysis temperature T_{final} .

$$\frac{dY_V(t)}{dt} = A_V \cdot \exp\left[\frac{E_{A,V}}{R \cdot T}\right] \cdot (Y_{V,p,T_{final}} - Y_V(t)) \quad (4.20)$$

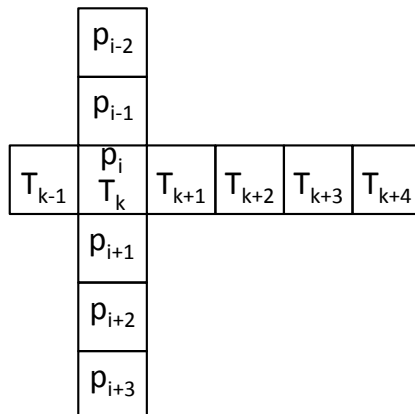


Figure 4.1: Set of experimental data required for implementation of the pyrolysis model

If the final temperature after devolatilisation is not known a priori, an iterative procedure has to be used. In a numerical incremental procedure, the maximum temperature of the fuel particle along its devolatilisation path can be used. For the adjustment of the parameters A_V and $E_{A,V}$, experimental data at different residence times and temperatures are required. The kinetic pyrolysis model can then be used to predict volatile yield as a function of time, temperature and pressure.

In summary, submodels that describe the influences of pressure, temperature, and time on volatile yield are presented. The choice of the proper devolatilisation model depends on the level of detail that is required, the experimental data, and other fuel information that are available. In Table 4.1 the possible stages of pyrolysis modelling are summarised.

Table 4.1: Different levels of devolatilisation modelling

Stage	Model equation	Influence of	Adjustable parameters
1.1	$Y_V = const$	-	-
1.2	$Y_{V,final} = Y_{V,p_{set},T_{set}} \cdot \Theta \cdot P$	p, T_{final}	ρ, ϑ
2	$\frac{dY_V(t)}{dt} = A_V \cdot \exp\left[\frac{E_{A,V}}{R \cdot T}\right] \cdot \left(Y_{V,p,T_{final}} - Y_V(t)\right)$	t, T, p	$A_V, E_{A,V}, \rho, \vartheta$

4.2 Development and Selection of Char Conversion Models

Char that is formed during devolatilisation further reacts in heterogeneous gasification reactions. As the char conversion in the heterogeneous reactions is the rate-determining step of fuel conversion in high temperature gasification processes, the focus of the model development is on the heterogeneous char-CO₂ and char-H₂O reactions.

4.2.1 Notation and Definition of Char Reactivity

The description of the char reaction rate is based on different definitions. In the simplest form the mass of reacting carbon is related to the char mass available for reaction and the terms *observed reaction rate* or *observed reactivity* are used:

$$r_{obs} = \frac{\text{reacting carbon}}{\text{time} \cdot \text{carbon mass}} = \frac{dm}{dt \cdot m} \left[\frac{g}{g \cdot s} \right] \quad (4.21)$$

The observed reaction rate can be directly derived from experimental data, for instance from the weight loss in a TGA experiment. In literature the observed reaction rate is also referred to as *overall rate* or *apparent rate*.

The term *intrinsic reactivity* denotes the reaction rate per surface area of the char and is also referred to as the true kinetics [Laurendeau1978]. The heterogeneous gasification occurs at the char surface. From a mechanistic point of view it is reasonable to normalise the reactivity to the surface available for reaction. The observed reaction rate for two chars with the same intrinsic reactivity then depends on the inner and outer char surface that is available for reaction, whereas the internal surface area of microporous char is by

far more important than the external particle surface². By measuring char specific surface area [m^2/g] the influences of porosity and surface reactivity can be separated and a more mechanistic understanding is possible. Intrinsic reactivity is defined as

$$r_{intr} = \frac{\text{reacting carbon}}{\text{surface area} \cdot \text{time}} = \frac{dm}{S \cdot dt} \left[\frac{\text{g}}{\text{m}^2 \cdot \text{s}} \right] \quad (4.22)$$

The calculation of the intrinsic rate requires information about the specific surface of the char. Under Regime I conditions, intrinsic and observed reactivity are correlated

$$r_{obs}^I = S \cdot r_{intr} \quad (4.23)$$

where the superscript *I* denotes Regime I conditions and *S* is the specific surface area of the char. Under Regime II conditions a concentration gradient within the char particle exists and the internal surface area is only partially available for reaction:

$$r_{obs}^{II} = S_{available} \cdot r_{intr} \quad (4.24)$$

In Regime III the observed reaction rate is only dependent on mass transport limitations within the particle boundary layer and there is no correlation to intrinsic reactivity.

Independent of the reaction regime the observed reaction rate is correlated to conversion rate

$$r_{obs} = \frac{dm}{dt \cdot m} = -\frac{dx \cdot m_0}{dt \cdot m} = -\frac{1}{(1-x)} \frac{dx}{dt} \quad (4.25)$$

where *x* is the instantaneous char conversion. Instantaneous char mass *m*, initial char mass *m*₀, and char conversion are correlated by the following equation:

$$x = \frac{m_0 - m}{m_0} \quad (4.26)$$

In the next section, first a simple model for the observed reactivity is presented. As the observed reactivity alone enables no mechanistic explanation of the char conversion process, different submodels based on intrinsic reactivity are presented in Section 4.2.3. These intrinsic models are later extended by submodels for pore diffusion, boundary layer diffusion, char surface area evolution, thermal deactivation, and char particle size and density variations.

4.2.2 Simple Model Approach for the Observed Reaction Rate

If no information about the intrinsic reactivity of a char is available, the model can only be based on the observed reaction rate. This is a purely empirical approach as a reaction mechanism is not taken into account and neither the influences of mass transport limitations nor char properties are considered. In the simplest form, only the temperature

²Assuming a specific surface area of 200 m^2/g , a char density of 1 g/cm^3 and a particle diameter of 100 μm , the internal surface area is more than 3000 times larger than the external particle surface area.

dependence of the reaction rate is modelled:

$$r_{obs} = r(T) = k_{0,obs} \cdot \exp \left[\frac{-E_{A,obs}}{R \cdot T} \right] \quad (4.27)$$

where $k_{0,obs}$ [g/(g·s)] and $E_{A,obs}$ are empirical constants that are derived from a fitting procedure to experimental data. As there are no influences of gas atmosphere and pressure included, the model is only valid for very limited operation conditions. The adjustable parameter $k_{0,obs}$ condenses all influences - except temperature - to a constant value. As, for example, gas concentrations change due to char conversion, the assumption of a constant $k_{0,obs}$ will always result in an inherent error.

It is possible to extend the model to include other operation parameters, but this would also be based on empirical formulations. As fully empirical models do not help to understand the reaction process, a further model extension is not made. In the following sections different submodels are presented that allow a deeper understanding of the char conversion process.

4.2.3 Submodels for Intrinsic Char Reactivity under Regime I Conditions

First, any mass transfer limitations are excluded and the chemical reaction at the char inner and outer surface is considered. The gasification reactions occur at active sites on the char surface. An active site can interact with a gas molecule and can form chemical bonds. Active sites can be carbon edges or dislocations, inorganic impurities [Laurendeau1978], defects in the carbon structure, and heteroatoms [Lahaye1991].

4.2.3.1 Overview of Char Reactivity Models from Literature

Due to its simplicity, an n th order type rate equation is often used to model intrinsic char gasification (e.g. [Laurendeau1978, Kajitani2006, Hodge2009]):

$$r_{intr} = k_0 \cdot \exp \left[\frac{-E_A}{RT} \right] \cdot p_i^n \quad (4.28)$$

The model constants k_0 , E_A , and n can be fitted to experimental data. This equation is used to describe single reactions where p_i denotes the partial pressure of gaseous reactants (e.g. CO₂, H₂O). A further simplification of the model is achieved by setting $n = 0$, i.e. any influence of the gas atmosphere is omitted.

The model does not include important phenomena that are reported in literature. These are a decreasing influence of the partial pressure due to the saturation of the char surface at higher pressure and a decrease in reaction rate due to the adsorption of reaction products at the char surface.

The adsorption and desorption processes at the char surface can be implemented by two approaches. Both were derived for catalytic reaction rate expressions at ideal surfaces in heterogeneous catalysis [Carberry1976]. The first approach was derived by Hinshelwood [Hinshelwood1940] and is commonly termed the Langmuir-Hinshelwood formulation. It expresses the reaction rate in terms of the surface coverage Θ and then employs the

Langmuir adsorption isotherm to relate Θ to the gas concentrations. A more explicit approach was derived by Hougen and Watson [Hougen1943] who correlated rate equations to surface concentrations of adsorbed species and free sites and then expressed these surface concentrations in terms of the Langmuir isotherm. The Hougen and Watson derivations are highly instructive extensions and refinements of the Langmuir-Hinshelwood theory and include further model equations [Carberry1976]. As the contributions of both approaches cannot be separated strictly, ideal-surface reaction models are referred to as Langmuir-Hinshelwood-Hougen-Watson (LHHW) formulations [Carberry1976]. However, most of the literature on char gasification refers to Langmuir-Hinshelwood rate equations when adsorption and desorption processes are involved, and a strict distinction between LH and LHHW is not made.

The theory of adsorption of gas molecules on active sites is based on four classical assumptions [Laurendeau1978]

1. The localised adsorption of gas molecules occurs via collisions with vacant active sites (the collision frequency is based on the kinetic theory from which the Arrhenius approach can be derived).
2. Only one molecule or atom can be adsorbed per active site.
3. The surface mechanism is constant throughout reaction and conversion.
4. The surface coverage is less than a complete monolayer.

For the classical Langmuir-Hinshelwood kinetics three further assumptions are required [Laurendeau1978]:

1. The surface is homogeneous and has a uniform average activity (uniform distribution of active sites).
2. No interactions occur among adsorbed species (the amount adsorbed has no effect on the adsorption rate).
3. Surface migration is nonexistent or so fast that only adsorption/desorption can be rate controlling.

The exact derivation of the LH and LHHW models and numerous examples can be found elsewhere [Laurendeau1978, Carberry1976].

In the simplest form, the classical LH approach is described by

$$r = \frac{k \cdot c}{1 + K \cdot c} \quad \text{or} \quad r = \frac{k \cdot p}{1 + K \cdot p} \quad (4.29)$$

where both k and K have Arrhenius form³ and c is the concentration of reactant gas. In the mechanistic development mass or molar gas concentrations ($[\text{g}/\text{m}^3]$ or $[\text{mol}/\text{m}^3]$) are applied, whereas practical investigations usually use the partial pressure⁴ p . In contrast to

³The parameters k and K can also be expressed by more fundamental rate constants.

⁴When converting the partial pressure to gas concentration ($c = m/V = pM/(RT)$) the influence of temperature is obvious. However, in contrast to the exponential influence of temperature in the activation energy term, this linear temperature influence is small and is almost always neglected.

gas concentrations, the partial pressure can be easily adjusted or measured in an experimental setup.

Equation 4.29 requires two pre-exponential factors and two activation energies. A simple LH rate equation is valid over a wide range of pressures and describes the saturation effect of the char surface at higher pressure. Equation 4.29 describes the adsorption and reaction of single gases like H₂O and CO₂.

Simultaneously to these main reactant gases, also product gases like CO adsorb on the char surface. A simple mechanism that incorporates the adsorption of CO during the CO₂ gasification is an oxygen-exchange mechanism first proposed by Ergun et al. [Ergun1961, Mentser1973]



where the number of free active sites C* is assumed to remain constant during burn-off [Ergun1961]. Applying the common LH theory, the following rate equation is derived for the CO₂ gasification [Laurendeau1978]

$$r = \frac{k \cdot c_{\text{CO}_2}}{1 + a \cdot c_{\text{CO}} + b \cdot c_{\text{CO}_2}} \quad (4.32)$$

where *k*, *a*, and *b* are reaction constants that can be described by an Arrhenius type equation. Again, in Equation 4.32 and similar formulations the partial pressures instead of gas concentrations are used in practical applications.

By assuming different reaction mechanisms, various other rate equations can be derived. If the chemisorption/adsorption step of CO₂ is assumed to be a two site process⁵ the rate equation proposed by Blackwood et al. [Blackwood1960] is more accurate. In this case the reaction rate equation is

$$r = \frac{k_1 \cdot c_{\text{CO}_2} + k_2 \cdot c_{\text{CO}_2}^2}{1 + a \cdot c_{\text{CO}} + b \cdot c_{\text{CO}_2}} \quad (4.33)$$

The derivation is based on a more complex mechanism with different oxygen-carbon complexes and is summarised by Laurendeau [Laurendeau1978]. An overview of different mechanistic explanations for the C-CO₂ reaction is given by Ma [Ma2006].

The rate equations can be derived for steam gasification in the same way and similar formulations arise. Furthermore, the inhibition of several product gases can be implemented in the equation by adding further terms to the denominator. In this way also the inhibition of CO₂ on the steam reaction can be implemented and vice versa.

The complexity of LHHW formulations increases with the assumption of a more complex surface mechanism and the implementation of more gas compounds for the adsorption/desorption processes. For example, Mühlen et al. [Muehlen1985] derived a rate

⁵In a two site process one CO₂ molecule adsorbs at two active sites which influences the reaction mechanism and therefore the model equation. Further information are found in [Laurendeau1978].

equation for the interaction of H₂O and CO₂ gasification of the following form

$$r = \frac{r_1 p_{CO_2} + r_9 p_{H_2O} + r_8 p_{CO_2}^2 + r_{14} p_{H_2O} p_{CO_2} + r_{11} p_{H_2O}^2 + r_{13} p_{CO_2} p_{H_2} + r_{12} p_{H_2O} p_{H_2}}{1 + r_2 p_{CO_2} + r_{10} p_{H_2O} + r_3 p_{CO} + r_5 p_{H_2}} \quad (4.34)$$

Each of the parameters r_i in the equation has Arrhenius form and is described by a pre-exponential factor and an activation energy. In order to validate the model, it is required to extract all the 22 parameters from experimental data by fitting procedures. Despite the sophisticated theoretical mechanism that was derived for the model, it is not desired to develop very complex formulations. For practical issues, there will always be a trade-off between a complex model derivation from first principles based on physical and chemical basics and an empirical simplification to improve the applicability of the model.

In Table 4.2 different model equations are compared in terms of their complexity and number of adjustable parameters.

Table 4.2: Comparison of different model equations for the heterogeneous char reactions under Regime I conditions

Model type	Experimental parameters	Model parameters	Adjustable parameters
Arrhenius (0th order)	T	k_0, E_A	2
Arrhenius (nth order) for CO ₂ and H ₂ O	T, p_{CO_2}, p_{H_2O}	$k_{0,i}, E_{A,i}, n_i$ $i = CO_2, H_2O$	6
LH (simple) $r = k_i \cdot p_i / (1 + K_i \cdot p_i)$	T, p_{CO_2}, p_{H_2O}	k_i, K_i $i = CO_2, H_2O$	8
LHHW (product gas inhibition)	T, p_i $i = CO_2, H_2O, CO, H_2$	k_j, K_j $j = CO_2, H_2O$	12

4.2.3.2 Definition of Different Intrinsic Char Reactivity Models

Based on the short literature review in the previous section, different levels of models for the heterogeneous char gasification are now defined. With increasing level number, the complexity of the model increases and more experimental data are required to derive the adjustable parameters. On the other hand, at a higher level also the predictive quality and the accuracy improve.

The model equations presented here or similar formulations can be found in literature. The definition of different levels enables a structured application of the models to experimental data in subsequent chapters.

Intrinsic Model - Level 1 - nth Order The influence of temperature is modelled by an Arrhenius approach and the influence of reactant partial pressure is incorporated by an nth order term:

$$r_{intr,L1} = r(T, p_i) = k_{0L1,i} \cdot \exp\left[\frac{-E_{AL1,i}}{RT}\right] \cdot p_i^{n_i} \quad (4.35)$$

where $i = \text{CO}_2, \text{H}_2\text{O}$. The constants $k_{0L1,i} [g / (m^2 \cdot s \cdot \text{MPa}^{n_i})]$ describe the surface properties of the char. The model is valid over a range of partial pressures, but does not account for the saturation of the char surface at higher pressure. Therefore, it likely overestimates the reaction rate at high pressure if there are no experimental data available. However, the Level 1 model can predict the influences of temperature and reactant partial pressure well.

Intrinsic Model - Level 2 - Simple LH In pressurised entrained flow gasifiers the partial pressures of the reactant gases CO_2 and H_2O are high and therefore saturation effects at the char surface might play a role. The Level 2 intrinsic reactivity model is based on simple LH rate equations for CO_2 and H_2O gasification:

$$r_{intr,L2} = \frac{k_{0L2,i} \cdot \exp\left[\frac{-E_{AL2,i}}{RT}\right] \cdot p_i}{1 + K_{0L2,i} \cdot \exp\left[\frac{-E_{aL2,i}}{RT}\right] \cdot p_i} \quad (4.36)$$

where again $i = \text{CO}_2, \text{H}_2\text{O}$. The four pre-exponential factors $k_{0L2,i} [g / (m^2 \cdot s \cdot \text{MPa})]$ and $K_{0L2,i} [1/\text{MPa}]$ and the four activation energies can be fitted to experimental data. A mutual influence of CO_2 and H_2O gasification is not implemented and also the inhibition by the adsorption of product gases is not considered. Despite the relative simple approach, a total of eight adjustable parameters have to be derived from experimental data.

Intrinsic Model - Level 3 - LHHW Kinetics The adsorption of gases at the char surface, the chemical reaction, and the desorption of products is considered by Langmuir-Hinshelwood-Hougen-Watson (LHHW) kinetic rate equations [Belfiore2003]. The final rate equation is dependent on the reaction mechanism that is assumed.

First, the gasification of char with CO_2 is considered. A widely applied ideal reaction mechanism is used that successfully correlates to experimental data [Laurendeau1978]. The reaction mechanism is assumed to consist of two steps. In the first step the CO_2 adsorption equilibrium is assumed on the char surface.



CO_2 adsorbs at an active carbon site (C^*). One oxygen atom remains at the surface, and an active CO-complex (CO^*) and gaseous CO is formed. Equation 4.37 is in chemical equilibrium and the position of the equilibrium is determined by the equilibrium constant K_{CO_2} . Simultaneously, other gases adsorb at the char surface. The adsorption of the other gases is also described by an equilibrium constant K_j for each gas. The coverage of the surface with the CO-complex is calculated to be

$$\Theta_{\text{CO}^*} = \frac{(K_{\text{CO}_2} \cdot p_{\text{CO}_2})^{1/\gamma_{\text{CO}_2}}}{1 + (K_{\text{CO}_2} \cdot p_{\text{CO}_2})^{1/\gamma_{\text{CO}_2}} + \sum_j (K_j \cdot p_j)^{1/\gamma_j}} \quad (4.38)$$

where $j = \text{H}_2\text{O}, \text{CO}, \text{H}_2$ if only main gas components are considered and the adsorption of N_2 is neglected. γ is the number of active sites that are required for the adsorption of

one gas molecule.

In a second step the CO-complex desorbs from the char surface



As it is assumed that Equation 4.37 is in chemical equilibrium and therefore very fast, the desorption of the CO-complex is the rate-determining step. Assuming $\gamma = 1$ for all gases, the rate of CO₂ gasification is

$$r_{C,CO_2} = k_{des,CO_2} \cdot \Theta_{CO} = \frac{k_{des,CO_2} \cdot K_{CO_2} \cdot p_{CO_2}}{1 + K_{CO_2} \cdot p_{CO_2} + \sum_j K_j \cdot p_j} = \frac{k_{CO_2} \cdot p_{CO_2}}{1 + K_{CO_2} \cdot p_{CO_2} + \sum_j K_j \cdot p_j} \quad (4.40)$$

where $k_{CO_2} = k_{des,CO_2} \cdot K_{CO_2}$.

Analogous to CO₂ gasification, a model for the intrinsic reaction rate of steam gasification is derived. Again, a two step mechanism is assumed



which results in the following rate equation

$$r_{C,H_2O} = k_{des,H_2O} \cdot \Theta_{CO} = \frac{k_{des,H_2O} \cdot K_{H_2O} \cdot p_{H_2O}}{1 + K_{H_2O} \cdot p_{H_2O} + \sum_j K_j \cdot p_j} = \frac{k_{H_2O} \cdot p_{H_2O}}{1 + K_{H_2O} \cdot p_{H_2O} + \sum_j K_j \cdot p_j} \quad (4.43)$$

As CO₂ and H₂O form different oxide complexes (CO*) that desorb at different rates [Liu2004], the rate constants $k_{des,i}$ are different. The units of k_i and $K_{i,j}$ are equal to the Level 2 model.

In the general form, the Level 3 model for intrinsic reactivity is

$$r_{intr,L3,i} = \frac{k_{L3,i} \cdot p_i}{1 + K_{L3,i} \cdot p_i + \sum_j K_{L3,j} \cdot p_j} \quad (4.44)$$

and

$$k_{L3,i} = k_{OL3,i} \cdot \exp \left[-E_{AL3,i} / (RT) \right] \quad (4.45)$$

$$K_{L3,i} = K_{OL3,i} \cdot \exp \left[-E_{aL3,i} / (RT) \right] \quad (4.46)$$

$$K_{L3,j} = K_{OL3,j} \cdot \exp \left[-E_{aL3,j} / (RT) \right] \quad (4.47)$$

4.2.4 Selection of a Submodel for the Variation of Reaction Rate with Conversion

In literature, different models are proposed that describe the variation of reaction rate as a function of char conversion x . Simple models do not consider char structural changes during reaction. The homogeneous model and the non-reacted core model are examples

of simple models [Molina1998]:

Homogeneous model

$$\frac{dx}{dt} = k \cdot (1 - x) \quad (4.48)$$

The mass specific reaction rate ($dm/dt/m$) does not change with conversion. The conversion rate dx/dt is reduced with conversion as less char is available in the later stages of reaction. Any variations of particle diameter, density, and surface area are not considered by the model equation.

Non-reacted core model

$$\frac{dx}{dt} = 3k \cdot (1 - x)^{2/3} \quad (4.49)$$

The char particle is represented by a solid sphere. The reaction only occurs at the outer surface of this sphere and the radius decreases as the gasification reactions advance. The particle density remains constant and the model does not consider the specific surface area. The non-reacted core model is most suited for reactions occurring under Regime III conditions.

In both models k is the kinetic constant. Other models are the Johnson model, the Dutta and Wen model, the Modified Volumetric model, and the Unification Theory model [Molina1998].

Due to the implementation of intrinsic kinetic data, the knowledge of specific surface area and its variation with conversion is important. During devolatilisation char particles with an initial specific surface area are generated. This surface can then change during conversion and the variation of reaction rate can be attributed to a change in surface area.

The most applied structural model that predicts surface area evolution is the Random Pore Model (RPM) derived by Bhatia and Perlmutter [Bhatia1980, Bhatia1981]. It predicts the total surface area at any given conversion x as a function of initial surface area and a pore structure parameter Ψ . Initially, the pore diameter grows due to conversion and the surface area increases. The effect is then overshadowed by the intersection of the growing surfaces in the later stages of conversion which results in a reduction of surface area. The variation of surface area with carbon conversion is described by [Feng2003b]:

$$S_v = S_{v0} \cdot (1 - x) \cdot \sqrt{1 - \Psi \ln(1 - x)} \quad (4.50)$$

$$S_g = S_{g0} \cdot \sqrt{1 - \Psi \ln(1 - x)} \quad (4.51)$$

where S_v, S_{v0} are instantaneous and initial surface areas on a volume basis [m^2/m^3] and S_g, S_{g0} are instantaneous and initial surface areas on a mass basis [m^2/g]. The initial random pore model has been further extended to correlate to solids that are dominated by micropores (Discrete Random Pore Model, [Bhatia1996]) and to model the change of surface reactivity with conversion (Modified Discrete Random Pore Model, [Gupta2000]). In spite of the mathematical modifications, the initial RPM is frequently used to describe the evolution of char surface area. Kajitani et al. [Kajitani2002] used the RPM equation on a volume basis (Equation 4.50) to relate mass specific surface area [m^2/g] to char conversion in a drop tube furnace. For steam gasification in the PDTF the parameter Ψ was 14 when fitted to surface area data for an Australian bituminous coal char. However,

the authors used $\Psi = 3$ for the modelling of conversion rates at high temperature. In their later publication [Kajitani2006], the Random Pore Model (Equation 4.50) was used to describe surface area (CO_2 -BET) on a volumetric basis (m^2/m^3). For an American bituminous coal char, Ψ was 10, and for a Chinese bituminous coal char, $\Psi=1$.

Matsumoto et al. [Matsumoto2009] used the RPM to model the surface variation of a biomass char during drop tube gasification and derived a value of 10 for the structure parameter Ψ .

Also at lower temperature, the RPM is used to describe the variation of the char conversion rate in TGAs. Feroso et al. [Feroso2009] derived values of Ψ from 0.5 to 15.2 for the CO_2 gasification of wood char.

The structural parameter Ψ can theoretically be calculated from the initial length of the non-overlapped pore system, the initial porosity, and the initial volume specific surface area [Bhatia1980]. As in the most cases, at least the length of the non-overlapped pore system is not known, Ψ is used as a fitting parameter to adjust the RPM to experimental data.

Several experimental studies attribute the variation of reaction rate with conversion to a change of the specific char surface area. As the model development in this dissertation is based on intrinsic reactions, the RPM is used as a submodel to describe the influence of char conversion on surface area and therefore also on observed gasification rate.

The RPM assumes that the particle diameter does not change with conversion as pore growth occurs within the particle structure. This is only valid under Regime I conditions. The variation of the particle diameter with conversion is considered by a different submodel in Section 4.2.8. As pore diffusion limitations result in a larger pore growth near the outer particle surface compared with the particle centre, the RPM is strictly speaking only valid under Regime I conditions. However, the local deviations of the surface area development within the char particle require more sophisticated model approaches that would make the application of the model difficult.

4.2.5 Development of Submodel for the Influence of Thermal Deactivation on Intrinsic Reactivity

Thermal annealing is a fast process that can reduce the reactivity of chars in very short time scales. However, char conversion under entrained flow conditions occurs within a few seconds and it is a priori not clear if an annealing process could substantially decrease the reactivity before the complete carbon conversion is achieved. Senneca et al. [Senneca1997] compared time scales that were measured for annealing processes in literature with estimated conversion rates of char in CO_2 and O_2 up to 1800°C . The combustion was at least one order of magnitude faster than the CO_2 gasification. The time scales of thermal annealing varied over more than one order of magnitude even for similar reaction temperatures, but generally decrease significantly with increasing temperature. Despite the broad scatter in the annealing data, Senneca et al. concluded that combustion is generally much faster than annealing, with possible exceptions at very high temperatures ($>1600^\circ\text{C}$), and CO_2 gasification and annealing are likely to take place over comparable time scales.

Therefore, it can be important to include a thermal deactivation submodel in a modelling

approach for entrained flow gasification. Due to the slower reaction during entrained flow gasification compared with combustion, a thermal annealing submodel could predict the decreasing reaction rates at the later stages of conversion. First a short literature review on model approaches for thermal annealing is presented, and then a simple model and a more comprehensive model are developed.

4.2.5.1 Literature Review on Modelling Thermal Deactivation

The loss of char reactivity at high temperature during devolatilisation and char conversion is observed in several experimental studies. Only a few models are found in literature that predict the influences of peak temperature and time at temperature on the loss of char reactivity, and only one model is found that describes thermal annealing for entrained flow gasification.

Cai et al. [Cai1996] used an empirical correlation to relate the standard reactivity in a TGA experiment to the peak temperature during pyrolysis in a wire mesh reactor. The experimental data could be represented by:

$$\ln R_{max} = a - b \cdot T \quad (4.52)$$

where R_{max} is the maximum char reactivity in air at 500°C (TGA measurement), T is the pyrolysis temperature in the wire mesh reactor, and a and b are empirical parameters. Experimental data compared with the adjusted model are shown in Figure 4.2. This model can only relate the loss of reactivity in a constant time interval. Predictions of the deactivation process with time are not possible. For this purpose more complex approaches are required.

The classic model that is used to describe the high temperature time dependent oxidation behaviour of chars is the Nagle and Strickland-Constable (NSC) model [Suuberg1991]. In the NSC model there are two distinct types of carbon surface atoms: sites A that are considered to be active sites and sites B that are rather unreactive. The reaction at the active sites is represented by



and the rate of reaction is expressed by a LH type equation

$$Rate = \frac{k_A \cdot p \cdot s}{1 + k_Z \cdot p} \quad (4.54)$$

where s is the surface fraction of A sites. The reaction of the unreactive sites is assumed to be



Therefore, new reactive sites A are produced during the reaction of the B sites. The reaction rate of B sites is represented by

$$Rate = k_B \cdot p \cdot (1 - s) \quad (4.56)$$

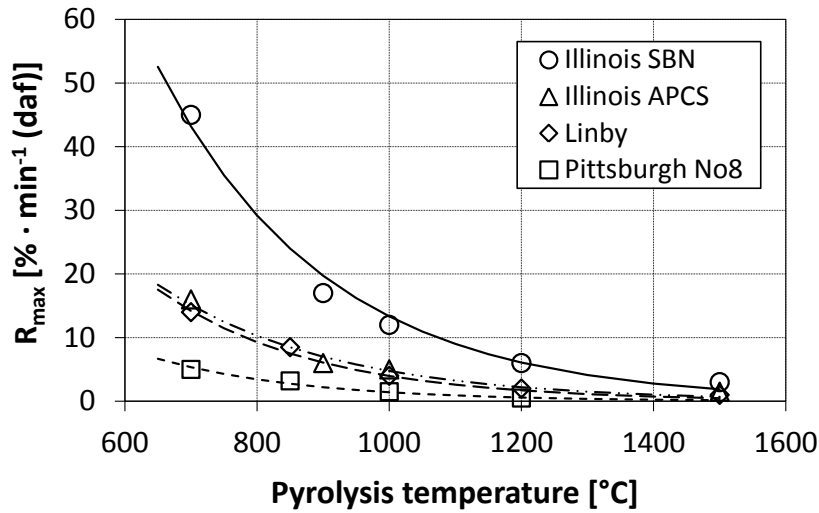


Figure 4.2: Reactivity (measured in a TGA in an oxygen atmosphere) of coal chars produced in a wire mesh reactor (helium atmosphere, heating rate 1000 K/s, holding time 2 s) as a function of pyrolysis temperature. Lines denote the model prediction (diagram derived from [Cai1996])

The A sites can react to unreactive B sites by a thermal annealing process that is modelled by a simple first order reaction



$$Rate = k_T \cdot s \quad (4.58)$$

where k_T is expressed by an Arrhenius type equation. Suuberg [Suuberg1991] proposed an activation energy for k_T of 406 kJ/mol and a pre-exponential factor of $6.3 \times 10^{12} \text{ s}^{-1}$. When assuming a stationary state during the reaction, the surface fraction s is constant and the overall rate of combustion is

$$rate = \frac{k_A \cdot p \cdot s}{1 + k_Z \cdot p} + k_B \cdot p \cdot (1 - s) \quad (4.59)$$

where

$$(4.60)$$

$$s = [1 + (k_T/k_B \cdot p)]^{-1} \quad (4.61)$$

The NSC model requires four activation energies and four pre-exponential factors that have to be derived from experimental data. Therefore, a large set of experiments is required to derive the adjustable parameters before the application of the model is possible.

In the NSC model, only two types of reaction sites are considered and the annealing is caused by a transition of the two types. In reality, many distinct chemical processes are contributing to thermal annealing. With increasing temperature some of these processes reach completion, and others just occur. Models of such a situation generally involve the concept of a distribution of activation energies for different reactions [Suuberg1991]. The fraction of active sites s/s_0 is then expressed by an integration over all sites and times

[Suuberg1991]:

$$\frac{s}{s_0} = \int_0^\infty \left(\exp \left[\int_0^t -A \cdot \exp(-E/(RT)) dt \right] \cdot f(E) \right) dE \quad (4.62)$$

where

$$f(E) = \frac{1}{\sigma \sqrt{2\pi}} \exp \left[- (E - E_0)^2 / (2\sigma^2) \right] \quad (4.63)$$

The distribution of activation energies can be expressed in a Gaussian form where σ is the standard deviation and E_0 is the mean of the distribution. Alternatively, the distribution of activation energies can be based on a shifted Γ -distribution or any other mathematical form. More information about this approach and a comparison to experimental data can be found in the review paper of Suuberg [Suuberg1991].

Zolin et al. [Zolin2001] combined an annealing model (distributed activation energy) with a char oxidation model and compared the results to experimental data from a combustion laminar flow reactor. Feng et al. [Feng2003] further improved this approach. However, the solution of distributed activation energy models is quite complex due to the activation energy distributions and the double integral.

The only annealing model that has been derived for CO_2 gasification is that of Salatino et al. [Salatino1999]. They used their experimental data derived from a TGA and a heated-strip reactor. A bituminous coal was heated in nitrogen to a final temperature with a defined heating rate followed by CO_2 gasification in a TGA at lower temperature. The data set is described by a kinetic annealing model. The course of annealing is quantified by an internal coordinate ξ ($\xi = 0$ for the non-annealed char and $\xi=1$ for the fully annealed one). The overall gasification rate is then expressed as a linear combination of the reactivity of the non-annealed (R_0) and the fully annealed char (R_∞)

$$R = R_0(1 - \xi) + R_\infty \cdot \xi \quad (4.65)$$

The variation of the coordinate ξ is modelled by a non-linear kinetic equation

$$\frac{d\xi}{dt} = k(T_{HT}) \cdot (1 - \xi)^n \quad (4.66)$$

where T_{HT} is the annealing temperature and $k(HT)$ is expressed by an Arrhenius type equation. It is assumed that the reactivity of the fully annealed char is negligible ($R_\infty = 0$). The annealing is then expressed by a thermo-deactivation factor with respect to an arbitrarily selected reference char whose gasification reactivity is R_0

$$\frac{R}{R_0} = \left([(n-1) \cdot k(T_{HT})]^{-1/(n-1)} \right) t_{HT}^{-1/(n-1)} \quad (4.67)$$

The model requires information about the activation energy and the pre-exponential factor in the $k(T_{HT})$ term, the parameter n , and the reactivity of the reference char.

Liu et al. [Liu2004b] report in their modelling study that a dynamic annealing model is incorporated and that the deactivation is implemented in the pre-exponential factors of their rate equation. However, they only publish a general equation of the form

$$A_i/A_{i0} = f(T_{HT}, t_{HT}) \quad (4.68)$$

and do not provide any other information. In the extended version of the carbon burnout kinetic model CBK/E that describes coal combustion, thermal annealing is based on a distributed activation energy model [Niksa2003]. The annealing rates are assumed to be so fast that the maximum temperature often determines the reduction of reactivity. The detailed annealing model is not described.

In entrained flow gasification, experimental data of annealing are rare and annealing mechanisms are not considered in state of the art model approaches. For example, Kajitani et al. [Kajitani2006] who published a char conversion model validated by experimental data did not consider char deactivation in their approach and used constant char reactivity throughout the conversion process.

No thermal char deactivation model is found in the open literature that describes the loss of char reactivity in a high temperature entrained flow gasifier. As annealing occurs in the time scales that are needed for fuel conversion, a thermal deactivation model could predict the loss of reactivity in the later stages of conversion and could improve the predictability of reaction rates in high temperature gasification.

4.2.5.2 Development of a Simple Thermal Deactivation Model for Chars

In the simple approach, only the influence of maximum temperature is considered as the maximum temperature even at a very short residence time is the main parameter that affects annealing [Beeley1996, Feng2003]. The model is based on the empirical equation (4.52) derived by Cai et al. [Cai1996]. This equation describes the effect of maximum temperature on the char reactivity typically measured in TGAs at lower temperature. The empirical equation requires two parameters that are adjusted to experimental data.

It is assumed that thermal deactivation is related to a loss of active sites on the char surface. With increasing temperature the concentration of active sites decreases. In each char gasification model (Level 1 to 3) the pre-exponential factor is a measure for the concentration of active sites. Therefore, thermal deactivation is assumed to lower the pre-exponential factor in each model equation. The ratio of the pre-exponential factors is defined as

$$A = \frac{k_{0Li,T}}{k_{0Li,T_{max}}} \quad (4.69)$$

where $k_{0Li,T}$ is the pre-exponential factor at the current gasification temperature and $k_{0Li,T_{max}}$ is the pre-exponential factor for a highly deactivated char. For the measurement of $k_{0Li,T_{max}}$ a char from a high temperature experiment in an entrained flow reactor is required. T_{max} is the maximum temperature in the entrained flow experiment. Alternatively, a realistic high temperature char can also be produced in a WMR that is capable of very high temperatures. The production of char in a high temperature TGA is questionable as the heating rate is usually low and volatiles are not removed from the char surface.

Equation 4.52 is modified by a normalisation with experimental data from the high temperature char

$$A = \frac{k_{0Li,T}}{k_{0Li,T_{max}}} = \exp \left[a - b \frac{T}{T_{max}} \right] \quad (4.70)$$

For $T = T_{max}$ the two adjustable parameters a and b are equal, and the equation can further be simplified

$$A = \frac{k_{0Li,T}}{k_{0Li,T_{max}}} = \exp \left[\omega \cdot \left(1 - \frac{T}{T_{max}} \right) \right] \quad (4.71)$$

where ω is the only adjustable parameter in the simple deactivation model. For the determination of ω , reactivity data of chars that are produced at different temperatures are required.

4.2.5.3 Development of a More Comprehensive Deactivation Model for Chars

In the more complex approach, the deactivation model for char reactivity describes the effects of temperature and time on the reactivity of the char surface. The influence of heating rate is not considered separately as it is not independent from temperature and time at temperature. Furthermore, only experimental data of chars that are produced at high heating rate (i.e. WMR and EFR) are used for the validation of the model. Similar to the approaches of Nagle and Strickland-Constable (NSC) [Suuberg1991] and Salatino et al. [Salatino1999], two different active sites on the char surface are considered. The sites F are produced during devolatilisation and are very reactive. With increasing heat treatment severity these sites are converted to sites D that are deactivated and are therefore less reactive. The heterogeneous char gasification occurs at both types of sites. The concept is graphically shown in Figure 4.3. The formulation of the reaction rates r_{Fresh} and r_{Deact} is dependent on the model for char intrinsic reactivity. The intrinsic reaction rate at the fresh sites is

$$r_{Fresh} = f \cdot k_{0Li,f,i} r'_{intr,Li} \quad (4.72)$$

where f is the fraction of fresh sites ($0 \leq f \leq 1$), $k_{0Li,f,i}$ is the pre-exponential factor for fresh sites in each of the intrinsic model rate equations, and $r'_{intr,Li}$ is the remaining term of the intrinsic rate equation. It is assumed that thermal deactivation only influences the pre-exponential factor and does not have an effect on activation energies and other model

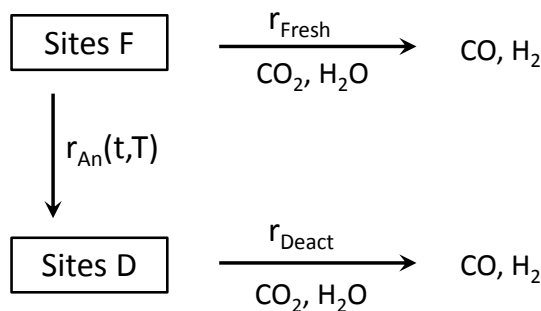


Figure 4.3: Concept of a simple thermal deactivation model based on two different types of active sites on the char surface

parameters. The assumption is supported by literature data (e.g. [Beeley1996, Shim2000]) and own experimental data shown later.

The intrinsic reaction rate for the deactivated sites is

$$r_{Deact} = (1 - f) \cdot k_{0Li,d,i} \cdot r'_{intr,Li} \quad (4.73)$$

When defining $A_{max} = k_{0Li,f,i}/k_{0Li,d,i}$, the total reaction rate becomes

$$r_{total} = r_{Fresh} + r_{Deact} \quad (4.74)$$

$$= [1 + f \cdot (A_{max} - 1)] \cdot k_{0Li,d,i} \cdot r'_{intr,Li} \quad (4.75)$$

where A_{max} is the reactivity ratio of a fresh char to a highly deactivated char. A_{max} is a fuel specific parameter and is constant during the reaction. In literature this ratio has been measured in TGA experiments at lower temperature and typical values are 20 [Hindmarsh1995], 30 to 50 [Beeley1996], and 50 [Cai1996]. The highest reported value is about 15000 for a lignite between 700°C and 2500°C [Shim2000].

The loss of fresh sites is time and temperature dependent and is approximated by a simple first order Arrhenius type equation

$$r_{An} = -\frac{df}{dt} = F_0 \cdot e^{-E_{A,F}/(RT)} \cdot f \quad (4.76)$$

where F_0 is the pre-exponential factor in the thermal annealing model and $E_{A,F}$ is the activation energy.

After the determination of intrinsic reactivity of a fresh and a deactivated char the thermal deactivation model can be described by

$$r_{intr} = [1 + f \cdot (A_{max} - 1)] \cdot k_{0Li,i} \cdot r'_{intr,Li} \quad (4.77)$$

$$A_{max} = \frac{k_{0Li,i,max}}{k_{0Li,i}} = \frac{\text{initial reactivity}}{\text{reactivity of deactivated char}}$$

$$f = \exp \left[-F_0 \cdot e^{-E_{A,F}/(RT)} \cdot t \right]$$

4.2.6 Submodel for Mass Transport Limitations under Regime II Conditions - Pore Diffusion

The quantitative description of the interaction of pore diffusion and chemical reaction at the char surface is only possible by using elaborate mathematical formulations. First, in Section 4.2.6.1 the basic modelling of diffusion-reaction processes is summarised and the effectiveness factor approach is introduced. Then, in Section 4.2.6.2 the fundamentals are used to derive diffusion-reaction models for the three levels of the intrinsic rate equations. As the gas diffusivity is an important parameter in the effectiveness factor approach, the fundamentals of gas diffusion are briefly described in Section 4.2.6.3.

4.2.6.1 Fundamentals about Pore Diffusion Limitations

During char gasification at high temperature, chemical surface reactions occur simultaneously to mass transfer processes within the porous char structure. Due to mass transfer limitations a gas concentration gradient within the char particle might be established and the surface in the particle centre is exposed to a lower reactant concentration (CO_2 , H_2O) than the surface near the particle external surface.

As the reaction within a porous structure is comparable to heterogeneous catalysis, most of the theoretical development is similar. However, due to the progressing conversion of char and the resulting continuously change in the pore structure, particle density, and size, the development of a model for mass transfer limitations in char gasification is a difficult task.

The historical development of quantitative descriptions of the factors that determine mass transfer limitations for porous catalysts is summarised by Satterfield [Satterfield1981]. The effect of diffusion is described by the effectiveness of a porous structure. An effectiveness factor is defined that accounts for all intraparticle diffusion effects. The effectiveness factor η is the ratio between observed reaction rate and proposed reaction rate if the reactant concentration at the particle outer surface c_s were constant throughout the particle [Bischoff1965]:

$$\eta = \frac{\text{observed reaction rate considering diffusion}}{\text{total rate if total internal surface were exposed to } c_s} \quad (4.78)$$

For the mathematical analysis of simultaneous reaction and diffusion processes, the porous particle in Figure 4.4 is considered. Within the particle (radius R) a spherical shell of thickness dr and radius r is located. The theoretical treatment of this simple system is based on the following assumptions [Satterfield1981]:

- the porous structure is isothermal;
- diffusion within the particle can be described by Fick's first law and an invariant effective diffusion coefficient, i.e. $J = -D_{eff}(dc/dr)$;
- the reaction involves a single reactant i , is irreversible, and the intrinsic rate is represented by an n th order rate equation, i.e. $k_S c_i^n$ (the index S denotes that the reaction rate is based on specific surface area).

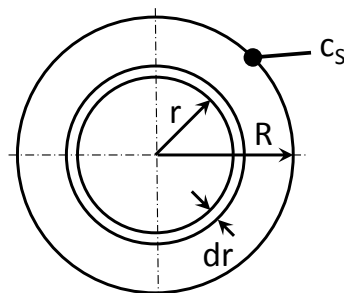


Figure 4.4: Spherical porous particle that is exposed to simultaneous diffusion and reaction

At steady state, a mass balance at the spherical shell results in

$$\begin{aligned} & (\text{Inward diffusion at } r+dr) - (\text{Inward diffusion at } r) \\ & = \text{Rate of reaction within the differential shell} \end{aligned} \quad (4.79)$$

$$4\pi(r+dr)^2 D_{eff} \left[\frac{dc}{dr} + \frac{d^2c}{dr^2} dr \right] - 4\pi r^2 D_{eff} \frac{dc}{dr} = (4\pi r^2 dr) S_v k_s c^n \quad (4.80)$$

where $4\pi r^2$ is the inner superficial area of the differential shell, D_{eff} is the effective diffusion coefficient, dc/dr is the concentration gradient at the radius r , and S_v is the volumetric surface area [m^2/m^3].

Equation 4.80 can be transformed to:

$$\frac{d^2c}{dr^2} + \frac{2}{r} \frac{dc}{dr} = \frac{S_v k_s c^n}{D_{eff}} \quad (4.81)$$

This differential equation describes the concentration gradient within a spherical porous particle. The right side of Equation 4.81 is simplified by defining a dimensionless quantity, termed the Thiele modulus ϕ_{sph} named after Thiele [Thiele1939], one of the fundamental researchers in this field:

$$\phi_{sph} = R \sqrt{\frac{S_v k_s c_s^{n-1}}{D_{eff}}} = R \sqrt{\frac{k_v c_s^{n-1}}{D_{eff}}} \quad (4.82)$$

where $k_v = S_v \cdot k_s$ is the reaction rate constant per unit of gross volume of the porous structure, and the subscript of ϕ_{sph} is to express the spherical geometry. Originally, Thiele [Thiele1939] developed the model for plane geometry.

For the solution of the differential equation, a first order reaction ($n=1$) is assumed. The Thiele modulus then becomes independent of concentration. The boundary conditions are

- $c = c_s$ at $r = R$ (constant concentration at the outside of the particle);
- $dc/dr = 0$ at $r = 0$ (no concentration gradient in the centre of the sphere).

The solution is derived following the procedure of Satterfield [Satterfield1981]. As a result, the concentration profile within the porous particle is dependent only on the Thiele modulus and the normalised distance r/R :

$$\frac{c}{c_s} = \frac{\sinh(\phi_{sph} \cdot r/R)}{(r/R) \sinh \phi_{sph}} \quad (4.83)$$

Using the concentration profile, the total reaction rate throughout the whole particle is obtained by an integration of the reaction rate in the spherical annulus over the entire particle. A simpler solution is achieved by recognising that the observed reaction rate is equal to the mass transfer rate into the particle:

$$r_{obs} = r_{ex} = 4\pi R^2 D_{eff} \left(-\frac{dc}{dr} \right)_{r=R} \quad (4.84)$$

After a differentiation of Equation 4.83 and the substitution of the result in Equation 4.84, the reaction rate throughout a spherical porous particle is calculated [Satterfield1981]:

$$r_{obs} = 4\phi_{Sph}\pi R D_{eff} c_S \left[\frac{1}{\tanh \phi_{Sph}} - \frac{1}{\phi_{Sph}} \right] \quad (4.85)$$

If no internal mass transfer limitations occur, i.e. under Regime I conditions, the rate would be

$$r_{obs} = \frac{4}{3}\pi R^3 k_v c_S \quad (4.86)$$

Following the definition in Equation 4.78, the effectiveness factor of the porous particle is the ratio of the two rates (Equation 4.85 and 4.86):

$$\eta_{Sph} = \frac{3}{\phi_{Sph}} \left[\frac{1}{\tanh \phi_{Sph}} - \frac{1}{\phi_{Sph}} \right] \quad (4.87)$$

and

$$\phi_{Sph} = R \sqrt{\frac{k_v c_S^{n-1}}{D_{eff}}} \quad (4.88)$$

Equation 4.87 is valid for a first order irreversible reaction in a sphere. The function is graphically shown in Figure 4.5. At low values of ϕ_{Sph} - under Regime I conditions - the effectiveness factor is unity. With increasing ϕ_{Sph} the overall rate is more and more limited by diffusion and η_{Sph} approaches $3/\phi_{Sph}$.

Analytical solutions relating η to ϕ are also developed in literature for other reaction rate equations and geometries.

Effectiveness factors for the n-th order rate equation Starting with the definition of the Thiele modulus in Equation 4.82, solutions for other nth order rate equations are derived. The mathematical procedure and example calculations can be found in literature [Belfiore2003].

Effectiveness factors in other geometries The simplest geometry for the mathematical analysis is a flat plate that is in contact with the gaseous reactants at one side and is sealed at the other side. The differential equation for this infinite or semi-infinite flat plate is [Satterfield1981]:

$$D_{eff} \frac{d^2 c}{dx^2} = c^n k_v \quad (4.89)$$

where x is the distance from the sealed side.

The Thiele modulus is defined as [Satterfield1981]:

$$\phi_{Pl} = L \sqrt{\frac{k_v c_S^{n-1}}{D_{eff}}} \quad (4.90)$$

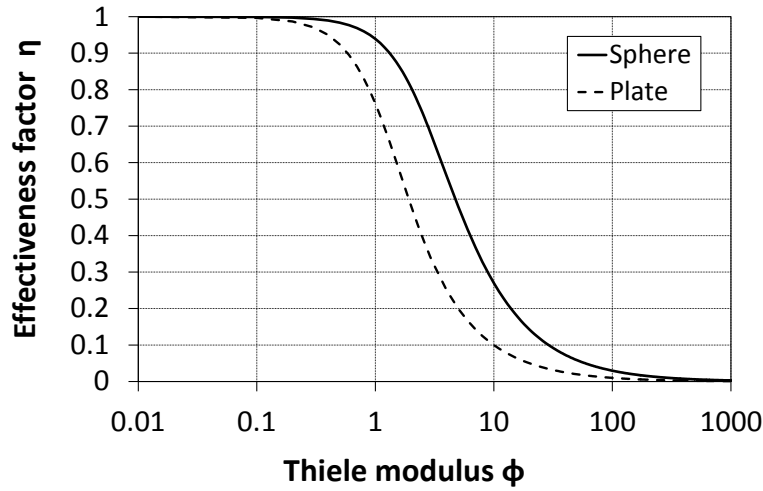


Figure 4.5: Functional dependency of effectiveness factor on Thiele modulus (spherical particle or flat plate, first order irreversible reaction)

where L is the thickness of the plate. If the plate is contacted by a reactive atmosphere from both sides, L is one-half of the thickness. Again, for a first-order irreversible reaction, the concentration term disappears and the solution for the effectiveness factor is [Satterfield1981]:

$$\eta_{pl} = \frac{\tanh \phi_{pl}}{\phi_{pl}} \quad (4.91)$$

Equation 4.91 is graphically shown in Figure 4.5. The definitions of the Thiele modulus for sphere and flat plate are different, but in both equations (4.87 and 4.91) the effectiveness factor approaches an asymptotic line at high Thiele moduli ($3/\phi_{sph}$ and $1/\phi_{pl}$). This is likewise true for any order reaction, although the magnitude of η at which the asymptotic relations are valid varies considerably with geometry and the nature of the kinetics [Satterfield1981].

General Treatment Bischoff [Bischoff1965] developed a general expression for the Thiele modulus in a semi infinite particle, referred to as the general modulus

$$\phi_{Gen} = \frac{L \cdot r(c_s)}{\sqrt{2}} \left[\int_0^{c_s} D_{eff}(\alpha) r(\alpha) d\alpha \right]^{-1/2} \quad (4.92)$$

where L is a characteristic length, r is an arbitrary rate expression, c_s is the gas concentration at the outer surface, D_{eff} is the effective diffusion coefficient and α is a substitute for the integration. This definition will result in all solutions for the effectiveness factor (arbitrary rate equation and geometry) coinciding for large ϕ_{Gen} and the differences are relatively small over the whole range of ϕ_{Gen} [Bischoff1965]. The coincidence of the solutions is also referred to as the general asymptotic solution. Earlier, Aris [Aris1957] used particle volume V_p and external surface area S_p to express the characteristic length L . In accordance with this definition, the general modulus can be used for arbitrary particle

shapes:

$$\phi_{Gen} = \left(\frac{V_p}{S_p} \right) \cdot r(c_s) \left[\int_{c_\infty}^{c_s} 2 \cdot D_{eff}(\alpha) r(\alpha) d\alpha \right]^{-1/2} \quad (4.93)$$

where c_∞ is the concentration in the particle centre or the boundary concentration for a semi infinite particle ($c_\infty = 0$ [Bischoff1965]). In case of a reversible reaction, c_∞ is the equilibrium concentration of the reactant, and in case of an irreversible reaction, $c_\infty = 0$ [Goto1990].

Equation 4.93 represents a general form of the Thiele modulus for heterogeneous reactions in porous particles. One must note that the calculation of the effectiveness factor slightly changes due to the shape uniformation of Aris [Aris1957]. For a spherical shape the effectiveness factor then is defined as⁶

$$\eta_{Sph} = \frac{1}{\phi_{Gen}} \left(\frac{1}{\tanh(3\phi_{Gen})} - \frac{1}{3\phi_{Gen}} \right) \quad (4.94)$$

The Equations 4.93 and 4.94 can now be used to derive formulations of the effectiveness factor for different rate equations and geometries. Equation 4.94 is the general asymptotic solution for large values of the effectiveness factor (arbitrary rate equation and spherical geometry).

4.2.6.2 Definition and Development of Different Models for Mass Transport Limitations under Regime II Conditions

The definition and the development of the combined reaction and diffusion models are based on the Equations 4.93 and 4.94. The char reactivity models derived in Section 4.2.3.2 are converted to Regime II conditions. The levels of model complexity therefore correspond to the intrinsic reactivity models.

The reaction rate in Regime I r_{intr} relates the conversion to the specific char surface.

$$r_{intr} \left[\frac{g}{m^2 \cdot s} \right] \quad (4.95)$$

In contrast, the reaction and diffusion formulations in Regime II are derived on a volumetric basis

$$r^{II} \left[\frac{g}{m^3 \cdot s} \right] \quad (4.96)$$

The two different definitions can be correlated by using the effectiveness factor, the specific surface area S , and the apparent density ρ_{app} of a char particle.

$$r^{II} = \eta \cdot \rho_{app} \cdot S \cdot r_{intr} \quad (4.97)$$

Pore Diffusion Model - Level 1 - nth Order In Level 1, the nth order rate equation is used to model the intrinsic reactivity. First, the units are converted to a volumetric

⁶Due to the shape uniformation in the general modulus (Equation 4.93, $V_p/S_p = d_p/6$ for a sphere) the mathematical formulation of the effectiveness factor for a spherical geometry is different to the initial formulation in Equation 4.87. For more information it is referred to [Aris1957] and [Bischoff1965].

basis and the partial pressure is substituted by mass concentration c_i assuming ideal gas behaviour.

$$r_{L1} = \eta_{L1} \cdot \rho_{app} \cdot S \cdot k_{0L1,i} \cdot \exp \left[\frac{-E_{AL1,i}}{RT} \right] \cdot \left(\frac{RT}{M_i} c_{S,i} \right)^{n_i} \quad (4.98)$$

In order to further show the influences of char density and surface area, these parameters are not summarised in a constant. As the partial pressure is temperature dependent, this effect is shown after the conversion to concentration units. In contrast to the exponential influence of temperature in the activation energy term, the influence of temperature on partial pressure is very low and is usually neglected in literature.

Following Equations 4.93 and 4.94, the general Thiele modulus and the effectiveness factor are calculated

$$\phi_{L1} = \frac{d}{6} \sqrt{\frac{\rho_{app} \cdot S \cdot k_{0L1,i} \cdot e^{-E_{AL1,i}/(RT)} (n_i + 1) (RT/M_i)^{n_i}}{2D_{eff,i}}} c_{S,i}^{n_i-1} \quad (4.99)$$

$$= \frac{d}{6} \sqrt{\frac{\rho_{app} \cdot S \cdot k_{0L1,i} \cdot e^{-E_{AL1,i}/(RT)} (n_i + 1) (RT/M_i)}{2D_{eff,i}}} p_{S,i}^{n_i-1} \quad (4.100)$$

$$= \frac{d}{6} \sqrt{\frac{\rho_{app} \cdot S \cdot r_{intr,L1} (n_i + 1) (RT/M_i)}{2D_{eff,i} \cdot p_{S,i}}} \quad (4.101)$$

$$\eta_{L1} = \frac{1}{\phi_{L1}} \left(\frac{1}{\tanh(3\phi_{L1})} - \frac{1}{3\phi_{L1}} \right)$$

Equation 4.94 is derived for a first order reaction. The effectiveness factor for n th order reactions can be approximated by the first order curve [Laurendeau1978]. Hong [Hong2000] calculated the maximum error that occurs from the approximation by the comparison to an exact numerical solution. The maximum error is 16% for $\phi = 0.7$ and $n = 0$, but is negligible for $\phi < 0.2$ and $\phi > 5$. For $n > 0.25$ the maximum error is always less than 10%. Equation 4.94 is also referred to as the general asymptotic solution of the effectiveness factor for a spherical geometry.

The adjustable parameters in the model are ρ_{app} , S , $D_{eff,i}$, $k_{0L1,i}$, n_i , and $E_{AL1,i}$. In entrained flow gasification the model should be implemented for CO_2 and H_2O gasification. When assuming that both reactions occur at the identical char surface area S , 10 parameters have to be measured, calculated, or derived from experimental data.

Beath [Beath1996] derived similar formulations and further included modifications to account for the effect of convective flow in the pore structure. Convective flow has to be considered if the product gas volume differs from the reactant gas volume which is true in case of the char gasification reactions. But, convective flow only increases the general Thiele modulus if the diffusion rate is limited by molecular diffusivity which occurs at larger pore diameters. As char has a microporous structure, Knudsen diffusion is expected to be more important and the effect of convective flow is assumed to be negligible.

Pore Diffusion Model - Level 2 - Simple LH The Level 2 intrinsic reactivity model is based on a simple LH rate equation. The model is transferred to a volumetric form and the partial pressure is substituted by concentration

$$r_{L2} = \eta_{L2} \cdot \rho_{app} \cdot S \frac{k_{0L2,i} \cdot e^{-E_{AL2,i}/(RT)} \cdot RT/M_i \cdot c_{S,i}}{1 + K_{0L2,i} \cdot e^{-E_{aL2,i}/(RT)} \cdot RT/M_i \cdot c_{S,i}} \quad (4.102)$$

In Level 2, the derivation of the Thiele modulus is complicated as the LH equation has to be integrated. The mathematical procedure leads to the following form

$$\phi_{L2} = \frac{d}{6} \cdot H_i \cdot \frac{a_i \cdot c_{S,i}}{1 + a_i \cdot c_{S,i}} \frac{1}{\sqrt{a_i \cdot c_{S,i} - \ln(a_i \cdot c_{S,i} + 1)}} \quad (4.103)$$

where

$$H_i = \sqrt{\frac{\rho_{app} S k_{0L2,i} e^{-E_{AL2,i}/(RT)} RT/M_i}{2D_{eff,i}}} \quad (4.104)$$

$$a_i = K_{0L2,i} e^{-E_{aL2,i}/(RT)} RT/M_i \quad (4.105)$$

The effectiveness factor is then derived using Equation 4.94. However, Equation 4.94 is valid for a first order reaction. The analytical solution for a LH rate equation is not possible, and therefore the general asymptotic solution (Equation 4.94) is used. Hong [Hong2000b] used a numerical solution for the effectiveness factor in a LH approach for char combustion and evaluated the maximum error that results from using the general asymptotic solution. The maximum error is 17 % at $\phi=0.707$. For $\phi < 0.2$ and $\phi > 5$ the error is negligible.

In Level 2, further variables are implemented into the model. In addition to the adjustable parameters in Level 1, these are $K_{0L2,i}$ and $E_{aL2,i}$. In entrained flow gasification the model should be implemented for CO₂ and H₂O gasification, which results in 14 parameters. Again, constant parameters can be contracted to reduce the number of variables.

There are only two studies in literature that combine a LH rate equation with an effectiveness factor approach. Hong et al. [Hong2000, Hong2000b] implemented an intrinsic LH rate equation in a conversion model for char combustion at high pressure and temperature. The model was compared with experimental data [Hong2000] and could quantitatively explain the effects of operation conditions. Liu et al. [Liu1999b] modelled the intra particle char-CO₂ reaction using a LH rate equation and implemented an effectiveness factor to account for pore diffusion. The model is able to predict local changes of surface area, local reaction rate, and carbon conversion, but numerical methods are required to derive the solution.

No theoretical development is known that derives an analytical effectiveness factor approach for char gasification based on a LH rate equation. The analytical solution derived here enables the straightforward implementation into a CFD software package or other simulation tools for gasification reactors.

Pore Diffusion Model - Level 3 - LHHW kinetics In entrained flow gasifiers the concentration of product gas is high, especially in the later stages of conversion. It is well known that gaseous products inhibit the reaction rate by the interaction with the char surface. LHHW kinetics that describe inhibition are used under Regime I conditions and predict the influence of product gas. So far, no mathematical or experimental approach is known, that considers product gas inhibition also under Regime II conditions for high pressure and high temperature fuel conversion.

The aim of the following mathematical derivation is to include the inhibition by product gases in an effectiveness factor approach. The intrinsic reaction rate is assumed to have LHHW form, according to Equation 4.40. The partial pressure is substituted by gaseous concentrations

$$r_{L3} = \eta_{L3} \cdot \frac{\rho_{app} \cdot S \cdot k_{L3,i} \cdot RT / M_i \cdot c_{S,i}}{1 + K_{L3,i} \cdot RT / M_i \cdot c_{S,i} + \sum_j K_{L3,j} \cdot RT / M_j \cdot c_{S,j}} \quad (4.106)$$

During reaction, a concentration gradient also develops for the product gas concentrations. The concentrations of CO and H₂ increase towards the char particle centre. The implementation of a concentration gradient for product gases would lead to a complex reaction and diffusion problem that is described by coupled differential equations for each gas component. A solution could then be derived by numerical calculations. However, a numerical procedure requires a lot of computing time and power, and would not lead to an analytical solution for the char reaction rate under Regime II conditions. Therefore, it is assumed that product gas concentrations are constant throughout the particle and equal to the gas concentrations at the outer char surface.

The Thiele modulus for the LHHW rate equation is derived from Equation 4.93:

$$\phi_{L3} = \frac{d}{6} G_i \frac{W_i \cdot c_{S,i}}{(1 + I_i + W_i \cdot c_{S,i})} \frac{1}{\sqrt{W_i \cdot c_{S,i} + (1 + I_i) \left[\ln \left(\frac{1 + I_i}{1 + I_i + W_i \cdot c_{S,i}} \right) \right]}} \quad (4.107)$$

where

$$G_i = \sqrt{\frac{\rho_{app} \cdot S \cdot k_{0L3,i} \cdot \exp \left[-E_{AL3,i} / (RT) \right] \cdot RT / M_i}{2D_{eff,i}}} \quad (4.108)$$

$$W_i = K_{L30,i} \cdot \exp \left[-E_{aL3,i} / (RT) \right] \cdot RT / M_i \quad (4.109)$$

$$I_i = \sum_j K_{0L3,j} \cdot \exp \left[-E_{aL3,j} / (RT) \right] \cdot RT / M_j \cdot c_{S,j} \quad (4.110)$$

Similar to the other levels, the effectiveness factor is calculated using Equation 4.94. As again the general asymptotic solution of the effectiveness factor is used, the analytical calculation presented here is only an approximation of the mathematical system. A numerical solution of the LHHW approach similar to the work of Hong [Hong2000] would be required to evaluate the maximum error of the analytical solution.

4.2.6.3 Fundamentals of Gas Diffusion within a Porous Particle

When mass transport limitations are involved, the diffusion of gases through porous char particles is described by the effective diffusion coefficient D_{eff} . Its quantity is required to calculate the reaction rate under Regime II conditions. In a porous char structure the transport of gas molecules can be influenced by molecular and Knudsen diffusion.

Molecular Diffusion In molecular diffusion one gas diffuses through another and the diffusion rate is limited by the collisions of the gas molecules. Binary diffusion coefficients with an accuracy of about 10 % can be calculated from a semi-empirical equation [Baerns2002]:

$$D_M(T, p_{total}) = \frac{18.583 \cdot T^{3/2} \cdot \sqrt{\frac{M_1 + M_2}{M_1 \cdot M_2}}}{p_{total} \cdot \sigma^2 \cdot \Omega} \left[\frac{cm^2}{s} \right] \quad (4.111)$$

where T [in K] is the gas temperature, M_i [in g/mol] are the molar masses, p_{total} [in 10^5 Pa] is the total pressure, Ω is the collision integral, and σ is the binary power constant of the Lennard Jones Potential. The equation is based on the kinetic gas theory. Values of Ω and σ for different binary gas mixtures can be calculated from tabulated parameters [Baerns2002].

As in the majority of cases more than two components are involved in real systems, diffusion can only be calculated by more complex approaches. However, binary diffusion coefficients are a good approximation for multicomponent mixtures.

Knudsen Diffusion If the gas pressure or the pore diameter in a porous structure are small, the diffusing molecules collide more often with pore walls than with other gas molecules. Then, the diffusion coefficient in a cylindrical pore is calculated from the kinetic gas theory [Baerns2002]:

$$D_K = \frac{d_{pore}}{3} \sqrt{\frac{8 \cdot R \cdot T}{\pi \cdot M_i}} \quad (4.112)$$

where d_{pore} is the pore diameter, R is the gas constant, M_i the molecular weight of the gas, and T the gas temperature. Knudsen diffusion is independent of the gas pressure.

Calculation of the Effective Diffusion Coefficient So far, molecular and Knudsen diffusion are considered in an unaffected gas atmosphere or in an ideal pore. In real porous structures diffusion is limited to the void space of the particle. Thus, the effective diffusion coefficient is calculated from the molecular or Knudsen diffusivity and the particle porosity ϵ . Furthermore, pores do not have an ideal cylinder shape, but have an irregular shape and are connected in a labyrinthine-like system. This is considered by a tortuosity factor τ . Usually the same values of ϵ and τ are taken both for molecular and Knudsen diffusion [Baerns2002], but strictly speaking both types of diffusion have to be separated. However, to reduce the number of parameters, identical values are assumed. The effective diffusivity

can then be calculated using the following equation:

$$\frac{1}{D_{eff}} = \frac{\tau}{\epsilon} \left(\frac{1}{D_M} + \frac{1}{D_K} \right) \quad (4.113)$$

Characteristic values of ϵ are 0.2 to 0.7. Due to the usually complex pore structure, τ cannot be calculated and it is required to determine τ experimentally. Typical values of τ are 3 to 4 [Baerns2002].

As the molecular diffusivity increases with temperature, the limitation by Knudsen diffusion dominates at high temperature and molecular diffusion at low temperature. The transition is dependent on the porous structure. For small pore diameters, Knudsen diffusion is dominant. As molecular diffusion decreases at higher pressure, Knudsen diffusion becomes also important at higher pressure.

4.2.7 Submodel for Mass Transport Limitations under Regime III Conditions - Boundary Layer Diffusion

The effectiveness factor approach and the calculation of reaction rate in the pore diffusion regime are based on the knowledge of the gaseous concentration at the particle surface c_s . The surface concentration is linked to bulk gas concentration by mass transport limitations in the boundary layer of a char particle. This second diffusion limitation is not considered by the effectiveness factor approach. Therefore, a further submodel is required to account for mass transport limitation within the boundary layer of a char particle.

In ideal Regime I and II conditions the diffusion within the boundary layer is fast and the surface concentration equals the bulk concentration and can be calculated from gaseous partial pressure p_i .

$$c_{S,i} = c_{bulk,i} = \frac{p_i}{RT} \quad (4.114)$$

Due to the slower intrinsic reaction rates compared to char combustion, Regime III conditions are usually not favoured in entrained flow gasifiers (except perhaps at over 2000 K) [Laurendeau1978]. However, a basic model approach for boundary layer diffusion is needed (i) to evaluate all influences of operation parameters and (ii) to quantitatively compare the film diffusion rates to other reaction regimes.

For the calculation of gas film diffusion in the particle boundary layer, a simple form of Fick's Law is used [Laurendeau1978]:

$$J_i = \beta \cdot M_i \cdot (c_{bulk,i} - c_{S,i}) \quad (4.115)$$

where J_i is the mass flux of reactant gas i [g/(m²·s)] at the particle outer surface, β is the mass transfer coefficient [m/s], M_i is the molar mass of the reactant gas, and $c_{bulk,i}$ and $c_{S,i}$ are molar concentrations in the bulk phase and at the outer particle surface, respectively. In order to relate the gas diffusion rate to the reaction rate of char, a gravimetric stoichiometric coefficient N is introduced [Laurendeau1978]:

$$N_i = \frac{M_C}{M_i \cdot \nu} \quad (4.116)$$

where M_C and M_i are the molar weights of carbon and the reactant gas, and ν is the molar stoichiometric coefficient of the gasification reaction. ν is defined as the molar ratio of reactant gas and carbon.⁷ Consequently, N for the char-CO₂ reaction is 3/11, and for the char-H₂O reaction 2/3. The reaction rate of carbon at the outer particle surface is then

$$r_{C,i,ext} = J_i \cdot N_i = N_i \cdot \beta \cdot M_i \cdot (c_{bulk,i} - c_{S,i}) \quad (4.117)$$

The mass transfer coefficient β is obtained from a Sherwood Number correlation for a sphere [Bird2007]:

$$Sh = \frac{\beta \cdot d}{D_{M,i}} = 2 + 0.6 \cdot Re^{0.5} \cdot Sc^{0.33} \quad (4.118)$$

In entrained flow gasification, gas and particles move at almost the same velocity and hence a stagnant atmosphere can be assumed around a char particle, i.e. $Re \cong 0$ and consequently $Sh \cong 2$. From the Equations 4.117 and 4.118 the observed reaction rate can be calculated:

$$r_{obs} \left[\frac{g}{g \cdot s} \right] = \frac{r_{C,i,ext}}{\rho_{app} \cdot V_{sph}/S_{ext}} = \frac{12 \cdot N \cdot D_{M,i} \cdot M_i}{d^2 \cdot \rho_{app}} \cdot (c_{bulk,i} - c_{S,i}) \quad (4.119)$$

where V_{sph} and S_{ext} are volume and external surface of the spherical particle and the ratio of both is $d/6$. d is the particle diameter, ρ_{app} the apparent density of the particle, and $D_{M,i}$ is the molecular diffusion coefficient for the gas i .

Under ideal Regime III conditions, the intrinsic reaction rate is so fast that the surface concentration approaches zero. The observed reaction rate is then only dependent on boundary layer diffusion. The diffusion coefficient can be calculated for binary gas mixtures [Baerns2002] by Equation 4.111. Furthermore, the gas concentration is expressed by partial pressure

$$(c_{bulk,i} - c_{S,i}) = c_{bulk,i} = \frac{p_i}{RT} \quad (4.120)$$

After substituting Equations 4.111 and 4.120 into Equation 4.119, it is obvious that

$$r_{obs}^{III} \sim \frac{T^{0.5} \cdot p_i}{p_{total} \cdot d^2 \cdot \rho_{app}} \quad (4.121)$$

The reaction rate in Regime III is only slightly dependent on temperature. Char particle properties like diameter and density are major influencing factors. Total gas pressure and partial pressure of reactant gas have also an influence on the reaction rate under Regime III conditions.

4.2.8 Submodel for the Change of Particle Size and Density during Conversion

The pore diffusion and boundary layer diffusion submodels require instantaneous particle density and particle diameter to calculate the char conversion rate. Submodels for the variation of these two parameters during the conversion process are briefly presented in

⁷The molar stoichiometric coefficient ν for both the char-CO₂ reaction and the char-H₂O reaction is 1.

this section.

Particle Swelling during Devolatilisation An increase in the particle diameter during devolatilisation is often observed in coal combustion and gasification systems. Swelling is caused by the fuel fluidity during the particle heat-up and is dependent on fuel properties and reaction conditions as summarised in Section 3.1.2. The swelling factor is dependent on fuel properties, heating rate, and devolatilisation pressure. Benfell [Benfell2001] developed a correlation for coal swelling that involves carbon content and operating pressure. The swelling ratio under pressurised conditions is

$$Sw = Sw_1^{0.7143+2.857 \cdot p_t} \quad \text{for } 0.1 \text{ MPa} \leq p_t \leq 0.8 \text{ MPa} \quad (4.122)$$

$$= Sw_1^{3.5-0.625 \cdot p_t} \quad \text{for } 0.8 \text{ MPa} \leq p_t \leq 4.0 \text{ MPa} \quad (4.123)$$

where p_t is the total pressure and Sw_1 is the swelling ratio at atmospheric pressure, which can be calculated from

$$Sw_1 = 8.67 - 0.0833 \cdot C_{daf} \quad \text{for } 89 \leq C_{daf} \leq 92, \quad (4.124)$$

$$= -0.0458 + 0.01459 \cdot C_{daf} \quad \text{for } 72 \leq C_{daf} \leq 89, \quad (4.125)$$

$$= 1.0 \quad \text{for } C_{daf} < 72 \quad (4.126)$$

where C_{daf} denotes the carbon content (wt%, daf) of the parent coal.

This correlation overestimates swelling ratios for high heating rate pyrolysis ($\sim 10^5$ K/s) [Zeng2005] as the influence of heating rate is not included. At higher heating rate, swelling is lower. However, the correlation indicates the trend in swelling behaviour and experimental data could be used to assess the influence of heating rate.

The implementation of a swelling model is required if the initial char particle size after devolatilisation is not known or if the influence of pressure on particle size needs to be expressed. If the initial char particle diameter is derived from experimental data the application of a swelling model is not required.

Particle Size and Density during Char Conversion Particle size and density can change during char conversion depending on the reaction regime. As particles only react at the outer surface under Regime III conditions, the particle size decreases, but the particle density remains constant. In contrast, in Regime I the reaction occurs at the internal particle surface and the particle density decreases whereas the diameter almost remains constant. In coal combustion modelling often power law relations are used to describe variations of the particle diameter and density with conversion [Ma2006]. The following expressions are often used to relate particle density ρ , diameter d_p and mass m during the

oxidation process [Ma2006]:

$$\frac{\rho}{\rho_0} = \left(\frac{m}{m_0} \right)^\alpha \quad (4.127)$$

$$\frac{d_p}{d_{p,0}} = \left(\frac{m}{m_0} \right)^\beta \quad (4.128)$$

The subscript 0 denotes initial char conditions after devolatilisation. For spherical particles, $\alpha + 3\beta = 1$, and for simplicity the parameters are assumed to be constant during conversion [Ma2006]. In Regime III, $\alpha = 0$ and $\beta = 1/3$, and particles burn at constant density. In Regime I, $\alpha = 1$ and $\beta = 0$, and the diameter remains constant. In entrained flow gasifiers, char conversion can occur in all three reaction regimes, thus $0 < \alpha < 1$ and $0 < \beta < 1/3$. When neglecting the mineral matter content, the mass ratio can be described by char conversion:

$$\frac{m}{m_0} = 1 - x_{char} \quad (4.129)$$

Furthermore, the particle diameter and density are correlated by the ratio of α/β :

$$\frac{\rho}{\rho_0} = \left(\frac{d_p}{d_{p,0}} \right)^{\alpha/\beta} \quad (4.130)$$

Essenhigh [Essenhigh1994] analysed an experimental combustion data base containing 37 values obtained from 15 literature sources. In spite of the different experimental methods, char types, fuel origins, particle sizes, and reaction temperatures, the ratio α/β was always in the range from 0 to 7, and in the majority of cases in the range 1 to 3. Liu and Niksa [Liu2004b] modelled char gasification in entrained flow and fluidised bed reactors and used a constant value of 0.95 for the parameter α assuming that the reaction occurs almost completely under Regime I conditions. Monson et al. [Monson1995] measured char combustion at elevated pressure and particle temperatures from 1123°C to 1723°C. The change of particle density with burn-off was best described by values for α between 0.5 and 0.65 indicating Regime II conditions.

In Regime I and III, the ratio α/β is:

$$\text{Regime I: } \frac{\alpha}{\beta} = \frac{1}{0} \rightarrow \infty \quad (4.131)$$

$$\text{Regime III: } \frac{\alpha}{\beta} = \frac{0}{1/3} = 0 \quad (4.132)$$

The reaction regime can be expressed by the quantity of internal and external char surfaces that are involved in the reaction. The internal surface area S_{int} is larger by far than the external surface area S_{ext} . In Regime II, the percentage of internal surface that is involved in the reaction is described by the effectiveness factor η . The ratio of involved internal surface area and external surface area is used to describe α/β :

$$\frac{\alpha}{\beta} = \frac{\eta \cdot S_{int}}{3 \cdot S_{ext}} \quad (4.133)$$

In Regime I, $\eta=1$ and α/β becomes a large number. In Regime III, $\eta \cdot S_{int} \approx S_{ext}$ and α/β becomes 1/3. Thus, the severity of pore diffusion in Regime II is described by the magnitude of η and the ratio α/β can be described in all three regimes. For a spherical particle, β is a function of α and the reaction conditions:

$$\beta = \frac{18 \cdot \alpha}{\eta \cdot S \cdot d_p \cdot \rho_0 \cdot (1-x)^\alpha} \quad (4.134)$$

where S [m^2/g] is the specific surface area and d_p is the particle diameter.

When using a constant value of α (for example 0.95 that is proposed by Liu and Niksa [Liu2004b]), the parameter β can be calculated from the effectiveness factor and particle properties.

4.2.9 State of the Art in CFD Modelling of Entrained Flow Gasifiers

After the theoretical development of the model framework for char conversion, the state of knowledge about the numerical simulation of entrained flow gasification is briefly summarised.

In recent years, computational fluid dynamics (CFD) are increasingly used as a predictive tool in fuel conversion systems. Due to the growing interest in entrained flow gasification, CFD calculations are developed that can predict the flow field and reaction network within a high temperature gasifier. This section briefly summarises some current approaches and compares the kinetic model equations used in the calculations.

Bockelie et al. [Bockelie2002, Bockelie2002b] developed a CFD model for a single stage, down fired gasifier and a two stage system with multiple feed inlets. The Chemical Percolation Devolatilisation (CPD) model was used to predict volatile and tar yield. By comparing the results from the model to literature data, Bockelie et al. noticed that the CPD model tends to under-predict the decrease in volatile yield with increasing pressure. The heterogeneous gasification rates are expressed by nth order rate equations, both for CO_2 and H_2O . It is indicated that mass transfer limitations at the boundary layer of a char particle and intra-particle diffusion resistance may occur at high temperature. However, it not described in the publications how this is implemented. Also, the adjustable parameters like pre-exponential factors and activation energies are not given in detail.

Watanabe and Otaka [Watanabe2006] modelled a two stage air blown coal entrained flow gasifier. The composition of volatiles released from coal is obtained by an equilibrium calculation. The devolatilisation rate is described by a single step model, and the reaction starts above the threshold temperature of 500 K. An nth order rate equation is used to model the heterogeneous reaction rates. The change in the rate-determining step, from chemical control to pore diffusion, is modelled by a change of the pre-exponential factor and the activation energy. For CO_2 the threshold temperature is 1200°C, and for H_2O it is 1260°C. Above these temperatures, the reactions are assumed to be limited by pore diffusion. A continuous transition between the regimes is not implemented. The development of pore structure with conversion and its influence on conversion rate is described by the Random Pore Model. The model parameters are taken from Kajitani et al. [Kajitani2002] who measured coal gasification in a PTDF and a PTGA.

Hla et al. [Hla2006, Hla2007] were the first to implement an effectiveness factor approach into CFD. Devolatilisation is described by a two-step model. Four reactants (O_2 , CO_2 , H_2O , and H_2) are considered for the reaction with char, and each reaction is described by an nth order rate equation. The heterogeneous char reaction is then dependent on the partial pressures of the reactants at the outer char particle surface and the effectiveness factor. The effectiveness factor was expressed as a function of the Thiele modulus. The partial pressure at the outer char surface is not known, but it is estimated by an iterative procedure using the bulk diffusion rate. As the surface area is an important parameter in this intrinsic approach, the change of surface area is expressed by the Discrete Random Pore Model [Bhatia1996] which is an extension of the original Random Pore Model. The kinetic parameters are derived from the experimental data set of CSIRO. The CFD calculations were applied to the PEFR geometry at CSIRO and a very good correlation to experimental data was observed.

Silaen and Wang [Silaen2010] recently analysed the effects of devolatilisation models on a one-stage entrained flow gasifier. The devolatilisation models used are the Kobayashi model with two-competing devolatilisation rates, a single rate model, a constant rate model, and the Chemical Percolation Devolatilisation (CPD) model. The heterogeneous reactions were modelled by Arrhenius type equations with a constant activation energy throughout the whole temperature range. Neither the influences of reactant partial pressure nor mass transport limitations are considered. The pre-exponential factors and activation energies were taken from literature data of graphite gasification. An entrained flow gasifier was simulated in a 2D and 3D case. Among the devolatilisation models, rather small deviations are detected. The Kobayashi model resulted the slowest rates, and the constant rate model produced the fastest devolatilisation rate. However, the reaction rates are strongly dependent on the adjustable parameters in the model equations and the rate calculated might not be related to the model equation. The authors did not provide an explanation for the difference and did not discuss which model is most suited for the prediction of realistic devolatilisation rates.

A commercial-scale, two-stage, upflow, slurry-fed, entrained flow gasifier is modelled by Slezak et al. [Slezak2010]. The focus of the numerical approach is on coal particle density and size fraction effects. The conversion is described by the two competing rate approach (Kobayashi devolatilisation model) and a shrinking core char conversion model. As in a shrinking core approach the reaction rate is determined by mass transport limitations in the boundary layer, kinetic data are not given in the paper. The results of the simulations show a strong dependence of particle trajectories on particle density and size.

The main assumptions for coal conversion in recent CFD simulations are summarised in Table 4.3. Different models for coal devolatilisation with varying complexity are implemented, but advantages and disadvantages are not discussed. A direct comparison to experimental data of devolatilisation and pyrolysis is not found. This might be due to the lack of experimental data at conditions relevant to entrained flow gasification. The implementation of the heterogeneous gasification reactions is mainly based on nth order rate equations. In most of the published simulations, the model parameters are not given and the model structure is not clear.

Only the researchers at CSIRO [Hla2006, Hla2007] implement directly the influence of

pore diffusion. Furthermore, their model parameters are derived from experimental data. To validate the simulations, the model results are compared with experimental data and a good correlation is found.

The short literature review on CFD modelling shows that current models - especially for the heterogeneous reactions - are simple. Furthermore, in almost all publications a comparison to experimental data is not shown which might be due to the lack of experimental data at high temperature and pressure. Therefore, it is hardly possible to evaluate the quality of the models, their transferability to entrained flow gasifier layouts, and their potential for optimisations on an industrial scale.

Table 4.3: Summary of devolatilisation and char gasification models used in CFD calculations for entrained flow gasification

Institution	Ref.	Devolatilisation	Heterogeneous reactions	Intraparticle diffusion
REI	[Bockelie2002]	CPD	nth order	-
CRIEPI	[Watanabe2006]	Single step	nth order	change of E_A
CSIRO	[Hla2006, Hla2007]	Two step	nth order	effectiveness factor
UNO	[Silaen2010]	4 types	Arrhenius type	-
NETL	[Slezak2010]	Two step	-	-

Chapter 5

Experimental Techniques, Procedures, and Results

The focus of the dissertation is the experimental investigation of entrained flow gasification at conditions relevant to industrial applications. Four experimental facilities are designed, built and operated to analyse gasification reactions at high pressure and high temperature. This chapter describes fuel preparation and the laboratory procedures for fuel and char analysis. Then, the experimental facilities are introduced and the experimental results are summarised.

5.1 Fuel and Reference Char Preparation

Seven fuels in the range from anthracite to biomass are analysed in this dissertation. The fuels were delivered from different suppliers. The fuel type, abbreviations, suppliers, and conditions as delivered are summarised in Table 5.1. The proximate and ultimate analysis of all fuels is shown in Table 5.2.

Table 5.1: Fuel supply and conditions as delivered

Abbreviations		Fuel type	Supplier	Conditions as delivered
K2-1	lignite R	Rhenish lignite	RWE ^a	raw, 45 wt% moisture
K3-3	lignite V	Lusatian lignite	Vattenfall ^b	milled, 11.5 wt% moist.
K2-3	anthracite	anthracite	RWE	raw, 3 wt% moist.
K2-4	bituminous coal A	high volatile bit. coal	RWE	raw, 13 wt% moist.
K2-5	bituminous coal B	high volatile bit. coal	RWE	raw, 10 wt% moist.
B1	biocoal	HTC ^c derived biocoal	TU Berlin ^d	raw, 12 wt% moist.
B2	wood	beech wood	-	chips, 10 wt% moist.

^aRWE Power AG

^bVattenfall Europe Mining AG

^cHydrothermal Carbonisation

^dInstitute for Energy Engineering, Technical University Berlin

5.1.1 Procedure for Processing Coal and Biomass

If fuel is delivered with a high moisture content, it is first dried to a moisture content of 20 wt% to 30 wt% prior to the pulverisation. Experiments are carried out in all facilities

Table 5.2: Proximate and ultimate analysis of the fuels

	K2-1	K3-3	K2-3	K2-4	K2-5	B1	B2
Proximate analysis (wt%, dry)							
Ash content	5.5	5.7	13.5	11.2	45.2	1.3	0.3
Volatile matter	52.7	52.4	6.2	41.3	22.8	67.2	71.1
Ultimate analysis (wt%, daf)							
Carbon	67.8	67.3	93.6	78.3	80.2	57.2	54.8
Hydrogen	5.2	5.3	3.0	5.3	4.9	5.7	6.2
Nitrogen	0.8	0.7	1.3	1.6	2.0	0.3	0.3
Sulphur	0.8	1.0	1.3	0.9	1.9	0.2	0.2

with pulverised fuel. A cross hammer mill (Retsch SK 100, for coal and biocoal) and a cutting mill (Retsch SM 100, for biomass) are used. After the milling, the fuel particles are sieved in defined size intervals using a tumbler screening machine (GKM KTS-V 600/3). If not indicated otherwise, the fuel is sieved between two meshes of width 80 μm and 160 μm . The moisture content of each fuel is adjusted in a conditioning cabinet (Mekko AD-02(T)) at a constant temperature of 40°C and a defined humidity. To prevent a change in moisture content prior to the experiments, the fuels are stored in air-tight containers. The two fuels that are mainly used in this work - lignite R and bituminous coal A - are analysed regarding their particle size distribution¹. Particles are suspended in deionised water using an anionic tenside and the size distribution is measured by a laser diffraction analyser (Quantachrome, CILAS 1090L). Results are shown in Figure 5.1. Due to the adhesion of fine matter, the particle size is shifted to lower values in comparison to the mesh width (between 80 μm and 160 μm). Because the pulverisation and adhesion properties of the two coals are different, the particle size distributions of the two coals vary, despite their identical preparation procedure.

5.1.2 Production of Reference Char

A laboratory char is produced from all fuels. The procedure is similar to the determination of volatile matter content following the standard procedure DIN 51720. 1 g of fuel is put in a small quartz glass container with an air-tight fitted lid. The glass is then placed in a muffle oven at 900°C for 8 minutes. Due to the devolatilisation, the pressure within the glass container increases and the quartz lid is lifted. Gaseous volatile matter can evolve from the fuel sample. After the devolatilisation process is finished the air-tight lid is closed by gravity preventing air contact with the sample. The quartz glass container is then removed from the muffle oven and cooled. Depending on the volatile matter content of the fuel, about 200 mg to 800 mg of char are produced during one run. The char generated in the laboratory procedure is referred to as *reference char* or *ref-char*.

Gaseous volatile matter is only partially removed from the vicinity of the char sample in this procedure. Secondary reactions like re-condensation or adsorption of tar compounds on the char surface are likely. The char yield measured in this laboratory analysis is expected

¹The particle size analysis is done by Quantachrome GmbH in their laboratories in Odelzhausen, Germany

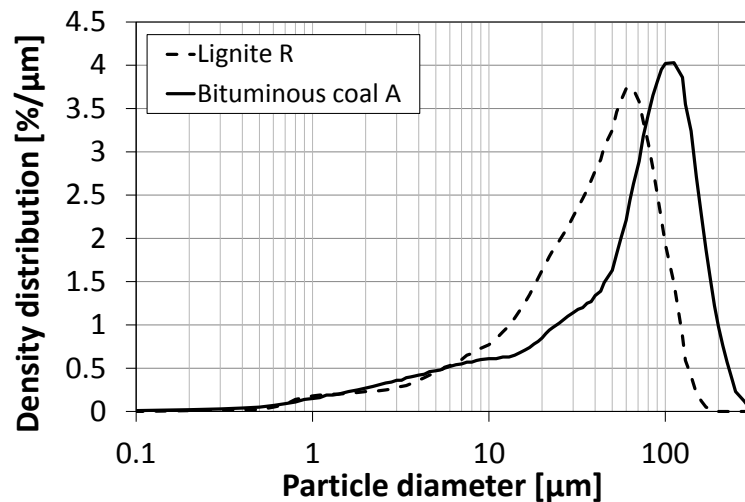


Figure 5.1: Particle size distribution of lignite R and bituminous coal A prior to their conversion in the entrained flow reactors

to be higher than under entrained flow conditions. Furthermore, ref-char is produced at a low heating rate at relatively low temperature (900°C) and is not representative of char that is generated under entrained flow conditions. For the setup and tests of analysis procedures, ref-char is used.

5.2 Methods used in the Laboratory Analysis

Coal and char samples that are collected from the different experimental facilities are analysed in laboratory. If not indicated otherwise, the analyses are carried out in the laboratories of the Institute for Energy Systems.

5.2.1 Proximate and Ultimate Analysis

The proximate analysis is carried out according to the standard procedures DIN 51718 (moisture content), DIN 51719 (ash content), and DIN 51720 (volatile matter).

The moisture content is measured in a moisture analyser (Denver IR-60) that slowly heats the sample to 106°C for about 1.5 minutes. The temperature of 106°C is used for all fuel and char samples. During the analysis, 1 g of sample is placed on a balance and the mass reduction due to water vapourisation is measured online.

The ash content is measured in a muffle oven. The dry sample after the moisture content measurement is directly used for the ash analysis. The sample (approx. 1 g) is filled in a ceramic crucible and put into a muffle oven at 815°C. Organic compounds are burned in hot air and mineral matter is left behind. The ash content is measured by weighing the fuel/char sample and the ash sample, and it is calculated on a dry basis. An uptake of moisture from air by the ash sample is prevented by directly determining the weight after cooling.

For the fuel samples, the volatile matter content according to DIN 51720 is measured. The procedure is identical to the production of reference char.

The ultimate composition is determined in an elemental analyser (elementar vario Macro)

and carbon, hydrogen, nitrogen, and sulphur contents of a sample are measured. The sample size is 10 mg to 100 mg depending on the sample mass that is available after the experiments. A test procedure with ref-char did not show an influence of sample mass on the results. As the elemental analyser only measures the total amount of hydrogen, the moisture content of the sample has to be known to calculate the organic bound hydrogen content.

5.2.2 Char Surface Measurement

The total surface area (TSA) is determined by CO₂ adsorption at 273 K (Quantachrome Autosorb 1C). In contrast to N₂ adsorption at lower temperature, CO₂ adsorption allows to include the contribution of the micropores to the total surface and to achieve micropore adsorption within a practical time frame [Hodge2009]. As the classical models (BET and DR) have limitations in determining the porosity of the microporous structures [Feng2003b], the density functional theory (DFT) method is used to analyse the adsorption isotherms. DFT is a molecular level statistical thermodynamic theory that correlates the measurement of the adsorption isotherm to the structure of the porous char [Feng2003b]. To allow a better comparison with literature data, also the DR method is used for the surface area determination.

The statistical error of the TSA measurement is determined in repeated measurements. The CO₂-DFT surface area and the CO₂-DR surface area of a PiTER char² is measured 8 times and the average TSA is 513 m²/g (DFT) and 567 m²/g (DR), respectively. The standard deviations are ±20 m²/g (DFT) and ±37 m²/g (DR). Both methods enable a good reproducibility and a low measurement uncertainty as the relative standard deviation is only ±4 % (DFT) and ±7 % (DR).

5.2.3 Measurement of Particle Size Distribution

Particle size distribution of the parent fuels and some pyrolysis and gasification chars collected from the PiTER are analysed in the laboratories of Quantachrome GmbH, Odelzhausen, Germany. The particle size is measured by laser diffraction (Quantachrome, CILAS 1090L) according to the standard procedure DIN ISO 13320. The fuel and char samples are prepared with an anionic tenside and then suspended in de-ionised water. The agglomeration of particles is prevented by using ultrasound. To control the quality of the measurement, each sample is analysed 5 times and a good reproducibility is achieved.

5.2.4 Particle Density Measurement

The apparent char density is determined by a tap density method. First, the sample is dried at 106°C and then filled into an empty glass tube of known volume (2.35 ml). The tube is tapped until the particles are settled and the volume remains constant. Then, the weight of the char sample is measured and char bulk density is derived. Assuming a constant packing factor of 0.42 [Ma2006], the apparent particle density is calculated. The

²ID: 20101220_PiTER_n. Each char sample is marked by an ID that includes the date of production, the experimental facility, and a letter for each test run.

density of each sample is estimated from the average of two repeated measurements. The average relative standard deviation of the apparent density measurement is $\pm 3\%$. Due to the simple procedure and the assumption of a constant packing factor, the true apparent char density is likely to deviate from the measurement.

5.3 Experimental Facilities and Procedures

5.3.1 Pressurised High Temperature Entrained Flow Reactor

The main experimental facility used in this work is the Pressurised High Temperature Entrained Flow Reactor (PiTER). The design, construction, built-up, and commissioning of the facility is a central part of this dissertation. The facility is designed to study gasification reactions under operation conditions relevant to industrial scale entrained flow reactors. Figure 5.2 shows the layout of the reactor.

5.3.1.1 Gas Supply and Preheating

A defined gas mixture is fed to the top of the reactor. The gases (N_2 , H_2 , O_2 , CO_2 , C_3H_8) are supplied in gas cylinders and the flow rate of each gas is controlled by a mass flow controller (MFC). The gases are mixed and preheated to 200-300°C in an external gas unit. Water steam is provided by a self-designed high pressure evaporator and mixed to the gas stream just before entering the PiTER. The gas flow capacities are summarised in Table 5.3.

5.3.1.2 Fuel Feeding System

Pulverised fuel is fed to the main reactor from a gravimetric dosing system with a highly controllable feed rate from 0.2 kg/h to 5.0 kg/h. The system is designed in cooperation with the company Dowitec in Nuremberg. It consists of two vibrational chutes that are connected by a batch weighing unit. The dosing system is adjusted to the needs of the PiTER in terms of geometry and pressure and is situated in a pressure vessel. Fuel is fed to the hot reaction zone by a water-cooled probe from the side at an angle of 40° from the vertical. The fuel flow is water-cooled to until 30 mm before entering the hot zone in order to prevent any reactions in the feeding tube.

Table 5.3: Gas flow capacities for the operation of PiTER

Gas	Unit	Capacity
Nitrogen	Nm ³ /h	100
Oxygen	Nm ³ /h	10
Hydrogen	Nm ³ /h	50
Carbon Dioxide	kg/h	35
Propane	kg/h	10
Water Steam	kg/h	10

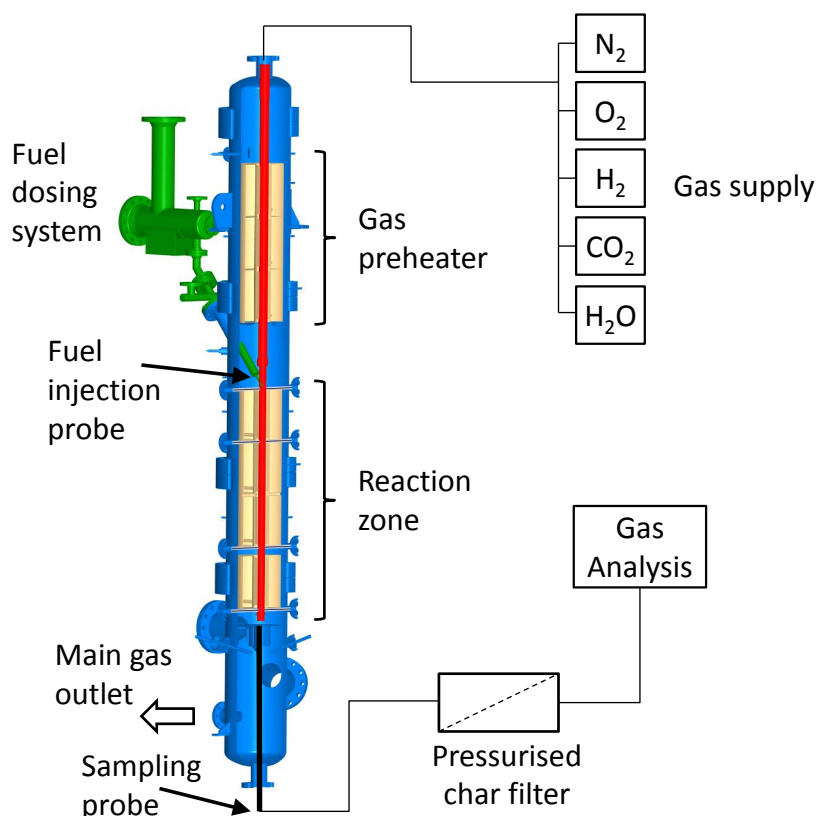


Figure 5.2: Sketch of the Pressurised High Temperature Entrained Flow Reactor (PiTER)

5.3.1.3 Reaction Zone

The reaction gases are enclosed in a system of ceramic tubes. The tube arrangement is shown in Figure 5.3. The tubes are made from high-grade alumina (>99.7 % Al_2O_3). Gas from the reactor top enters the preheater tube (60 mm i.d.) that can be heated up to 1800°C. The hot gas is then fed to a ceramic nozzle assembly and the tube diameter is reduced. The nozzle consists of an orifice and a smaller tube (30 mm i.d.) that accelerates the gas flow rate. The pulverised fuel is fed from the side, is injected into the accelerated gas flow, and then dispensed into the main reaction tube (inner diameter 70 mm, length 2.3 m).

Fuel Injection The flow rate of fuel carrier gas to main reaction gas is calculated according to a constant gas velocity ratio. For the calculation, identical temperatures of both gas streams are assumed. As the particles are injected near the reaction tube wall, a higher carrier gas velocity is required to transport the particles to the reaction tube centre. In the experiments a velocity ratio of approximately 5 between the carrier gas and the main reaction gas in the reaction tube is used. Due to the higher velocity of the main reaction gas at the inlet to the reaction tube and the in reality lower velocity³ of the carrier gas, the true velocity ratio at the mixing point is considerably lower. The carrier gas accounts

³The carrier gas is cooled up to about 30 mm before entering the reaction tube. Therefore, the true gas temperature will be lower than the gas temperature of the main reaction gas. The assumption of identical gas temperatures overestimates the gas velocity of the carrier gas.

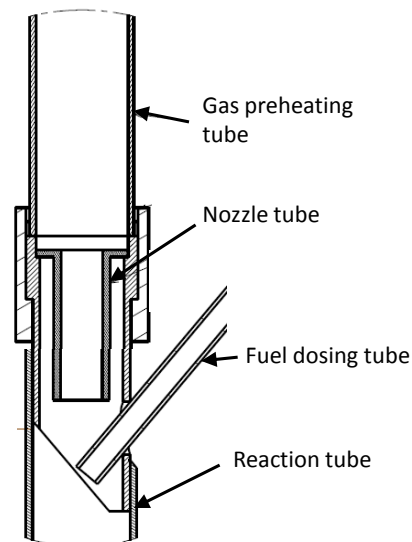


Figure 5.3: Sketch of the ceramic tube assembly of the PiTER facility

for only approx. 15 % of the total gas flow rate in the reaction tube. The assumption of a velocity ratio of about 5 is confirmed by CFD calculations. The particle injection is simulated using different boundary conditions. Particle trajectories at the point of injection are shown in Figure 5.4. Only the reaction tube and the dosing tube are shown. The preheated reaction gas enters the reaction tube through the nozzle tube (not shown) from the top. The colours denote the particle velocity that is highest at the point of injection and then approaches the average gas velocity of about 1 m/s in the simulation. Due to the particle injection from the side, turbulence occurs and a good mixing of particles with the hot reaction gas is achieved. This enables high heating rates and a defined starting point of the reaction. Furthermore, the particles are distributed in the cross section of the reaction tube. The good particle distribution is confirmed by a homogeneous fouling of the reaction tube circumference that is observed after the experiments. Particle wall contacts occur along the length of the reaction tube and are an indicator that particles are not only in the middle of the gas flow and that the particle distribution in the reaction tube is not shifted to one side.

Particle Heating Rate The injection system is designed to simulate heating rates that are also achieved in larger scale entrained flow reactors. In industrial gasifiers coal particles enter the reaction chamber through a burner and are heated very fast. As for industrial gasifiers, the particle heating rate in the PiTER cannot be measured directly, but the determination from a calculation is possible. The particle heating rate is determined by the convection and thermal radiation between a single particle and the surrounding gas atmosphere and the hot ceramic walls. The mathematical equations for radiation and convection are taken from [Polifke2005]. The calculation is based on the following parameters and assumptions:

- Fuel particles are spheres defined by a certain diameter.
- The particle outer surface area is small compared to the surrounding hot surface (ceramic tube).

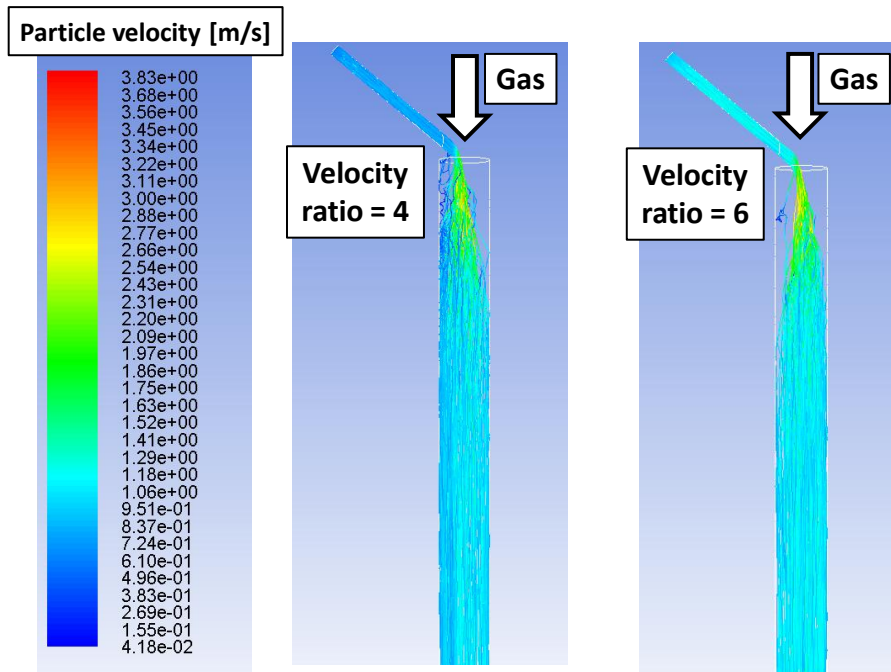


Figure 5.4: Particle injection in PiTER experiments modelled by CFD calculations at 2.0 MPa and 1200°C. The coloured lines denote particle trajectories. The nominal velocity ratio between the carrier gas and the main reaction gas is given in the diagrams and colours indicate the particle velocity.

- Convection between gas and particle is based on the particle free fall velocity.
- Fuel particles have a high thermal conductivity and temperature gradients within the particles are negligible.
- Particle emissivity is 0.8.
- Particle heat capacity is 2000 J/(kg K).
- Particle density is 1000 kg/m³.
- Gas and wall temperature is 1400°C.
- Gas pressure is 1.0 MPa.
- Gas properties are determined by the ideal gas law.

The most significant parameter is the particle diameter that mainly determines the heating rate. Figure 5.5 shows time-dependent heating rates and temperature profiles for fuel particles with different diameters. The initial heating rates are between 10⁴ K/s and 10⁶ K/s and correspond to industrial scale facilities where similar boundary conditions occur. Depending on the particle size, the particle is heated to gas temperature in 20 ms (50 μm diameter), 60 ms (100 μm), and 100 ms (150 μm).

Entrained Flow Operation Mode After the gas and particle mixing, the fuel-gas reactions occur within the reaction tube. The particles are entrained in the gas stream if their free fall velocity $v_{particle}$ is negligible compared with the gas velocity. The particle

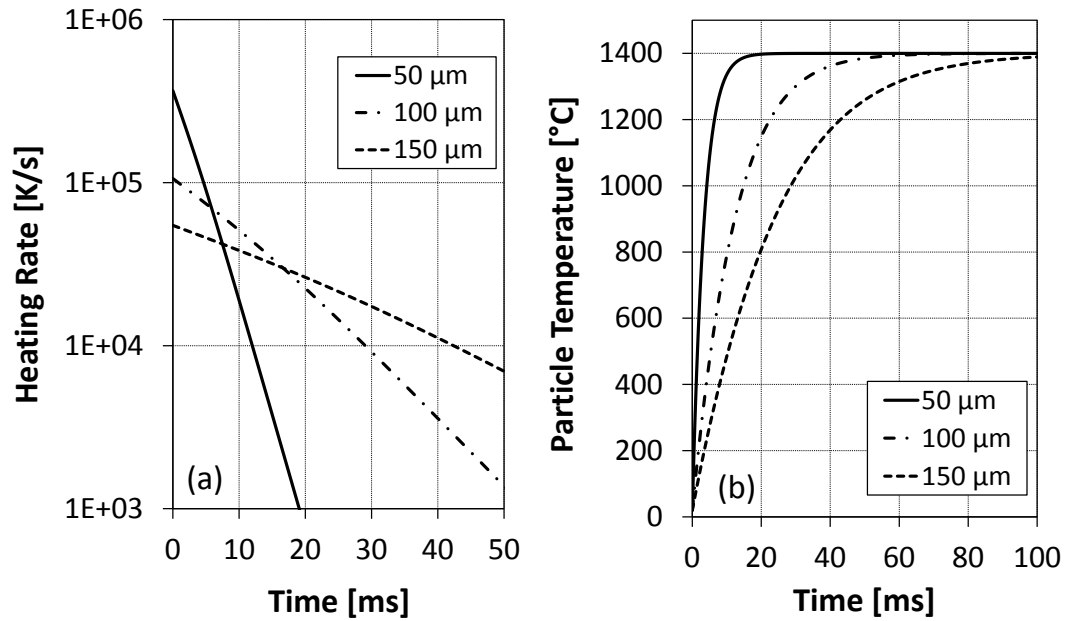


Figure 5.5: Particle heating rate (a) and particle temperature history (b) calculated for typical PiTER operation conditions and particles with different diameter

entrainment E is defined as the relative deviation from the gas velocity:

$$E = \frac{v_{gas} - v_{particle}}{v_{gas}} \quad (5.1)$$

The free fall velocity and the entrainment are calculated based on the following parameters and assumptions:

- Particles fall with steady state velocity free from acceleration effects.
- Gas and particle temperature is 1400°C.
- Gas pressure is 1.0 MPa.
- Gas velocity is 1 m/s.
- Gas properties for nitrogen are assumed.

The influence of the two most significant parameters particle diameter and density is shown in Figure 5.6. A laminar flow is assumed for the calculation. This assumption is valid for particles below certain threshold values for diameter and density. For an operation pressure of 1.0 MPa and a particle size of 200 μm the threshold particle density is 1500 kg/m³. An increase in the operation pressure to 2.0 MPa changes the gas properties and decreases the tolerable maximum particle density to 900 kg/m³. The char densities are assumed to be around or below this value and particle size is usually far below 200 μm. For small particles with a low density, the free fall velocity is very low and consequently the entrainment is approaching 100 %. For a typical density of coal char of 1000 kg/m³ and a typical particle size of 100 μm used in PiTER experiments, the entrainment is above 90 % proving the PiTER entrained flow operation mode.

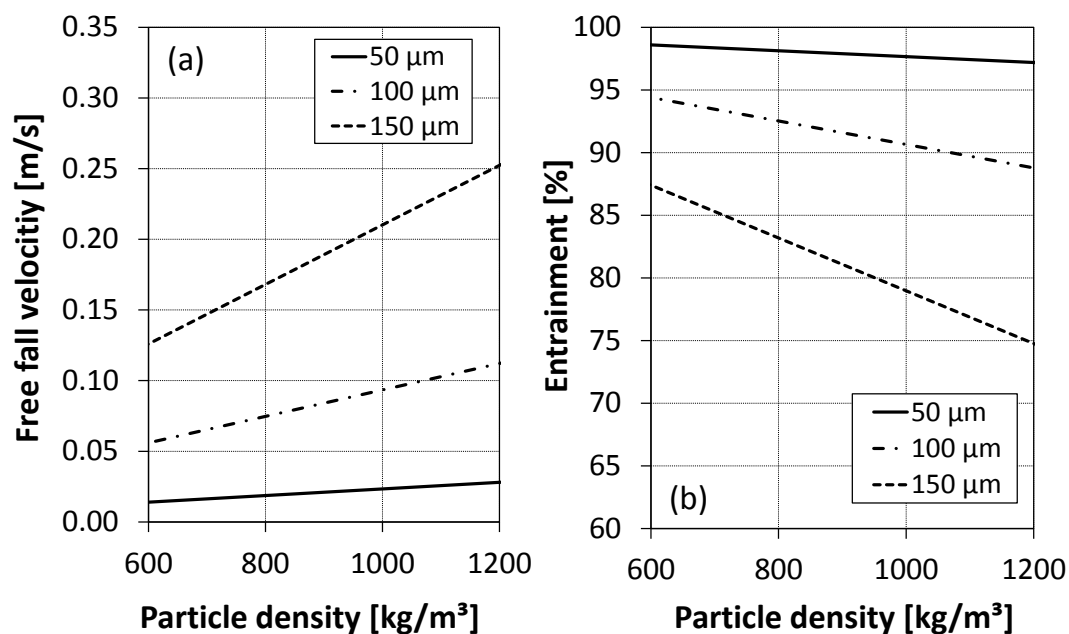


Figure 5.6: Particle free fall velocity (a) and entrainment (b) calculated for typical PiTER operation conditions (1400°C, 1.0 MPa) and a gas velocity of 1 m/s

Flow Profile The reaction tube has an inner diameter of 70 mm and a length of 2.3 m. By adjusting the gas flow rate a mean residence time of the gas within the reaction tube is achieved. The flow profile within the reaction tube is mainly dependent on the gas velocity. At a low gas flow rate a laminar profile is developing after the nozzle system. With an increasing gas flow rate the Reynolds number of the gas flow increases and the flow profile shifts to the turbulent region (transition: $Re \sim 2320$). In the experiments the Reynolds number is between 800 and 4000 depending on gas flow rate, temperature, and pressure. Therefore, there are different flow profiles in the reaction tube due to different operation parameters.

5.3.1.4 Heating Zones

The gas preheating tube is surrounded by three heating zones; the reaction tube is surrounded by four heating zones. All seven heating zones are identical and each zone has a height of 500 mm. The schematic layout of a heating zone is shown in Figure 5.7.

A graphitic cylinder is used as a resistance heater. Due to its meander shape the geometrical length is prolonged and the electrical resistance is increased. Furthermore, the electrical current is directed throughout the whole cylinder and a uniform heat production is achieved around the ceramic tube. Each heater is contacted by two graphitic screw bolts that also hold the heater mechanically in an upright position. The heater is surrounded by a tube made from graphite that prevents convective radial flow. Graphitic felt serves as thermal insulation. The insulation material is radially framed by a stainless steel cylinder and supported by a carbon fibre-reinforced carbon (CFC) plate at the bottom. The CFC plate is mechanically connected to the stainless steel cylinder and also holds the inner graphitic tube. The graphitic bolts connect the heater to the outside of the stainless steel cylinder and are electrically isolated by ceramic tubes. The maximum power output of

each heating zone is 36 kW (40 V, 900 A).

The heating zones are stacked and connected at the outer stainless steel cylinders preventing radiative or convective heat loss between the heating zones. An interlayer made from graphitic foil is situated between two heating zones. This interlayer has a central gap fitted to the outer diameter of preheating or reaction tube and minimises the vertical radiative and convective heat transfer between heating zones. Outside the stainless steel cylinders, the graphitic bolts are contacted by copper bars that connect the heating elements with a current feedthrough at the pressure vessel.

5.3.1.5 Water Quench System

The reaction tube determinates within a refractory basement that separates the heated reaction zone from a cold quench zone. The hot gas and particle mixture is then directly sprayed by cold water from up to six nozzles. Pressurised cold water is supplied by two redundant high pressure pumps. The water flow rate is adjusted to the heat capacity of the hot gas and particle mixture. The temperature within the quench zone is monitored by a thermocouple.

The water level is held constant by an overfall that prevents the quench zone from floating. The waste water flows to a water tank that is repeatedly drained by two redundant ball valves. The higher and lower water levels in the waste water tank are monitored by each two redundant level meters preventing over-floating or complete drainage. This configuration prevents that any toxic or explosive gases are released from the reactor through the waste water system. However, at high pressure small amounts of gases are dissolved in the quench water and leave the waste water tank in the liquid phase. To avoid a release of toxic gases to the environment, the waste water is depressurised within a container that is constantly ventilated by the university's waste gas system.

5.3.1.6 Pressure Vessel

The gas preheating, reaction, and quench zones are enclosed in a pressure vessel. The cylindrical vessel has an inner diameter of 600 mm and a height of about 7 m and is made of stainless steel (material number 1.4571). The design parameters are a maximum pressure of 5.0 MPa at a steel temperature of 300°C. Due to the loss of tensile strength of stainless steel at higher temperatures, the vessel has to withstand a pressure of 10.0 MPa at ambient temperature and the main design class for standard components (e.g. flanges and valves) is PN 100.

For over-temperature protection of the pressure vessel the outer surface is water-cooled by heat plates. These plates consist of two layers of stainless steel that are flown through by cooling water and can be fitted to the curvature of the pressure vessel. In comparison to a standard double layer pressure vessel, heat plates can be removed and the single layer pressure vessel can be re-designed easily, e.g. for the adaption of an additional flange. The disadvantages of heat plates are a poorer thermal contact of cooling water and pressure vessel and some construction-conditioned un-cooled spots at the pressure vessel. Cooling water is supplied by the university's central cooling water system and is fed to the heat plates vessel by six closed loops. The water flow rate and reflux temperature of each loop

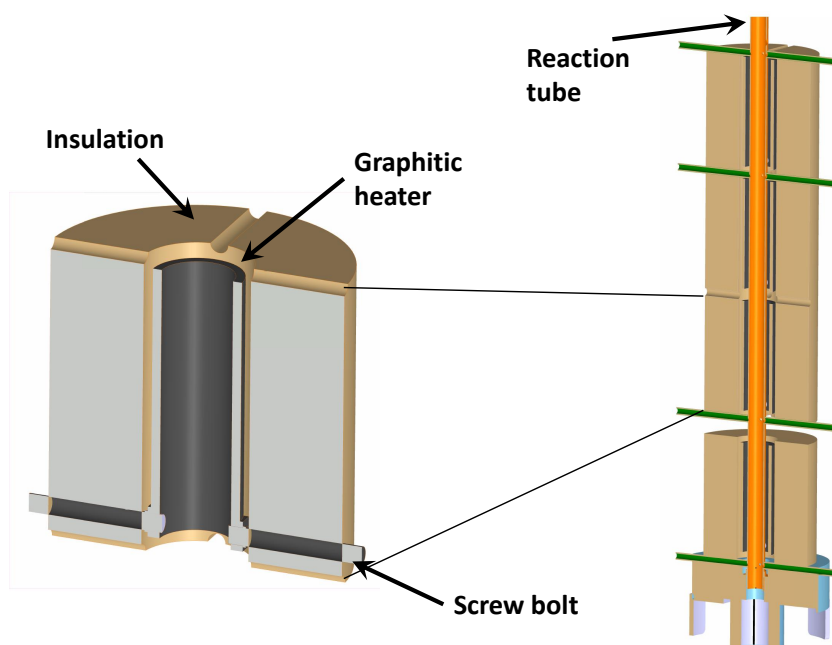


Figure 5.7: Schematic design of the heating zones of the PiTER

are monitored. In case of a breakdown of the cooling system, an emergency cooling system is installed that is operated with mains water.

5.3.1.7 Char Sampling and Gas Analysis

Char and gas samples are taken from the hot reaction tube through a stainless steel probe that is cooled with water or tempered with oil. This probe is inserted at the bottom of the pressure vessel and can be moved upwards into the reaction tube. By adjusting the height of the sampling probe char and gas samples are taken at different stages of conversion. The probe can be inserted in the reaction tube over a length of 1200 mm. Therefore, the top sample point is about 1000 mm below the fuel injection. The lowest sample point is at the outlet of the reaction tube after a reaction length of 2.3 m.

At given operation conditions (pressure, temperature, gas flow rate) char is sampled at different residence times and the progress of char conversion can be observed. The char is separated from the gas phase in a porous stainless steel filter. The filter is situated in a small pressure vessel that is located directly below the sampling probe. The small pressure vessel and all gas lines are heated to avoid steam condensation. The gas flow rate through the sampling probe is adjusted by a MFC. A pressurised cold trap removes water steam and other condensable gases to protect the MFC. Char and gas is drawn from the reaction tube isokinetically by adjusting the gas flow rate.

A continuous gas flow from the sampling probe is fed to the gas analysis system. The concentrations of the gas components CO, CO₂, H₂, and CH₄ are measured by the combination of a NDIR sensor and a heat conductivity sensor. The O₂ concentration is measured by an electrochemical sensor. Due to the susceptible sensors, the gas is cleaned in a series of filters and particle load and condensable trace elements are removed. The filter causes a response time of the gas analysis system of about one minute.

Additionally, in about half of the experiments also mass spectroscopy (MS) is used to analyse the gas composition. A small amount of hot gas after the char filter is fed directly to the MS. As there are no gas filters installed before the MS, the resulting response time of the gas analysis is only about 5 s, which allows not only gas analysis but also process monitoring. Small fluctuations in the fuel feeding system can be monitored online. The concentrations of CO, CO₂, H₂, CH₄, H₂O, and O₂ are measured. Due to the overlap of the main CO peak with the main N₂ peak at a mass of 28, the exact determination of the CO concentration is difficult. The uncertainty in the CO measurement is ± 3 mol%. As the CO concentrations are in the range 5 mol% to 20 mol%, the measurement error especially at lower gas concentrations is high. Future measurements should also use argon as the inert gas (despite the higher costs) to enable a precise gas analysis by mass spectroscopy.

5.3.1.8 Process Control and Safety System

Due to the high temperature, high pressure, and the use of toxic and/or explosive gases, a highly reliable process control and safety system is mandatory. The process control system is based on the programmable logic controller (PLC) Siemens Simatic S7. A program code is written that enables the control of all process parameters. The program code is visualised by the software Siemens WinCC that runs on a standard personal computer. The main user interface is shown in Figure 5.8. The user interface enables the setting of target process temperature, pressure, and gas flow rates. The process setpoint values are calculated by programmable ramp functions that enable a stable change of process conditions. Furthermore, the user interface indicates deviations from the current setpoints by warnings and alerts that are accompanied by light and sound signals. The system allows the user to identify critical operation conditions and to interfere by changing the setpoints. Independent of the process control system, a safety system is installed. This safety system is based on hard wire circuits and is responsive to lower and upper limits of certain process parameters. In a hazard and operability study (HAZOP) with experts from the German Association for Technical Inspection (TÜV-Süd) critical operation parameters have been identified whose overstepping could lead to major hazards for users and the environment. The most critical process parameters are summarised in Table 5.4. A critical process parameter is classified according to the SIL system (safety integrity level). The higher the SIL number, the higher the risk for persons and environment. The potential financial risk in case of a failure is evaluated by the AIL (automation integrity level). The highest SIL/AIL number is 4. The most critical process parameters have to be controlled by safety instrumented systems (SIS) (German: Prozessleittechnik PLT).

5.3.1.9 Experimental Procedure for the PiTER Experiments

In each experiment the steady state conditions within the reaction tube are achieved. The setpoints of the heating zones are set to reaction temperature. In all experiments an isothermal temperature profile is applied. The operation pressure is adjusted by the pressure control valve at the main gas outlet. The gas flow rates are chosen according to the desired residence time in the reaction tube and according to the required gas

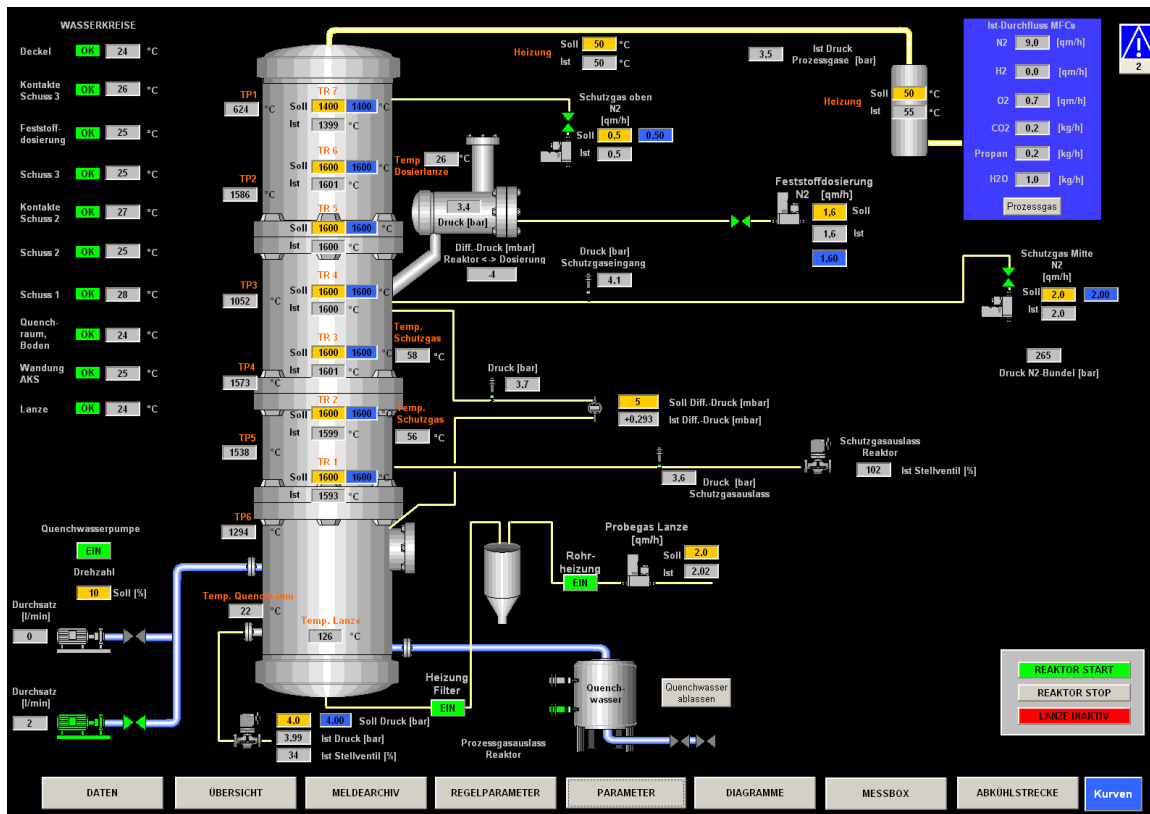


Figure 5.8: User Interface for the PiTER operation based on the Siemens WinCC software package

Table 5.4: The most critical process parameters during the operation of the PiTER

Parameter and event	SIL	AIL	SIS
Backflow of hot gases to the gas supply system	SIL0	AIL3	Hardwire thermocouple non-return valve
Water level increase within the reactor	SIL1	AIL3	Hardwire level indicator
Failure of the sampling probe and the cooling circle	SIL1	AIL3	Hardwire pressure indicator

composition. The gas composition depends on the type of experiment:

Pyrolysis experiment Pyrolysis experiments are carried out in an inert gas atmosphere and pure nitrogen is used. In some experiments minor amounts of hydrogen are mixed to the reaction gas to analyse the devolatilisation behaviour in a reducing gas atmosphere. In these experiments an inlet hydrogen concentration of 8 mol% is adjusted.

Integral gasification experiments Integral gasification experiments are used to simulate the complete reaction sequence in an industrial scale entrained flow gasifier. The most important parameter in these experiments is the adjustment of a defined stoichiometry between the fuel mass flow rate and the oxygen flow rate in the reaction gas. The stoichiometry is defined by the molar ratio between oxygen atoms in the gas phase and

carbon atoms in the fuel:

$$O/C = \frac{\text{molar oxygen atom flow rate in the gas phase}}{\text{molar carbon atom flow rate in the fuel mass flow}} \quad (5.2)$$

The O/C ratio is set to unity in all integral gasification experiments. This is in accordance with entrained flow gasification experiments at CSIRO [Harris2006].

To adjust the residence time in the reaction tube, nitrogen is used as a balance in the reaction gas. The fuel carrier gas consists of pure nitrogen. After the fuel particles enter the reaction tube, the devolatilisation, the combustion of volatiles, and the char conversion occur partly simultaneously, and partly subsequently.

Differential Gasification Experiments In the integral experiments single reactions cannot be studied independently. For example, char conversion is always influenced by both CO_2 and H_2O gasification. Furthermore, the gas composition is continuously changing during conversion. In order to measure the rate of single reactions and to achieve constant operation conditions in the reaction tube, differential gasification experiments are carried out. In these experiments the gas composition and residence time are adjusted by the MFCs. As the fuel conversion influences the gas composition, the fuel mass flow rate has to be low.

An extensive differential measurement campaign is not carried out. However, the procedures for differential experiments are evaluated and test measurements are done in pure CO_2 and mixtures of CO_2 , H_2O , H_2 , and CO .

5.3.2 Baby High Temperature Entrained Flow Reactor

A second entrained flow reactor that is developed within the framework of this dissertation is the Baby High Temperature Entrained Flow Reactor (BabiTER). In contrast to the PiTER, it is designed for atmospheric pressure and on a smaller scale. However, it is possible to study gasification reactions at conditions relevant to high temperature entrained flow reactors. Figure 5.9 shows the layout of the facility.

5.3.2.1 Gas Mixing Unit and Gas Preheater

Different gases can be premixed and fed to the gas preheating unit. These gases are N_2 , O_2 , H_2 , CO_2 , CO , CH_4 , and air. The gas flow rate of each gas is adjusted by mass flow controllers. The gases are premixed in a gas collecting tube and then fed to the horizontal gas preheater that consists of a ceramic tube (inner diameter 25 mm, length 800 mm, 99.7 % Al_2O_3). The preheating tube is surrounded by a spiral shaped electrical resistance heater that is connected to a transformer. The temperature is monitored by a type S thermocouple that is directly placed at the outer wall of the ceramic tube. The gas mixture can be heated to a maximum temperature of 1300°C and then enters the main reaction tube.

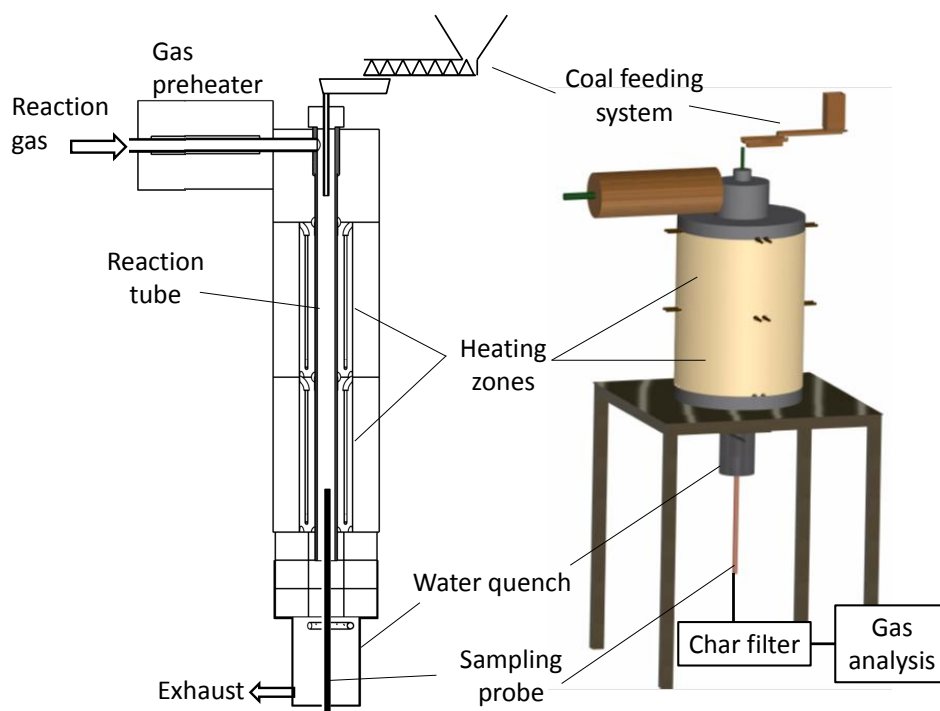


Figure 5.9: Schematic layout of the Baby High Temperature Entrained Flow Reactor

5.3.2.2 Reaction Tube

After the gas is preheated from the side, a laminar flow is achieved by a flow straightener and the gas mixture streams downwards within the reaction tube (i.d. 40 mm, length 1000 mm, 99.7 % Al_2O_3). By adjusting the gas flow rate an average gas residence time within the reaction tube is achieved. The reaction tube is surrounded by two heating zones. Each heating zone consists of four MoSi_2 heating elements that are designed for a maximum temperature of 1800°C . The heating elements in each zone are arranged in series and are connected to a transformer. The temperature within each heating zone is controlled by a type B thermocouple that is situated at the outer wall of the reaction tube. A second thermocouple is connected to a safety relay that shuts down the facility in case of an over temperature.

5.3.2.3 Fuel Feeding System

Pulverised fuel is fed to the reaction tube from a dosing system at the top of the reactor. A constant fuel mass flow is achieved by a combination of screw feeder and vibrational chute and is controllable in the range 50 g/h to 500 g/h. The dosing system is situated on a balance allowing an online monitoring of the fuel feeding rate. To prevent air from entering the reactor through the feed line, the feeding system is enclosed in a container. Inert gas fed to the container is used as a carrier gas for the fuel particles. The feeding system is connected to the reaction tube by a ceramic tube (inner diameter 8 mm, 99.7 % Al_2O_3). This tube determines after the flow straightener and particles enter the gas flow in the hot zone. As hot gas from the preheating unit flows around the feeding tube, it is heated to preheating temperature. The carrier gas and fuel particles are also heated within the feeding tube and devolatilisation reactions might occur. However, the residence

time of the particles in the hot section of the feeding tube is 30 ms to 60 ms which leads only to partial devolatilisation. In terms of the carrier gas atmosphere, two options are available:

Inert Gas Feeding In the normal configuration, the feeding tube is unchanged and particles are fed to the reaction tube in an inert gas atmosphere. Due to the slower heat-up in the feeding tube, the particle heating rate is expected to be slightly lower than in the PiTER. In the feeding tube partial pyrolysis occurs, and volatiles and char enter the reaction tube.

Burner Like Design In an industrial scale entrained flow reactor, fuel and oxygen are mixed at the burner outlet and ignite in the hot reaction zone. Fuel is fed by an inert carrier gas and is then injected into an oxygen rich atmosphere. This configuration is imitated by the second feeding option. Within the 8 mm feeding tube a concentric stainless steel tube with an inner diameter of 4 mm is situated. The fuel particles are first fed to this inner metallic tube that determinates within the transition to the hot zone. The configuration is shown in Figure 5.10. Pure oxygen is fed to the annular gap between the two tubes. Within the transition to the hot zone, the particles and oxygen are mixed and ignited in the ceramic feeding tube. A large temperature increase is observed by the partial combustion of volatiles. Although the temperature cannot be measured in the transition zone, it is expected to be higher than the gas preheater temperature. Again, the gas-particle mixture enters the main reaction tube after the flow straightener. The residence time in the hot section of the feeding tube is again in the range 30 ms to 60 ms, but might be slightly lower due to the higher temperature. The heating rate is expected to be higher than in the normal inert gas configuration and comparable to industrial scale applications. However, with this second setup pyrolysis experiments in an inert gas atmosphere are not feasible due to the oxygen supply.

5.3.2.4 Water Quench System, Sampling Probe, and Char Filter

After leaving the reaction tube, the hot gas and particle mixture is directly cooled by spray water from a ring-shaped nozzle. The gas and the quench water are constantly removed from the quench zone.

Char and gas samples are collected from the hot reaction tube through a water tempered probe. This probe (outer diameter 22 mm, inner tube 8 mm) is inserted at the bottom of the quench zone and can be moved upwards into the reaction tube. By adjusting the height of the sampling probe, char and gas samples are taken at different stages of conversion. At a given set of operation conditions (temperature, gas flow rate) char and gas samples with different residence times are taken along the reaction tube. The samples are isokinetically sucked in, whereby the gas flow rate is adjusted by a membrane pump.

Char is separated from the reaction gas in a char filter. The char filter and the probe are heated to prevent any condensation of water steam. A continuous gas flow from the sampling probe is analysed using a NDIR /heat conductivity analyser, and the concentrations of CO, H₂, CO₂ and CH₄ are recorded. Simultaneously, the gas concentrations can also

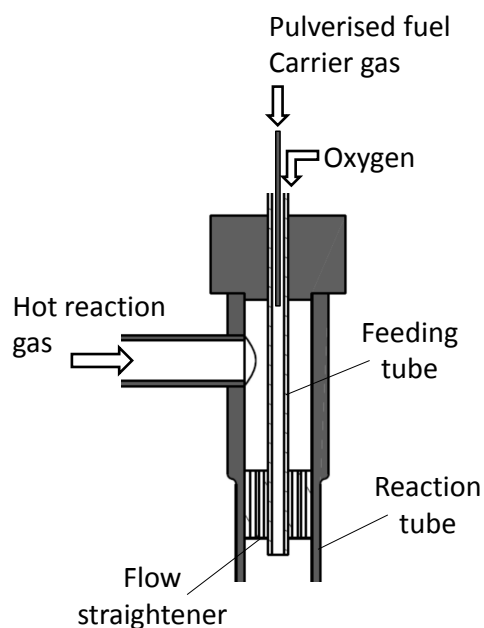


Figure 5.10: Burner like feeding design of the Baby High Temperature Entrained Flow Reactor

be measured by mass spectroscopy.

5.3.2.5 Process Control and Safety System

There is no central process control system for the BabiTER facility. Mass flow controllers are adjusted either by software or manually. The operator has to prevent manually that combustible (e.g. H_2 , CH_4) and oxidising gases (O_2 , air) are fed together to the gas mixing unit. Before starting the fuel feeder, the feeding unit has to be flushed with inert gas to prevent a backfiring from the hot reactor through the feeding tube. The temperature in the gas preheater and the two reaction zones is monitored by PID controllers and further secured by over temperature protection relays. The reaction gas that leaves the quench zone is vacuumed and removed by a ventilation system. However, due to several ceramic connectors the reactor is not absolutely gas tight and minor amounts of explosive and toxic gases can leave the reactor. Furthermore, a damage of ceramic parts can cause a major leakage. Therefore, the operator of the facility has to be equipped with gas sensors and the gas monitoring system that is installed in the laboratory has to be activated.

5.3.3 Pressurised Wire Mesh Reactor

Fuel devolatilisation at high pressure and high heating rate is analysed in the Pressurised Wire Mesh Reactor (PWMR). The main components of this bench-scale rig are developed during this dissertation. The PWMR can be operated at temperatures of up to 1100°C , at heating rates up to 5000 K/s , and at pressures of up to 5.0 MPa .

5.3.3.1 Layout and Design of the PWMR

The central part of the PMWR is a metal mesh that is clamped between two electrodes. A quadratic mesh with a width of $42\ \mu\text{m}$ is used in all experiments. The mesh material is stainless steel (material number 1.4841) that allows a maximum temperature of approx. 1100°C . Two layers of mesh are placed on top of each other and are welded together at three of the four edges. Therefore, a small bag is formed for the fuel sample. The surface area of this bag between the electrodes is $20\ \text{mm} \times 20\ \text{mm}$. The two wires of a thermocouple (type K, diameter $25\ \mu\text{m}$) are directly welded onto the upper surface of the mesh in order to measure the mesh temperature. The electrodes are connected to a power supply (SM 15-200 D, Delta Elektronika) that can provide a maximum voltage of $15\ \text{V}$ and a maximum current of $200\ \text{A}$. The mesh between the electrodes is used as a resistance heater. By controlling the power supply, the mesh temperature is adjusted. The electrodes are placed within a small pressure vessel that is designed for a maximum pressure of $5.0\ \text{MPa}$. Experiments in a defined gas atmosphere and at a defined pressure are feasible. In order to continuously remove volatiles from the fuel sample, the mesh is swept by a gas stream. A flow straightener is located below the mesh and the flushing gas passes through the mesh at a defined gas flow rate. Volatiles are removed and a re-condensation on the char surface is prevented.

5.3.3.2 Real-Time Control System

The critical part of a wire mesh reactor is the temperature control unit. A very fast control algorithm is required to achieve a precise and repeatable temperature profile. The control system of the PWMR is based on a real-time processor (NI cRIO-9072) that can operate at a frequency of $1000\ \text{Hz}$, i.e. 1000 calculation steps are carried out in $1\ \text{s}$. Due to the thermal inertia of the thermocouple and the electrical inertia of the power supply unit a control frequency of $100\ \text{Hz}$ is chosen. The control algorithm is based on the LabView software package (Version 8.6) and consists of a PID controller that adjusts the power output according to the temperature requirements. The temperature profile is monitored during each experiment and always lies in a range of $\pm 10^\circ\text{C}$ around the current setpoint.

5.3.3.3 Experimental Procedure

For the PWMR experiments a standard procedure is developed that allows pyrolysis of different fuels to be analysed at high heating rate and under pressure. An experiment consists of the following steps:

Mesh preparation For each experiment, a new mesh is prepared. A strip of mesh is cut and folded at one end. The two layers are welded together. The two thermocouple wires are welded on top of each other, and then onto one side of the mesh. Then the mesh is rinsed with acetone to remove oil and other impurities. The mesh is dried at 106°C and its weight is measured.

Sample preparation A fuel sample is first pulverised and sieved between two meshes (80 μm and 160 μm). A sample mass of 10 mg to 20 mg is placed in the mesh bag. To remove fines that stick to larger particles, the mesh is blown out from both sides by clean compressed air. The remaining fuel particles are larger than the mesh width of 42 μm and a loss of fines during the experiment is prevented. Finally, the sample and mesh are dried at 106°C and the weight is measured ⁴. By subtracting the mesh weight, the fuel mass on a dry basis is calculated. The mesh is stored in a gas tight container to prevent any uptake of moisture.

Experimental run The mesh is mounted between the electrodes and the thermocouple wires are connected to the control unit. Then, the sample holder is placed in the pressure vessel. A vacuum pump is used to remove air from the reaction chamber, and the pressure vessel is flushed three times by argon (grade 5.0). Pressure and gas flow rate are adjusted using a pressure regulator and a rotameter. The laminar flow velocity of argon through the mesh is set to 0.1 m/s in all experiments. At higher pressure the mass flow rate is increased to maintain a constant gas velocity. After switching on the temperature controller, the setpoint temperature profile is activated and the heat treatment occurs. The heating period is observed optically through the sight glasses of the pressure vessel. In case of an unsuccessful attempt or an inhomogeneous temperature distribution of the mesh, the run is excluded from the further analysis. The cool-down of the sample is achieved by convection and radiation. As the convection is more significant at higher pressure, the cooling at higher pressure is faster, as shown in Figure 5.11.

Volatiles that are removed from the coal samples are entrained in the gas flow and condense either on cold surfaces within the pressure vessel or leave the pressure vessel. After the experiment the mesh is removed, dried again at 106°C, and its weight is measured.

⁴The mesh is placed on the balance directly after drying and the weight is recorded above room temperature. The procedure is applied to prevent moisture from re-adsorbing on the fuel particles

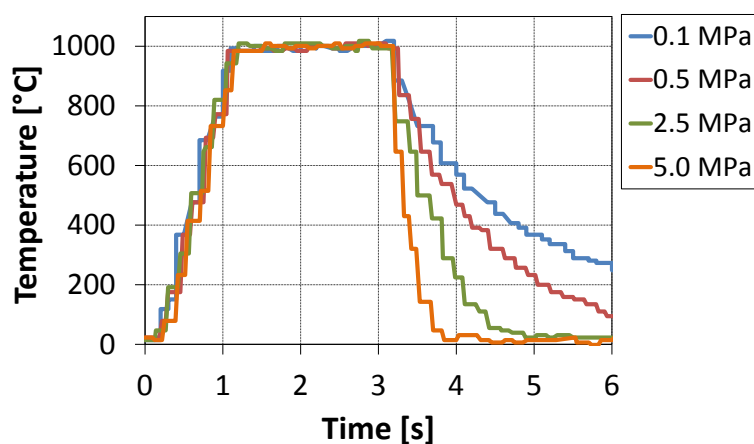


Figure 5.11: Temperature profile for PWMR experiments at constant setpoint temperature and different pressure

Calculation of volatile yield Volatile yield on a dry basis is calculated using

$$Y_{V,dry} = \frac{m_{fuel} - m_{char}}{m_{fuel}} \quad (5.3)$$

The fuel ash content from the proximate analysis is used to calculate the volatile yield on a dry-ash-free basis (daf)

$$Y_{V,daf} = \frac{Y_{V,dry}}{1 - a_{dry}} \quad (5.4)$$

where a_{dry} is the fuel ash content on a dry basis.

5.3.4 Pressurised Thermogravimetric Analyser

The reaction rate of the heterogeneous char reactions is usually measured in thermogravimetric analysers. At low temperature (600°C to 900°C, depending on char properties) char gasification is only limited by the chemical surface reactions and mass transfer limitation do not occur. The reaction rate of chars that are collected from the PiTER is measured in the Pressurised Thermogravimetric Analyser (PRETA). The facility is designed, built up and commissioned within the framework of a joint research project [Stetka2011] in cooperation with the company Linseis GmbH in Selb, Germany, and is commercially available (Linseis STA PT HP/2). The partial design, the commissioning, the development of the measurement procedure, and the experiments are part of this dissertation. The PRETA can be operated at up to 5.0 MPa in variable gas atmospheres of N₂, Ar, O₂, H₂, CO₂, CO, and H₂O. The thermobalance is designed for a maximum temperature of 1800°C. The PRETA was operated at up to 1650°C during commissioning. Char reactivity measurements are usually carried out at 650°C to 850°C.

5.3.4.1 Layout of the PRETA

The schematic layout of the PRETA is shown in Figure 5.12. The balance beam and the weighing unit are situated in the lower horizontal pressure vessel. The sample holder is extended from the balance beam by a ceramic rod that enables the sample to be placed in the reaction tube. The ceramic reaction tube is surrounded by a graphitic heating element and thermal insulation material (graphitic and ceramic). The graphitic heater is connected by two graphitic bolts to copper bars that are situated outside the thermal insulation. These copper bars are connected with a current feedthrough at the pressure vessel. Power is supplied by a transformer. The configuration is similar to the PiTER heating zones and construction and operation experience could be used. The reaction tube, heater, and insulation are situated within the upper vertical pressure vessel. The upper vessel and part of the lower pressure vessel are water-cooled to prevent an over-temperature. The pressure vessels are designed for a maximum operation pressure of 5.0 MPa at a steel temperature of 300°C. The two pressure vessels are connected by a central flange. To remove the sample holder from the reaction tube, the lower pressure vessel can be moved vertically. The reaction gas is fed to the sample from the top. Gas flow rates of N₂, Ar, O₂, H₂, CO₂, and CO can be adjusted by mass flow controllers. The reaction gas is preheated

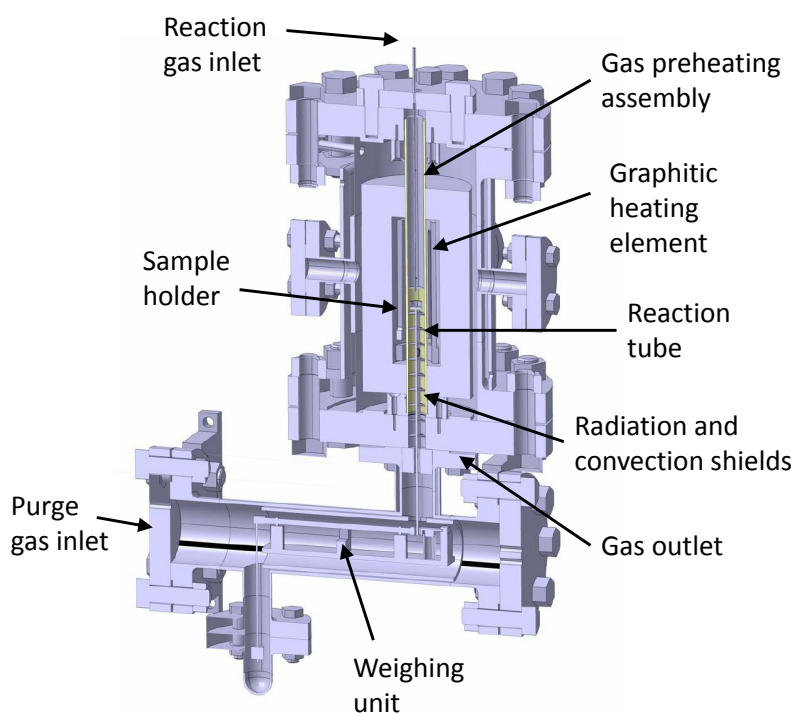


Figure 5.12: Schematic layout of the Pressurised Thermogravimetric Analyser (PRETA)

to reaction temperature in an assembly that is integrated in the upper part of the reaction tube. Furthermore, the assembly prevents convection and radiation losses from the isothermal reaction zone, especially at higher pressure when the convection forces are high. To minimise the convection and radiation losses below the sample holder, several ring-shaped plates are situated in the lower part of the reaction tube. These plates reduce the free flow cross section of the reaction gas and prevent the backflow of cold gas.

A purge gas is fed to the lower pressure vessel. Both reaction and purge gas are mixed in the lower part of the reaction tube and leave the pressure vessels together. The purge gas prevents reaction gas from entering the weighing unit. The pressure in the PRETA is controlled by a needle valve in the off-gas.

Mass flow controllers, pressure valve, and temperature controller are monitored by a personal computer and the weight loss during the experiment is recorded.

5.3.4.2 Experimental Procedure for the PRETA

Different chars collected during the operation of the PiTER are analysed in the PRETA. As the char samples consist partially of fine matter that could easily be blown away by the reaction gas in the experiment, the char sample (50 mg) was first placed within a mesh bag (stainless steel 1.4841, mesh width 42 μm). The mesh bag was strapped to the thermocouple on top of the sample holder by two stainless steel wires that are welded to the mesh bag. In test experiments in a CO_2 atmosphere without a char sample, a mass increase of the mesh bag was recorded. This weight gain was also confirmed by an external balance and was in the range of 1 mg to 2 mg. The increase in weight is likely caused by a reaction of CO_2 with the mesh material. As the weight gain is expected to be dependent on temperature, time, and reaction gas composition, it leads to an unknown error in the

reaction rate measurement of char.

Hence, experiments without a stainless steel mesh are carried out. The char sample is placed in a ceramic crucible (diameter 20 mm, height 4 mm). The rim of the crucible is very narrow to minimise mass transport limitations between the bulk gas phase and the char surface. The crucible is put on the sample holder. The thermocouple (type K) is recessed in the ceramic plate of the holder and the thermocouple tip has a direct thermal contact to the bottom of the crucible.

Due to the low rim of the crucible, the removal of fine matter by the reaction gas is likely, especially when the gas flow rate is changed in an experiment. Therefore, the char sample is first placed into a mesh bag, and the fine matter is removed by clean compressed air. Then the remaining char is filled into the crucible. In all experiments the initial sample size is between 40 mg and 60 mg.

After the char sample is placed within the reaction tube and all flanges of the PRETA are closed, the inner volume is vacuumed to remove air. Then the pressure is slowly increased in an inert gas atmosphere (N_2 or Ar). When the setpoint pressure is reached, the gas flow rate and temperature controllers are started.

The nominal gas flow rate (standard conditions) in the experiments is adjusted in order that the true volumetric gas flow rate at different pressures is constant. At 0.5 MPa the reaction gas flow rate is $500 \text{ ml}_N/\text{min}$ (273 K, 101.3 Pa). This is then increased to $1 \text{ l}_N/\text{min}$ at 1.0 MPa, $1.5 \text{ l}_N/\text{min}$ at 1.5 MPa, $2 \text{ l}_N/\text{min}$ at 2.0 MPa, and $2.5 \text{ l}_N/\text{min}$ at 2.5 MPa.

In all experiments the reaction gas flow rate is high enough to ensure a product gas concentration (e.g. CO) below 1 mol%.

The purge gas flow rate is adjusted to be equal to the reaction gas flow rate. The minimum threshold value of purge gas is $1 \text{ l}_N/\text{min}$. Therefore, the purge gas flow rate is higher than the reaction gas flow rate in low pressure experiments. This has no influence on the weight data.

Experiments with two different types of temperature profiles are carried out:

Experiment at a constant temperature In experiments at a constant temperature the reaction rate of char at constant conditions is measured. A typical temperature and weight profile is shown in Figure 5.13. The temperature is increased to the setpoint temperature of 750°C with a heating rate of $15 \text{ K}/\text{min}$. The weight of the sample changes during heat-up because the gas density (buoyancy) and the gas velocity (flow resistance) are influenced by temperature. When the constant temperature plateau at 750°C is reached, the weight remains stable. After 105 min the gas atmosphere is changed to CO_2 which is indicated by a small discontinuity in the weight curve. Directly after the CO_2 reaches the char sample, the gasification reaction is initiated and weight decreases. At about 400 min the weight remains constant because the organic matter of the char sample is completely converted. At 475 min the gas atmosphere is switched back to N_2 which is detected by a small discontinuity in the weight profile. At 510 min the heater is switched off and the temperature rapidly decreases.

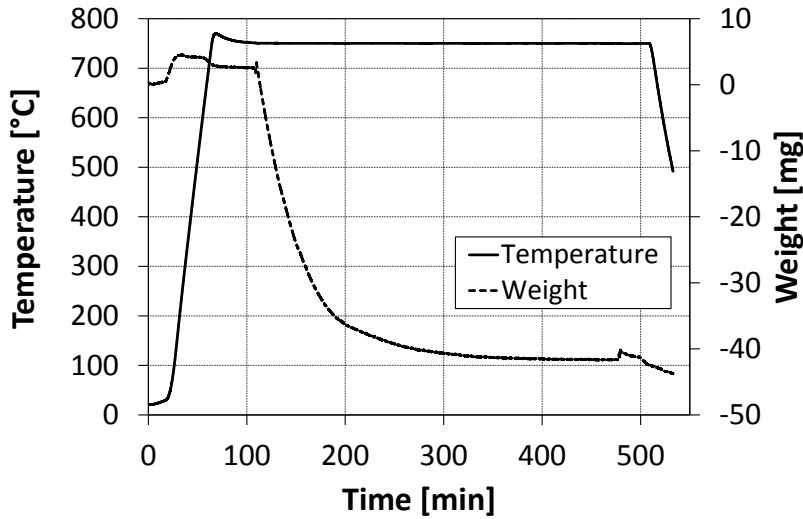


Figure 5.13: Temperature and weight curve in a PRETA experiment with a char sample of lignite R (sample ID: 20101220_PiTER_c) ($T=750^{\circ}\text{C}$, $p_{\text{CO}_2}=0.5\text{ MPa}$, $p_{\text{total}}=0.5\text{ MPa}$)

The reaction rate is calculated from the weight curve.

$$r_T = \frac{dm}{dt \cdot m} = \frac{dx}{dt \cdot (1-x)} \quad (5.5)$$

where the observed reaction rate r_T is dependent on char conversion x . For example, the reaction rate at 750°C ($r_{750^{\circ}\text{C}}$) and the conversion rate dx/dt derived from the data in Figure 5.13 are shown in Figure 5.14. Due to the continuously decreasing sample mass, the conversion rate (dx/dt) decreases. The reaction rate ($dm/(dt \cdot m)$) first increases slightly and reaches a maximum at $x = 0.6$ to 0.7 , but then decreases at higher conversions. The curve shape is dependent on char properties.

Experiment at a constant heating rate In experiments at a constant heating rate, the influence of temperature on char reaction rate is evaluated. Figure 5.15 shows a temperature and weight profile of an experiment with a lignite R char. The char sample is first heated to 600°C in an inert gas atmosphere. When the temperature is stable at 600°C , the gas atmosphere is switched to CO_2 indicated by the narrow discontinuity in the weight profile at 85 min. As a temperature of 600°C is too low for the char reaction with CO_2 , the weight initially remains constant. At 100 min the sample is heated at 10 K/min up to 1000°C . The start of weight loss is observed at 105 min when the temperature is about 680°C . Due to the continuous temperature increase, the reaction rate accelerates and the weight loss becomes faster. At 130 min the weight loss levels off as the organic matter of the char is converted completely.

As the weight curve is also influenced by buoyancy effects during the heating period from 600°C to 1000°C , the weight is corrected with a reference curve that is recorded when no char sample is in the crucible. Then the reaction rate is calculated from the weight curve according to Equation 5.5. The mass specific reaction rate r_T ($=dm/(dt \cdot m)$) and the conversion rate dx/dt are shown in Figure 5.16. The reaction rate strongly increases with temperature until the char sample is converted completely at about 880°C . Then dx/dt

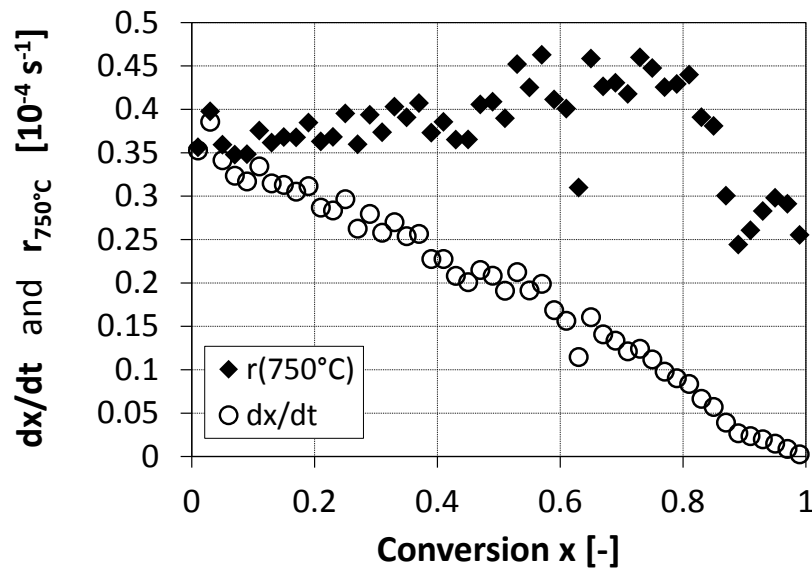


Figure 5.14: Conversion rate dx/dt and reaction rate ($dm/(dtm)$) as a function of conversion for a char sample of lignite R (sample ID: 20101220_PiTER_c) ($T=750^{\circ}\text{C}$, $p_{\text{CO}_2}=0.5$ MPa, $p_{\text{total}}=0.5$ MPa)

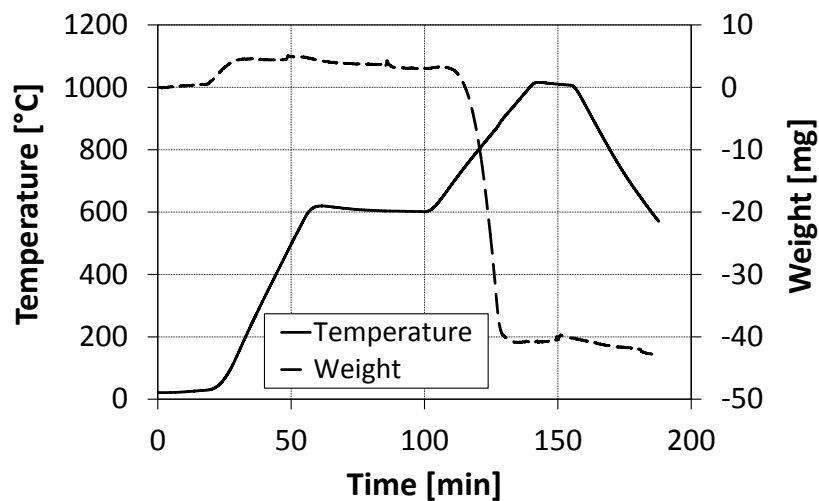


Figure 5.15: Temperature and weight curve in a PRETA experiment at constant heating rate for a char sample of lignite R (sample ID: 20101220_PiTER_c) (10 K/min, $p_{\text{CO}_2}=0.5$ MPa, $p_{\text{total}}=0.5$ MPa)

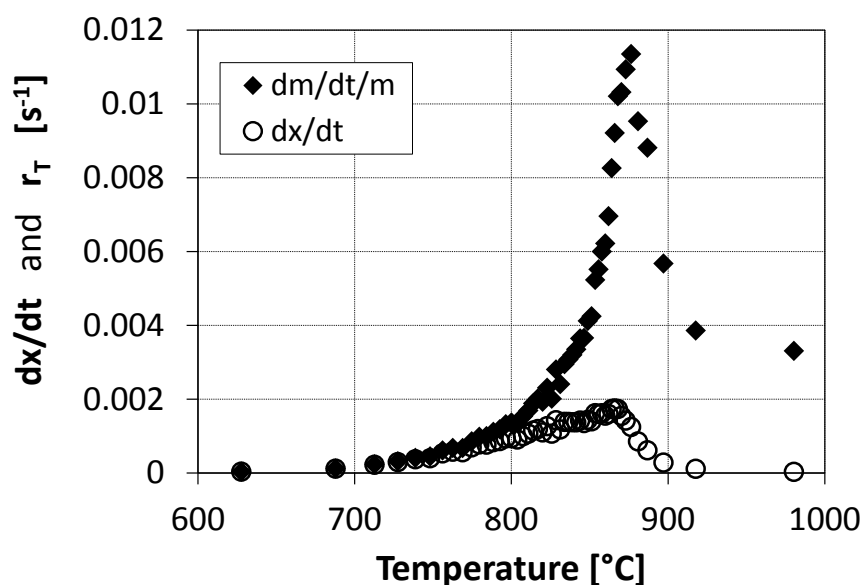


Figure 5.16: Conversion rate dx/dt and reaction rate ($dm/(dtm)$) as a function of temperature for a char sample of lignite R (sample ID: 20101220_PiTER_c) (10 K/min, $p_{CO_2}=0.5$ MPa, $p_{total}=0.5$ MPa)

rapidly approaches zero. As the reaction rate is related to instantaneous mass and the remaining char mass is very small, tiny weight changes result in a high reaction rate. The reaction rate that is shown above 880°C is caused by small weight fluctuations that are independent of the char reaction. When the organic char mass is low, the error in the reaction rate data is high and the data are not considered for further analysis.

5.3.5 Atmospheric Thermogravimetric Analyser

Char samples collected from the entrained flow reactors and the wire mesh reactor are analysed in an atmospheric thermogravimetric analyser (ATGA) (Linseis STA PT 1600). The weight loss rate at a low temperature in an oxygen containing atmosphere is measured. This data are used to calculate reactivity of different chars at standardised experimental conditions.

A char sample is placed between two layers of mesh (mesh width 42 μm , stainless steel 1.4841) that are welded together at three sites to form a small bag. In contrast to the PRETA experiments in a CO_2 containing atmosphere and at higher temperature, a variation of the mesh weight during the experiment in the oxygen containing atmosphere is not observed. Clean compressed air is used to remove fines from the char sample that could otherwise get lost in the experiment and falsify the conversion data.

The sample holder consists of a ceramic plate (Al_2O_3 , diameter 20 mm). The thermocouple (type S) is situated within a central pin that protrudes approx. 15 mm from the centre of the ceramic plate. The mesh bag is strapped to the thermocouple by two stainless steel wires that are welded to the bag. This configuration enables a direct thermal contact between the thermocouple tip and the char sample in the mesh bag. The mesh material allows a good gas exchange between the char sample and the surrounding atmosphere, prevents the accumulation of product gases, and minimises gas concentration gradients

within the char sample.

Due to the high reactivity of the lignites, a low experimental temperature (350°C to 400°C) is chosen. The chars are heated in a nitrogen atmosphere to setpoint temperature. Then, the atmosphere is switched to 5 mol% oxygen in nitrogen and the weight loss is recorded. The gas flow rate is held constant at 200 ml/min (at 0°C, 0.1013 MPa). From the weight loss data, the reaction rate is calculated:

$$r = \frac{dm}{dt \cdot m} = \frac{dx}{dt \cdot (1 - x)} \quad (5.6)$$

where m is the instantaneous mass of the sample. As the reaction rate is dependent on conversion, an average reaction rate is chosen to compare the reactivity of different chars. The initial weight loss up to 0.075 conversion is excluded to eliminate effects of the gas change and possible effects of volatiles combustion that have remained within the char structure during devolatilisation at a very short residence time. At a higher conversion the relative measurement uncertainty increases due to the lower sample mass. Furthermore, not all char samples achieved complete conversion in the reaction time given. Therefore, the conversion interval from 0.075 to 0.325 is chosen to calculate an average reactivity. This average reaction rate is referred to as *standard reactivity*.

A larger sample mass improves the measurement accuracy. However, with increasing sample size, mass and heat transfer limitations within the char sample might occur. The measured reaction rate is then not only dependent on the char surface reactivity. As the sample size must not influence the standard reactivity measured, experiments with different amounts of char are carried out. The reference char of the lignite R is used in the tests. Figure 5.17 shows the effect of sample size on reaction rate at a temperature of 400°C. The weight recording interval is 1 s. This leads to a high scatter in the data as very small weight deviations result in large differences in the reaction rate calculation. When calculating average reaction rates in an interval of 2 minutes, a clear trend in the data is shown.

An amount of 25 mg is chosen as the lowest sample size⁵. With this sample size, there are only a few layers of char particles in the mesh bag and a very good gas exchange is feasible. The doubling to 50 mg sample size does not influence the reaction rate data. A further increase to 75 mg and 100 mg results in a significant rise of the reactivity at up to 0.4 conversion. The temperature measurement at the char sample shows in both cases an increase to approx. 410°C. This indicates a significant influence of the exothermic combustion reaction for the larger samples size and the heat-up of the sample. Due to the large sample size the reaction heat cannot be removed from the sample surface and an internal heat-up is observed. Therefore, the reaction conditions are not longer stable and the reaction rate increases which is shown in Figure 5.17. If a smaller sample size (25 mg and 50 mg) is used, the reaction heat can be removed by the gas flow and an internal heat-up does not occur. The temperature in these experiments remains constant at 400°C.

In all the standard reactivity experiments a sample size of 40 mg to 50 mg is used. The

⁵In test experiments with 10 mg of char, relative large weight fluctuations were recorded and the measurement uncertainty was high.

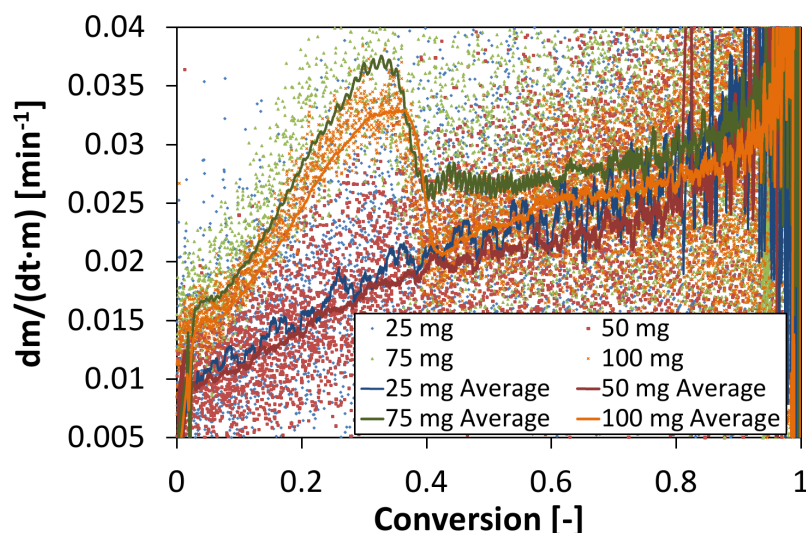


Figure 5.17: Effect of sample size (lignite R ref-char) on reaction rate measured at 400°C in a 5 mol% O₂ in N₂ atmosphere in the atmospheric TGA

reaction temperature of chars of bituminous coal is set to 400°C. As the reactivity of lignite chars that are produced under entrained flow conditions at a short residence time is expected to be higher than the lignite reference char reactivity, the temperature in the experiments is decreased to 375°C. The reaction time in all experiments is set to 300 min.

5.4 Experimental Results

5.4.1 Results from the Entrained Flow Reactors

The two entrained flow reactors PiTER and BabiTER are used to measure fuel conversion in pyrolysis and gasification experiments. Several measurement sets are carried out and a total number of over 250 entrained flow experiments is available. The measurement matrix in Figure 5.18 gives an overview of the experimental parameters used in the entrained flow reactors. Data at different residence times are available for each measurement point in temperature and pressure.

In this section first the methods to determine particle residence time and fuel conversion are discussed and then experimental data are presented.

5.4.1.1 Calculation of Particle Residence Time in the Entrained Flow Experiments

The total gas flow rate is used to adjust the average gas residence time in the reaction tube. However, the average particle residence time may deviate from the gas residence time. Possible deviations are caused by different effects that are discussed in the following paragraphs.

Increase in gas amount by fuel gasification During the devolatilisation and gasification reactions the gas flow rate in the reaction tube continuously increases. This leads to a decrease in the true gas residence time compared with the adjustments of the MFCs. The

Lignite R					Lignite V				
	1000°C	1200°C	1400°C	1600°C		1000°C	1200°C	1400°C	1600°C
0.1 MPa		X O	X O	X O	0.1 MPa		X O	X O	X
0.5 MPa		X O	X O	X O	0.5 MPa	X	X	X	
1.0 MPa		O							
2.5 MPa		X	X						

Bituminous coal A					Anthracite				
	1000°C	1200°C	1400°C	1500°C		1000°C	1200°C	1400°C	1600°C
0.5 MPa		O	X O	O	0.1 MPa		X O	X	X O
1.0 MPa		X O	X		0.5 MPa		X O	X O	
2.0 MPa			X		Biocoal				
3.0 MPa		X			0.1 MPa	O	O	O	
4.0 MPa		X							

Figure 5.18: Measurement matrix for entrained flow experiments in BabiTER (0.1 MPa) and PiTER (higher pressure). Crosses (X) indicate pyrolysis experiments, and circles (O) denote gasification experiments.

decrease in the average gas residence time is dependent on the gas to fuel ratio. For fuels with a high volatile matter content that are mainly used in the experiments, devolatilisation contributes to gas production more significant than the heterogeneous gasification reactions. Therefore, the potential influence of solid fuel devolatilisation is calculated for each experimental run and heterogeneous reactions are neglected. In a worst case calculation, the devolatilisation occurs instantly at the point of fuel injection and a higher gas flow rate exists along the whole reaction tube. Then, the deviation between true average gas residence time and adjusted value is 0 % to 7 % for the PiTER experiments.

In the atmospheric BabiTER experiments the influence of devolatilisation is higher. The true average gas residence time can be 2 % to 22 % lower than the setpoint residence time, depending mainly on fuel type and gas flow rate.

The uncertainties in both reactors arise from the fact that it is not known a priori at which time and at which position in the reaction tube the increase in the gas amount occurs. If a linear increase in the gas amount along the reaction length is assumed, the deviation of residence time is only half the worst case values mentioned above. It is assumed that devolatilisation in the experiments occurs between these boundary cases. Therefore, the average gas residence time is reduced by three quarters of the worst case values mentioned above and the error interval is equal at both sides of this value.

Incomplete entrainment If the free fall velocity of the particles is significant compared to the gas velocity, the particles are moving faster than the surrounding gas atmosphere. Both PiTER and BabiTER are designed as entrained flow reactors where the gas flow rate is high. In a laminar gas flow the deviation can be calculated analytically as shown in Figure 5.6. For each experimental run, the entrainment is calculated assuming a particle

density of 1000 kg/m^3 and a diameter of $100 \text{ }\mu\text{m}$ which is a worst case consideration as the mean particle size is smaller in the experiments.

The particle entrainment in the PiTER experiments is between 82 % and 95 % with the average at 90 %. This reduces the average particle residence by approx. 10 % compared to the average gas residence time. However, the assumption of a laminar flow along the whole reaction tube is a worst case consideration since fuel injection causes turbulence in the upper part of the reaction zone. Hence, the true deviation between average particle residence time and average gas residence time caused by incomplete entrainment is less than 10 %.

The BabiTER is operated at atmospheric pressure. This decreases the gas density and increases the particle free fall velocity. However, the BabiTER is operated on average with a slightly higher gas velocity. Therefore, the entrainment is high and is between 82 % and 97 % with the average at 90 %. In BabiTER experiments the assumption of a laminar flow is a good approximation as there is a flow straightener installed before the particle injection and the particles are injected in gas flow direction. Furthermore, the gas density at atmospheric pressure is low resulting in low Reynolds numbers. Hence the deviation between the true particle residence time and gas residence time is approx. 10 %.

By the determination of the laminar free fall velocity of the particles, a maximum reduction of particle residence time is calculated for each experimental run. The true reduction is assumed to be half the maximum deviation, and the uncertainty at both sides of this value is 50 % of the maximum deviation. For example, if the maximum reduction of the particle residence time due to incomplete entrainment is 0.2 s in an experiment, the true deviation is assumed to be 0.1 s and the uncertainty is $\pm 0.1 \text{ s}$.

Flow velocity distribution within the reaction tube For each experimental run the Reynolds number of the gas flow profile within the reaction tube is calculated. The gas properties are calculated using material constants of pure nitrogen. The Reynolds number is dependent on the gas flow rate, temperature and pressure.

In **PiTER** experiments values of the Reynolds number range from 800 to 4000 with the average being 1800. As the critical Reynolds number that indicates the transition between the laminar and the turbulent region is 2320, most experiments are nominally performed in the laminar region. However, in these experiments turbulence occurs during fuel injection and therefore in the upper part of the reaction tube. A laminar flow profile is only expected at the lower part of the reaction tube. The gas velocity in the centre of a laminar flow profile is higher than the average flow velocity⁶. Therefore, particles that are in the centre of the reaction tube move faster than particles that are near the wall. In the turbulent region, the flow profile is described by a plug flow where the gas velocity is equal along the radial position. The particle velocity is then not dependent on the radial position.

As the flow profile of all experiments can be described neither by complete laminar nor by complete turbulent flow, an exact analytical calculation of the particle velocity as a function of radial position is not possible. A solution to this problem is the positioning of the sampling probe. If the sampling probe were placed exactly in the centre of the reaction tube, the residence time of collected particles would be shorter than the average gas res-

⁶In an ideal laminar flow profile the centre velocity is twice as high as the average gas velocity.

idence time in a laminar flow, but equal to the average gas residence time in a turbulent flow. The sampling probe is therefore placed between the centre of the reaction tube and the wall as shown in Figure 5.19. The exact position is calculated assuming a laminar flow profile within the reaction tube. As a result, the centre of the sampling probe is shifted 21 mm to the side and the ideal position is shown in the figure. The probe position in between test runs is checked by a borescope and photos are shown in Figure 5.19.

In a laminar flow the average gas residence time in the cross section of the sampling probe at the selected position approaches the average gas residence time in the cross section of the reaction tube. Therefore, also the residence time of particles collected with the probe approaches the average gas residence time in the reaction tube. In a turbulent flow the position of the probe does not influence the average residence time of the particles collected. The residence time of particles collected with the probe equals the average gas residence time independent of the flow regime.

The position of the sampling probe cannot be controlled during the operation when the reaction tube is heated. In gasification experiments the fuel conversion should be dependent on the radial position. This cannot be proved experimentally as a radial movement of the probe after the assembly is not possible.

Furthermore, a displacement is possible during a measurement set due to the vertical movement of the probe that might also influence the radial position. Hence, a deviation in the experiments is expected. The distance between the sampling probe and the reaction tube wall is 2 mm. The maximum positive deviation is therefore 2 mm. For the maximum negative deviation 5 mm are assumed. In a worst case consideration a pure laminar flow is assumed which results in an uncertainty of the average gas residence time within the probe cross section of -33 % and +8 %.

In **BabiTER** experiments the Reynolds number is between 90 and 370. A laminar flow profile is expected in all experiments. Due to the flow straightener and the particle injection in flow direction, only small turbulences are likely in the upper part of the reaction tube. The velocity of the particle carrier gas is 4 to 5 times higher than the velocity of the main reaction gas. This leads to a distribution of the particles in the cross section of the reaction tube. However, the particle concentration in the centre of the reaction tube is still higher than near the wall. An analytical calculation of the flow profile shows that particles are concentrated within a diameter of ~ 20 mm around the centre of the reaction tube. Due to the small fuel mass flow rate in BabiTER experiments, this effect is desired as particle wall impacts are reduced. The calculation is substantiated by the observation that there are only minor slag deposits on the reaction tube wall even after a prolonged operation. Due to the high gas diffusivity at high temperature, a homogeneous gas concentration in the cross section of the reaction tube is expected.

Because of the small fuel mass flow, the sampling probe is placed in the centre of the reaction tube to collect a sufficient char mass in an appropriate time interval. As the true gas residence time in the centre of a laminar flow profile is lower than the average gas residence time in the whole cross section, the residence time of the collected particles is reduced. Char and gas is sampled isokinetically, i.e. the gas flow above the cross section of the sampling probe is sucked into the probe with the same velocity as the main gas that passes the probe. In each experiment the average gas residence time in this cross section

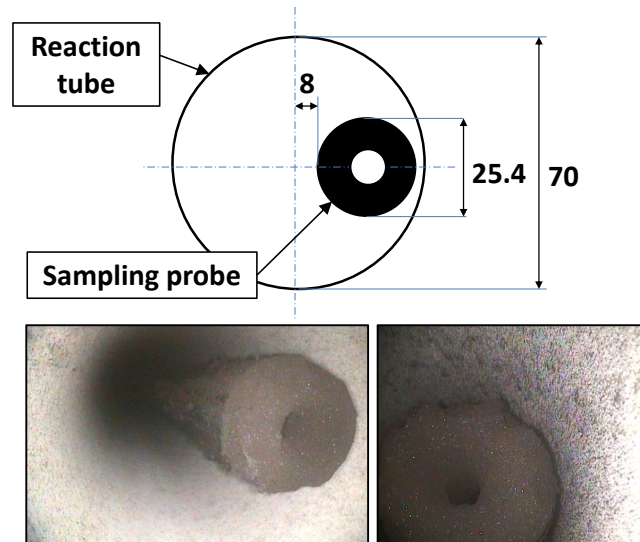


Figure 5.19: Position of the sampling probe in the reaction tube for the PiTER experiments

(diameter 22 mm) is calculated. As only particles are removed that are within this cross section, the average particle residence time equals the average gas residence time in this cross section. Due to the laminar flow in each experiment which yields identical flow profiles, the deviation between the particle residence time and the average gas residence time is constant. The particle residence time is 41 % lower than the average gas residence time that is adjusted by the MFCs. Due to an uncertainty in the isokinetic conditions that are caused by the unprecise measurement of the gas volume flow through the sampling probe⁷, the uncertainty of the particle residence time is $\pm 8\%$ for each experiment.

Due to the combined effects of the devolatilisation, the incomplete entrainment, and the flow profile in the reaction tube, the true particle residence time of the char collected differs from the average gas residence time that is adjusted in each run. For each experimental run the true particle residence time and the uncertainty are calculated. The uncertainties of the three effects are combined by an error propagation method:

$$\tau_{\text{true, particle}} = \tau_{\text{MFC, adjusted}} - \Delta_{\text{Devolatilisation}} - \Delta_{\text{Particle Free Fall}} - \Delta_{\text{Sampling Probe}} \quad (5.7)$$

$$u(\tau_{\text{true, particle}}) = \sqrt{\sum_{k=1}^3 \left(\frac{\partial \tau_{\text{true, particle}}}{\partial \Delta_i} \right)^2 \cdot u^2(\Delta_i)} \quad (5.8)$$

Table 5.5 summarises the range of deviations and average uncertainties of all experimental runs. For each experimental run the deviations caused by the three effects are combined and the average particle residence time is calculated. The average particle residence time

⁷The uncertainty of the gas flow rate through the sampling probe is $\pm 30\%$ (± 90 l/min). This leads to an uncertainty in the cross section from which particles are sucked into the sampling probe of $\pm 20\%$ (± 4 mm).

Table 5.5: Particle residence time of char collected in the entrained flow experiments. The maximum and minimum deviations of residence time are given whereas the uncertainty denotes an average value for all experiments.

Deviation of particle residence time by	PiTER	BabiTER
	Min/Max Uncertainty	Min/Max Uncertainty
Devolatilisation	-(0.01-0.18)s (\pm 0.02 s)	-(0.01-0.19)s (\pm 0.02 s)
Incomplete entrainment	-(0.01-0.29)s (\pm 0.10 s)	-(0.01-0.10)s (\pm 0.03 s)
Flow profile	0 s (\pm 0.38 s)	-(0.08-0.59)s (\pm 0.03 s)
Total deviation	-(0.03-0.40)s (\pm 0.40 s)	-(0.09-0.83)s (\pm 0.05 s)

is used in the subsequent presentation of the entrained flow results.

In order to minimise the uncertainties, CFD aided experiments would be required. In an iterative procedure the flow profile of each experimental run could be evaluated. As the increase in gas amount influences the flow profile and the particle properties may change during conversion, experimental data with an analytical evaluation of the particle residence time would be required in the first step. Then, the experimental data could be used to improve the model prediction and to correct particle residence time. However, this is beyond the scope of this dissertation.

5.4.1.2 Calculation of Conversion in the Entrained Flow Experiments

The conversion in the entrained flow experiments can either be calculated from the gas analysis or the char analysis.

In the first approach it is assumed that the nitrogen molar flow rate is constant within the reaction tube. The total flow rate can be calculated from the N_2 concentration and the N_2 flow rate. Gaseous nitrogen produced during fuel conversion is neglected. The molar flow rate of carbon in the gas phase is known from the gas analysis as CO_2 , CO , and CH_4 concentrations are measured. As the mass flow rate of carbon in the fuel is known from the fuel analysis, the carbon conversion can be calculated from the gas analysis. However, the uncertainty in the CO measurement by mass spectroscopy is about ± 3 mol%. The accuracy of the IR analyser depends on the calibration quality in the measurement range and is estimated to be ± 1 mol%. As in the pressurised experiments the nitrogen molar flow rate is high to achieve a short residence time within the reaction tube. the gas concentrations measured are low and the relative errors are high. An uncertainty in the CO analysis of 1 mol% results in a deviation of carbon conversion of up to 15 %. Also, uncertainties in other gas concentrations contribute to the error.

Furthermore, at a low residence time and a low-temperature tar compounds or hydrocarbons are in the gas phase. These cannot be detected by the gas analysis. Therefore, carbon conversion measured by the gas analysis is likely too low.

Hence, the calculation of conversion from the gas analysis is not considered in the data evaluation. Elemental and overall conversions are calculated by an ash tracer method that is widely applied in literature for the determination of coal and biomass conversion (e.g. [Kobayashi1977, Monson1995, Rosenberg1996, Yeasmin1999, Simone2009,

Yoshiie2011]). It is assumed that the amount of mineral matter in the char is constant during conversion. Ash devolatilisation is neglected. The calculation procedure is summarised in the Appendix A. The quality of an ash tracer method is discussed in literature. Monson et al. [Monson1995] calculated the conversion after pyrolysis and oxidation of three bituminous coals in a drop tube reactor by an ash tracer method. They compared the results with Ti and Al⁸ as a tracer and concluded that burn-off calculated from each of the tracers correlated within a few percent. Yeasmin et al. [Yeasmin1999] studied the pyrolysis of brown coal in a drop tube reactor at up to 1000°C and calculated conversion with ash, Al, Ca, Mg, Fe, and Ti as tracers. It was found that the difference of the tracer methods was less than 4%daf of coal and that there is negligible evaporation of the ash. For PiTER and BabiTER experiments the uncertainties in conversion calculations caused by the char analysis are discussed in the Appendix A. The confidence intervals are summarised in Table 5.6.

Table 5.6: Average absolute extended uncertainties in conversion data for entrained flow experiments (based on ash content measurement and elemental analysis)

Confidence Level	68.3 %	95 %
Carbon Conversion	1.0 %	2.0 %
Sulphur Conversion	42.1 %	84.2 %
Nitrogen Conversion	7.9 %	15.8 %
Overall Conversion	0.8 %	1.6 %

The char sample mass is not always large enough to measure ash content (especially in BabiTER experiments). The oxygen concentration in a char sample after devolatilisation is very low. Therefore, the ash content can be calculated directly from the CHNS analysis assuming an oxygen concentration of 0 wt%. This results in a higher uncertainty of ± 0.47 wt% of the ash content. The average absolute extended uncertainty of carbon conversion is then 3.4 wt% (95 % confidence interval) and of overall conversion 3.0 wt% (95 % confidence interval).

The calculation of conversion from the gas analysis and char analysis are directly compared in a parity plot in Figure 5.20. The data set contains all experimental runs from the BabiTER where both methods of conversion calculation are applied. The error analysis showed that the scatter and deviation from the diagonal is mainly caused by the uncertainty in gas analysis. In general, carbon conversion from the gas analysis is lower than from the char analysis which indicates the effect of hydrocarbons and tar compounds that are not considered in the gas analysis.

5.4.1.3 Pyrolysis in the Entrained Flow Reactors

Pyrolysis experiments are carried out in both entrained flow reactors. The PiTER is operated at 0.5 MPa to 4.0 MPa. Pyrolysis at atmospheric pressure is analysed in the BabiTER. The temperature in both reactors ranged from 1000°C to 1600°C. The results are presented and discussed for each fuel separately.

⁸Due to the high evaporation temperature of Ti and Al the devolatilisation of these elements is not expected.

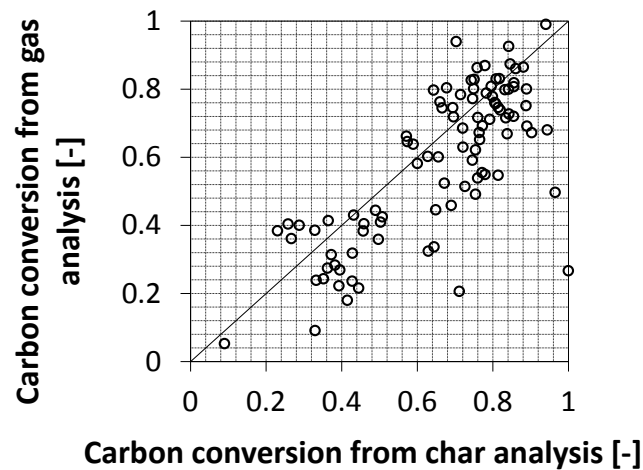


Figure 5.20: Parity plot of the calculation of carbon conversion from gas and char analysis from BabiTER experiments

Lignite R Pyrolysis experiments using lignite R are carried out in inert and reducing gas atmospheres. The PiTER is operated either with pure nitrogen or with a mixture of hydrogen and nitrogen. The hydrogen molar concentration is adjusted to 8 mol% in the reaction tube. In Figure 5.21, pyrolysis experiments in both atmospheres are compared directly.

A significant dependence of conversion on the gas atmosphere is not observed. In inert and reducing atmospheres, the volatile yield increases with residence time and temperature. The final conversion is not dependent on the gas atmosphere. A significant increase in volatile yield⁹ or a contribution of the hydrogenation reaction is not observed up to 2 s residence time even at very high temperature. The reaction rate of hydrogen with char is slow and is not expected to increase significantly the overall reaction rate during heterogeneous char gasification. In the further data analysis, experiments in both reducing and inert gas atmospheres are not distinguished.

Figure 5.22 summarises pyrolysis data of lignite R at atmospheric pressure and 0.5 MPa. The particle residence time is varied between 0.2 s and 2 s and the temperature between 1200°C and 1600°C. Both carbon conversion and overall conversion (equal to volatile yield) increase with particle residence time. At a low residence time an influence of temperature is observed. This is due to the faster devolatilisation reactions at higher temperature. At longer time scales the differences diminish and there is no significant influence of temperature on volatile yield. The char samples at atmospheric pressure in the BabiTER are generally collected at a lower residence time and therefore a direct comparison to experiments at pressure is not possible. However, the trends of data from both reactors are in good agreement within the measurement uncertainty. A significant influence of pressure on volatile yield is not observed from 0.1 MPa to 0.5 MPa.

In the PiTER experiments the pressure is further increased. Figure 5.23 shows experimental data at 1.0 MPa and 2.5 MPa. Within the measurement uncertainty there is no significant influence of pressure on volatile yield. At a particle residence time above 1.0 s there is also no influence of temperature and the average final volatile yield of lignite R under entrained

⁹In pyrolysis experiments the overall fuel conversion equals volatile yield as char conversion does not occur.

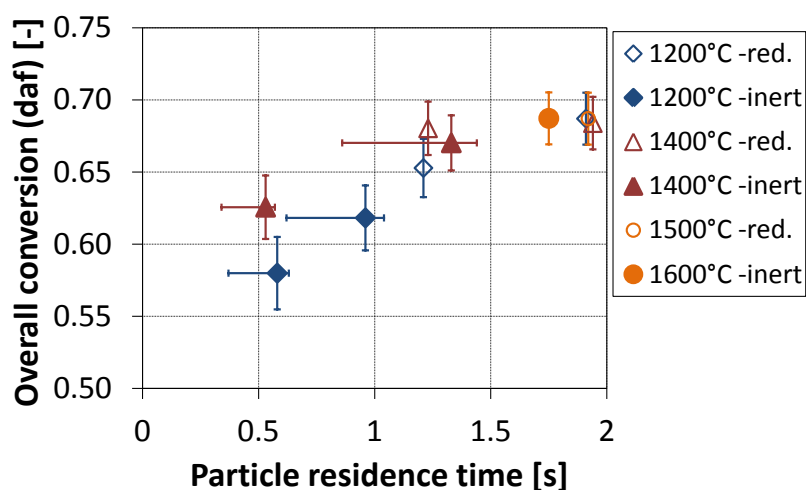


Figure 5.21: Entrained flow pyrolysis experiments with lignite R at 0.5 MPa in different gas atmospheres. Open symbols denote experiments in N_2 ; closed symbols denote experiments in a reducing (H_2/N_2) atmosphere. The particle residence time denotes the gas residence time that is corrected by the influences of devolatilisation, incomplete entrainment, and flow profile. Error bars are shown exemplary.

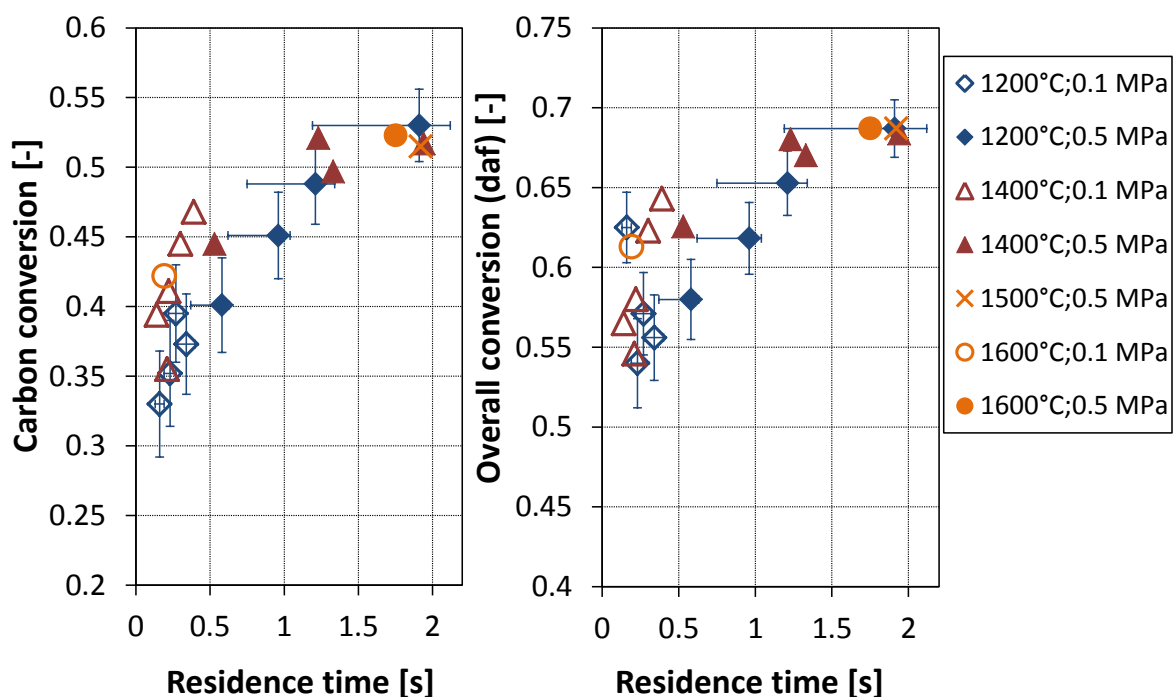


Figure 5.22: Conversion during the pyrolysis of lignite R at atmospheric pressure (BabiTER) and at 0.5 MPa (PiTER). Error bars are shown exemplary for the 1200°C data and are comparable for the other data points.

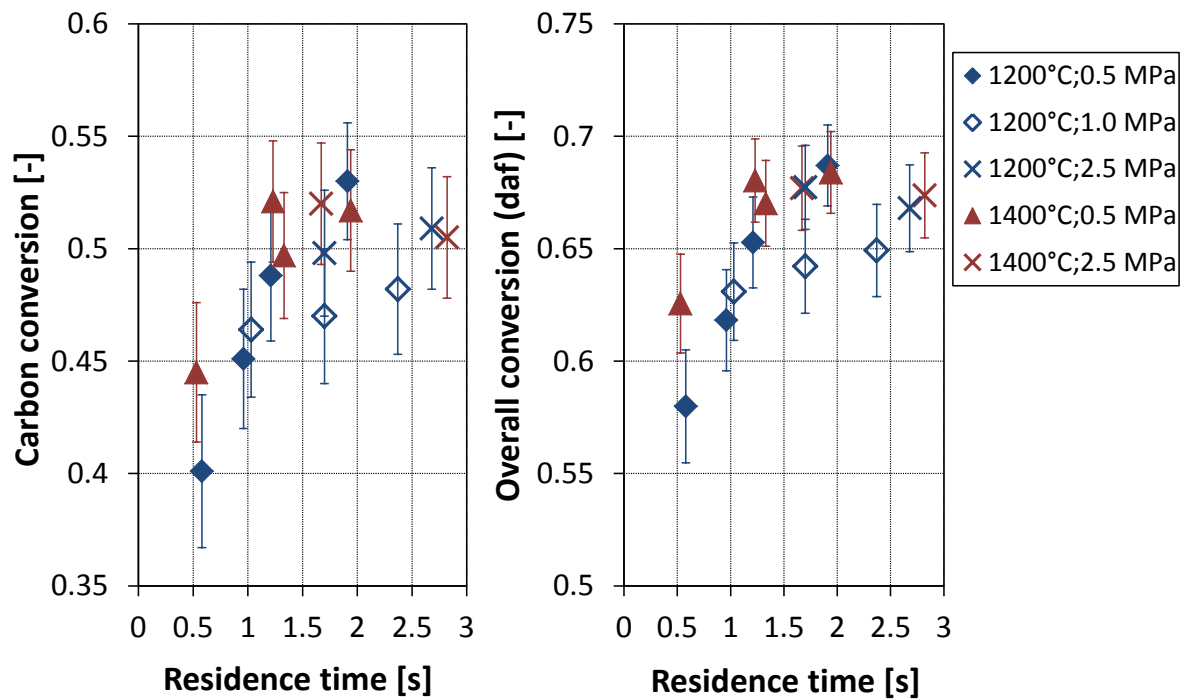


Figure 5.23: Conversion during the pyrolysis of lignite R at 0.5 MPa, 1.0 MPa, and 2.5 MPa in the PiTER as a function of particle residence time and temperature

flow conditions is 68 wt% (daf). Carbon conversion at 2 s is on average 52 %, i.e. about half of the carbon remains within the char structure.

In the BabiTER experiments at shorter residence times, the carbon conversion is lower. The average value is 39 %.

Lignite V Similar pyrolysis experiments are carried out with lignite V. The pressure in the PiTER is 0.5 MPa and the BabiTER is operated at atmospheric pressure. The conversion data in a nitrogen atmosphere from 1200°C to 1600°C are shown in Figure 5.24. Error bars denote uncertainties of the calculation of conversion from char analysis and uncertainties in particle residence time, respectively.

At 1200°C the conversion increases with particle residence time. However, there is some scatter in the data as shown by the two measurement points at 2 s residence time. The average overall conversion (volatile yield) at 2 s is 67.5 wt%. At 1400°C the conversion in the BabiTER is slightly higher. At a longer residence time in the PiTER the deviation diminishes. Both carbon and overall conversion at 1600°C are lower than at 1400°C. This can only be explained by measurement errors. A small deviation of residence time could cause a large deviation of conversion during the devolatilisation phase. Furthermore, ash devolatilisation could have an influence.

At a temperature of 1400°C a higher conversion at 0.1 MPa than at 0.5 MPa is observed. This might indicate an influence of the devolatilisation pressure. However, the difference is not significant and can also be explained by the measurement uncertainty.

The carbon conversion under entrained flow conditions is calculated from the average of conversion between 1.5 s and 2 s residence time (1200°C and 1400°C data) and is 49 %. The volatile yield at longer residence times under entrained flow conditions is on average

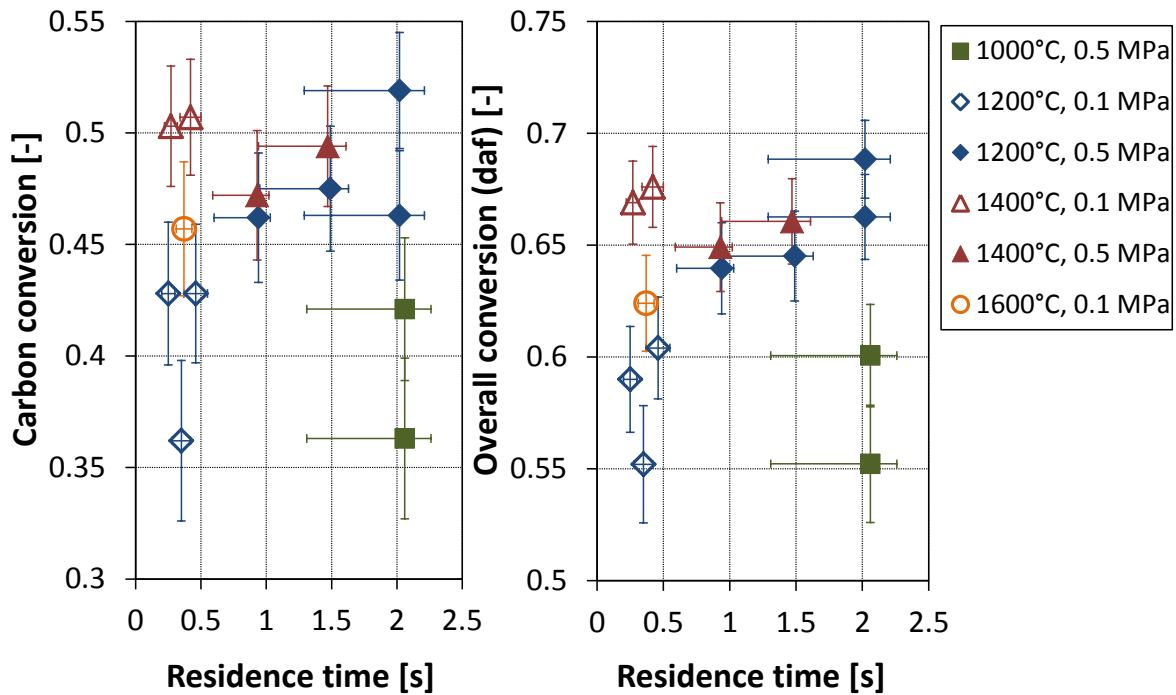


Figure 5.24: Conversion during the pyrolysis of lignite V at atmospheric pressure (BabiTER) and at 0.5 MPa (PiTER) as a function of particle residence time and temperature

66 wt%.

At a shorter residence time (BabiTER), the carbon conversion is slightly lower and the average value of all BabiTER data is 45 %.

Bituminous coal A All pyrolysis experiments with bituminous coal A are carried out in the PiTER. The operation pressure ranges from 0.5 MPa to 4.0 MPa and the reaction temperature is 1200°C and 1400°C, respectively. Experimental data are shown in Figure 5.25. Error bars denote the uncertainties in the char analysis and in the particle residence time calculation, respectively.

Compared with the two lignites there is a large scatter in the data and a clear influence of particle residence time or temperature is not observed. The highest conversion is detected at 1400°C and 0.5 MPa (closed triangles). At 1.0 MPa and 2.0 MPa the conversion is lower indicating a possible influence of pressure. At 1200°C the highest conversion is measured at 1.0 MPa and also a decrease is observed when the pressure is increased to 3.0 MPa and 4.0 MPa. However, the quality of the data set is low and deviations within a data series cannot be explained by the uncertainty in the char analysis.

Therefore, other effects are likely that influence the conversion data. Ash devolatilisation at higher temperatures would lower the conversion data. This is not observed in the data set as conversion at 1400°C is mostly higher than at 1200°C.

The PiTER experiments with bituminous coal A were the last test runs and were carried out after a few weeks of operation using different coals. Some ash and slag particles were already attached to the reaction tube surface. When changing the gas atmosphere to oxygen after the pyrolysis experiments considerable amounts of CO and CO₂ were detected. This is an indicator that coal and char sticks to the reaction tube surface. The accumu-

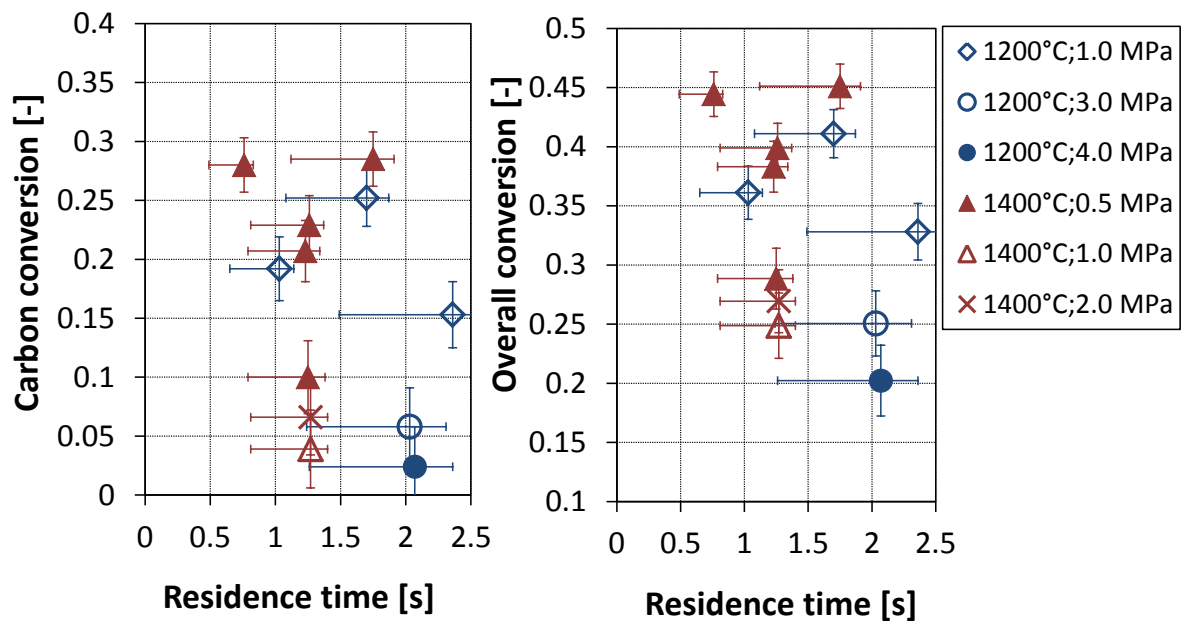


Figure 5.25: Conversion during the pyrolysis of bituminous coal A from 0.5 MPa to 4.0 MPa in the PiTER as a function of particle residence time and temperature

lated char in the experiment might fall down and is collected by the sampling probe. This strongly falsifies the char sample and could also be a reason for the large scatter in the pyrolysis data.

Another effect is soot formation. Tar compounds and hydrocarbons that are released during the pyrolysis can form soot particles in the gas phase. As the oxygen content of the bituminous coal A is much lower than that of the lignites, the probability of soot formation in pyrolysis experiments with the bituminous coal is higher. Oxygen atoms that are also released during the pyrolysis of lignite promote the formation of CO and CO₂ and prevent soot generation. The formation of soot is also indicated by particle size measurements that are discussed later. Therefore, soot formation is likely that could influence the conversion data. As the generation of soot is also dependent on temperature and pressure, the scatter in the conversion data could be explained.

For the calculation of char conversion in later gasification experiments the carbon conversion during the pyrolysis phase is required. As the conversion during the 1400°C/0.5 MPa experiments is highest, soot formation for this data series is neglected and an average carbon conversion is calculated. This is 22 %. The uncertainty of the data is expressed by the large absolute standard deviation of 7.5 %. The average overall conversion (volatile yield daf) of these experiments is 39 wt%, and the maximum value is 45 wt%.

Anthracite Entrained flow pyrolysis experiments with anthracite are carried out in the BabiTER at atmospheric pressure and in the PiTER at 0.5 MPa. Experimental conversion data are shown in Figure 5.26. Error bars denote measurement uncertainties from the char analysis and from the particle residence time calculation.

An increase in carbon and overall conversion is observed with progressing particle residence time. At a short residence time and at atmospheric pressure the conversion is dependent on temperature and continuously increases from 1200°C to 1600°C. In the PiTER experiments

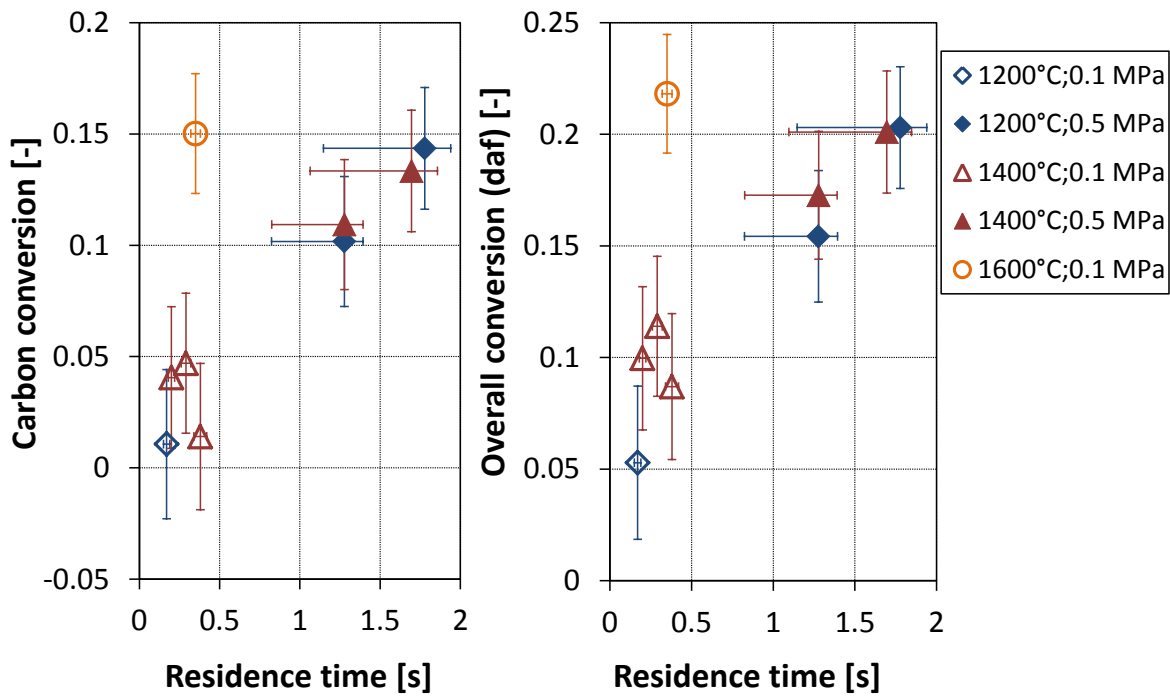


Figure 5.26: Conversion during the pyrolysis of anthracite in the BabiTER (0.1 MPa) and PiTER (0.5 MPa) at 1200°C and 1400°C

at longer residence times there is no clear difference between the 1200°C and the 1400°C data. The conversion at a short residence time (0.4 s) and at 1600°C is similar to the data at 1200°C/1400°C and longer residence time (1.7 s) indicating the kinetic effect of temperature on devolatilisation.

The final carbon conversion during the pyrolysis is assumed to be the average data at 1.7 s residence time. It is 14 % and the absolute standard deviation is 1 %. In BabiTER experiments at a lower residence time the carbon conversion is on average 5 %, but the absolute standard deviation of 6 % is relatively high.

5.4.1.4 Gasification in the Entrained Flow Reactors

The gasification experiments are carried out in both entrained flow reactors. In all experiments a constant stoichiometry is applied. For each carbon atom in the fuel mass flow one oxygen atom in the reaction gas is provided. This results in a constant oxygen to carbon ratio (O/C) of 1 ± 0.1 . The uncertainty results from deviations of the MFCs and the fuel mass flow rate. The temperature in both reactors is varied between 1000°C and 1600°C and the pressure is increased up to 1.0 MPa. Experimental data at 2.5 MPa are not used in the evaluation as there were fluctuations in the fuel mass flow rate that were noted after the experiments.

Char that was collected during the experiments is used to calculate the elemental and overall conversion of the fuel. The char conversion is a further important parameter for the understanding of the fuel conversion behaviour, but cannot be measured directly. The pyrolysis experiments have shown that most of the conversion during devolatilisation occurs at a very short residence time below 0.2 s. Both reactors are not designed to further reduce the residence time and still achieve a high measurement resolution. But even at a

low residence time some char is already converted in heterogeneous reactions due to the reactive gas atmosphere. In the BabiTER experiments the first measurement point is after 0.2 s to 0.3 s and in the PiTER experiments after about 0.5 s. Therefore, the resolution of gasification experiments at high temperature is limited to the medium and later stages of char conversion and in both reactors the conversion during devolatilisation and during the first stages of char gasification cannot be separated.

The data from the pyrolysis experiments are used to measure the progress of char conversion. During the pyrolysis stage, the amount of char that is produced is measured precisely as heterogeneous gasification reactions are excluded. The carbon conversion during the pyrolysis experiments is used to calculate char conversion C_{char} in the gasification experiments:

$$C_{char} = \frac{C_{C,gasification} - C_{C,pyrolysis}}{1 - C_{C,pyrolysis}} \quad (5.9)$$

where $C_{C,gasification}$ is the carbon conversion in the gasification experiment and $C_{C,pyrolysis}$ is the carbon conversion in the corresponding pyrolysis experiment that is carried out at identical pressure and temperature. It is assumed that char only consists of carbon and mineral matter. Small amounts of hydrogen, oxygen, and other trace elements are neglected in this calculation. The carbon conversion during pyrolysis has been measured separately for each fuel as shown before.

For the calculation of the overall conversion in the gasification experiments, all organic elements of the fuel (carbon, hydrogen, oxygen, nitrogen, sulphur, and trace elements) are considered. The determination of the overall conversion is based on the ash content of the parent fuel and the char sample. The overall conversion shown in the following diagrams includes the conversion during devolatilisation and char conversion.

Conversion results are presented and discussed in the following paragraphs for each fuel:

Lignite R In the pyrolysis experiments the carbon conversion is not dependent on temperature at a particle residence time of 1.5 s to 2 s. The average carbon conversion is 52 % that is used for the calculation of char conversion at longer residence time. The absolute standard deviation of the data is 1 % and it is used for the calculation of the uncertainty in char conversion. At a short residence time (BabiTER experiments) the carbon conversion during pyrolysis is lower. The average carbon conversion up to 0.4 s residence time is 39 % that is used for the calculation of char conversion. The scatter in data is higher which is indicated by the standard deviation of 4 %.

The entrained flow gasification data of lignite R are shown in Figure 5.27. Experiments at a low particle residence time and under atmospheric pressure are carried out in the BabiTER. In the PiTER the residence time is increased up to 2.4 s. The temperature range in both reactors is 1200°C to 1600°C.

Both overall and char conversion increase rapidly with particle residence time. The temperature has a significant influence on the conversion. However, the difference in conversion between 1200°C and 1400°C is small and decreases further between 1400°C and 1600°C. In the early stages of conversion there is a steep increase in char conversion indicating a fast reaction rate. After a residence time of 0.5 s about 50 % of the char is already gasified. The reaction rate slows down at higher residence times and conversions.

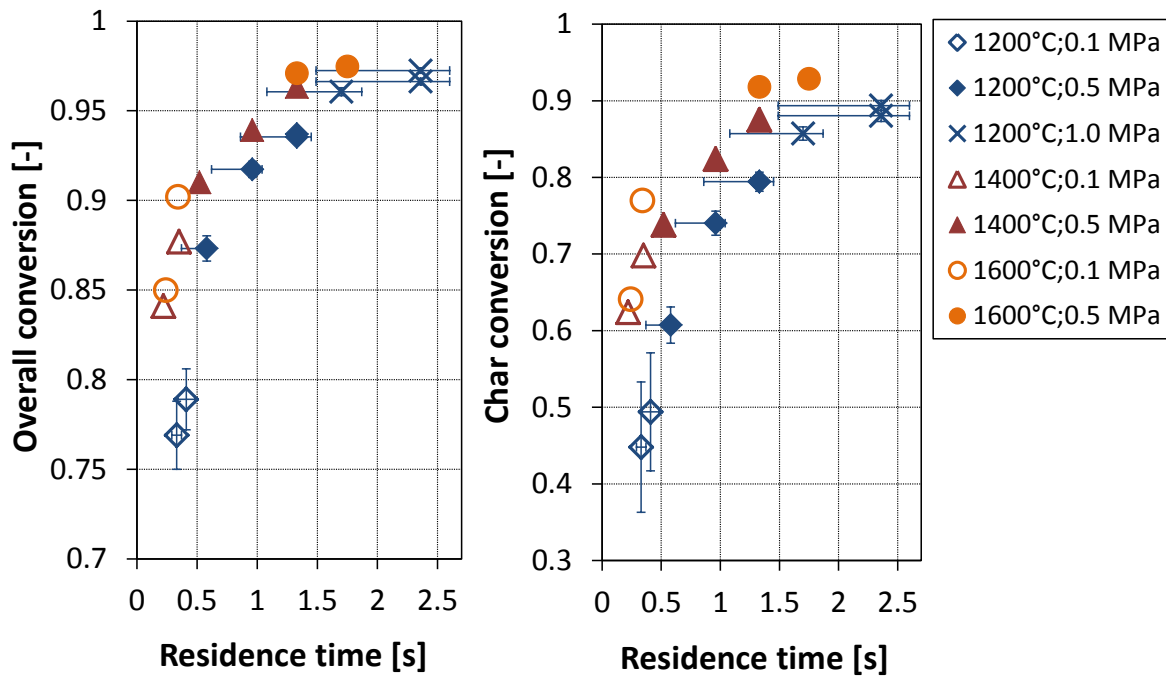


Figure 5.27: Gasification results of lignite R at a constant stoichiometry of $O/C = 1 \pm 0.1$ as a function of particle residence time, temperature, and pressure. Error bars are shown exemplary for the 1200°C data and are comparable for all measurement points.

There is a continuous trend in the data from 0.1 MPa to 1.0 MPa when particle residence time is increased as the data for a constant temperature lie within a small band. This trend is independent of the operation pressure indicating no significant influence of the total pressure on reaction rate.

Lignite V The gasification experiments with lignite V are carried out in the PiTER and the BabiTER. However, the fuel mass flow rate in PiTER experiments was inhomogeneous and these data are not used for the analysis. In BabiTER experiments the temperature is 1200°C and 1400°C. The stoichiometry is adjusted by a constant O/C ratio of 1. The overall and char conversions are shown in Figure 5.28. The average carbon conversion in the BabiTER is 45 % during the pyrolysis experiments which is used for the calculation of char conversion in the gasification experiments. The absolute standard deviation is 5 % which results in the relatively large error bars of char conversion in Figure 5.28.

Both overall and char conversions are very high even at a short residence time indicating the high reactivity of lignite V. At 1200°C no significant influence of residence time is detected which is caused by the narrow residence time interval and the measurement uncertainties. A rise of temperature to 1400°C significantly increases the conversion and results in 93 % overall conversion after a particle residence time of 0.4 s.

Bituminous coal A The gasification kinetics of bituminous coal A are analysed in the PiTER at 0.5 MPa and 1.0 MPa. A constant stoichiometry of $O/C = 1$ is applied and the temperature is varied between 1200°C and 1500°C. The experimental data are shown in Figure 5.29. Error bars denote the measurement uncertainty in char analysis, particle residence time, and calculation of char conversion. The large error bars of the char conversion

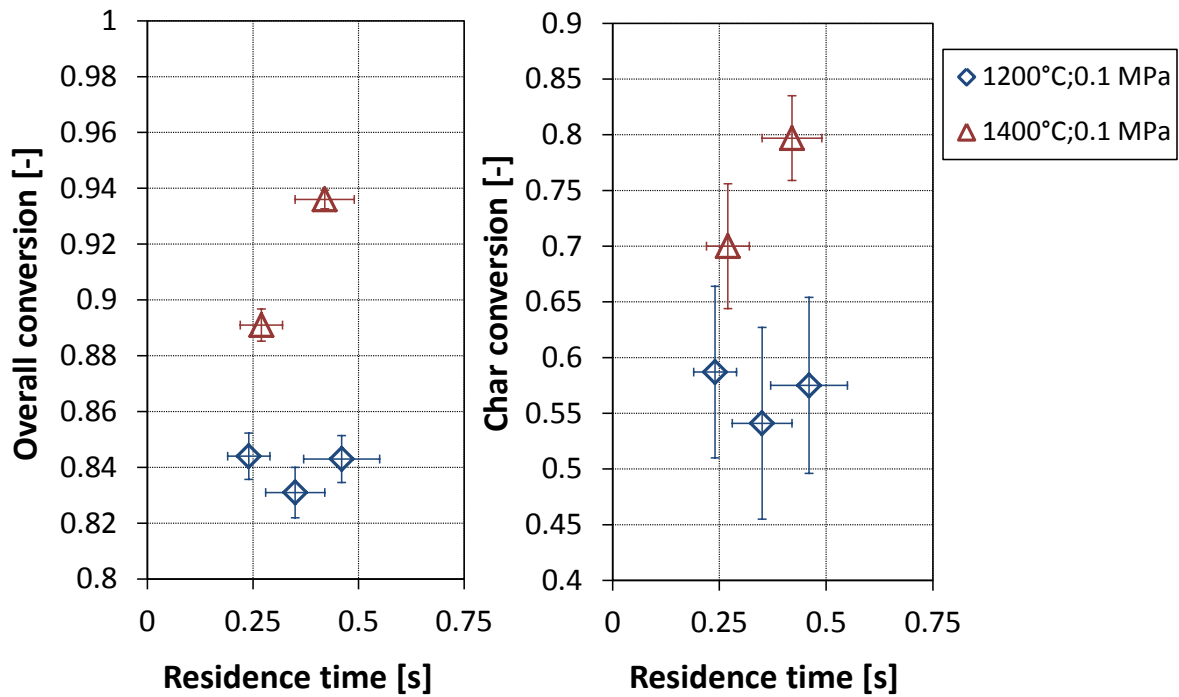


Figure 5.28: Gasification results of lignite V at a constant stoichiometry of $O/C = 1 \pm 0.1$ as a function of particle residence time and temperature in the BabiTER experiments

are mainly caused by the uncertainty of carbon conversion during the pyrolysis experiments that is 22 % (standard deviation 7.5 %).

At 0.5 MPa the overall and char conversions considerably increase from 1200°C to 1400°C. A further rise of temperature to 1500°C does not increase the conversion. An increase in pressure to 1.0 MPa seems to promote the conversion rate especially in the early stages, but a direct comparison at identical residence times is not possible. The overall conversion at 1.7 s residence time and 1400°C/1500°C is 80 wt%. As a higher temperature is not expected to further increase the conversion, a longer residence time is required to observe higher levels of conversion.

Anthracite The lowest conversion is observed during the gasification of anthracite. The experiments are carried out in the PiTER at 0.5 MPa and in the BabiTER under atmospheric pressure. The stoichiometry is adjusted by an O/C ratio of 1. The experimental data are shown in Figure 5.30. The char conversion is calculated using the carbon conversion during the pyrolysis experiments (14 % for PiTER data, 5 % for BabiTER data). A significant influence of residence time and gasification temperature is shown in the data. Due to the low volatile yield of anthracite (on average 18 wt% in the PiTER pyrolysis experiments) the overall and char conversions deviate only slightly. The maximum overall conversion at 1400°C is 54 wt% at a particle residence time of 1.3 s. In order to measure higher conversion levels, experiments at longer residence times are required.

Biocoal To evaluate the reaction behaviour of biogenous fuels under entrained flow conditions, biocoal is converted at a constant stoichiometry of $O/C = 1$ in the BabiTER. The temperature is varied between 1000°C and 1400°C. When feeding biocoal with nitrogen

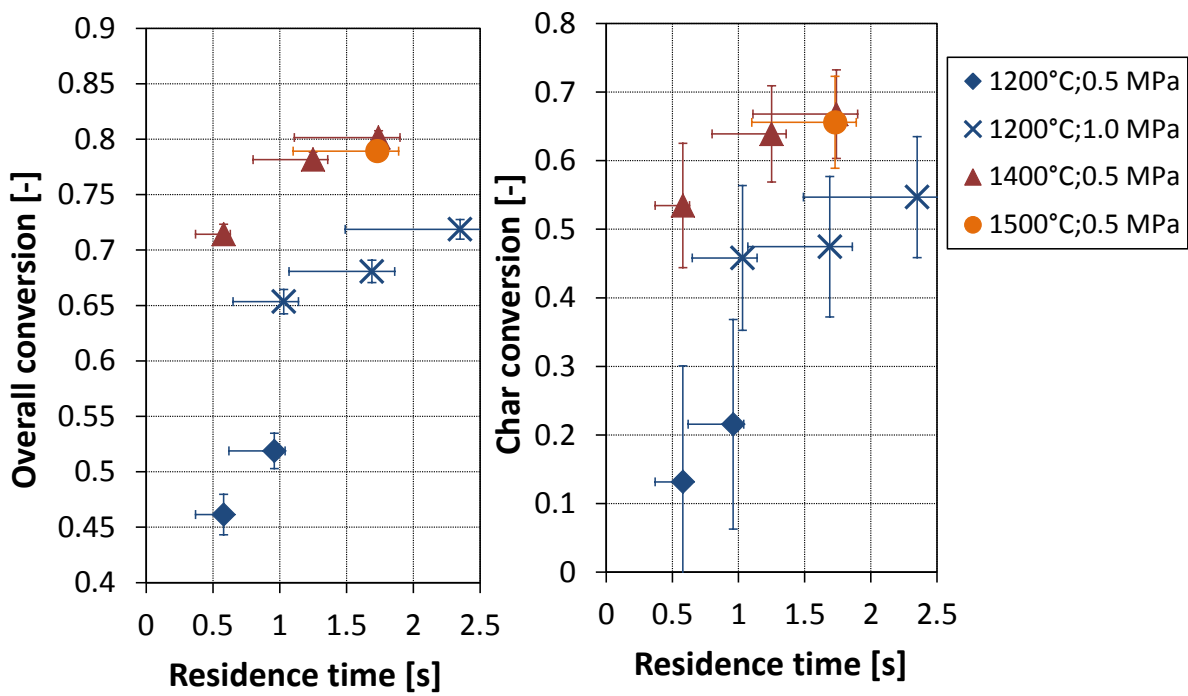


Figure 5.29: Gasification results of bituminous coal A at a constant stoichiometry of $O/C = 1 \pm 0.1$ as a function of particle residence time, temperature, and pressure

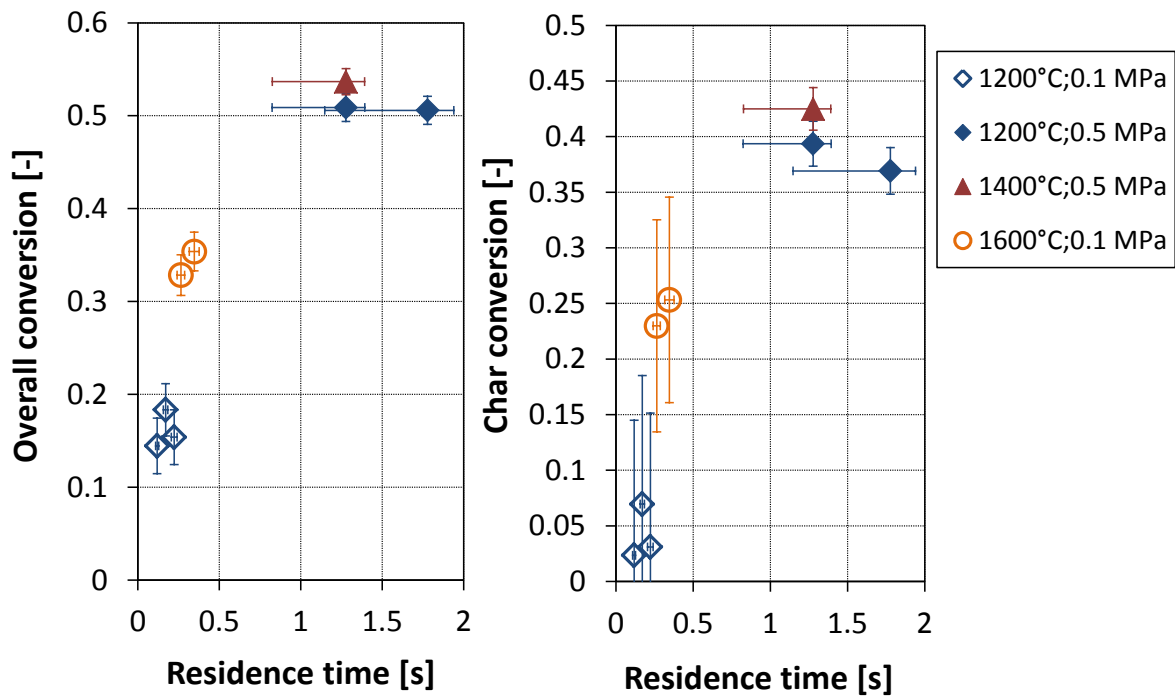


Figure 5.30: Gasification results of anthracite at a constant stoichiometry of $O/C = 1 \pm 0.1$ as a function of particle residence time, temperature, and pressure

as the carrier gas to the hot reaction zone, the partial devolatilisation caused a plugging within the feeding tube. Therefore, the feeding system is changed to the burner like design¹⁰ described in Section 5.3.2.3. Biocoal is fed to the inner feeding tube with nitrogen as the carrier gas. Pure oxygen is fed to the annular gap between the two feeding tubes and is mixed with biocoal upon entering the hot zone. The oxygen concentration at the mixing point is 40 mol%. The volatiles that are released during heat-up are ignited preventing a blockage of the feeding tube. Due to the volatiles combustion, the temperature within the feeding tube is expected to be partially higher than in the main reaction tube (at least for the 1000°C and 1200°C experiments). The residence time within the feeding tube is only 30 to 60 ms.

The carbon and overall conversion of biocoal are shown in Figure 5.31. Due to the high conversion only low amounts of char are collected. The calculation of conversion is based only on the ultimate analysis which results in relatively large uncertainties. Because of the large uncertainties, the significance of the conversion data is low. However, there is a trend in the data that conversion increases with increasing residence time and temperature. After short residence times high levels of conversion are achieved indicating the high reactivity of biocoal.

The char conversion cannot be readily calculated as entrained flow pyrolysis experiments of biocoal are not available. Therefore, the carbon conversion during devolatilisation is estimated from the proximate and the ultimate analysis and comparable entrained flow data of lignite R. The carbon conversion in the proximate analysis (900°C) of lignite R is 34.8 %. In the entrained flow experiments at a low residence time (BabiTER) an average carbon conversion of 39.5 % is measured. The higher temperature and the particle entrainment result in an increase in the carbon conversion by a factor of 1.14. The carbon conversion in the proximate analysis of biocoal is 44.2 %. The influence of entrained flow conditions is assumed to be identical to the lignite R experiments (factor 1.14) and the carbon conversion during devolatilisation of biocoal is assumed to be 50.2 %. Based on this assumption, char conversion is calculated and shown in Figure 5.32.

Char conversion even at a short residence time is high and the residence time and temperature have an influence on conversion. However, an error analysis that is not shown in the diagram shows that the differences are not significant. The experiments with biocoal clearly show the high reactivity under entrained flow conditions. The application of the experimental data to develop kinetic models that can predict the gasification behaviour under industrial scale conditions is limited. Based on the experimental data, a prediction of conversion at variable temperatures and longer residence times is possible, but the uncertainty is high. The transfer of the data to larger scale gasifiers is difficult due to the relative large measurement uncertainty in the data.

5.4.1.5 Analysis of Char Specific Surface Area during Conversion

The specific surface area is measured by adsorption of CO₂ on the char surface at 273 K. The adsorption isotherms are analysed using density functional theory (DFT) and Dubinin-Radushkevich (DR) methods. As the heterogeneous gasification reactions take place at the

¹⁰In this dissertation the burner like design is only used for biocoal. Experiments were also carried out using lignite R as a fuel, but results are not shown here.

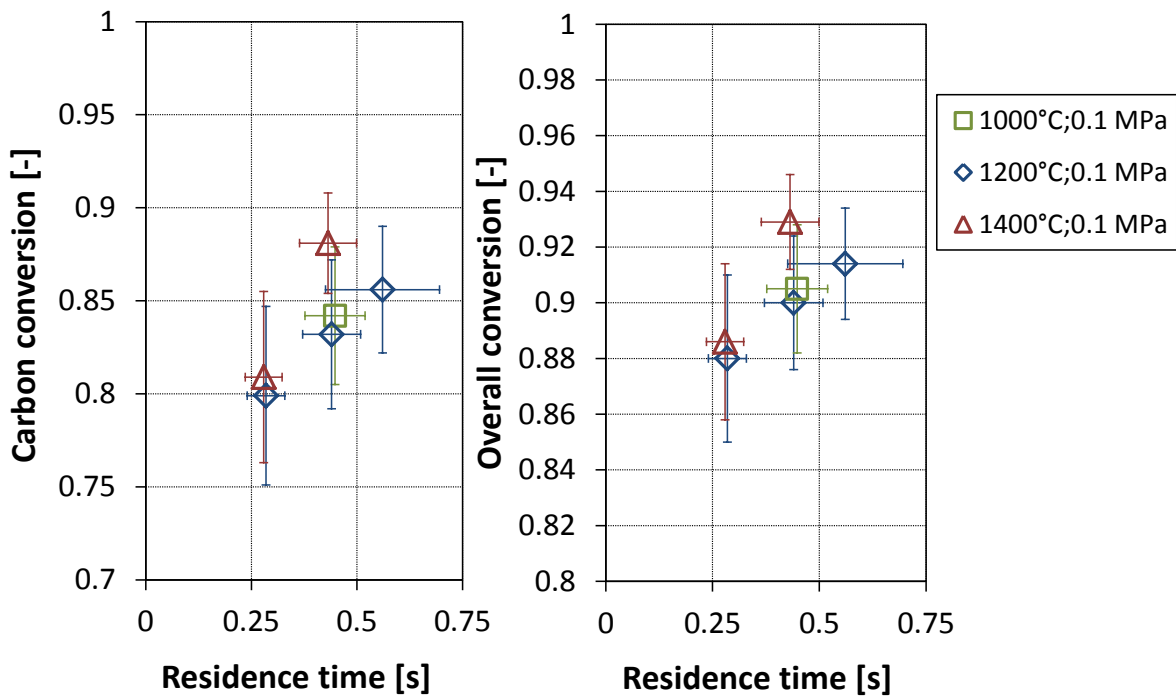


Figure 5.31: Carbon and overall conversion of biocoal after gasification at a constant stoichiometry of $O/C = 1$ in the BabiTER

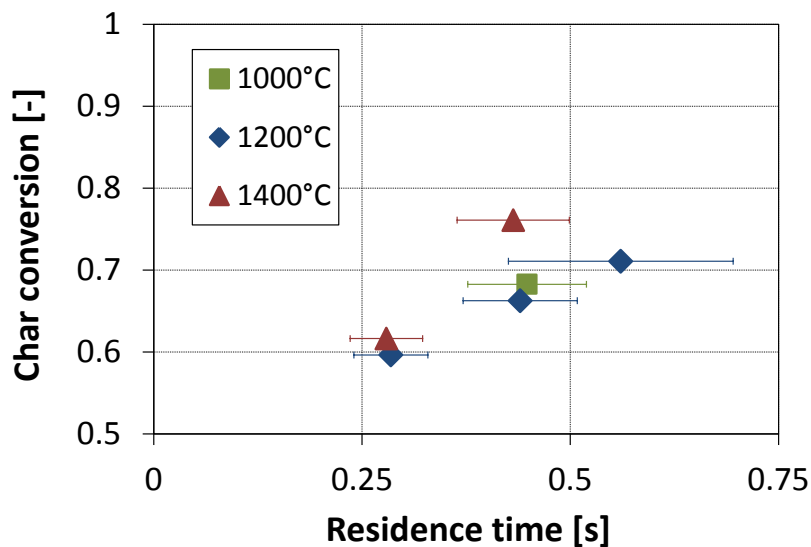


Figure 5.32: Char conversion of biocoal at atmospheric pressure and constant stoichiometry ($O/C=1$) calculated from the carbon conversion in entrained flow experiments and from the proximate analysis

char surface, the quantity of surface area can be a measure for char reactivity. The more area is available for reaction, the faster the overall reaction rate is. At a high temperature when the reaction rate is partially limited by pore diffusion the effect of surface area is expected to be lower. However, even in the pore diffusion regime a large part of the surface area is still accessible and the specific surface area is still an important parameter. Furthermore, pore diffusion is dependent on char porosity, and chars with a high porosity are also expected to show a large surface area. Hence, the specific surface area could also be a measure of char reactivity under Regime II conditions.

The specific surface area of about half of the chars that are collected during the pyrolysis and gasification experiments is measured. The results are analysed and discussed in the following paragraphs. The standard deviation in repeated measurements¹¹ is 21 m²/g for the DFT analysis, and 38 m²/g for the DR analysis. For further information see Section 5.2.2.

Lignite R The specific surface areas of 21 pyrolysis chars of lignite R that are produced at different temperatures, pressures, and residence times are shown in Figure 5.33. Both methods, DFT and DR, lead to similar results.

The initial surface area at a low residence time is 500 m²/g to 650 m²/g. For chars that are produced at 1200°C only a small initial decrease in surface area with particle residence time is observed. At a low residence time the devolatilisation is not complete which may cause the measurement of initially higher surface areas, especially in the DFT analysis. At a longer residence time the surface area almost remains constant at 1200°C. In contrast, at 1400°C and 1600°C the surface area rapidly decreases at longer time at temperature. The effect of pressure is shown in Figure 5.34 by a re-ordering of the data. The lines are linear regression fits to the experimental data. At very low residence time in the BabiTER experiments (atmospheric pressure) the surface area is very large, both at 1200°C and 1400°C. However, this may not be an influence of pressure as devolatilisation is not completed. At higher pressure data at comparable residence times are shown. The linear regression lines show a clear effect of pressure. At higher pressure surface area increases. Therefore, the total pressure during devolatilisation has an effect on char structure.

Specific surface area of 20 chars that are collected during gasification experiments of lignite R are shown in Figure 5.35.

When plotted against residence time, there is a clear difference between chars that are produced at 1200°C and at 1400°C/1600°C. The surface area of the 1200°C chars decreases almost linearly. The initial decrease in the surface area of 1400°C/1600°C chars is initially higher leading to significantly lower surface areas at higher temperatures. The surface area change of chars produced at different temperatures can be unified when the surface area is plotted against char conversion. All chars fall within a narrow band and the surface area rapidly decreases with char conversion. The effect of temperature is mainly explained by a higher level of char conversion at a higher temperature. Notwithstanding, the trend of a lower surface area at higher temperatures is still observed. The gasification

¹¹For the error analysis a PiTER pyrolysis char that was produced at 1400°C, 0.5 MPa and 1.3 s is used. Specific surface area is measured 8 times with the average at 513 m²/g (DFT) and 567 m²/g (DR), respectively.

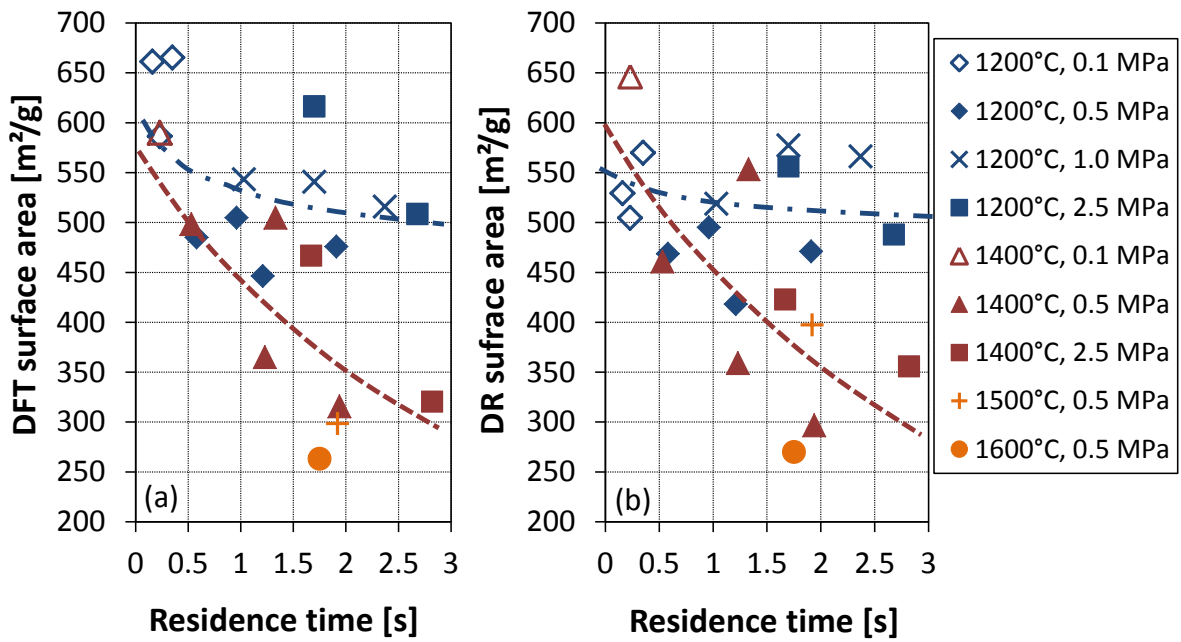


Figure 5.33: CO₂ surface area of pyrolysis chars of lignite R measured at 273 K: (a) DFT-method; (b) DR-method

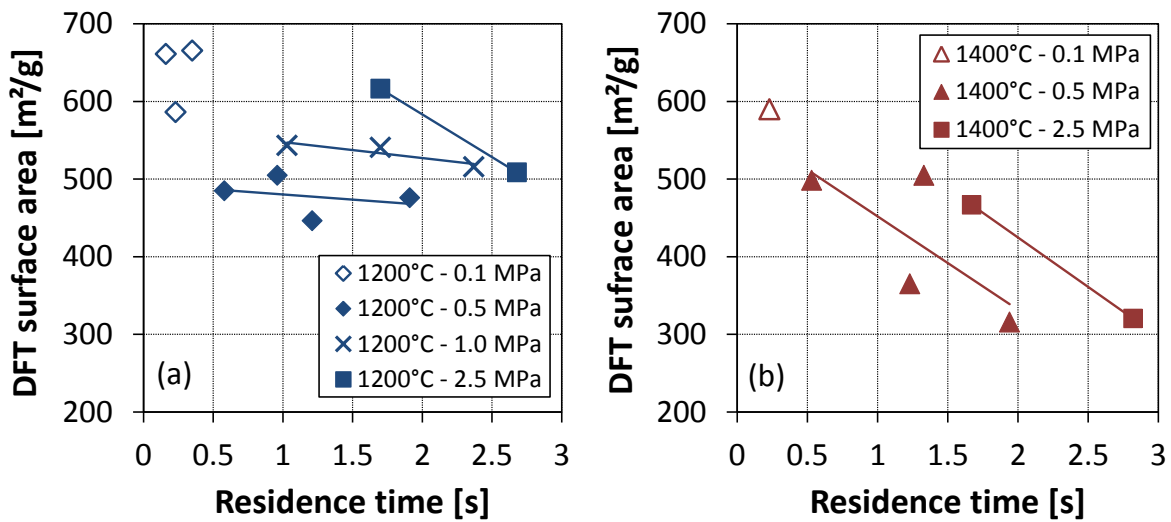


Figure 5.34: Specific surface area (CO₂-DFT) of pyrolysis chars of lignite R produced at different pressures: (a) experiments at 1200°C; (b) experiments at 1400°C

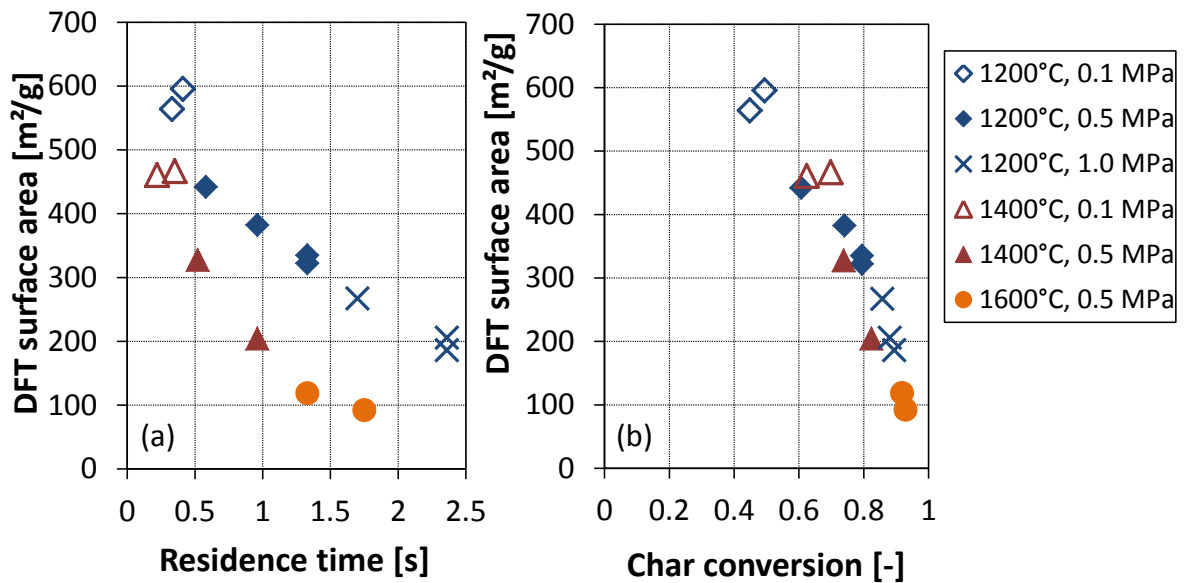


Figure 5.35: Specific surface area (CO₂-DFT) of gasification chars that are collected during gasification experiments of lignite R at different temperature, pressure, and residence time: (a) dependence on particle residence time; (b) dependence on char conversion

experiments are carried out at 0.1 MPa, 0.5 MPa, and 1.0 MPa. In contrast to the pyrolysis experiments, a significant effect of pressure on the surface area during gasification is not observed.

In Figure 5.33 it is shown that the surface areas evaluated by DFT and DR methods are similar. This is also confirmed by the gasification data (not shown here). In Figure 5.36 parity plots of DFT vs. DR surface area are shown for pyrolysis and gasification chars. In both diagrams, a good correlation between the DFT and DR methods is observed. For the pyrolysis chars (Figure 5.36(a)) the two methods yield no systematic difference. In the case of gasification chars (Figure 5.36(b)), the DFT method yields slightly lower surface areas than the DR method, but the difference is only marginally larger than the standard deviation of repeated measurements. Therefore, surface area derived from the two methods is considered as equal and in the following analysis only char surface areas that are calculated by the DFT method are presented.

Lignite V For lignite V the specific surface area is measured after the entrained flow pyrolysis experiments. The data are shown in Figure 5.37. In contrast to the lignite R chars, there is no clear influence of temperature. After the pyrolysis at 1000°C, 1200°C, and 1400°C the surface area is almost equal. The particle residence time seems to have an influence, as the surface area slightly increases at longer time at temperature. A re-organisation of the char surface or a partial pore opening might occur that both increase the specific surface area.

Bituminous coal A Pyrolysis and gasification chars of bituminous coal A are available to measure the specific surface area. The data of pyrolysis experiments at different temperatures and pressures are shown in Figure 5.38.

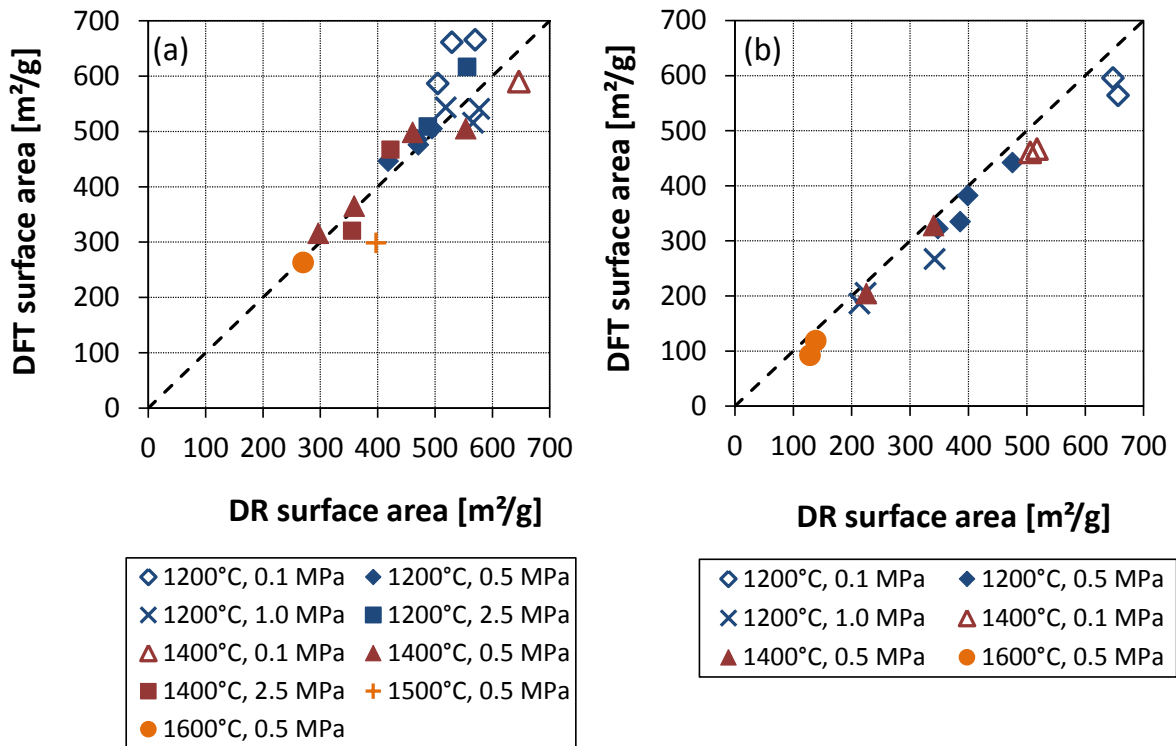


Figure 5.36: Surface area parity plots of pyrolysis (a) and gasification (b) chars using experimental data of lignite R

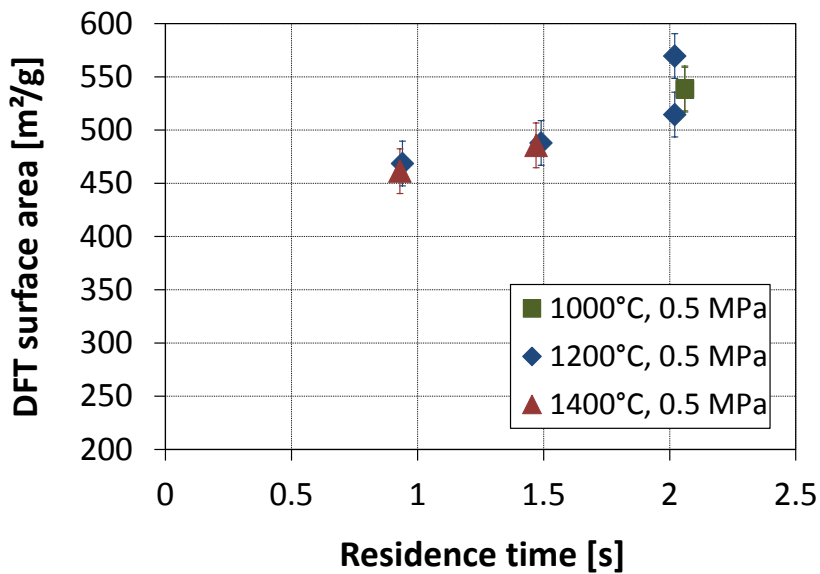


Figure 5.37: Specific surface area (CO₂-DFT) of pyrolysis chars of lignite V at different temperature and at a pressure of 0.5 MPa

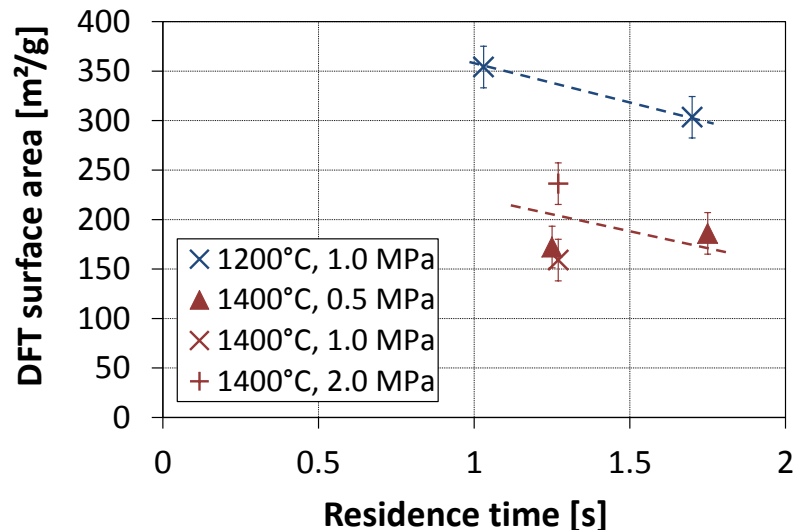


Figure 5.38: Specific surface area (CO_2 -DFT) of pyrolysis chars of bituminous coal A at different temperatures and pressures

Despite the low number of measurements, a significant effect of temperature is observed. The 1200°C chars have a larger surface area than the 1400°C chars. This is in agreement with surface area measurements of the lignite R chars. At a residence time of 1.3 s chars that are generated at 0.5 MPa, 1.0 MPa, and 2.0 MPa are compared. The 2.0 MPa char has the largest surface area, but the surface area at 0.5 MPa and 1.0 MPa is similar. Therefore, the pressure might have an influence, but more data are required for a quantitative analysis.

In the gasification data similar observations are made. When ordering the char surface area by residence time (Figure 5.39(a)), the surface area of the 1400°C chars is significantly lower than of the 1200°C chars. However, at 1400°C the char conversion is higher. After a rearrangement of the data (Figure 5.39(b)), the influence of the char conversion is shown. The surface area decreases almost monotonously with char conversion. This is in agreement with data of the lignite R shown in Figure 5.35.

Anthracite The pyrolysis and gasification data of the anthracite are shown in Figure 5.40. At 1400°C the specific surface area is much lower than at 1200°C . The pyrolysis at 1400°C results in surface areas below $50 \text{ m}^2/\text{g}$. The influence of temperature in the gasification experiments cannot completely be explained by char conversion as the char conversion at 1400°C is only slightly higher than at 1200°C .

Biocoal The surface area after the gasification of biocoal in the BabiTER is shown in Figure 5.41. Neither the residence time nor the temperature have a significant influence and the surface area is always between $340 \text{ m}^2/\text{g}$ and $400 \text{ m}^2/\text{g}$. As the conversion in all gasification experiments is similar, it is not possible to detect an influence of char conversion.

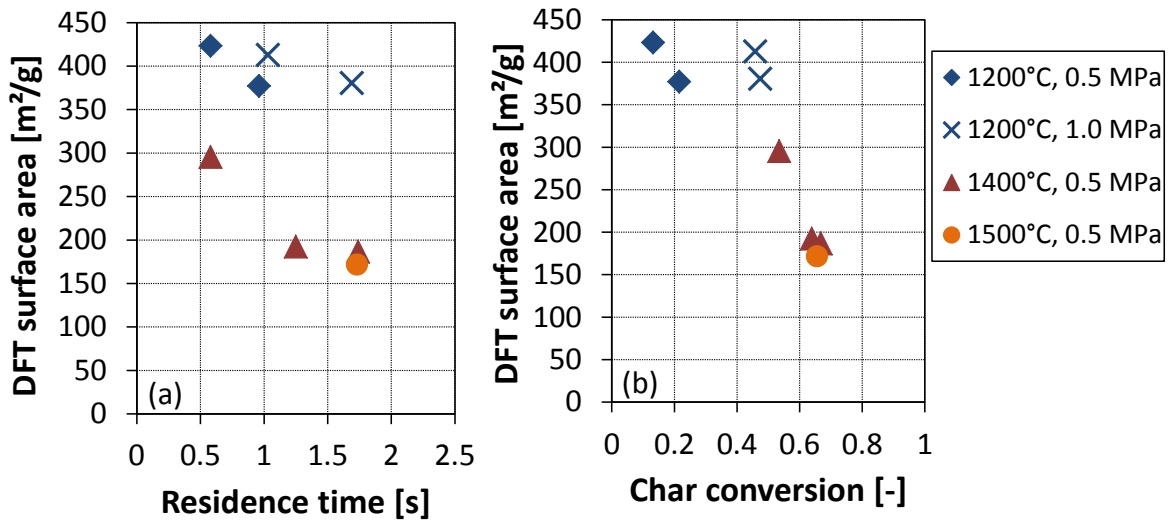


Figure 5.39: Specific surface area (CO₂-DFT) of gasification chars of bituminous coal A at different temperature and pressure: (a) influence of residence time; (b) dependence on char conversion

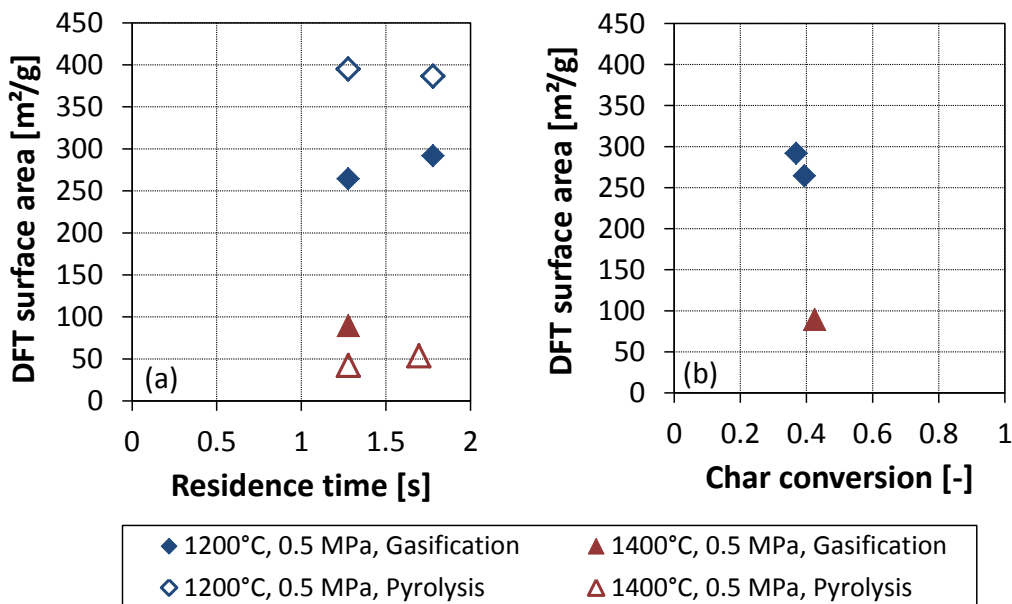


Figure 5.40: Specific surface area (CO₂-DFT) of char after pyrolysis and gasification of anthracite at different temperatures and at a pressure of 0.5 MPa: (a) influence of residence time; (b) dependence on char conversion for the gasification chars

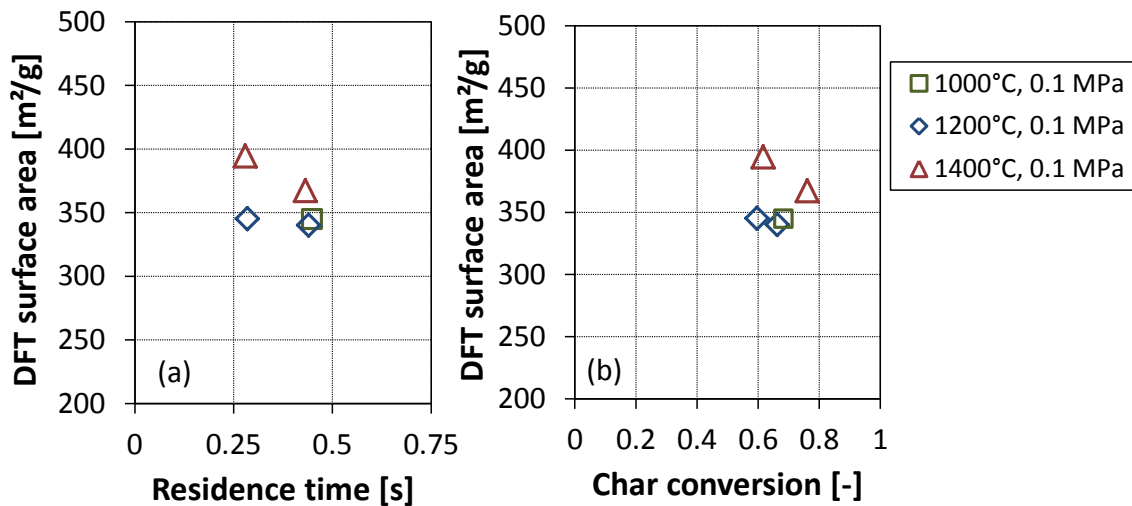


Figure 5.41: Specific surface area (CO_2 -DFT) of biocoal char after gasification at atmospheric pressure and a temperature of 1000°C, 1200°C, and 1400°C: (a) influence of residence time; (b) dependence on char conversion

5.4.1.6 Analysis of the Particle Size during Entrained Flow Gasification

After the pyrolysis and gasification experiments some char samples are analysed regarding their particle size distribution. The measurements are carried out by the laboratories of Quantachrome GmbH in Odelzhausen, Germany.

Lignite R Five chars produced at different operation conditions are analysed and the particle size distributions are shown in Figure 5.42. All particle size distributions are shifted to smaller particles compared with the parent coal. After the pyrolysis at 1400°C and 1.3 s residence time the overall conversion (daf) is 67 wt% and the maximum of particle size is at 50 μm which is 15 μm lower than the maximum of the parent coal. Coal swelling during pyrolysis is not detected. In the gasification experiments the temperature has an effect on particle size. Although the overall conversion (daf) in the gasification experiment at 1200°C is already 93.5 wt%, the particle size is similar to the pyrolysis experiment at 1400°C. It is assumed that the conversion results in an decrease in particle density which is an indicator for Regime I conditions. A further increase in temperature to 1400°C lowers the particle size. Both at 1.0 s and 1.3 s residence time the particle size distribution is similar, but significantly smaller than after the gasification at 1200°C. The overall conversion at 1400°C is 94 wt% and 96 wt%, respectively. As the particle size is reduced, it is assumed that pore diffusion and/or boundary layer diffusion limit the reaction rate and that the particles are converted mainly in their outer region. The 1400°C curves show two maxima which might be an indicator for a fragmentation of particles.

The 1600°C data do not confirm the trend in particle size. The particles sizes are between the 1200°C and 1400°C gasification experiment. The conversion in this experiment is very high (>97 wt%) and the char mass that is collected is considerable lower than in the 1400°C experiment. Small variations in the coal mass flow rate that are not detected, but are likely due to the sloped feeding tube could lead to a locally lower O/C ratio in the reaction tube. When the fuel feeding system is operated independently of the PiTER,

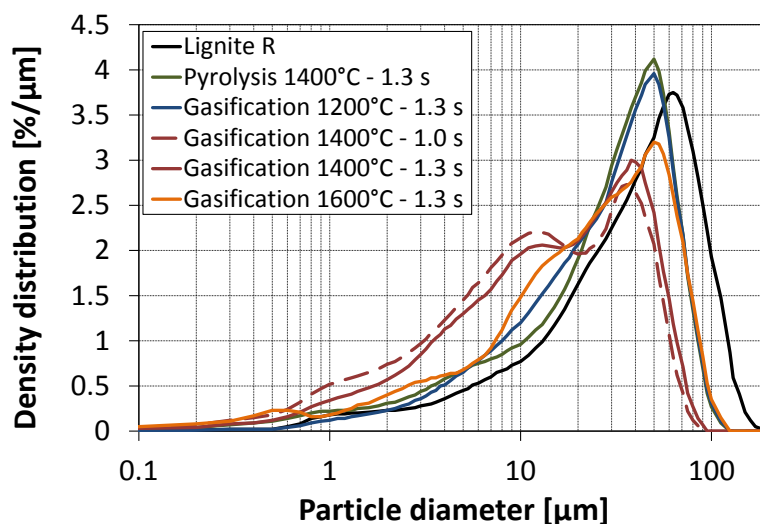


Figure 5.42: Particle size distributions of different chars of lignite R (operation conditions are indicated in the legend, pressure always 0.5 MPa)

fluctuations are usually not detected by the human eye. However, if the flow rate of the carrier gas is significantly reduced, small fluctuations occur. These are expected to be present also at higher gas flow rates, and might be only detected at a very high conversion in the PiTER.

Due to the entrained flow operation mode a back mixing of reactant gases is prevented. This might result in a lack of reactant gases for the conversion of some particles. These particles then react more in a pyrolysis environment and prevent the achievement of 100 % conversion. As the overall conversion at 1600°C is >97 wt%, the influence on the conversion data must be low, but the influence on particle size distribution might be large. The weight of the char sample of the 1600°C experiment is only 100 mg which is about a factor 10 to 30 lower than at comparable experiments at 1400°C and 1200°C. Therefore, the error in the particle size distribution of the 1600°C data is expected to be high which is also confirmed by the non-uniform curve progression. The maximum at 50 μm coincides with the maximum of the pyrolysis char at 1400°C and is expected to be caused by particles that are converted more in a pyrolysis gas atmosphere and therefore did not reach complete conversion. At a very small particle diameter ($< 1 \mu\text{m}$), the particle size of the 1600°C char is higher than of the 1200°C and 1400°C char. This could indicate the existence of very small char particles that are left over after conversion, but could also be an indicator for soot formation.

Bituminous coal A The particle size distributions of a pyrolysis and a gasification char of bituminous coal A are compared with the parent fuel in Figure 5.43. The particle diameter after the pyrolysis is smaller than the initial coal particle size. The maximum of the pyrolysis char is at 40 μm whereas the coal has its maximum particle diameter at 100 μm . The overall conversion after the pyrolysis at 1400°C, 0.5 MPa, and 1.25 s is 40 wt% which leads to a reduction of the particle size. Particle swelling is not indicated, but partially a fragmentation might have occurred.

After the gasification at the same particle residence time (1.25 s) the particle size distri-

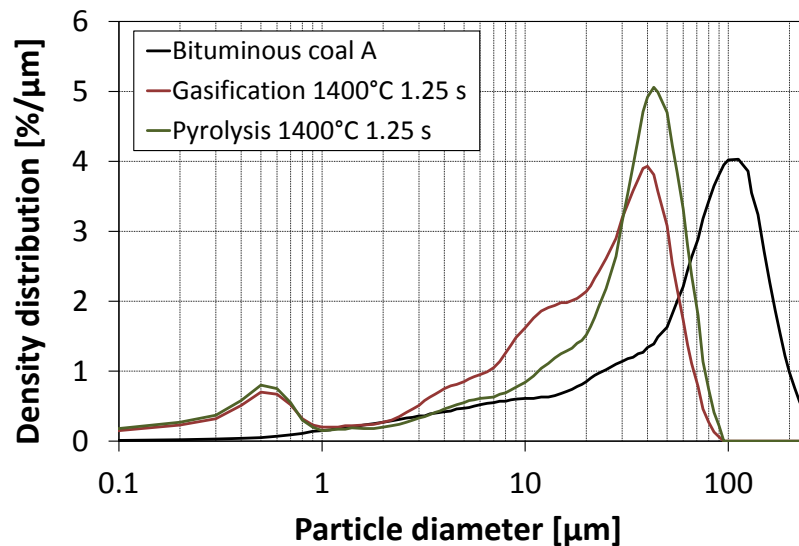


Figure 5.43: Particle size distributions of a pyrolysis and a gasification char of bituminous coal A compared to the initial coal particle size (operation temperature and residence time as indicated, operation pressure 0.5 MPa)

bution is further shifted to smaller diameters and its shape is wider. The overall conversion is then 78 wt%. The particle size is reduced during char gasification which indicates either an influence of mass transport limitations or the fragmentation of particles.

Both char size distributions show a second maximum at a lower particle diameter of about $0.5 \mu\text{m}$ that is not present in the initial coal size distribution. This maximum is attributed to the formation of soot during devolatilisation. The generation of soot in a laminar diffusion flame begins at temperatures between 1312°C and 1427°C for a range of hydrocarbons [Stanmore2001]. The pyrolysis and the gasification temperature during the PiTER experiments are in this temperature range and hydrocarbons are released during devolatilisation. Therefore, the formation of soot is likely. Stanmore et al. [Stanmore2001] group soot into three size ranges. Initially, soot forms *spherules* that are in the range of 10 nm to 50 nm. These can agglomerate to form *particles* in the range $0.1 \mu\text{m}$ to $1 \mu\text{m}$. A further grouping of these particles leads to *agglomerates* with a typical size of $100 \mu\text{m}$. The particle size distribution in Figure 5.43 indicates the formation of soot particles that consist of smaller spherules. As there are also particles detected at the lower measurement limit of 40 nm, the presence of single spherules is also likely. Yoshiie et al. [Yoshiie2011] analysed particle emissions from a coal gasification reactor and found a similar peak in the char particle size distribution after the gasification of a Chinese bituminous coal at 1200°C to 1400°C in a drop tube furnace. They assigned this peak to soot generation.

In summary, the particle size distributions of the initial coal and the chars after pyrolysis and gasification show a variation of the particle diameter with operation conditions. The gasification of lignite R at 1200°C yields almost the same particle size distribution than the pyrolysis experiment indicating the conversion under Regime I conditions where the particle size remains constant. At 1400°C the particle diameter significantly decreases which is an indicator for the transition to Regime II or III conditions. The gasification of bituminous coal A at 1400°C results in a decrease in the particle size compared to

the pyrolysis experiment. This is a further indicator for the conversion under Regime II or III conditions. Soot formation is observed during the pyrolysis and the gasification of bituminous coal A at 1400°C. In the particle size distributions of lignite R chars, there is also a portion of particles with a diameter $< 1 \mu\text{m}$. This might also be an indicator for soot generation; the quantity is much lower than for bituminous coal A.

5.4.1.7 Analysis of Apparent Char Density of Pyrolysis and Gasification Chars

A simple tap density method is used to measure the particle density of fuel and char. The results are summarised in Table 5.7. The particle density of the parent fuels is

Table 5.7: Measurements of fuel and char density with a tap density method using a constant packing factor of 0.42 (Particle residence time ~ 1 s)

Sample	Char preparation conditions	Apparent particle density
Lignite R		
fuel	-	1.82 g/m ³
char	pyrolysis, 1200°C, 1.0 MPa	1.04 g/m ³
char	gasification, 1200°C, 0.5 MPa	1.01 g/m ³
Bituminous coal A		
fuel	-	1.75 g/m ³
char	pyrolysis, 1200°C, 1.0 MPa	0.94 g/m ³
char	gasification, 1200°C, 1.0 MPa	0.76 g/m ³

considerably lower than the density of graphite (2.27 g/cm³ [Fedoseev1986]) indicating an initial porosity of the coal particles. The particle density decreases after the pyrolysis stage and then further after the gasification as organic matter is gasified within the char structure. The particle porosity can be estimated by the ratio of particle density and density of solid graphite. The porosity of lignite R is 0.54 after the pyrolysis and 0.56 after the gasification. Bituminous coal A particles have a porosity of 0.59 after the pyrolysis and 0.67 after the gasification.

5.4.2 Results from the Wire Mesh Reactor

Pyrolysis experiments in an argon atmosphere are carried out in the Pressurised Wire Mesh Reactor. The heating rate in all experiments is 1000 K/s, the maximum temperature is 1000°C, and the sweep gas velocity is constantly 0.1 m/s (at ambient temperature and experimental pressure). For a wide range of fuels, the volatile yield is measured as a function of pressure. The holding time in these experiments is 1 s at the maximum temperature of 1000°C. As 1 s is required to heat the sample to 1000°C, the total time at temperature is approximately 2 s. The experimental data are shown in Figure 5.44. The volatile yield is strongly dependent on fuel properties. For wood and biocoal, the conversion during pyrolysis is very high. The lignites and the bituminous coals release about 40 wt% to 60 wt% of their organic matter in the pyrolysis stage. On the other end, the volatile yield of the anthracite is only 5 wt% to 10 wt%. The error bars denote the standard deviation of

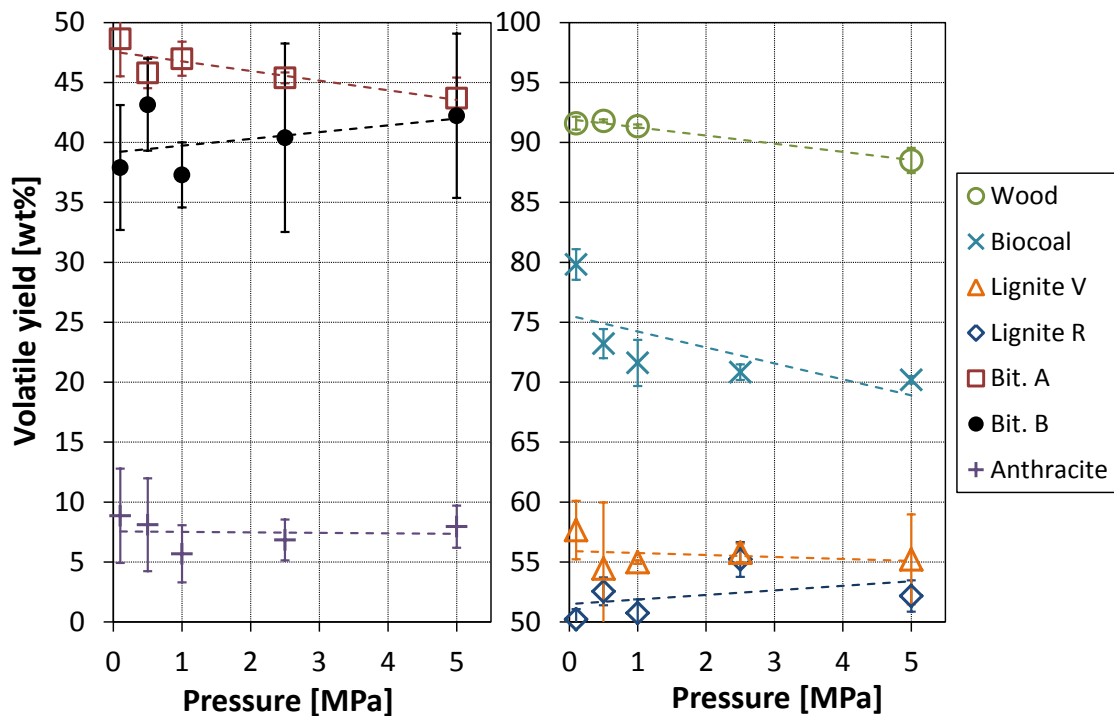


Figure 5.44: Volatile yield (dry ash free basis) as a function of pressure in PMWR experiments with different fuels (heating rate 1000 K/s, max. temperature 1000°C, holding time 1 s)

a minimum of 3 repeated measurements and are generally small. However, for the bituminous coal B the data comprise only two experimental runs for each pressure and also the standard deviation is very high.

Pressure has a significant influence on the conversion for some fuels as shown by linear regression lines. The volatile yields of wood, biocoal, and bituminous coal A decrease with pressure. For the two lignites there is no significant effect of pressure and deviations can be explained by the standard deviation. The data of bituminous coal B indicates an increase in volatile yield with pressure. However, for this coal the data quality is low as indicated by the standard deviation and the measurement uncertainty is too high to detect any significant influence of pressure.

As the particle density of the anthracite is very high, the sample mass is unintendedly large (30 mg to 70 mg) and effects of particle interactions cannot be excluded. For all other experiments the sample mass is 10 mg to 20 mg, and the particles are distributed within the two mesh layers almost forming a monolayer. The sample mass in these experiments did not have an influence on volatile yield as shown in Figure 5.45. The lines are linear regression lines for each fuel.

Wood and lignite R show a minor increase in volatile yield with sample mass, for lignite V the volatile yield remains almost constant. The two data points at approximately 22 mg (experimental pressure 0.5 MPa and 1.0 MPa) indicate that even higher samples masses do not significantly lower the volatile yield. The decrease for biocoal, bituminous coal A, and bituminous coal B is low. In case of the biocoal, the two data points at a sample mass of 10 mg are generated at atmospheric pressure. Therefore, the low pressure is likely to cause the high volatile yield, but not the low sample mass. In conclusion, there is no significant influence of the sample mass on volatile yield. The effects of fuel properties

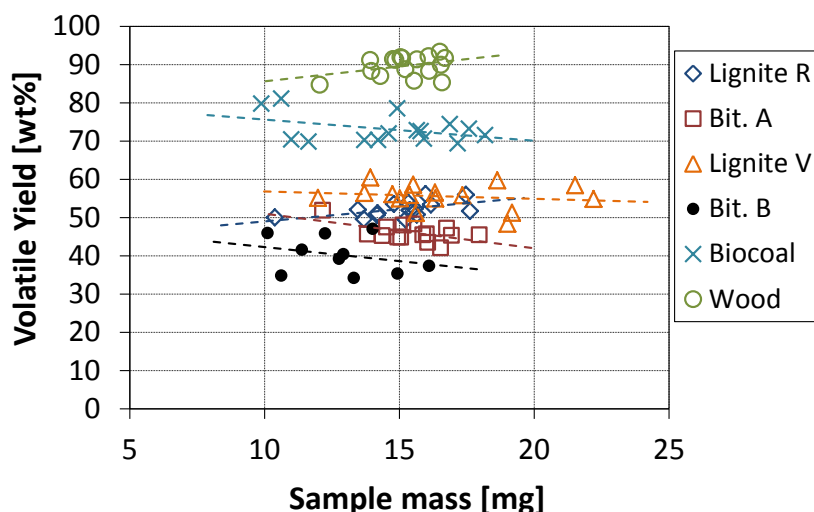


Figure 5.45: Volatile yield as a function of initial sample mass in PWMR experiments (heating rate 1000 K/s, maximum temperature 1000°C, holding time 1 s, pressure 0.1 MPa to 5.0 MPa)

and pressure are more significant.

Experiments with lignite R and bituminous coal A are also carried out at a longer holding time of 2 s. A direct comparison of the experiments at a holding time of 1 s and 2 s is shown in Figure 5.46. At a lower pressure a holding time of 2 s increases the volatile yield of both fuels. The effect on lignite R is higher than on the bituminous coal A. At a higher pressure the influence of holding time diminishes. Therefore, at a holding time of 2 s the influence of pressure on volatile yield is more significant than at a lower holding time.

5.4.3 Results from the Pressurised Thermogravimetric Analysis

The heterogeneous char gas reactions are analysed in the PRETA. In all experiments any mass transfer limitations are excluded and the reaction rate is only dependent on the intrinsic surface reaction. The model parameters required to describe the reaction rates under Regime I conditions are derived from the thermogravimetric analysis. The influence of temperature, reactant gas concentrations (partial pressure), and product gas concentrations (partial pressure) on the reaction rate are evaluated. In the experimental analysis only char samples that are collected from the PiTER are used. The chars are produced under operation conditions (high temperature, high heating rate) relevant to industrial scale applications.

5.4.3.1 Influence of Carbon Dioxide Partial Pressure

The observed reaction rates at different CO₂ partial pressures are measured and the influence of reactant gas partial pressure is evaluated. The PRETA experiments are carried out using a char of lignite R (sample ID: 20101221_PiTER_o). The char is produced in the PiTER at a pressure of 0.5 MPa, at a temperature of 1600°C, and at a particle residence time of 1.75 s.

In a first series of experiments the total pressure in the PRETA is kept at 2.5 MPa. The

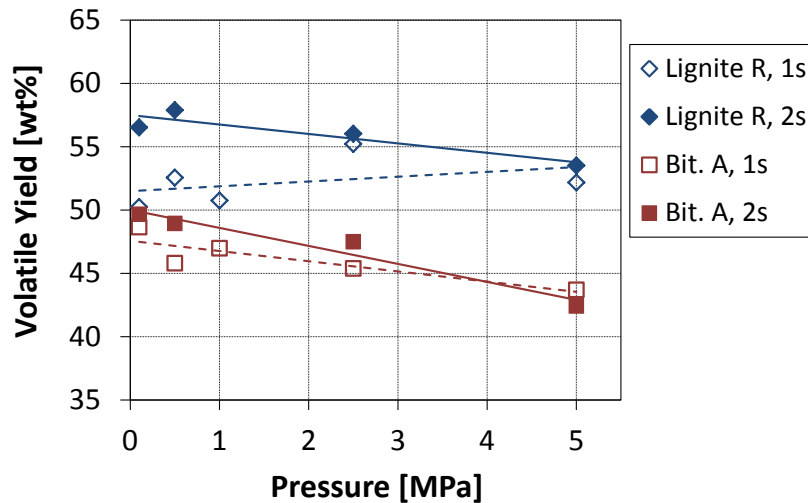


Figure 5.46: Volatile yield as a function of holding time (1 s and 2 s) and pressure in the PWMR experiments with lignite R and bituminous coal A (heating rate 1000 K/s, maximum temperature 1000°C)

CO₂ partial pressure is increased from 0.5 MPa to 2.5 MPa, and N₂ is used as the balance gas. The temperature is kept constant at 750°C. The weight loss data are used to calculate the observed reaction rate in Figure 5.47. The reaction rate is dependent on conversion and increases towards higher CO₂ partial pressures. Initially at low conversion, there might be an influence of the gas change from N₂ to CO₂ as the gas flow rates are changed which might influence the weight recorded. Hence, the data that are recorded below a conversion of 0.05 are excluded from the further analysis. Then, at a medium conversion the observed reaction rate is almost constant in all experiments. At a higher conversion an increase in observed reaction rate is measured. This might be caused by an increase in the specific surface area. As at higher conversions the char structure might be significantly changed and is then no longer representative for entrained flow char, the observed reaction rate should be measured at the lowest possible conversion. Therefore, the average rate in the conversion interval 0.05 to 0.2 is used for the further analysis. A further reduction of the interval (for example 0.05 to 0.1) is not required as the observed reaction rate is constant at low to medium conversion. The larger interval of 0.05 to 0.2 leads to a reduction of the measurement uncertainty as the average observed reaction rate can be calculated over a wider range.

Due to limitations of the CO₂ mass flow controller, the partial pressure could not be decreased further. In a second series of experiments the total pressure is set to 0.5 MPa, and the CO₂ partial pressure is varied. The results are shown in Figure 5.48. Again, the observed reaction rate increases at a higher CO₂ partial pressure.

The standard deviation in the conversion interval 0.05 to 0.2 is a measure for the uncertainty in reaction rate. In both series of experiments the relative standard deviation of the reaction rate is about 10 %.

5.4.3.2 Influence of Total Pressure

The observed reaction rates at a CO₂ partial pressure of 0.5 MPa are different in the diagrams 5.47 and 5.48. Both experiments are carried out at different total pressures, but

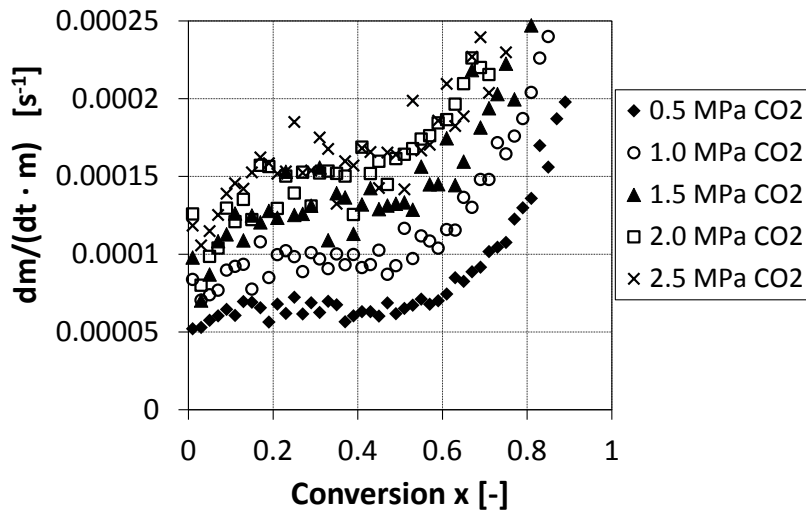


Figure 5.47: Observed reaction rate of lignite R char as a function of CO₂ partial pressure and conversion in the PRETA (total pressure 2.5 MPa, balance gas N₂, temperature 750°C)

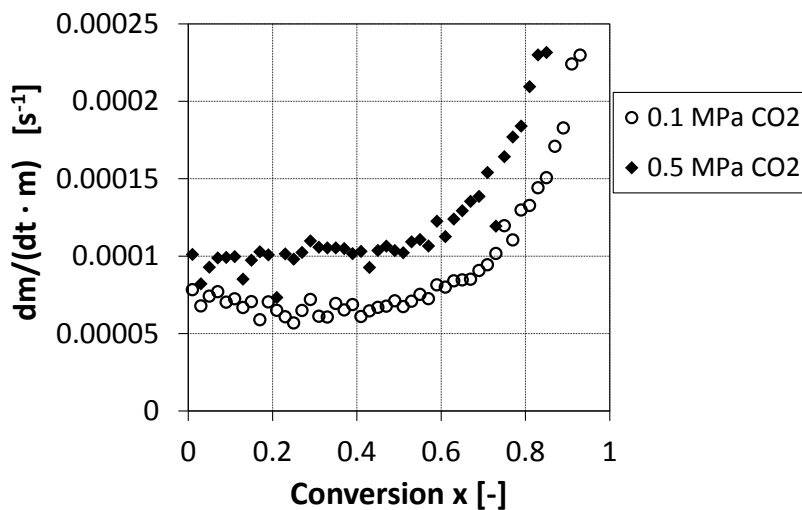


Figure 5.48: Observed reaction rate of lignite R char as a function of CO₂ partial pressure and conversion in the PRETA (total pressure 0.5 MPa, balance gas N₂, temperature 750°C)

otherwise identical operation conditions. Therefore, the total pressure seems to have an influence on reaction rate. To further analyse this parameter, experiments at a constant CO₂ partial pressure and at different total pressures are performed. In a first series, the lignite R char (ID: 20101221_PiTER_o) is used. The temperature is kept constant at 750°C, and N₂ and Ar are used as balance gases. Figure 5.49 shows the influence of balance gas partial pressure and conversion on observed reaction rate $dm/(dt \cdot m)$. As it is assumed that the high gas mass flow rate in the high pressure experiments could cause a cooling of the char sample¹², experiments with the standard gas flow rate (i.e. 2.5 l_N/min) and a reduced gas flow rate (half the standard flow rate) are carried out. The reaction rate in experiments that use Ar as balance is independent of the balance gas pressure (i.e. total pressure). If N₂ is used as the balance gas, the reaction rate significantly decreases.

¹²The residence time of the reaction gas in the preheating unit of the PRETA is independent of pressure. It was assumed that this time is not sufficient to preheat the reaction gas to sample temperature at high mass flow rates that occur at higher pressure.

The reduction of the gas flow rate does not increase the reaction rate. An influence of an incomplete gas preheating at higher mass flow rate is not detected. The small reduction of reaction rate at the reduced gas flow rate may result from a higher partial pressure of CO that could inhibit the reaction, or from the measurement uncertainty.

At a low conversion, some discontinuities are observed that could result from the gas change to CO₂. Therefore, again the conversion interval 0.05 to 0.2 is used for the further data evaluation.

In a second series of experiments another lignite R char (sample ID: 20100831_PiTER_i) is used. The char is produced in the PiTER at a temperature of 1400°C, at a pressure of 2.5 MPa, and at a residence time of 1.7 s. The reaction rates in the PRETA at a CO₂ partial pressure of 0.5 MPa and different partial pressures of N₂ are shown in Figure 5.50. The reaction rate is clearly dependent on the partial pressure of the balance gas N₂. A higher N₂ partial pressure and therefore total pressure reduces the reaction rate. This behaviour is later discussed in Section 7.1.1.

5.4.3.3 Influence of Temperature

The influence of temperature on the reaction rate is analysed for different char samples. For each char, two different types of experiments are carried out: in the first experiment the reaction rate at a constant temperature of 750°C and at a constant CO₂/H₂O partial pressure of 0.5 MPa is measured; in the second experiment the heating rate is kept constant at 10 K/min and the temperature is increased from 600°C to 1000°C.

Influence of Temperature on the Char-CO₂ Reaction The partial pressure of the reactant gas CO₂ is 0.5 MPa and no further gas components are used. Four different chars that are produced at different operation conditions are used in the experiments. These operation conditions are summarised in Table 5.8.

Table 5.8: Operation conditions (PiTER pyrolysis) for the production of chars (lignite R) that are used in the analysis of the temperature influence on char reactivity

Abbreviation	Sample ID	Temperature	Pressure	Residence time
1200°C char	20101220_PiTER_c	1200°C	0.5 MPa	1.3 s
1400°C char	20101220_PiTER_n	1400°C	0.5 MPa	1.3 s
1600°C char	20101221_PiTER_o	1600°C	0.5 MPa	1.7 s
2.5 MPa char	20100831_PiTER_i	1400°C	2.5 MPa	1.7 s

The observed reaction rates in the two different types of experiments are shown in Figure 5.51. The reaction rates at constant temperature and at constant heating rate are dependent on the char preparation temperature. The higher the pyrolysis temperature is the lower the observed reaction rate. The reactivity of the 2.5 MPa char is slightly higher than the reactivity of the 1400°C char indicating an effect of the devolatilisation pressure. In the experiments at a constant temperature, the observed reaction rate is almost independent from the level of conversion. As the temperature is increased in the experiments at a constant heating rate and the conversion progresses, the effect of conversion cannot be evaluated.

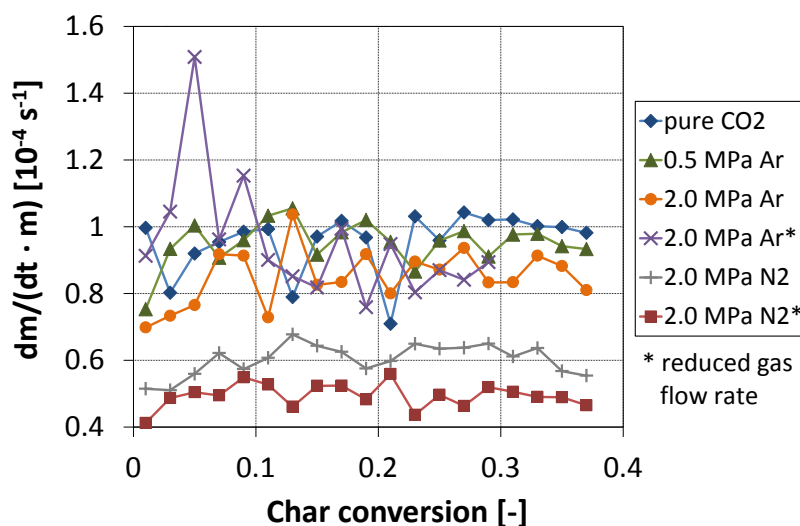


Figure 5.49: Influence of balance gas partial pressure (N_2 or Ar) on observed reaction rate in PRETA experiments (Sample ID: 20101221_PiTER_o, $T=750^\circ\text{C}$, $p_{CO_2}=0.5\text{ MPa}$)

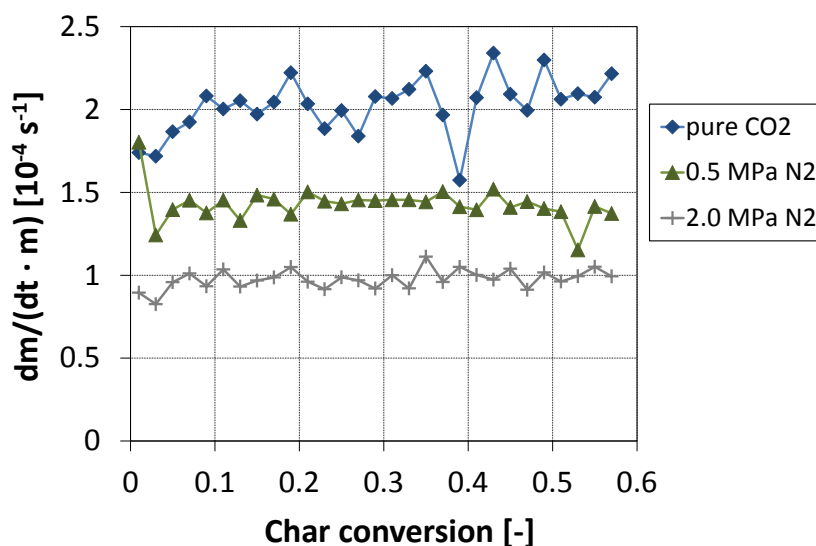


Figure 5.50: Influence of balance gas partial pressure (N_2) on observed reaction rate in PRETA experiments (Sample ID:20100831_PiTER_i, $T=750^\circ\text{C}$, $p_{CO_2}=0.5\text{ MPa}$)

Influence of Temperature on the Char- H_2O Reaction The partial pressure of H_2O is set to 0.5 MPa and the total pressure is 1 MPa using Ar as the balance gas. The experiments are carried out with the 1600°C char from Table 5.8. The observed reaction rates in the two types of experiments are shown in Figure 5.52. Due to the slightly discontinuous water feed pump and the evaporation, small fluctuations in the gas supply cause a higher level of noise in the weight data compared with the CO_2 experiments. To balance the temporal unsteadiness, the weight signal is smoothed by calculating the continuous average of a 2 minutes interval. The variation of the observed reaction rate with char conversion is larger than in the CO_2 experiments. Initially, the reaction rate is $8 \cdot 10^{-4}\text{ g}/(\text{g} \cdot \text{s})$, then declines, but increases again at the later stages of conversion. The observed reaction rate is on average about 5 times higher than in the CO_2 atmosphere. Despite the data smoothing, the difference of data points next to one another is relatively large indicating the high uncertainty in the char- H_2O rate measurements.

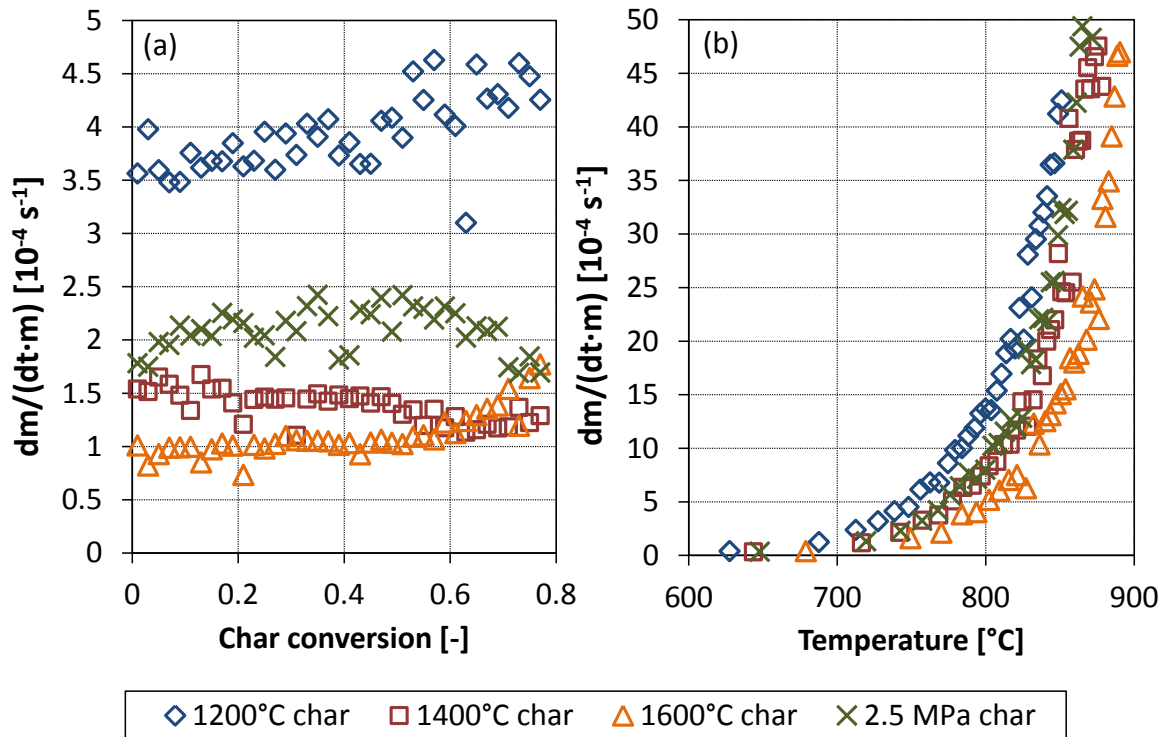


Figure 5.51: Influence of pyrolysis conditions of lignite R char on observed reaction rate (PRETA, $p_{\text{CO}_2} = p_{\text{total}} = 0.5 \text{ MPa}$): (a) experiment at a constant temperature of 750°C; (b) experiment at a constant heating rate of 10 K/min

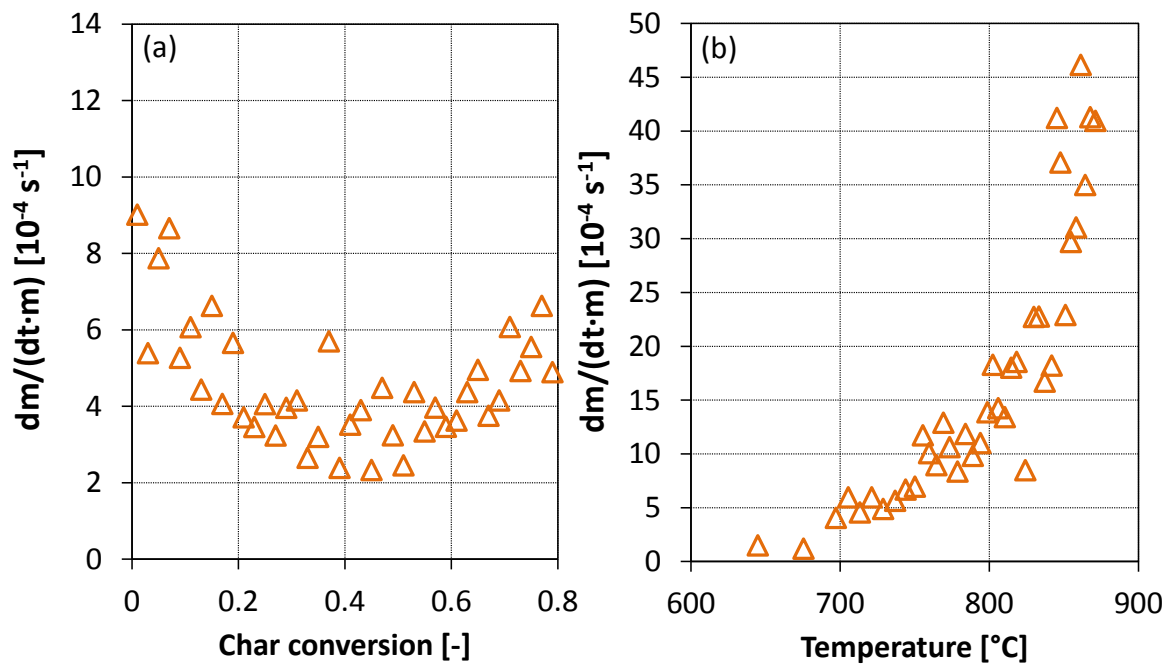


Figure 5.52: Observed reaction rate of steam gasification of a lignite R char in the PRETA (Sample ID: 20101221_PiTER_o, $p_{\text{H}_2\text{O}} = 0.5 \text{ MPa}$, $p_{\text{total}} = 1 \text{ MPa}$, balance Ar): (a) experiment at a constant temperature of 750°C; (b) experiment at a constant heating rate of 10 K/min

5.4.3.4 Combined Analysis of the Influences of Carbon Dioxide Partial Pressure and Temperature

In Langmuir-Hinshelwood type (or LHHW type) models the effects of reactant gas partial pressure and temperature cannot be separated as the temperature has an influence on the sorption processes at the char surface. It is therefore required to vary the reactant partial pressure at different temperatures. The determination of the model parameters requires more experimental data and the experimental effort is higher. To reduce the number of experiments, the gas atmosphere is varied within one experimental run. Figure 5.53 shows observed reaction rate at two different temperatures and different CO₂ partial pressures. The sample is the 1600°C char. Usually, the reaction rate of a char is changing with conversion because the surface area or the char reactivity are dependent on conversion. In general, the reaction rates measured at different levels of conversion cannot be compared directly. However, experiments with the same char sample (Figures 5.47 and 5.48) show that the observed reaction rate $dm/(dt \cdot m)$ is almost constant in the conversion range up to 0.6 when the initial discontinuities due the gas changes are excluded. This range is used to vary the CO₂ partial pressure.

The total pressure in the experiments shown in Figure 5.53 is 1.0 MPa and Ar is used as the balance gas. Initially, the CO₂ partial pressure is 1.0 MPa and the highest reaction rate is observed at the two temperatures. Then, the gas atmosphere is switched to Ar and the reaction rate rapidly decreases. As CO₂ molecules that are adsorbed at the char surface continuously desorb in the Ar atmosphere, the sample reduces slowly its weight and the reaction rate calculated is above zero. In the PRETA experiments it is not possible to separate weight changes from char conversion and weight changes from adsorption and desorption processes. The true char conversion does not proceed if the sample weight changes due to the desorption of CO₂, and the true char conversion is lower than shown in Figure 5.53. The use of the conversion interval 0 to 0.6 is therefore a conservative choice because the true char conversion is lower.

The observed reaction rates at a constant CO₂ partial pressure are calculated by averaging the measurements in these intervals and are summarised in Table 5.9. The observed

Table 5.9: Observed reaction rates at different CO₂ partial pressures and temperatures derived from Figure 5.53

CO ₂ partial pressure [MPa]	Conversion interval at 750°C	Reaction rate at 750°C [g/(g·s)]	Conversion interval at 775°C	Reaction rate at 775°C [g/(g·s)]
1.0	0.05-0.21	$1.34 \cdot 10^{-4}$	0.05-0.21	$2.44 \cdot 10^{-4}$
0.5	0.35-0.45	$1.05 \cdot 10^{-4}$	0.45-0.51	$1.97 \cdot 10^{-4}$
0.25	0.51-0.55	$0.75 \cdot 10^{-4}$		

reaction rate increases at a higher CO₂ partial pressure and at a higher temperature. As the reaction rates are derived by an average determination, the standard deviation is an indicator for the uncertainty. The relative standard deviation is 7 % to 17 % which is considerably higher than in experiments in constant gas atmospheres. Therefore, the error in this procedure is high, but only two experimental runs are required to evaluate the

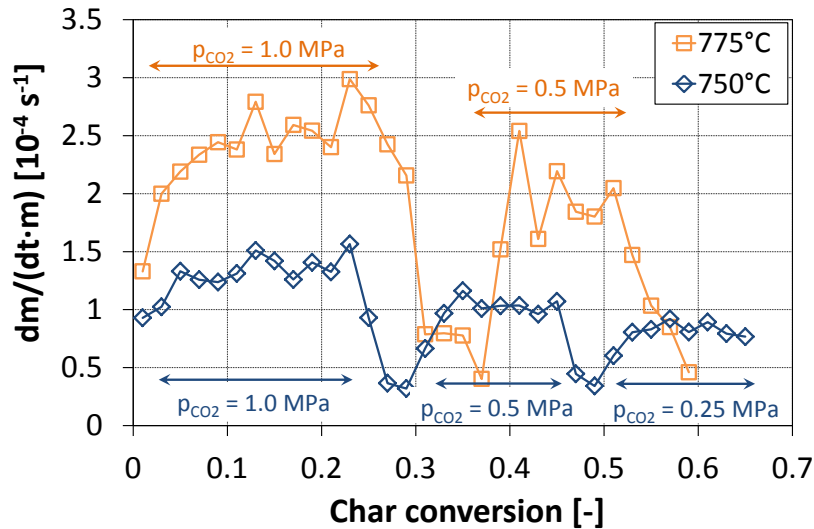


Figure 5.53: Influence of CO₂ partial pressure and temperature on reaction rate in a PRETA experiment using a lignite R char ($p_{total}=1.0$ MPa, balance argon)

influence of reactant partial pressure and temperature.

5.4.3.5 Influence of Product Gas Inhibition

To evaluate the influence of the product gas on the CO₂-char reaction, experiments with gas mixtures of CO₂ and CO are carried out using the 1600°C char. All data are recorded at a total pressure of 1.0 MPa (balance gas Ar) and a CO₂ partial pressure of 0.5 MPa. The partial pressure of CO is 0.1 MPa, 0.2 MPa, and 0.3 MPa, and it is varied within an experiment at a constant temperature. The weight loss curves of experiments at 750°C and 775°C are shown in Figure 5.54. At 750°C the CO partial pressure is increased from 0.1 MPa to 0.3 MPa. At 775°C its partial pressure is decreased from 0.3 MPa to 0.1 MPa. In between the gas atmosphere is changed to pure argon. When the atmosphere is switched to CO₂-CO a rapid increase in weight is observed. This is probably due to the adsorption of these gases at the char surface. After the atmosphere is switched back to pure Ar, a rapid decrease in the weight is observed. This might be due to the desorption of CO₂ and CO.

Compared with the initial char mass of 44 mg (daf) in both experiments, the weight loss within the reactant gas intervals is very low. At a CO partial pressure of 0.3 MPa, a weight change is hardly recorded at both temperatures. With decreasing CO partial pressures the mass loss rate increases. As the total char conversion in the two experiments is very low, the reaction rate cannot be visualised as a function of char conversion. Instead, the observed reaction rate is calculated from average mass loss rate divided by average char sample mass (daf) in the sample interval:

$$\frac{dm}{dt \cdot m} = \frac{\Delta m}{\Delta t} \cdot \frac{1}{m_{char,daf}} \quad (5.10)$$

The resulting observed reaction rates are shown in Table 5.10. For comparison the reaction rate of the CO₂-char reaction without CO inhibition from Figure 5.53 is shown.

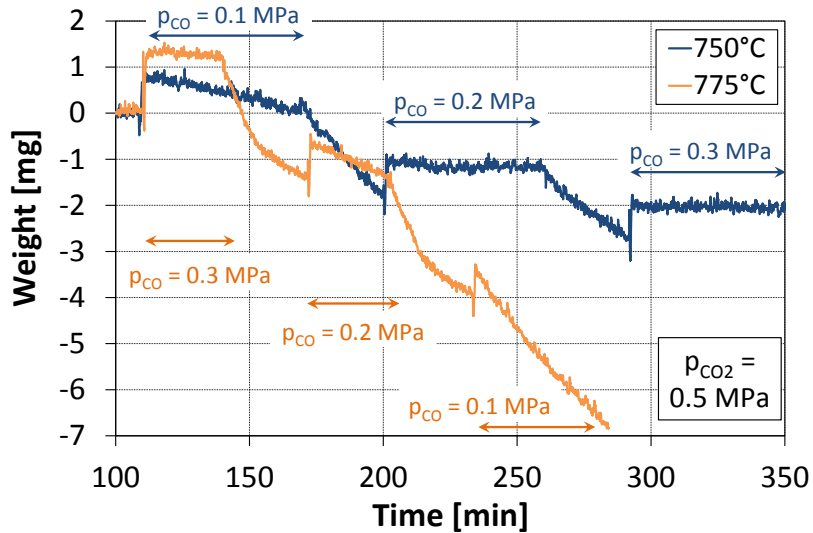


Figure 5.54: Weight loss curve for PRETA experiments at 750°C and 775°C with mixtures of CO₂ and CO using a lignite R char ($p_{CO_2}=0.5$ MPa, $p_{total}=1.0$ MPa, balance Argon)

Even at a low CO partial pressure of 0.1 MPa the reaction rate decreases severely. The

Table 5.10: Reaction rates at different CO partial pressures (CO₂ partial pressure always 0.5 MPa) and temperatures derived from the Figures 5.54 and 5.53

CO partial pressure [MPa]	Reaction rate at 750°C [g/(g·s)]	Reaction rate at 775°C [g/(g·s)]
0.0 MPa	$1.05 \cdot 10^{-4}$	$1.97 \cdot 10^{-4}$
0.1 MPa	$0.061 \cdot 10^{-4}$	$0.255 \cdot 10^{-4}$
0.2 MPa	$0.012 \cdot 10^{-4}$	$0.093 \cdot 10^{-4}$

increase to 0.2 MPa leads to a further loss of reactivity. At a CO partial pressure of 0.3 MPa the weight loss is too low to calculate the reaction rate. The influence of the product gas is significant at these low temperatures (750°C and 775°C) and reduces the reaction rate by more than one order of magnitude.

As only two experiments are carried out and the char conversion in these experiments is too low to calculate the reaction rate at different levels of conversion, the determination of the standard deviation in the measurements or any other measure for uncertainty is not possible.

5.4.4 Results from the Atmospheric Thermogravimetric Analysis

Chars of lignite R, lignite V, and the bituminous coal A are analysed in a standard procedure in an atmospheric thermogravimetric analyser. The detailed setup and the measurement procedure is described in Section 5.3.5. The weight loss rate at low temperatures (375°C to 400°C) in an atmosphere of 5 mol% O₂ in N₂ is recorded and the reactivity is calculated using Equation 5.6. Figure 5.55 summarises reactivities for different chars as a function of conversion in the ATGA.

In order to compare the reactivity of different chars, the definition of a representative mass

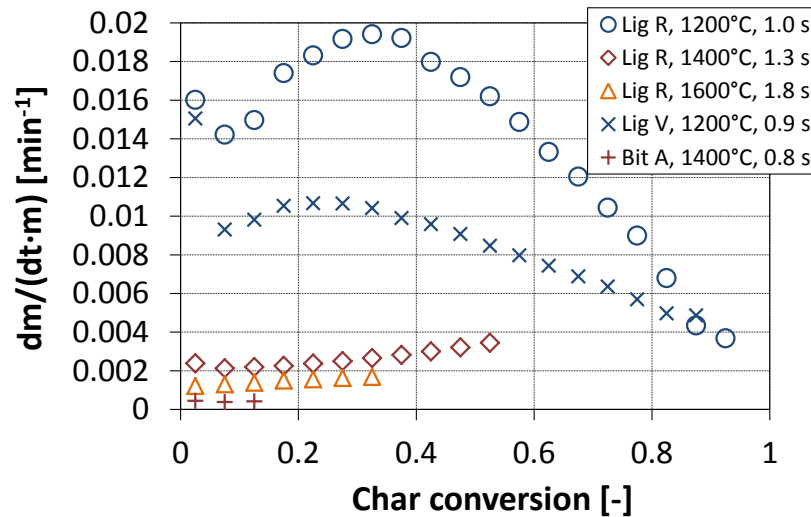


Figure 5.55: Weight loss rate $dm/(dt \cdot m)$ of chars of lignite R, lignite V, and bituminous coal A in the ATGA at 375°C (oxidising atmosphere, 5% O₂ in N₂)

loss rate per char is necessary. As the reaction rate changes with conversion a defined conversion interval is chosen and the standard reactivity is defined as the average reaction rate within this conversion interval. In the initial stages of conversion possible influences of the gas change are likely. Furthermore, low amounts of volatile matter that remain in the char structure after the pyrolysis are likely to be burned after switching to the oxygen atmosphere. Therefore, the measurement point at the lowest char conversion (0.025) is excluded from the average determination.

In the reaction time of 300 min, most of the chars - especially those with a low reactivity - are only partially converted. As most of the chars reach a conversion level of 0.325, the conversion interval 0.075 to 0.325 is chosen to calculate an average reactivity. If the maximum conversion in the ATGA is lower, the upper boundary of the interval is adjusted. The average reaction rate in the conversion interval is defined as *standard reactivity* and chars can be compared directly using this parameter.

The uncertainty in the standard reactivity measurement is estimated by repeated measurements. The reference char of lignite R is used. In 5 measurements the standard reactivity is on average $5.5 \cdot 10^{-3} \text{ min}^{-1}$ with a standard deviation of only $2.3 \cdot 10^{-4} \text{ min}^{-1}$. This corresponds to a relative uncertainty of $\pm 4.2\%$. The reproducibility and accuracy of the standard reactivity measurements are very high.

A series of lignite R chars that are produced under different operation conditions are analysed. The standard reactivity as a function of temperature, particle residence time, and pressure is shown in Figure 5.56. The pyrolysis data at 1200°C and 1400°C are approximated by an exponential line fit to visualise the trend in reactivity.

The pyrolysis data can be compared directly as the conversion in these experiments is similar. The char conversion in the gasification experiments is higher and can also influence char reactivity. However, the gasification data confirm the trend in the pyrolysis chars. The standard reactivity decreases with increasing temperature and time at temperature. The chars produced at 2.5 MPa seem to be more reactive than the 0.5 MPa chars.

The pyrolysis chars of lignite V are analysed using the same procedure. The standard

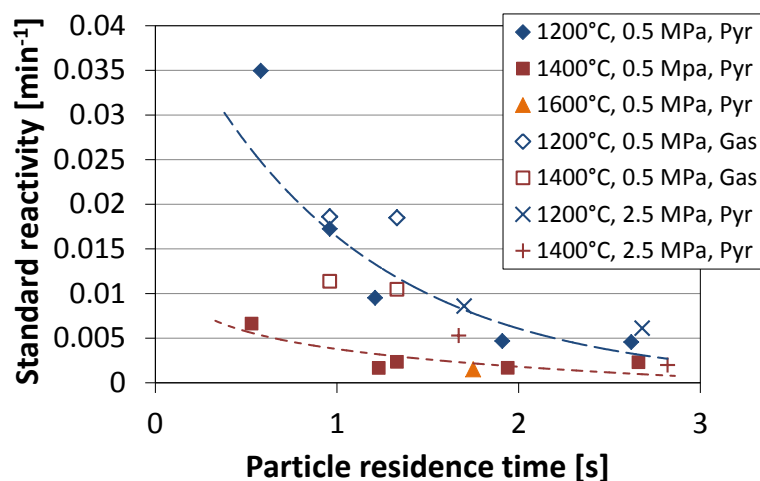


Figure 5.56: Standard reactivity (ATGA, 375°C, 5 % O₂ in N₂) of lignite R chars produced at different operation conditions (Pyr = pyrolysis experiment; Gas = gasification experiment)

reactivity as a function of temperature and time at temperature is shown in Figure 5.57. At 1200°C the standard reactivity decreases with increasing time at temperature. At 1400°C there is no influence of particle residence time on char reactivity. It is assumed that the deactivation process at the higher temperature is fast and that char is strongly annealed before the first measurement point. Compared with lignite R, the standard reactivity of lignite V char is slightly lower.

The chars of bituminous coal are less reactive than the lignite chars. The experiments with chars of bituminous coal A at 375°C result in almost no conversion in the experimental time of 300 min. The temperature is increased to 400°C and the reaction rate and the conversion are higher, but a direct comparison to the lignite data at 375°C is not possible. However, the reactivity of chars of bituminous coal A can be compared with one another and the thermal annealing process is described. Experimental data are shown in Figure 5.58. Similar to the lignites, the standard reactivity decreases with particle residence time and temperature. As the pyrolysis of bituminous coal A is not analysed in the PiTER at 1500°C or 1600°C, the standard reactivity of a gasification char at 1500°C is shown.

All chars analysed so far are collected from PiTER experiments at particle residence times from 0.5 s to 3.0 s. Due to the high temperature, char deactivation has already occurred even at the shortest residence time. The estimation of the initial char standard reactivity from the entrained flow experiments is only possible if the residence time is very short or the temperature can be kept low. Both is not possible in the experimental setup. Defined residence times in the milliseconds range are not adjustable and it is expected that the operation at low temperature would not result in complete devolatilisation in the given reaction time of only a few seconds. A solution to this problem is the use of the Pressurised Wire Mesh Reactor. Defined pyrolysis conditions at a lower temperature and a longer holding time are feasible. Chars are prepared at a heating rate of 1000 K/s, a maximum temperature of 700°C, and a holding time of 10 s. The temperature is chosen in accordance to experiments of Cai et al. [Cai1996] and Feng et al. [Feng2003]. Both used a minimum pyrolysis temperature of 700°C for their char reactivity analysis. Feng et al. [Feng2003] proved experimentally that the char reactivity of Cerrejon bituminous

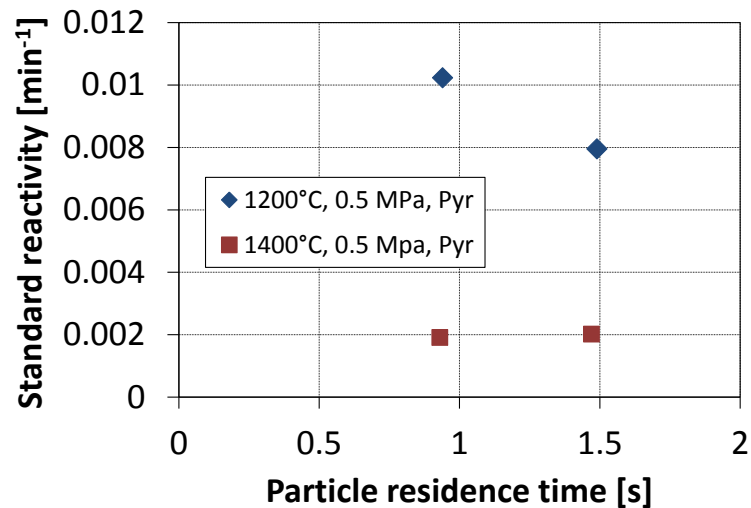


Figure 5.57: Standard reactivity (ATGA, 375°C, 5 % O₂ in N₂) of lignite V chars produced at 0.5 MPa in the PiTER

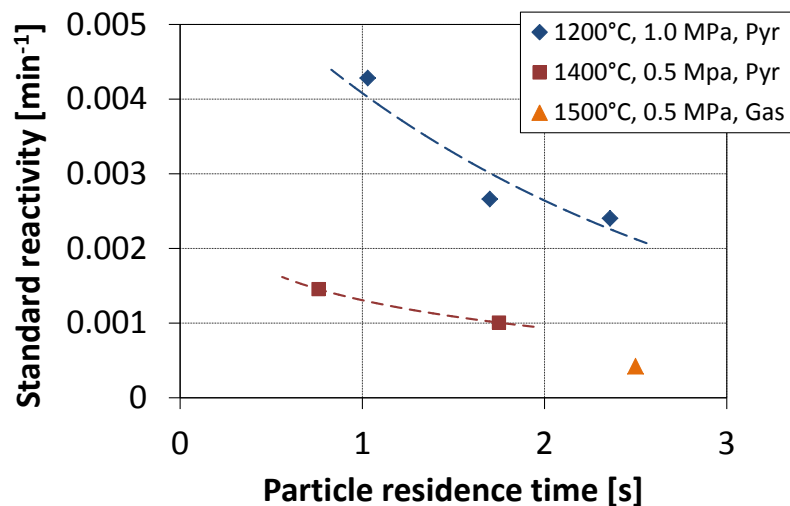


Figure 5.58: Standard reactivity (ATGA, 400°C, 5 % O₂ in N₂) of bituminous coal A chars produced in the PiTER

coal does not decrease with residence time at 700°C. Therefore, the thermal annealing at 700°C is negligible and char produced at this temperature is considered to be the most reactive char.

The pyrolysis of fuel is observed in the PWMR through the optical view ports. The holding time of 10 s is chosen as the devolatilisation is visually completed after this time interval. Several char samples of lignite R and bituminous coal A are produced in the PWMR. As in each experiment only 6 mg to 8 mg of char are produced, several repeated experiments are required for each fuel to produce enough char for the ATGA measurement. The standard reactivity is then measured at 375°C (lignite R char) and 400°C (bituminous coal A char). In both experiments a temperature increase of about 10°C is observed after the gas atmosphere is changed to oxygen. This is due to the high reactivity of the 700°C chars and the exothermic oxidation reactions within the char sample. Due to the temperature instability in the initial stages of conversion, the reaction conditions in the ATGA are less defined and mass transfer limitations might have an influence. The temperature

in the ATGA is measured at the outside of the mesh bag. The temperature within the char sample might even be higher. This could increase the reaction rate significantly and mass transport limitations are possible. The measured standard reactivity might be lower than the true standard reactivity in the absence of any mass transport limitations. Furthermore, the increase of temperature in the char sample raises the local reaction rate. Therefore, the mass loss is recorded at a partially higher temperature than 375°C/400°C. Then, the measured standard reactivity might be higher than the true standard reactivity at 375/400°C. Both effects lead to a larger (and unknown) uncertainty in the standard reactivity of the 700°C char, but these measurement are required to estimate the reactivity of a fresh, not-deactivated char.

The decrease in the setpoint temperature in the ATGA experiments with the 700°C chars would improve the measurements, but is not possible as this would disable the direct comparison to the PiTER chars. The standard reactivity of the 700°C chars of lignite R and bituminous coal A are summarised in Table 5.11. The standard reactivity of both PWMR chars are considerably higher than the standard reactivity of the chars shown in the Figures 5.56 and 5.58. It is assumed that the PWMR chars represent the reactivity of a fresh, not-deactivated char that is also generated in entrained flow reactors in very short reaction times.

Table 5.11: Standard reactivity of PWMR chars that are produced at a heating rate of 1000 K/s, a maximum temperature of 700°C, and a holding time of 10 s.

Parent fuel	ATGA temperature	Standard reactivity
	[°C]	[min ⁻¹]
Lignite R	375	0.066
Bituminous coal A	400	0.020

Chapter 6

Validation of Pyrolysis Models for Entrained Flow Gasification

The volatile yield at different operation conditions is measured in the PWMR and the two entrained flow reactors PiTER and BabiTER. In different measurement sets, temperature, pressure, and particle residence time are varied and the conversion after pyrolysis is measured. The data are shown in Section 5.4 and are now used to derive the fuel specific parameters in the pyrolysis models derived in Chapter 4.

6.1 Volatile Yield as a Function of Pressure and Temperature for Different Fuels

The model equations that describe the influence of pressure and temperature on volatile yield (Equations 4.3 to 4.19) are applied to the experimental data from Chapter 5.

The influence of temperature on volatile yield is modelled by the assumption of a temperature dependent linear decrease in the volatiles concentration in the solid fuel. The effect of pressure is included in the pyrolysis model by an analogy to vapour pressure calculations. The influence of **pressure** on volatile yield is then described by Equation 4.16:

$$Y_V(p) = Y_{V,p_{set}} - \frac{\ln p/p_{set}}{\rho}$$

The experimental data at 1000°C are provided by the PWMR experiments. As the pyrolysis at 1000°C is probably not completed after a holding time of 1 s, the experimental data at a holding time of 2 s are used if available (lignite R and bituminous coal A). The data of wood, biocoal, lignite V, and anthracite are measured at a holding time of 1 s. p_{set} is 0.5 MPa as this is in accordance with most of the entrained flow data. In the model, both parameters $Y_{V,p_{set}}$ and ρ are derived by a least square fitting method.

If the measurement point at 0.5 MPa was used for $Y_{V,p_{set}}$, the model would predict exactly this value (including the measurement error) at 0.5 MPa. By fitting both parameters ($Y_{V,p_{set}}$ and ρ) to all data points, $Y_{V,p_{set}}$ is determined by the trend in all the experimental data. Figure 6.1 shows the model predictions compared with the experimental data. Table 6.1 summarises the model parameters for six fuels ranging from wood to anthracite.

ρ is a measure for the magnitude of the pressure influence. The volatile yield decreases considerably with pressure at low values of ρ . If ρ is large, the operation pressure has

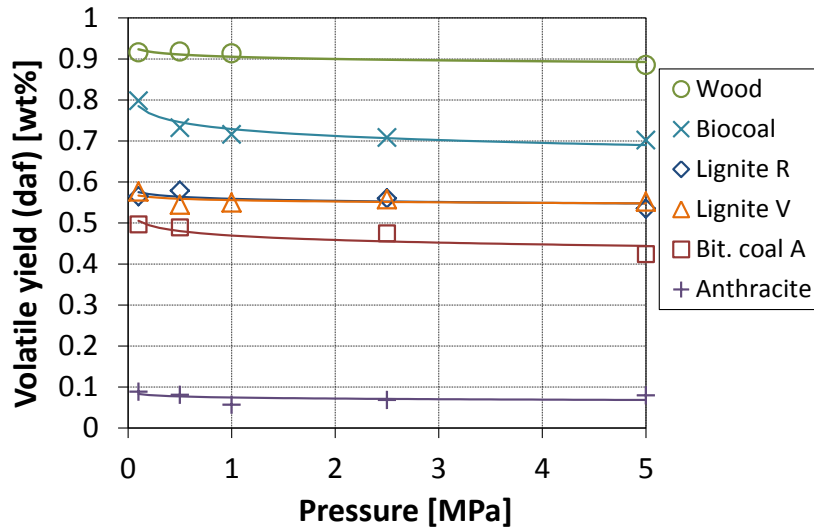


Figure 6.1: Model predictions of volatile yield (daf) as a function of the pyrolysis pressure. Symbols denote experimental data from the PWMR shown in Figure 5.44.

Table 6.1: Model parameters of the pyrolysis model in the pressure range 0.1 MPa 5.0 MPa for different fuels

Fuel	$Y_{V,p_{set}}$	p_{set}	ρ
Wood	0.911	0.5 MPa	126.6
Biocoal	0.746	0.5 MPa	41.1
Lignite R	0.564	0.5 MPa	141.0
Lignite V	0.559	0.5 MPa	207.6
Bituminous coal A	0.480	0.5 MPa	63.8
Anthracite	0.077	0.5 MPa	267.3

almost no influence on volatile yield.

Also **temperature** influences volatile yield. The volatile yield in the entrained flow experiments above 1200°C is significantly higher than in the PWMR at 1000°C. In the PiTER and in the BabiTER particles are entrained in a gas flow and are surrounded by a gas atmosphere. This environment is also imitated in the PWMR as the sample is flown through by an inert gas. In both configurations, the recondensation of volatile matter is prevented. The temperature and not the experimental setup is expected to have the major effect on volatile yield. The influence of temperature in the pyrolysis model is described by Equation 4.10:

$$Y_V(T) = Y_{V,T_{set}} + (Y_{V,T_{max}} - Y_{V,T_{set}}) \cdot (1 - \exp[-\vartheta(T - T_{set})]).$$

As a large number of experimental data is available at 0.5 MPa, the influence of temperature is evaluated at this pressure. $Y_{V,T_{set}}$ is chosen to be equal to $Y_{V,p_{set}}$ in Table 6.1 for each fuel because then the submodels for pressure and temperature effects intersect in a common data point and both can be applied together. $Y_{V,T_{max}}$ is the volatile yield in the entrained flow experiment at the highest temperature. ϑ is determined by minimising the least squares between the model equation and the experimental data. If the volatile yield is measured in more than one entrained flow experiment at the same temperature, the average of data at a particle residence time ≥ 1 s is calculated. Suitable PWMR and en-

trained flow experiments are available for the two lignites. The PWMR reactor is operated at 1000°C, whereas pyrolysis experiments in the PiTER are carried out at temperatures from 1200°C to 1600°C. The model predictions are compared with experimental data in Figure 6.2 and the model parameters are summarised in Table 6.2. Entrained flow pyrolysis experiments of bituminous coal A are carried out. The volatile yield in the entrained flow experiments is lower than the volatile yield in the PWMR. The reason for this is soot formation. The volatile matter can form soot particles in the gas phase under certain operation conditions. The existence of soot during pyrolysis and gasification of bituminous coal A is shown in the particle size analysis in Section 5.4.1.6. Soot is collected simultaneously with char by the sampling probe. In the char analysis, the soot fraction increases the carbon content and decreases the ash content of the char sample. The calculation of overall and carbon conversion leads to values that are much lower than the true fuel conversion.

Soot is probably also generated in the PWMR experiments. However, the mesh purge gas transports soot particles away from the char sample. The weight analysis and the calculation of volatile yield are not influenced.

Due to the lack of usable entrained flow data, the influence of temperature on devolatilisation of bituminous coal A cannot be determined in the model. As entrained flow pyrolysis data of the other fuels are not available, the model parameters are only presented for the lignites.

Table 6.2: Model parameters of the pyrolysis model that describe the influence of temperature on volatile yield

Fuel	$Y_{V,T_{set}}$	$Y_{V,T_{max}}$	T_{set}	ϑ
Lignite R	0.564	0.687	1000°C	0.0066
Lignite V	0.559	0.655	1000°C	0.0141

6.2 Analysis of the Devolatilisation Kinetics

So far, the volatile yield after a longer time at temperature is described as a function of pressure and temperature. The devolatilisation rate that describes the evolution of volatiles with time is expressed as a single first-order reaction (SFOR) rate equation (Equation 4.20):

$$\frac{dY_V(t)}{dt} = A_V \cdot \exp\left[\frac{E_{A,V}}{R \cdot T}\right] \cdot \left(Y_{V,p,T_{final}} - Y_V(t)\right)$$

where $Y_{V,p,T_{final}}$ is the final volatile yield at the operation pressure and the maximum pyrolysis temperature. The BabiTER results at 0.1 MPa and the PiTER data at 0.5 MPa are used for the parameter determination. An average yield at both pressures from the pyrolysis model in Section 6.1 is selected as the final volatile yield. The pre-exponential factor A_V and the activation energy $E_{A,V}$ are determined in a least squares fitting method. The model predictions and the experimental data are compared in Figure 6.3 for the lignite R. The experimental data at a residence time < 0.3 s are excluded in the fitting procedure as a small error in residence time of these experiments would result in a large deviation

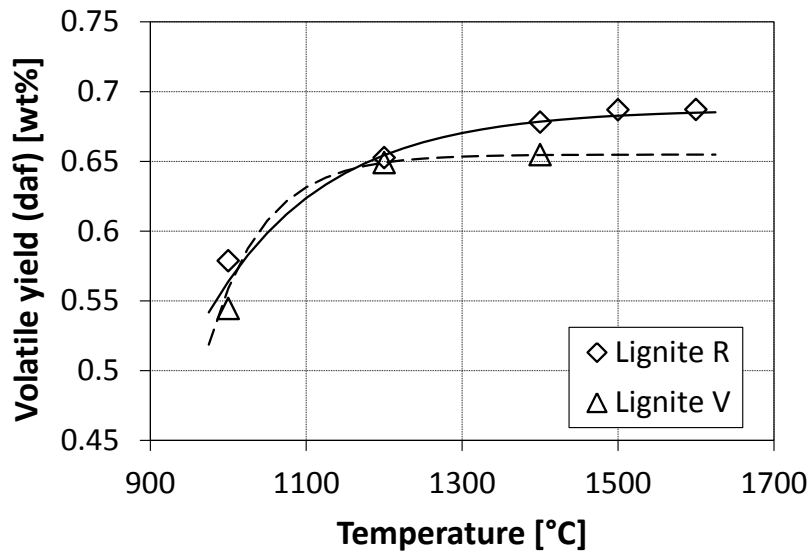


Figure 6.2: Model predictions of volatile yield (daf) in the pyrolysis model as a function of temperature. Symbols denote experimental data from the PWMR (see Figure 5.44; data only at 1000°C available) and the PiTER (see Figures 5.22 and 5.24; 1200°C to 1600°C) at a devolatilisation pressure of 0.5 MPa.

from the model. This is due to the strong increase in volatile yield at a low residence time. The model parameters are determined from the 1200°C and the 1400°C data, and the 1600°C measurement points are shown for comparison. The pre-exponential factor A_V is 293 s^{-1} and the activation energy $E_{A,V}$ is 51 kJ/mol. However, in the fitting procedure it is assumed that the particle heating rate is very high and the particle temperature equals the gas temperature. If a defined particle heating rate is applied to the parameter determination, the pre-exponential factor and the activation energy slightly change as shown in Table 6.3.

The initial heating rate in the entrained flow experiments is calculated to be $\geq 10^5 \text{ K/s}$

Table 6.3: Influence of the assumption of different heating rates on the determination of pre-exponential factor and activation energy in the pyrolysis model of lignite R

Heating rate [K/s]	A_V s^{-1}	$E_{A,V}$ kJ/mol
∞	293	51
10^6	293	51
10^5	325	52
$5 \cdot 10^4$	371	53
10^4	4742	81

(particle size $\leq 100 \mu\text{m}$, see Figure 5.5). Therefore, the assumption of an infinite heating rate in the model evaluation does not significantly influence the parameters.

The similar procedure is used to evaluate the adjustable parameters in the pyrolysis model of lignite V. The pre-exponential factor A_V is $5.88 \cdot 10^5 \text{ s}^{-1}$ and the activation energy $E_{A,V}$ is 142 kJ/mol.

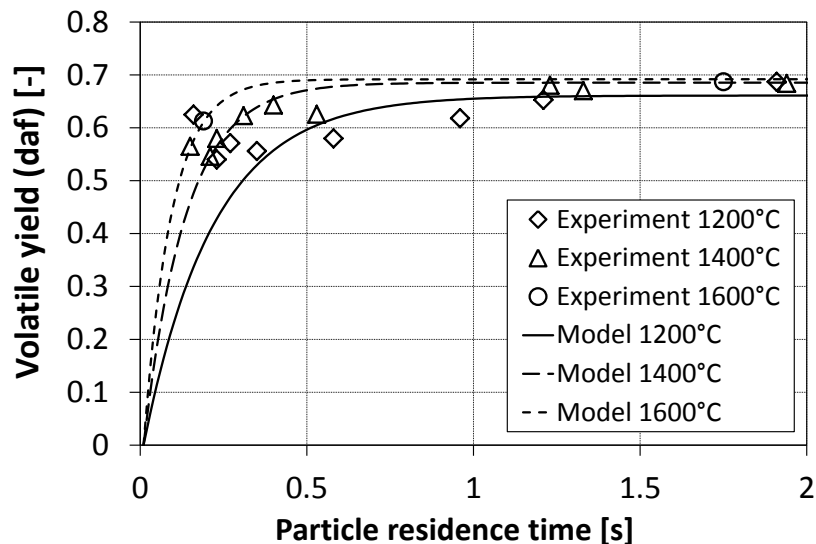


Figure 6.3: Model predictions of volatile yield (daf) of lignite R in the pyrolysis model as a function of residence time and temperature. Symbols denote experimental data (see Figure 5.22) from the BabiTER and the PiTER.

The kinetic pyrolysis model cannot be validated for other fuels as the amount of time dependent pyrolysis data is too low.

The pre-exponential factor and the activation energy of both lignites significantly deviate in the models despite similar physical and chemical processes during devolatilisation. This can be explained by the simplicity and the empirical nature of the model. All devolatilisation reactions are approximated by a single reaction rate with constant activation energy. The model is purely empirical and the parameters have no mechanistic importance. Furthermore, the uncertainties in the experimental data are not considered in the model evaluation, but would lead to deviations of the model parameters. The activation energies of 51 kJ/mol and 142 kJ/mol lie within the range that is reported in literature. For example, Brown et al. [Brown2001] modelled pyrolysis kinetics by a simple Arrhenius type rate equation. They used an activation energy of 140 kJ/mol for the entrained flow pyrolysis of ethyl ether, a model compound for biomass studies.

Simone et al. [Simone2009] integrated a SFOR model in a CFD code for biomass devolatilisation and compared the results to experimental drop tube data. The activation energy was adjusted to represent the experimental data and the final value was between 20.4 kJ/mol and 43.9 kJ/mol depending on the fitting procedure.

Chapter 7

Validation of the Char Conversion Models for Entrained Flow Gasification

In Chapter 4 different char reaction submodels are proposed that can be combined to describe the reaction rate in high temperature entrained flow gasifiers. The basic structure of the char conversion model and the interaction of the submodels are shown in Figure 7.1.

The experimental data from Section 5.4 are now used to determine the adjustable parameters in the submodels and to build model equations that predict the gasification behaviour of solid fuels in pilot and industrial scale reactors.

7.1 Validation of the Char Gasification Submodels

The experimental data from different facilities are used to determine fuel and char specific properties. Submodels are developed for the intrinsic reactivity, for the evolution of surface area, and for the thermal deactivation of char. These submodels can then be combined to describe the reaction rates of char during conversion under Regime I conditions. The two submodels for mass transport limitations (pore diffusion and boundary layer diffusion) are then validated by entrained flow conversion data.

The largest number of experiments is available for the lignite R. Therefore, the submodels are first validated for char of lignite R. If the amount of data of other fuel chars is sufficient, submodels of other fuels are presented.

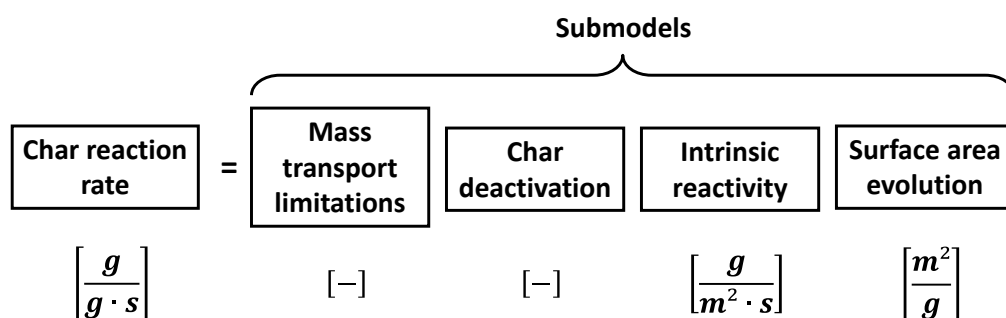


Figure 7.1: Structural combination of different submodels to describe the char conversion rate in high temperature entrained flow gasifiers

7.1.1 Validation of the Intrinsic Reactivity Submodels

Three levels of submodels for the intrinsic reaction rate are developed in Section 4.2.3.2. At a higher level number, the complexity of the model equations increases and more adjustable parameters are required to describe the reaction behaviour. The adjustable parameters of the model equations are evaluated using experimental data of the PRETA experiments. As the operation conditions in thermogravimetric analyses are very defined, the influence of single operation parameters on the intrinsic reactivity can be determined precisely.

7.1.1.1 Level 1 - nth Order

In Level 1, single char-gas reactions are considered and the model describes the influences of temperature and reactant pressure on the char conversion rates. The nth order rate equation is given by Equation 4.35:

$$r_{intr,L1,i} = r(T, p_i) = k_{OL1,i} \cdot \exp\left[\frac{-E_{AL1,i}}{RT}\right] \cdot p_i^{n_i}$$

In the following, the influence of reactant partial pressure and then the influence of temperature on the reaction rate are evaluated:

Influence of the CO₂ Partial Pressure As the experiments are performed at different total pressure, a possible effect of total pressure is incorporated in the model equation by an mth order term:

$$r_{intr,L1,CO_2} = k_{OL1,CO_2} \cdot \exp\left[\frac{-E_{AL1,CO_2}}{RT}\right] \cdot p_{CO_2}^{n_{CO_2}} \cdot p_{total}^m \quad (7.1)$$

For the evaluation of the parameter n_{CO_2} the observed reaction rates in both experimental series (Figures 5.47 and 5.48) are normalised using the data at $p_{norm} = 0.5$ MPa:

$$r_{norm} = \frac{r_{obs,p_{CO_2}}}{r_{obs,0.5MPa}} = \frac{S(x) \cdot r_{intr,L1,CO_2}}{S(x) \cdot r_{intr,L1,0.5MPa}} \quad (7.2)$$

$$= \frac{k_{OL1,CO_2} \cdot \exp\left[\frac{-E_{AL1,CO_2}}{RT}\right] \cdot p_{CO_2}^{n_{CO_2}} \cdot p_{total}^m}{k_{OL1,CO_2} \cdot \exp\left[\frac{-E_{AL1,CO_2}}{RT}\right] \cdot (p_{norm})^{n_{CO_2}} \cdot p_{total}^m} \quad (7.3)$$

Then constant parameters in this type of experiments are summarised and reduced, and on both sides the logarithm is taken:

$$r_{norm} = const. \cdot p_{CO_2}^{n_{CO_2}} \quad (7.4)$$

$$\ln[r_{norm}] = \ln[const.] + n_{CO_2} \cdot \ln[p_{CO_2}] \quad (7.5)$$

When plotting $\ln[r_{norm}]$ as a function of $\ln[p_{CO_2}]$, the reaction order n_{CO_2} is derived from the slope of the curve. The corresponding diagram is shown in Figure 7.2. The data points are approximated by a linear least squares fitting method and the reaction order

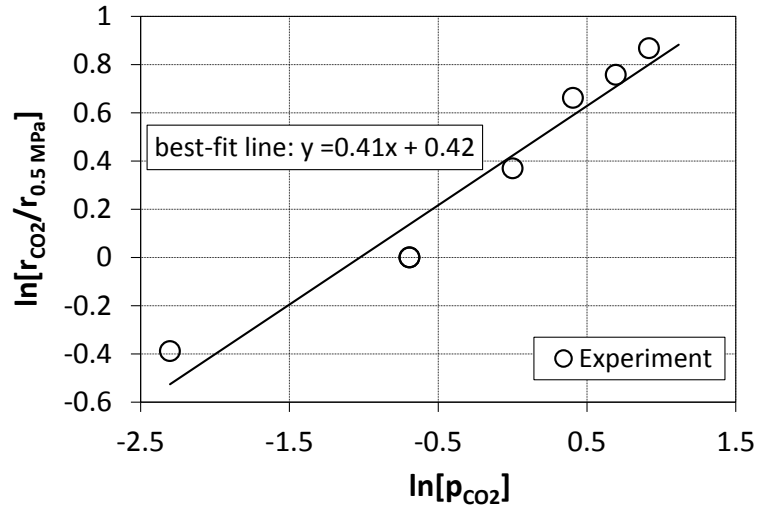


Figure 7.2: Graphical evaluation of reaction order n_{CO_2} in PRETA experiments for lignite R char. (Data derived from Figures 5.47 and 5.48)

n_{CO_2} is determined to be 0.41. The average standard deviation in the reaction rate data is taken as a measure of uncertainty of the reaction order. This results in an uncertainty of 0.04. The reaction order n_{CO_2} is then 0.41 ± 0.04 .

Influence of the H₂O Partial Pressure Experiments at different H₂O partial pressures are not available. As the uncertainty in reaction order has only a small effect on the reaction rate, the reaction order of the CO₂ reaction is also assumed for the char-H₂O reaction. This is 0.41. The assumption of identical reaction orders is supported by drop tube experiments of Matsumoto et al. [Matsumoto2009]. They measured the char reaction rate in CO₂ and steam and observed identical orders for the two reactions.

Influence of the Total Pressure Some indications are found in the PRETA experiments in section 5.4.3.2 that suggest an influence of total pressure on the observed reaction rate. As N₂ and Ar are used as balance gases in the PRETA experiments, also an influence of the balance gas partial pressure could be possible. To quantify the effect of total pressure and balance gas partial pressure an m th order formulation is used:

$$\frac{dm}{dt \cdot m} = S(x) \cdot k_{OL1,CO_2} \cdot \exp\left[\frac{-E_{AL1,CO_2}}{RT}\right] \cdot p_{CO_2}^{n_{CO_2}} \cdot p_{total}^m \quad (7.6)$$

For the graphical analysis of the parameter m , the logarithm on both sides is taken:

$$\ln\left[\frac{dm}{dt \cdot m}\right] = \ln\left[S(x) \cdot k_{OL1,CO_2} \cdot \exp\left[\frac{-E_{AL1,CO_2}}{RT}\right] \cdot p_{CO_2}^{n_{CO_2}}\right] + m \cdot \ln[p_{total}] \quad (7.7)$$

The first term on the right side is constant, if only the total pressure is varied in the experiments. The partial pressure of CO₂ is kept constant. The conversion is assumed to be constant because only a small amount of char is converted. The parameter m is determined by plotting the logarithm of the observed reaction rate as a function of the logarithm of the total pressure as shown in Figure 7.3.

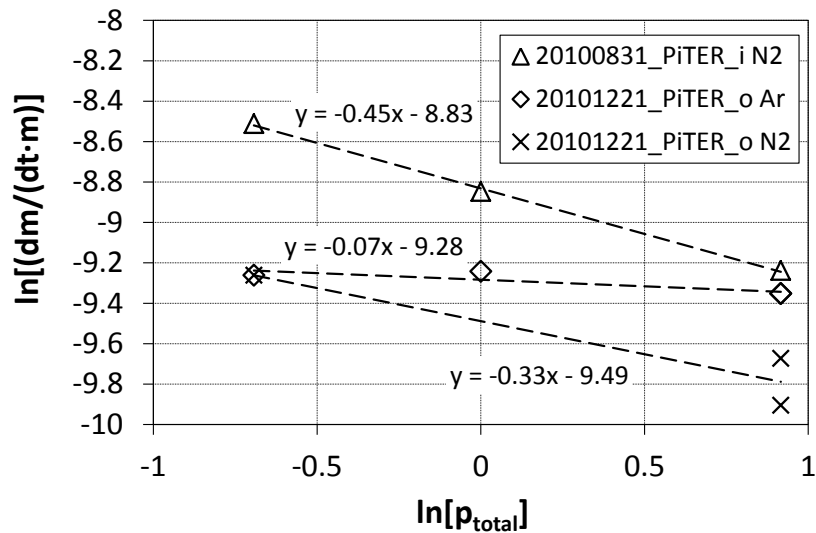


Figure 7.3: Graphical evaluation of the total pressure order m and the effect of balance gas (N_2 and Ar) in PRETA experiments for two different lignite R chars

The slopes of the curves denote the total pressure order m . In experiments with N_2 , the reaction order for the two chars is -0.45 and -0.33 , respectively. In the experiments that use Ar as the balance gas, the reaction order is only -0.07 . This implies that the properties of the balance gas and not the total pressure have an influence on the reaction rate. The application of a high partial pressure of N_2 results in a reduced reaction rate. Possible explanations for this observation might be the influence of gas diffusion or the adsorption at active sites:

- The diffusion rate of CO_2 in Ar might be higher than in N_2 . A high partial pressure of N_2 could inhibit the diffusion of reactant gas to the char outer surface and within the pore structure, and might lead to a reduction in observed reaction rate. This explanation is very unlikely, as the molecular gas diffusion coefficient of a CO_2 - N_2 mixture is higher than for a CO_2 -Ar mixture¹. Furthermore, the operation parameters in the PRETA are chosen to measure reaction rates under Regime I conditions. Effects of diffusion are excluded.
- Argon is a noble gas and the interactions with other gas molecules and surfaces are weak. In most applications N_2 is also an inert gas. But the thermogravimetric observations indicate that the adsorption of N_2 molecules at active sites on the char surface might occur. At a high partial pressure, N_2 molecules block active sites and prevent the reaction with CO_2 molecules.

For a more detailed analysis of the effects of the balance gas and the total pressure, more experiments are required. These should also evaluate the effect of temperature as diffusion and sorption processes are temperature dependent.

The influence of total pressure is not clear from the experiments. Also, studies from literature do not consider total pressure as an influencing factor. Therefore, the total

¹Binary diffusion coefficients can be calculated by a semi-empirical equation [Baerns2002]. The molecular gas diffusion coefficient of a CO_2 - N_2 mixture is about 6 % higher than that for a CO_2 -Ar mixture independent of temperature and pressure.

pressure is not included in the model equations and only the partial pressures of reactant gases are considered.

Influence of Temperature The influence of temperature on conversion is evaluated for four different char samples. The reaction rates in an experiment at a constant temperature ($T_{norm} = 750^\circ\text{C}$) and at a constant heating rate (600°C to 1000°C) are shown in Figure 5.51 for the char- CO_2 reaction and in Figure 5.52 for the char- H_2O reaction. For each char sample the reaction rate ($dm/(dt \cdot m)$) in the thermogravimetric analysis is dependent on char conversion as the specific surface area $S(x)$ changes during conversion. This effect is excluded by a normalisation of the observed reaction rate at a constant heating rate r_{HR} with the observed reaction rate at a constant temperature $r_{750^\circ\text{C}}$:

$$\frac{r_{HR}(x)}{r_{750^\circ\text{C}}(x)} = \frac{S(x) \cdot r_{intr,HR}(x)}{S(x) \cdot r_{intr,750^\circ\text{C}}(x)} = \frac{r_{intr,HR}}{r_{intr,750^\circ\text{C}}} \quad (7.8)$$

This approach assumes that the variation of surface area with conversion $S(x)$ is not dependent on temperature in the PRETA experiments. All experiments are carried out under Regime I conditions. Therefore, the evolution of surface area is not influenced by mass transport limitations and a temperature influence is not expected.

The intrinsic reactivity is described by the n th order rate equation and the activation energy $E_{AL1,i}$ is derived from an Arrhenius plot.

$$\begin{aligned} \frac{r_{HR}}{r_{750^\circ\text{C}}} &= \frac{k_{OL1,i} \cdot \exp\left[\frac{-E_{AL1,i}}{RT}\right] \cdot p_i^{n_i}}{k_{OL1,i} \cdot \exp\left[\frac{-E_{AL1,i}}{R \cdot T_{norm}}\right] \cdot p_i^{n_i}} \\ &= \exp\left[\frac{E_{AL1,i}}{R} \cdot \left(\frac{1}{T_{norm}} - \frac{1}{T}\right)\right] \end{aligned} \quad (7.9)$$

$$\ln\left[\frac{r_{HR}(x)}{r_{750^\circ\text{C}}(x)}\right] = \frac{E_{AL1,i}}{R \cdot T_{norm}} - \frac{E_{AL1,i}}{R} \cdot \frac{1}{T} \quad (7.10)$$

The Arrhenius plot ($\ln[r_{HR}/r_{750^\circ\text{C}}]$ vs. $1/T$) of the char- CO_2 reaction of four different chars is shown in Figure 7.4. All data points fall within a narrow band, and the activation energies of all chars are similar. For the determination of the activation energy, the first data point at the lowest temperature (= lowest conversion) is excluded as an influence of the gas change to CO_2 in the PRETA is likely. At a higher temperature (=higher conversion) the sample mass decreases and the error in the data increases. Furthermore, at a high temperature mass transport limitations may exist within the char pore structure or at the transition to the gas bulk phase. The activation energy is calculated from the conversion interval 0.03 to 0.25. In the constant heating rate experiment the temperature increases with conversion. The maximum temperature at 25 % conversion is dependent on the reactivity of the char sample. Table 7.1 summarises the activation energy and the maximum temperature derived from the analysis.

The activation energy tends to increase for chars that are produced at higher temperatures. However, more data are required for the evaluation of a clear dependence. Therefore, the dependence of activation energy on char heat treatment temperature is

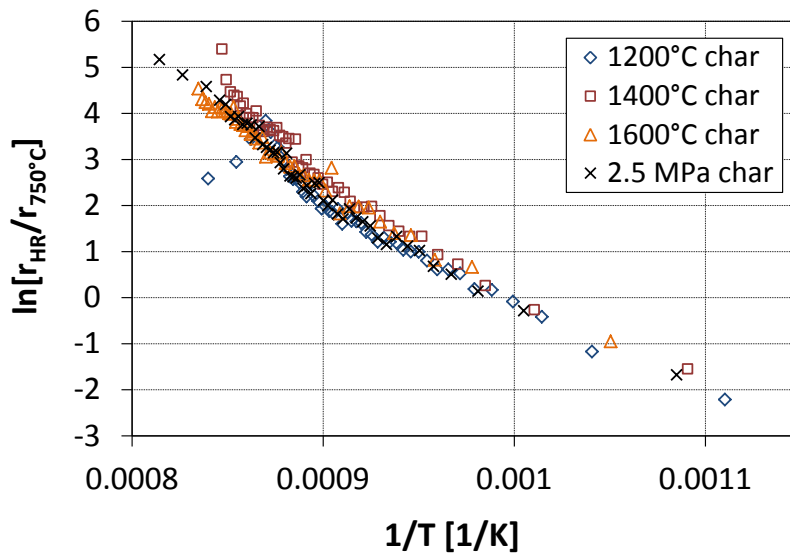


Figure 7.4: Temperature dependence of the reaction rate of different lignite R chars ($p_{CO_2} = p_{total} = 0.5$ MPa). Experimental data is shown in 5.51.

Table 7.1: Activation energy for the char- CO_2 reaction of different lignite R char samples measured in the PRETA analysis. Temperature denotes the sample temperature at a conversion of 0.25 in the constant heating rate experiment.

Char type	Sample ID	Activation energy E_{AL1,CO_2}	Temperature ($x=0.25$)
1200°C char	20101220_PiTER_c	182 kJ/mol	788°C
1400°C char	20101220_PiTER_n	211 kJ/mol	817°C
1600°C char	20101221_PiTER_o	206 kJ/mol	840°C
2.5 MPa char	20100831_PiTER_i	192 kJ/mol	817°C

not considered. An average activation energy is included in the model. As any influences of devolatilisation pressure are implemented in other submodels, the 2.5 MPa char is not considered for the calculation of the average activation energy. The average of the other three char samples that are produced at 0.5 MPa is 200 kJ/mol, and the standard deviation is 16 kJ/mol.

The temperatures in Table 7.1 are also an indicator for char reactivity. They denote the temperature in the constant heating rate experiment when the char conversion reaches 25 %. This temperature increases with char production temperature. The 1600°C char has the lowest reactivity because the highest temperature is required.

The influence of temperature on the H_2O reaction is only measured for the 1600°C char. The identical procedure described for the char- CO_2 measurements is applied to the H_2O data. The activation energy is 212 kJ/mol and therefore slightly higher than for the char- CO_2 reaction. Due to the uncertainty in the char- H_2O measurements the uncertainty of activation energy is expected to be at least in the range of the CO_2 activation energy. The temperature in the constant heating rate experiment for 25 % char conversion is 765°C and therefore significant lower than in the corresponding char- CO_2 experiment. This indicates the higher reactivity of char towards steam than towards CO_2 . Due to the larger activation energy, this higher reactivity will be more pronounced at higher temperatures.

Determination of the Pre-exponential Factor Reaction rates that are measured in the thermogravimetric analysis are on a mass basis [$g/(g \cdot s)$] whereas the reaction rate in the intrinsic model is on a surface area basis [$g/(m^2 \cdot s)$]. The specific surface area of chars is known from adsorption measurements with CO_2 at 273 K. In the thermogravimetric experiments the specific surface area of char is expected to change with conversion. As the evolution of surface area is dependent on the reaction conditions, the variation of surface area in PRETA experiments is likely to deviate from the evolution in entrained flow experiments at higher temperatures.

The conversion up to 0.05 is excluded due to possible effects of the gas change to CO_2 in the experiment. At a higher conversion a significant change of specific surface area in the PRETA is expected that is not representative for the surface area evolution in the entrained flow experiments. Thus, the maximum conversion for the average determination is set to 0.2. The variation of surface area can be detected in the mass specific reaction rate if there is a change with conversion. From 5% to 20% conversion, the mass specific reaction rate is constant for all three char samples which proves that there is no significant variation of the surface area.

Mass specific (= observed) reaction rates of the 1200°C char, the 1400°C char, and the 1600°C char are used to determine the pre-exponential factor of the char- CO_2 reaction. The average reaction rates at 750°C in the conversion interval 0.05 to 0.2 are: $3.64 \cdot 10^{-4} g/(g \cdot s)$ (1200°C char), $1.53 \cdot 10^{-4} g/(g \cdot s)$ (1400°C char), and $0.97 \cdot 10^{-4} g/(g \cdot s)$ (1600°C char).

Initial DFT surface areas of the chars are: 449 m^2/g (1200°C char), 513² m^2/g (1400°C char), and 263 m^2/g (1600°C char). The pre-exponential factor is then calculated analytically from Equation 4.35 using $n_{CO_2}=0.41$ and $E_{AL1,CO_2}=200$ kJ/mol. The pre-exponential factors together with the other model parameters are shown in Table 7.2. The pre-

Table 7.2: Model parameters of the Level 1 intrinsic char- CO_2 reaction model for different char samples

Char type	Pre-exponential factor k_{0L1,CO_2} $\left[\frac{g}{m^2 \cdot s \cdot MPa^{n_{CO_2}}} \right]$	Activation energy E_{AL1,CO_2} [kJ/mol]	Exponent n_{CO_2} -
1200°C char	16525	200	0.41
1400°C char	6068	200	0.41
1600°C char	7516	200	0.41

exponential factor decreases considerably when the char pyrolysis temperature is increased from 1200°C to 1400°C. Although the mass specific reaction rate decreases from the 1400°C char to the 1600°C char, the pre-exponential factor slightly increases. Compared with the strong decline from 1200°C to 1400°C the further variation is only marginally. The loss of mass specific reaction rate from 1400°C to 1600°C can be explained by the loss of specific surface area. Intrinsic reactivity decreases from 1200°C to 1400°C and then remains almost constant up to 1600°C.

The pre-exponential factor of the char- H_2O reaction is determined for the 1600°C char.

²The surface area of this char is unusual large in comparison to other chars that are produced at similar conditions. The calculation of the pre-exponential factor could results in a value that is too low.

Using the aforementioned procedure, the value $144770 \text{ g}/(\text{m}^2 \cdot \text{s} \cdot \text{MPa}^{0.41})$ is derived. The corresponding activation energy is 212 kJ/mol and the reaction order is 0.41.

7.1.1.2 Level 2 - Simple LH Type Rate Equation

The adsorption and the desorption of reactant gases and the saturation of the char surface area at higher reactant partial pressures are integrated in the Level 2 char gasification model. The model equation (Equation 4.36) is:

$$r_{intr,L2} = \frac{k_{L2,i} \cdot p_i}{1 + K_{L2,i} \cdot p_i} = \frac{k_{0L2,i} \cdot \exp\left[\frac{-E_{AL2,i}}{RT}\right] \cdot p_i}{1 + K_{0L2,i} \cdot \exp\left[\frac{-E_{aL2,i}}{RT}\right] \cdot p_i}$$

The experimental data from the combined analysis of the influences of reactant partial pressure and temperature (Section 5.4.3.4) of the PRETA are used. These data are only available for the char-CO₂ reaction of the lignite R.

The parameters k_{L2,CO_2} and K_{L2,CO_2} are derived graphically by a rearrangement of Equation 4.36:

$$\frac{1}{r_{intr,L2}} = \frac{1}{k_{L2,CO_2}} \cdot \frac{1}{p_{CO_2}} + \frac{K_{L2,CO_2}}{k_{L2,CO_2}} \quad (7.11)$$

and the plot of $1/r_{intr,L2}$ vs. $1/p_{CO_2}$. This is shown in Figure 7.5 for the data in Table 5.9. As the observed reaction rate of the lignite R char does not change with conversion up to 60% (see for example Figure 5.51), it is assumed that the surface area is almost constant up to 60% conversion and the intrinsic reactivity is calculated from the observed reaction rate and the initial surface area ($263 \text{ m}^2/\text{g}$). From the correlation between the slope and the axis intercept in Figure 7.5, k_{L2,CO_2} and K_{L2,CO_2} at temperatures of 750°C and 775°C are calculated. Then, Arrhenius plots ($\ln[k]$ vs. $1/T$) are used to determine the pre-exponential factors and activation energies of k_{L2,CO_2} and K_{L2,CO_2} . The data are summarised in Table 7.3. The model predictions are compared with the thermogravimetric data in Figure 7.6.

At a low CO₂ partial pressure ($1 \gg K_{L2,CO_2} \cdot p_{CO_2}$) the model becomes a first order

Table 7.3: Model parameters of the Level 2 intrinsic char-CO₂ reaction model

Model parameter	Value at 750°C	Value at 775°C	Pre-exponential factor	Activation energy
$k_{L2,CO_2} [\text{g}/(\text{m}^2 \cdot \text{s} \cdot \text{MPa})]$	$1.92 \cdot 10^{-6}$	$3.86 \cdot 10^{-6}$	$8.82 \cdot 10^6$	248 kJ/mol
$K_{L3,CO_2} [1/\text{MPa}]$	2.81	3.15	362	41 kJ/mol

equation. The activation energy of k_{L2,CO_2} should then approach the activation energy of the nth order model (Level 1 intrinsic model). However, in the LH approach the activation energy is 48 kJ/mol higher than in the nth order rate equation. The reason for the deviation in this analysis might be the uncertainty of the data. The data is collected in only two experimental runs. The error in these measurements cannot be balanced by the trend in a series of measurements. For example, the deviation of the measured reaction rate of only 5 % could change the activation energy up to 80 kJ/mol. Therefore, the values presented here are a first estimation, but more measurements are required to determine

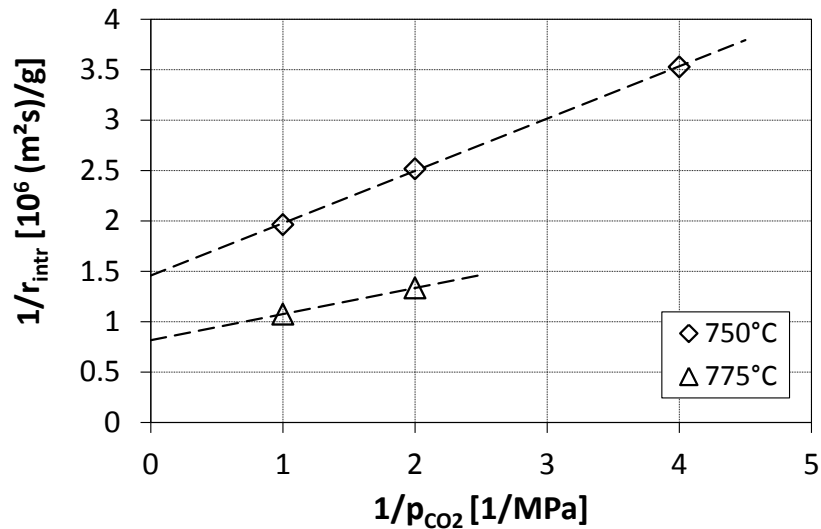


Figure 7.5: Graphical determination of the parameters k_{L2,CO_2} and K_{L2,CO_2} in the Level 2 intrinsic reaction model

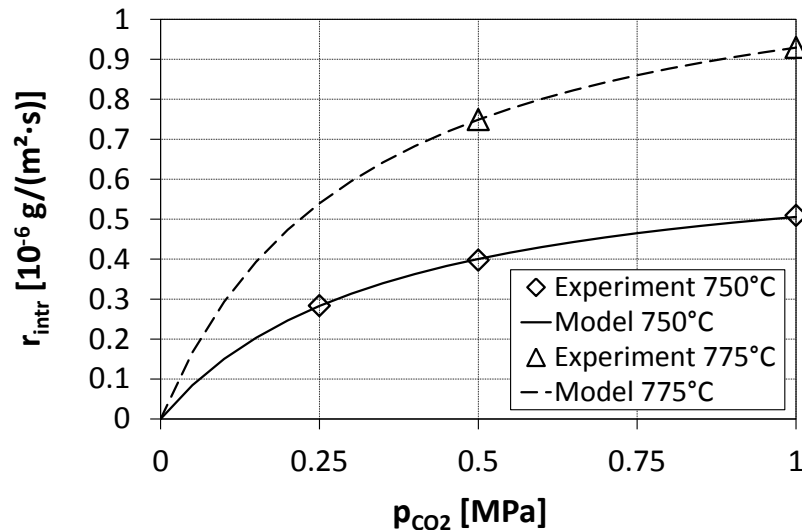


Figure 7.6: Comparison of the model predictions of the Level 2 intrinsic model compared with the experimental data set from PRETA measurements.

reliable parameters for the Level 2 intrinsic model.

In Table 3.3, literature data of the char-CO₂ reaction are shown. Several studies [Ollero2003, Cetin2005, Feroso2009] use nth order and LH rate equation to describe reaction rate and the deviations between the two activation energies are even larger than reported here.

7.1.1.3 Level 3 - LHHW Kinetics

The Level 3 intrinsic model is based on the data evaluation of the Level 2 model and the PRETA experiments with mixtures of CO₂ and CO (see Section 5.4.3.5). The general form of the model is described by Equation 4.44. For the char reaction with CO₂ and CO this equation becomes

$$r_{intr,L3} = \frac{k_{L3,CO_2} \cdot p_{CO_2}}{1 + K_{L3,CO_2} \cdot p_{CO_2} + K_{L3,CO} \cdot p_{CO}} \quad (7.12)$$

Again, a graphical procedure is chosen to derive the model parameters. Equation 7.12 is rearranged:

$$\frac{1}{r_{intr,L3}} = \left(\frac{1}{k_{L3,CO_2} \cdot p_{CO_2}} + \frac{K_{L3,CO_2}}{k_{L3,CO_2}} \right) + \frac{K_{L3,CO}}{k_{L3,CO_2} \cdot p_{CO_2}} \cdot p_{CO} \quad (7.13)$$

and $1/r_{intr,L3}$ is plotted vs. p_{CO} in Figure 7.7.

The parameters $k_{L3,CO_2} = k_{L2,CO_2}$ and $K_{L3,CO_2} = K_{L2,CO_2}$ are taken from the Level 2 model. The only unknown parameters are then the pre-exponential factor and the activation energy of $K_{L3,CO}$. From the slope of the two linear regression curves, the values of $K_{L3,CO}$ at 750°C and 775°C are calculated. The pre-exponential factor $K_{0L3,CO} = 3.4 \cdot 10^{-22}$ 1/MPa and the activation energy $E_{aL3,CO} = -479$ kJ/mol are derived from an Arrhenius plot.

The negative activation energy indicates a decrease in the CO inhibition at higher temperature. However, the model parameters of the Level 3 intrinsic model are derived from too little data to reliably predict the reaction of char with CO₂ and CO. More experiments are required to underpin the validity of the model parameters.

Negative activation energies for the inhibition of product gases are also reported in the literature (see Table 3.3 and Table 3.4). Hence, the influence of product gases is lower at a higher temperature. The strong reduction of the reaction rate that is observed in the PRETA experiments is not expected at higher temperatures in an entrained flow gasifier.

7.1.2 Validation of the Surface Area Submodel

For a range of solid fuels, specific surface areas of chars after pyrolysis and gasification are measured. The experimental data are shown in Section 5.4.1.5. The pyrolysis at a higher temperature results in a decrease in the surface area for lignite R, bituminous coal A, and anthracite. An increase in temperature from 1200°C to 1400°C at a particle residence time of 1.5 s to 2 s results in a loss of surface area by a factor of about 8 for the anthracite, and by a factor of 1.5 to 2 for the bituminous coal and the lignite R, respectively. In contrast, no influence of temperature is observed between 1000°C and 1400°C in the data set of lignite V.

Less data are available to evaluate the effect of pyrolysis pressure on surface area. Within the lignite R chars, the specific surface area is larger at a higher pyrolysis pressure. This trend is partially supported by the surface area of bituminous coal A char that is generated at different pressure.

Char surface area measurements are available for the gasification of lignite R, bituminous coal A, anthracite, and biocoal. In all gasification and pyrolysis experiments a similar effect of temperature is observed. With increasing temperature the char surface area decreases. Only biocoal char is an exception. The influence of pressure during the conversion cannot be analysed in detail as there are too little data available. The gasification experiments result in different levels of conversion dependent on parent fuel, temperature, and residence time. For each fuel, char specific surface area is analysed as a function of char conversion. In the data sets of all four fuels, a decrease in surface area in the medium and later stages of conversion is detected.

For the development of a submodel that predicts the specific surface area in entrained flow gasification, the influence of pressure on surface area after devolatilisation and the

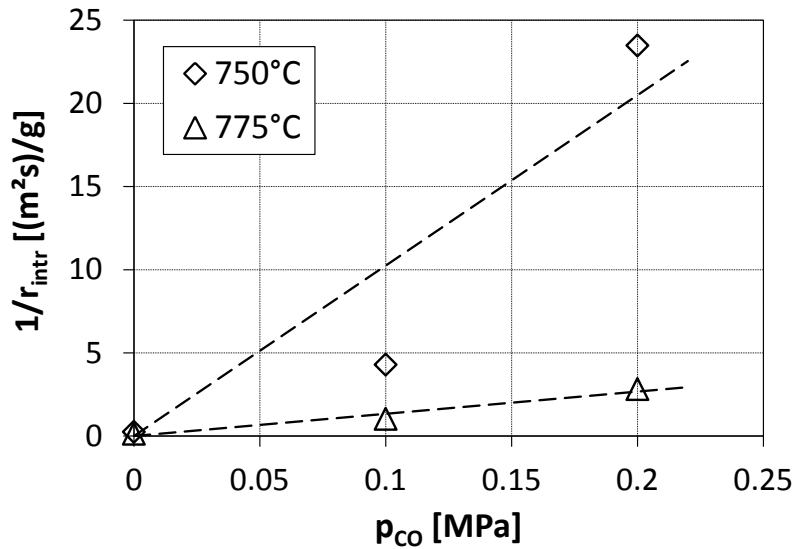


Figure 7.7: Plot of $1/r_{intr}$ vs. p_{CO} for the evaluation of CO inhibition in PRETA experiments

influence of char conversion and temperature on surface area during gasification are implemented. The model development is shown for the lignite R.

The initial char surface area after devolatilisation is determined from the pyrolysis experiments. As specific surface area at a low residence time is almost independent of pyrolysis temperature (see Figure 5.33), the 1200°C data are used to evaluate the effect of pressure on the initial char surface area. The average char surface area in the residence time interval 0.5 s to 3.0 s at different pyrolysis pressures is summarised in Table 7.4.

In the model an empirical linear approximation of the data is applied:

Table 7.4: Average specific surface area (DFT, CO₂ at 273 K) of pyrolysis chars of lignite R that are produced at different pressure and in the residence time interval 0.5 s to 3.0 s

Pyrolysis pressure [MPa]	DFT surface area [m ² /g]
0.5	478
1.0	533
2.5	563

$$S_{ini} \left[\frac{m^2}{g} \right] = 475 + 37 \cdot p \left[MPa \right] \quad (7.14)$$

where S_{ini} is the initial char surface area of lignite R after devolatilisation and p is the pyrolysis pressure.

In the gasification experiments the surface area decreases in the medium and later stages of conversion as shown in Figure 5.35. As the surface area after the pyrolysis is lower than the maximum surface area in the gasification experiments, there is a maximum in surface area during char conversion. This maximum is predicted by the Random Pore Model (RPM) (see Section 4.2.4). However, the initial form of the RPM predicts surface area on a volumetric basis [m²/m³]. Based on char mass [m²/g], the RPM describes an increase in surface area in the later stages of char conversion. The continuous decrease in mass specific surface area in the experimental data is therefore contradictory to the

theoretical background of the model. But, due to its simple form and the prediction of a maximum, the mathematical description of the RPM is used as an empirical equation to predict mass specific surface area of lignite R char. The initial char surface area after devolatilisation is estimated by Equation 7.14 and the model parameter Ψ is evaluated by a least squares fitting procedure. The experimental data and the model predictions are shown in Figure 7.8. The parameter ψ is estimated to be 4.7 in the temperature range 1200°C to 1600°C and the complete mathematical description of surface area is:

$$S \left[m^2/g \right] = (475 + 37 \cdot p \text{ [MPa]}) \cdot (1 - x) \cdot \sqrt{1 - \Psi \cdot \ln[1 - x]} \quad (7.15)$$

In the model, the char surface area is dependent on devolatilisation pressure and char conversion. Both influencing parameters are detected to be the most important in the evaluation of experimental data. The model is able to predict an increase in char reactivity due to an increase in surface area at higher pressure that is also reported in literature [Roberts2003].

Another parameter that might influence surface evolution is the gasification temperature. The decrease in specific surface area for some coals at a higher temperature in pyrolysis and gasification experiments indicates a significant change in the char structure. A possible explanation is the melting of mineral matter that blocks the pore structure and lowers the surface area. Liu et al. [Liu2006] and earlier Lee et al. [Lee1996] detected a rapid decrease in reactivity and surface area above a threshold temperature. Liu et al. related this temperature to the ash fusion temperature of several coals and found a good correlation. SEM photos proved that the melting of ash occurred if the operation temperature was above the ash melting temperature. Furthermore, a fast reorganisation (structural ordering) of the char surface is expected at higher temperatures leading to a loss of surface area. The dataset of lignite R gasification at 0.5 MPa is analysed regarding the influence of conversion temperature on surface area. The structure parameter Ψ is determined for the gasification temperatures 1200°C, 1400°C, and 1600°C. Figure 7.9 shows a clear trend in the data: the structure parameter Ψ decreases at higher gasification temperatures.

The amount of data points at a single temperature is low and data are only available at higher levels of conversion. The RPM curves are least squares fits to the experimental data, but for a better description of the temperature influence more data - especially at lower conversion - are required.

For the other fuels, the amount of surface area data is lower. In the following paragraphs, the model predictions and simplifications for char surface area of bituminous coal A, anthracite, lignite V, and biocoal are summarised.

Bituminous coal A The pyrolysis experiments indicate an influence of pressure on the surface area after devolatilisation (see Figure 5.38). However, the amount and significance of the data are too low to develop an empirical formulation. Therefore, the char specific surface area of 354 m²/g after pyrolysis at 1200°C, 0.5 MPa, and 1.0 s is used as an initial value after devolatilisation. Then, the parameter Ψ is estimated by a least squares fitting method using the char surface data of the gasification experiments. In Figure 7.10 the model predictions are compared with the experimental data measured at temperatures from 1200°C to 1500°C. The development of specific surface area of bituminous coal A

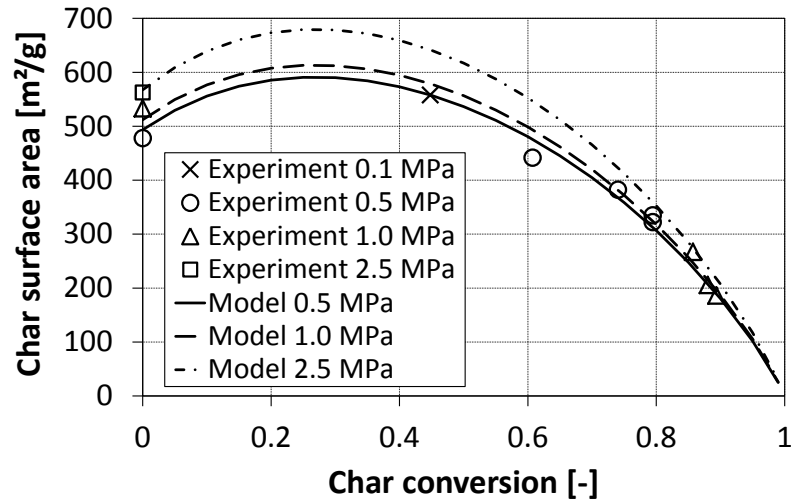


Figure 7.8: Model prediction of specific surface area of lignite R char compared with measurements of char surface area (DFT, CO₂ at 273 K) at different levels of conversion and at gasification temperatures from 1200°C to 1600°C

char during conversion is mathematically described as:

$$S \left[\frac{m^2}{g} \right] = 354 \cdot (1 - x) \cdot \sqrt{1 - \Psi \cdot \ln [1 - x]} \quad (7.16)$$

with $\Psi = 3.0$. The scatter in the data is high which may be caused by the influence of soot formation.

Anthracite The specific surface area of anthracite chars during pyrolysis and gasification is shown in Figure 5.40. As the amount of data is low and a clear influence of char conversion on surface area is not observed, the empirical form of the Random Pore Model is not applied. The data show a significant influence of temperature on surface area. The char conversion does not increase significantly from 1200°C to 1400°C at 1.3 s residence time, but the surface area decreases from 265 m²/g to 90 m²/g. The loss of surface area is faster than char conversion which additionally decreases the reaction rate. Further experimental data are required to analyse this phenomenon in more detail. As the temperature in an entrained flow gasifier is usually higher than 1400°C, a constant char surface area of 90 m²/g might be a good assumption in a gasification model.

Lignite V Gasification experiments of lignite V are not carried out. During pyrolysis, a slight increase in surface area with residence time is observed (see Figure 5.37), but there is no influence of temperature from 1000°C to 1400°C. The average surface area at 0.9 s residence time is 465 m²/g.

Biocoal As only a few surface measurements of biocoal chars are available, the complex Random Pore Model formulation is not applied. The specific char surface area of biocoal is assumed to be constant and the average value of 353 m²/g can be used for further analysis.

Matsumoto et al. [Matsumoto2009] measured the surface area (N₂-BET) of a biomass

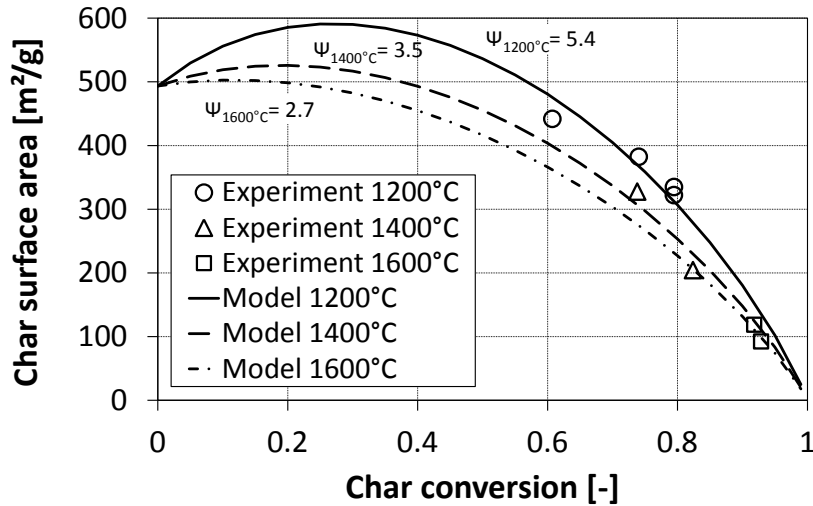


Figure 7.9: Model prediction of specific surface area of lignite R char compared with measurements of the char surface area (DFT, CO₂ at 273 K) at different levels of conversion, different temperatures, and a gasification pressure of 0.5 MPa.

char at different stages of conversion in a PDTF. There was no significant difference of surface evolution in CO₂ and H₂O which is also assumed for this model evaluation.

7.1.3 Validation of the Thermal Deactivation Submodels

Two thermal annealing submodels are proposed in Section 4.2.5. The evaluation of the annealing submodels is based on the standard reactivity data from the ATGA measurements (see Section 5.4.4) and the surface area measurements (see Section 5.4.1.5). From both, intrinsic standard reactivity can be calculated. In the simple model only the influence of maximum temperature on the deactivation of char is predicted. The annealing factor A is defined in Equation 4.71 as

$$A = \exp \left[\omega \cdot \left(1 - \frac{T}{T_{max}} \right) \right] \quad (7.17)$$

where ω is the only adjustable parameter and T_{max} is the highest experimental temperature where a strongly deactivated char is produced.

A equals the ratio of the pre-exponential factors of a fresh and a deactivated char in the intrinsic model. It is assumed that this reactivity ratio is equal at high (entrained flow conditions) and at low (TGA conditions) temperature, and that it can be described by the ratio of intrinsic standard reactivity in the ATGA experiments

$$A = \frac{r_{Stand,T}/S_T}{r_{Stand,T_{max}}/S_{T_{max}}} \quad (7.18)$$

where S_T and $S_{T_{max}}$ are the specific surface areas of the chars that are produced at T and T_{max} , respectively.

The standard reactivity data and the specific surface areas of chars of lignite R, lignite V, and bituminous coal A are available. For lignite R and bituminous coal A the PWMR char (1000 K/s, 700°C, 0.5 MPa, 10 s) and the PiTER chars are used to determine ω . Specific

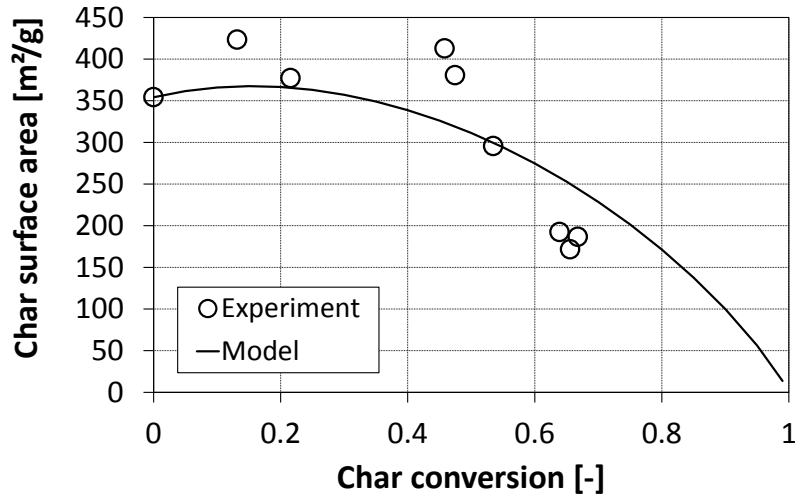


Figure 7.10: Model prediction of specific surface area of bituminous coal A char compared with measurements of char surface area (DFT, CO₂ at 273 K) at different levels of conversion, 0.5 MPa and 1.0 MPa pressure, and in the temperature range 1200°C to 1500°C

surface area of the PWMR chars is not measured due to the low sample mass. The value of surface area is taken from the surface area model. The uncertainty of the assumption is low as the range of surface area after pyrolysis is low. For lignite V only PiTER chars are available. The parameter ω is determined by a least squares fitting method using the experimental data. ω for the different fuels and the corresponding maximum temperatures T_{max} are summarised in Table 7.5. The experimental data and model predictions are shown in Figure 7.11.

In the more comprehensive annealing model, the char deactivation is dependent on re-

Table 7.5: Annealing parameter ω and T_{max} in the simple thermal annealing submodel for different fuels

Fuel	T_{max} [K]	ω
Lignite R	1873	6.3
Lignite V	1673	11.4
Bituminous coal A	1773	6.8

action time and temperature. The mathematical formulation of the model is given in Equation 4.77 and the model parameters are A_{max} , F_0 , and $E_{A,F}$. A_{max} is the ratio of initial intrinsic char reactivity to reactivity of completely deactivated char. This ratio is described by the intrinsic standard reactivity of PWMR char (1000 K/s, 700°C, 0.5 MPa, 10 s) and the 1600°C PiTER char. Although chars are available for lignite R, lignite V and bituminous coal A, the quantity of the data is only sufficient for lignite R and the comprehensive annealing model is applied for this fuel.

A_{max} of lignite R char is measured to be 23. The pre-exponential factor F_0 is 21000 s⁻¹, and the activation energy $E_{A,F}$ is 117 kJ/mol. Both are derived by a least squares fitting method using standard reactivity data of PiTER pyrolysis chars. The experimental data and the model predictions for the deactivation of lignite R char are shown in Figure 7.12. The model approaches always an annealing factor of 1 at high temperatures and residence times, i.e. the intrinsic char reactivity is equal to the reactivity of the most deactivated

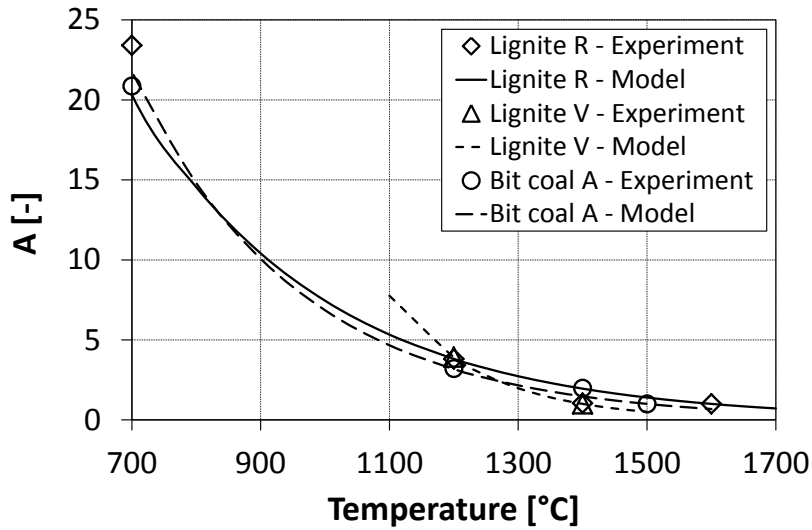


Figure 7.11: Predictions of the simple thermal annealing submodel compared with intrinsic standard reactivity data

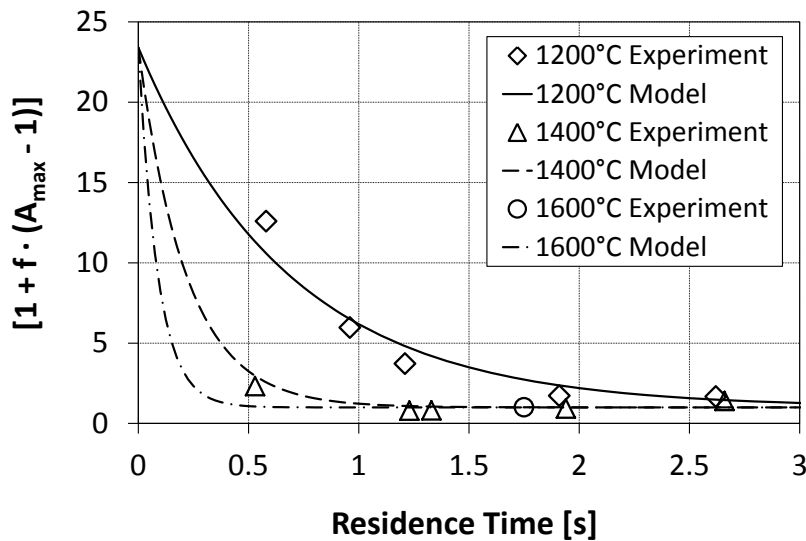


Figure 7.12: Comprehensive thermal annealing model of lignite R char in comparison to experimental data of intrinsic standard reactivity of PiTER pyrolysis chars

char from the experimental data. If the model is used to predict the char reactivity at temperatures above the experimental temperature range, the true char reactivity might be lower since a further deactivation could occur. The model overestimates char reactivity at temperatures above the experimental range. However, at high temperature the deactivation is only weakly dependent on temperature as shown in Figure 7.11. When the experimental temperature range is overstepped the error is low, but experiments should aim at the highest possible temperature.

7.2 Validation of the Model Framework by Using Entrained Flow Data

Char conversion experiments separated from devolatilisation are only carried out in the thermogravimetric analysis because all entrained flow experiments are carried out using fuel (coal or biomass). Therefore, the devolatilisation occurs as the first reaction step followed by progressing char conversion. The mathematical description of the fuel conversion requires the combination of a pyrolysis model and a char conversion model. In the following evaluation of entrained flow data, the volatile yield and the devolatilisation kinetics are based on the pyrolysis model described in Chapter 6, i.e. a simple single first order reaction rate model.

Due to the combination of several submodels and the implementation of process parameters that are not constant during conversion (e.g. gas concentrations), numerical methods are used to combine the submodels and to calculate fuel conversion.

The PiTER (total length of the reaction tube 2265 mm) is assumed to be a one-dimensional plug flow reactor, and it is divided into cells in gas flow direction. For each cell, the reaction rates are calculated based on process parameters. The progress in fuel conversion is calculated using the gas flow and the conversion rate in each cell. At the cell outlet the main gas concentrations (H_2 , CO , H_2O , CO_2 , N_2 , and O_2) are calculated assuming chemical equilibrium³. This gas composition is an input parameter for the next cell. If the amount of gas increases due to the gasification reactions, this is considered for the calculation of the gas flow rate and residence time in the next cell. The temperature in each cell can be varied. As all experiments are carried out with a constant temperature of the reaction tube, a constant gas temperature of all cells is assumed. An energy balance is not applied because the reaction enthalpy of the gasification process is negligible compared with the heat capacity and thermal power of the electrically heated reaction tube.

The fuel conversion is subsequently divided into three processes that occur consecutively within the reaction tube:

Gas and Particle Mixing In the first cell gas and fuel particles are mixed. As the average temperature of the main reaction and fuel carrier gas is far above the vaporisation temperature of water, the fuel moisture is assumed to be in the vapour phase. Gas concentrations are calculated from the inlet gas concentrations and from the fuel moisture content. The particle temperature at the inlet to the reaction tube is assumed to be 200°C as water is then in the vapour phase even at higher pressure.

Devolatilisation and Char Combustion The devolatilisation process is modelled in 6 cells that are equal in length. The total length of the devolatilisation zone is dependent on operation conditions (e.g. gas flow rate, temperature) and can be adjusted. The total length is 150 mm to 400 mm, and the length of one cell 25 mm to 65 mm. The heating rate

³The calculation of chemical equilibrium is based on a mass balance and on the equilibrium position of the water gas shift reaction. Only the main gas components H_2 , CO , H_2O , CO_2 , N_2 , and O_2 are considered. The occurrence of methane and hydrocarbons at lower temperature and at very short residence time is neglected. The detailed procedure is described in Appendix C

of the fuel particles is assumed to be $5 \cdot 10^4$ K/s. In each cell the devolatilisation kinetics of the pyrolysis model are applied and the total volatile yield after each cell is calculated. The elemental composition of volatiles is based on the ultimate analysis (carbon, hydrogen, nitrogen, and oxygen content) of the fuel. Sulphur, chlorine and other minor components are not considered.

In the last cell, the equilibrium composition of the volatiles is calculated. It is assumed that the total amounts of hydrogen, nitrogen and oxygen are part of the volatile matter. The amount of volatile carbon is calculated by a total volatile mass balance. Char produced during devolatilisation consists of remaining solid carbon and mineral matter. Furthermore, in the last cell gaseous volatiles are burned with oxygen. After a stoichiometric combustion, some oxygen might still be present in the gas phase for low volatile fuels. In this case, char is partially burned. As the subsequent char gasification reactions are much slower, a model for the combustion rates of volatiles and char is not implemented. At the outlet of the last devolatilisation cell, a rapid achievement of chemical equilibrium in the gas phase is assumed.

The discretisation of the devolatilisation zone is varied, ranging from 1 cell to 10 cells. To avoid the release of volatiles in discontinuous steps even at very short residence times a minimum number of cells is required. A medium number of 6 cell leads to good results.

Char Gasification The focus of the model development is on the heterogeneous char reactions. After the devolatilisation, char conversion occurs in the remaining length of the reaction tube. The remaining length is divided into cells of equal size. In each cell char conversion rate can be calculated using the instantaneous process parameters (e.g. temperature, gas concentrations, pressure), char properties (e.g. surface reactivity, density, particle diameter), and chemical/physical properties (e.g. diffusivity). The influence of the cell size on the results is evaluated in a model calculation that includes an nth order rate equation for CO_2 and H_2O gasification. Submodels for specific surface area evolution, thermal char deactivation, and pore diffusion are used and fuel conversion and gas concentrations are calculated for different discretisations. The results of the subdivision of the char gasification zone into 10 to 40 cells are shown in Figure 7.13.

There are small deviations between the different cell numbers. An increase in cell number from 10 to 20 results in a decrease in char conversion of 2 percent points. Also, there is a small difference in the gas concentrations (CO_2 is shown as an example). The larger the first cell is, the higher the residence time and conversion time within this cell. As it is a numerical stepwise calculation and the reaction rate is calculated from the inlet conditions of this cell, a progressing thermal deactivation and a progressing conversion are not considered within this cell. The deviations result from an overestimation of the char conversion rate in the first cells where the char reactivity is high. With increasing cell number these discretisation effects diminish. The difference in char conversion between 30 and 40 cells is less than 0.2 percent points. In the following evaluations the char gasification zone of the reaction tube is divided into 40 cells. The cell length is 55 mm to 60 mm depending on the total devolatilisation length.

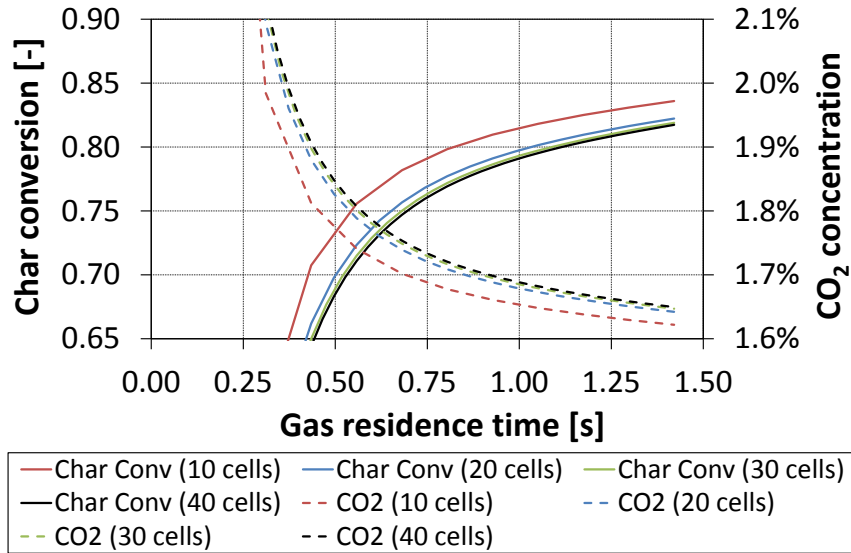


Figure 7.13: Influence of cell number on char conversion and gas concentration in the numerical model of the PiTER

7.2.1 Validation of the Simple Empirical Char Gasification Model

With no information from the laboratory and bench-scale analysis, the simple char conversion model described in Section 4.2.2 is applied. The high temperature entrained flow data are compared with Equation 4.27:

$$r_{obs} = r(T) = k_{0,obs} \cdot \exp \left[\frac{-E_{A,obs}}{RT} \right]$$

and the adjustable parameters $k_{0,obs}$ and $E_{A,obs}$ are derived. The parameters of the pyrolysis model that are derived in Chapter 6 for different fuels and that are applied in the numerical simulation are summarised in Table 7.6.

As the pyrolysis rate is temperature dependent, the reactor length required to achieve the volatile yield is larger at lower temperature. The pyrolysis length is adjusted in each simulation to achieve a smooth transition of the overall conversion from the pyrolysis to the char conversion region. The pyrolysis length ranges from 0.15 m to 0.4 m which corresponds to a residence time interval of 120 ms to 250 ms. Compared with the residence time for char conversion in the range 1.4 s to 2 s, a possible error in the assumption of the pyrolysis length is small.

The experimental data of char and overall conversion are compared with the model predictions for different fuels. The adjustable parameters $k_{0,obs}$ and $E_{A,obs}$ are derived by a least squares fitting procedure. In the following, the model simulations are compared with experimental data for different fuels. Experimental data of overall fuel conversion can be directly derived from the entrained flow experiments. Char conversion is calculated from the overall conversion in a gasification experiment and the conversion during devolatilisation in a pyrolysis experiment at comparable operation parameters (see Equation 5.9).

Table 7.6: Summary of pyrolysis parameters used in the entrained flow gasification simulations of the PiTER

Fuel	Lignite R	Bituminous coal A	Lignite V	Biocoal
Particle heating rate [K/s]	$5 \cdot 10^4$	$5 \cdot 10^4$	$5 \cdot 10^4$	$1 \cdot 10^{5a}$
p_{set} [MPa]	0.5	0.5	0.5	0.5
T_{set} [°C]	1000	1000	1000	1000
$Y_{V,pset,Tset}$ [-]	0.564	0.48	0.559	0.746
$Y_{V,pset,Tmax}$ [-]	0.687	0.55^b	0.655	0.746^c
ϑ [-]	0.0066	0.01^d	0.0141	0.01^e
ρ [-]	141	63.8	207.6	41.1
A_V [s ⁻¹]	293^f	293	293	586^g
$E_{A,V}$ [kJ/mol]	51	51	51	51

^aHigher heating rate due to the burner like injection in the experiments

^bAssumption: volatile yield is increased by a factor of 1.15 at high temperature

^cA further increase in volatile yield is not assumed

^dAssumption

^eAssumption

^fAssumption: All fuels have identical devolatilisation kinetics

^gThe devolatilisation rate is increased due to the burner like injection and the higher expected heating rate

Lignite R The results of the simulations compared with experimental data for the gasification of lignite R at a pressure of 0.5 MPa and different temperatures are shown in Figure 7.14. The experimental data at 0.1 MPa are shown for comparison.

The adjustable parameters are $E_{A,obs} = 64$ kJ/mol and $k_{0,obs} = 351$ s⁻¹. The low value of the observed activation energy indicates the occurrence of mass transport limitations. However, both parameters have no mechanistic meaning. At higher temperatures the simulation overestimates the experimental conversion data. The design of a gasifier based on the simulation would underestimate the residence time that is required for complete conversion. The predicted particle residence time to achieve 99.5 % fuel conversion at 1600°C is 0.77 s which is very short compared with the experimental data.

If the model is extended with the simple form of the thermal deactivation submodel (mass specific $\omega = 7.8$), a slightly better fit to the experimental data is achieved. Then, the model parameters are $E_{A,obs} = 148$ kJ/mol and $k_{0,obs} = 60100$ s⁻¹. The particle residence time to achieve 99.5 % fuel conversion at 1600°C is then extended to 0.93 s. But this value is still very low in comparison to the experimental data. It is expected that the further implementation of submodels would improve the simulations.

Bituminous Coal A The quality of the entrained flow data is low due to soot formation. As the calculation of char and overall conversion is based on the carbon and ash content of the char samples, soot formation strongly influences the conversion data. In spite of the large uncertainty, the PiTER data set is used to develop a kinetic model that predicts entrained flow gasification of bituminous coal A. Equation 4.27 is fitted to the experimental data (overall conversion) at 0.5 MPa, and the activation energy $E_{A,obs} = 129$ kJ/mol and the pre-exponential factor $k_{0,obs} = 5860$ s⁻¹ are derived. In the bench-scale analysis two

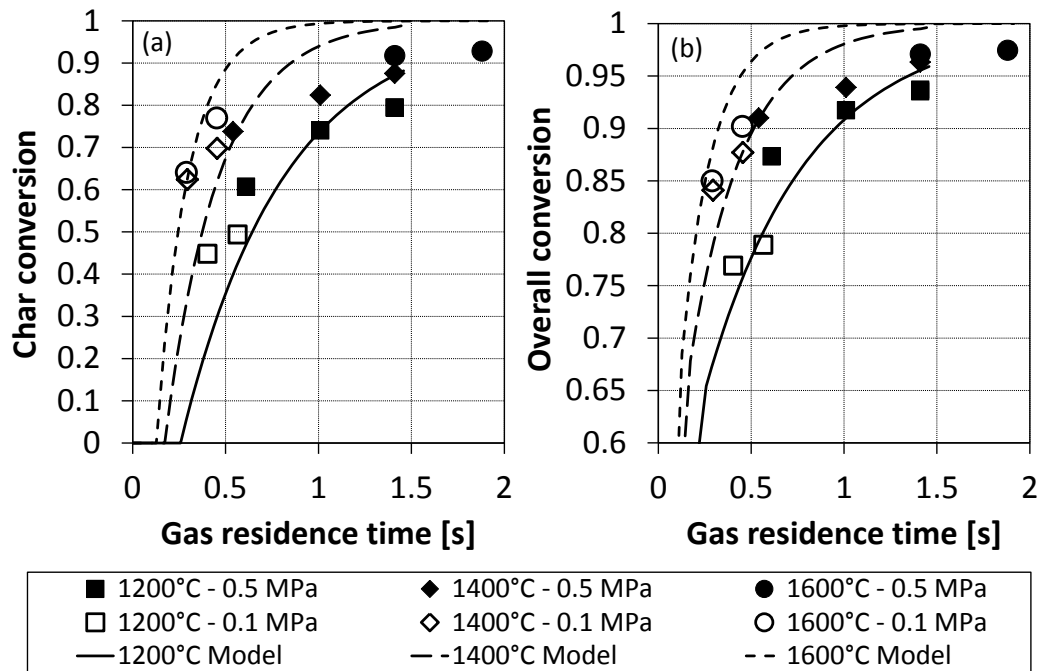


Figure 7.14: Simple Arrhenius type model simulation of PiTER and BabiTER entrained flow gasification compared with experimental data (lignite R): (a) char conversion; (b) overall conversion (experimental data as a function of particle residence time are shown in Figure 5.27)

submodels are derived for bituminous coal A: the surface area submodel and the simple type of the thermal annealing submodel. The implementation of both submodels improves the correlation between simulation and experimental data. The sum of the least squares of the char conversion data is reduced from $3.43 \cdot 10^{-2}$ to $2.89 \cdot 10^{-2}$. The activation energy changes to $E_{A,obs} = 243$ kJ/mol and the new pre-exponential factor is $k_{0,obs} = 4.41 \cdot 10^4$ s⁻¹. The simulation of the overall conversion at 0.5 MPa compared with experimental data is shown in Figure 7.15.

The simulation overestimates volatile yield as the measurement points of overall conversion at 1200°C are lower than the overall conversion predicted by the model after a residence time of about 0.25 s. The overall conversion after devolatilisation in the model is the sum of volatile yield (including volatiles combustion) and char combustion. At the given stoichiometry a reduction of pyrolysis yield would increase the amount of char that is burned, but would not change the conversion after devolatilisation. Therefore, the model predicts a reasonable value for fuel conversion after devolatilisation, but the experimental data is influenced by soot formation and therefore the experimental conversion level is too low. The simple model enables the simulation of entrained flow gasification of bituminous coal A. However, the large uncertainty has to be considered.

Lignite V Entrained flow data of lignite V gasification are available at atmospheric pressure. As the devolatilisation in the BabiTER occurs partially in the feeding tube, this is considered in the experimental data⁴. The Arrhenius type model in Equation 4.27 is fitted to the experimental data (overall conversion), and the activation energy $E_{A,obs} =$

⁴The residence time in the feeding tube at high temperature is approximately 60 ms that is added to the gas residence time in the reaction tube

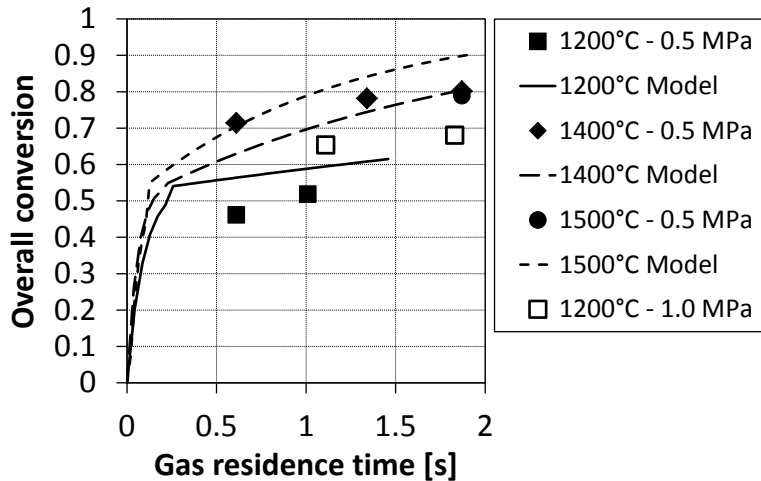


Figure 7.15: Simple Arrhenius type model simulation of PiTER entrained flow gasification compared with experimental data (bituminous coal A; integration of thermal annealing and surface area submodels; experimental data as a function of particle residence time are shown in Figure 5.29)

66 kJ/mol and the pre-exponential factor $k_{0,obs} = 510 \text{ s}^{-1}$ are derived. Both values are similar to the lignite R parameters derived for the simple model. The implementation of the simple thermal annealing model⁵ ($\omega = 11.4$ on a mass basis) of lignite V char does not change the deviation between model and experimental data, but significantly changes the model parameters ($E_{A,obs} = 207 \text{ kJ/mol}$, $k_{0,obs} = 1.27 \cdot 10^7 \text{ s}^{-1}$). The decrease in char reactivity at higher temperatures is balanced by the increase in activation energy. The model predictions and the experimental data of lignite V gasification at atmospheric pressure are shown in Figure 7.16. Further submodels are not available for the lignite V.

As only data are available up to 1400°C, the effects of a further increase in temperature can only be derived from the model. Without the implementation of the annealing submodel the residence time that is required to achieve an overall fuel conversion of 98 % at 1600°C is 0.66 s, but after the implementation it increases to 0.84 s. Therefore, the simple model predicts very high conversion rates at high temperature. The implementation of the thermal annealing model predicts lower conversion rates which is more consistent with experimental experience with the lignite R at higher temperature.

Biocoal Biocoal is gasified using the burner like injection system shown in Figure 5.10. Therefore, the input parameters for the model validation have to be slightly adjusted. Due to the high concentration of oxygen in the feeding tube, the temperature is rapidly increased by volatiles combustion. This will increase the heating rate and also the devolatilisation rate of the particles. A heating rate of $1 \cdot 10^5 \text{ K/s}$ and the doubling of the devolatilisation rate are assumed. As no entrained flow pyrolysis data are available, a temperature effect on volatile yield is not considered and volatile yield is constant 78.5 wt% (daf). The simple char conversion model (Equation 4.27) is fitted to the experimental data at 1200°C and 1400°C and a low activation energy of 20 kJ/mol and a pre-exponential factor of 10 s^{-1} are derived. The influence of temperature on the gasification rate is low which is also

⁵The quality of the char deactivation model of lignite V is rather low as only the standard reactivity of char samples produced at two temperatures could be measured.

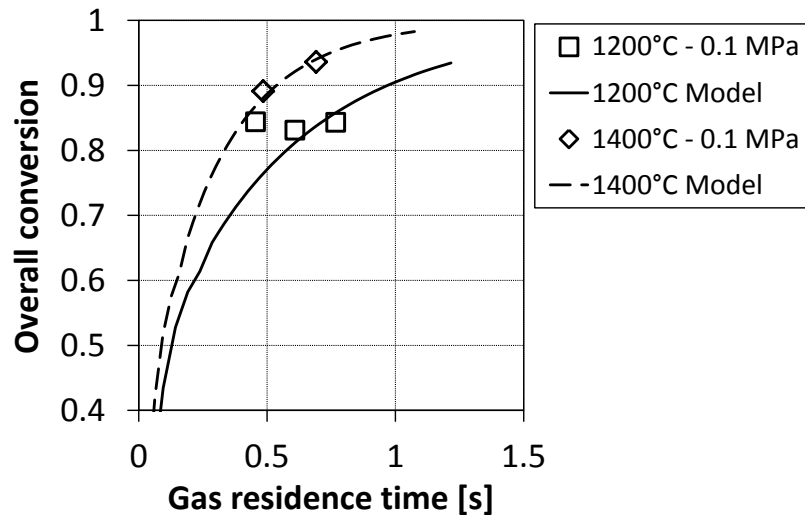


Figure 7.16: Simple Arrhenius type model simulation with integrated thermal annealing submodel of BabiTER entrained flow gasification compared with experimental data (lignite V; experimental data as a function of particle residence time are shown in Figure 5.28)

shown by the experimental data.

Anthracite Anthracite has a low proportion of volatiles and is expected to produce a char with a high density. Furthermore, no weight loss is observed in the ATGA experiments at 400°C. Both observations indicate that the conversion rate in entrained flow reactors will be low. In entrained flow experiments the conversion of anthracite is significantly lower than of the other fuels. As oxygen is still measured in some gasification experiments at high temperature and low residence time (BabiTER, 1600°C), the char combustion rate is also very low. The model that is described here uses an infinite rate for the char-oxygen reaction. Hence, a progressing combustion with residence time cannot be simulated. Therefore, the simple char gasification model is not used to describe the gasification of anthracite.

The kinetic parameters in the simple char gasification model are derived for four fuels ranging from biocoal to bituminous coal. The reaction rate parameters are summarised in Table 7.7. As the parameters are calculated from experimental data in the temperature range 1200°C to 1600°C, the model cannot simply be extrapolated to higher or lower temperatures.

Table 7.7: Kinetic parameters of the simple char gasification model for different fuels

Fuel	Lignite R	Lignite V	Bituminous coal A	Biocoal
$k_{0,obs}$ [s^{-1}]	351	510	5860	10
$E_{A,obs}$ [kJ/mol]	64	66	129	20

During the validation thermal annealing and surface area submodels for different fuels were integrated that improve the predictive quality of the entrained flow gasification model. The few examples showed the advantage of the implementation of submodels that are derived

on a mechanistic basis. In the next section all submodels are combined to validate the comprehensive model framework.

7.2.2 Validation of the Comprehensive Model Framework for the Simulation of Entrained Flow Gasification

In order to improve the model predictions for high temperature gasification processes, different submodels are developed based on experimental data mainly from bench-scale analysis and theoretical derivations. The implementation of single submodels and the effects on the predictability of the simple model have already been discussed. Generally, the extension of the simple model (Equation 4.27) with one or more submodels decreases the deviation between simulation and experimental data and enhances the predictive quality. A combination of all submodels is expected to predict fuel behaviour under entrained flow conditions without any empirical adjustments of the simulation. The different submodels are:

- Pyrolysis submodel to simulate the volatile yield as a function of pressure, temperature, and particle residence time
- Intrinsic reactivity submodel to describe intrinsic reaction rate of the char-CO₂ and char-H₂O reaction dependent on gas partial pressures and temperature
- Surface area submodel to predict the development of specific surface area after devolatilisation and during char conversion as a function of pressure, temperature, and conversion
- Thermal annealing submodel to implement the deactivation of the char surface with increasing heat treatment severity
- Particle size and density submodel to describe the variation of particle size and char apparent density with conversion
- Pore diffusion submodel to implement the limitation of the reaction rate by mass transport limitations within the char structure
- Boundary layer diffusion submodel to predict the maximum reaction rate due to mass transport limitations within the boundary layer of the char particles

The submodels are combined in the numerical simulation to calculate fuel conversion in the PiTER. As all parameters in the submodels are available for the lignite R, the simulation is based on this fuel. The parameters used in the models are summarised in Table 7.8. The parameters of the submodels are derived from the bench-scale analysis of chars or from calculations based on literature data. No adjustment is made to conversion data measured in the entrained flow reactors. Figure 7.17 compares the model predictions with char and overall conversion measured in the PiTER at 0.5 MPa and in the BabiTER at atmospheric pressure. The simulation is run for boundary conditions used in the PiTER experiments (e.g. reaction length 2.265 m, gas flow rates according to the experimental setpoints, pressure 0.5 MPa, stoichiometry O/C = 1). It is expected that the conversion at atmospheric pressure (BabiTER) does not differ much. Therefore, the BabiTER data

Table 7.8: Summary of model parameters of lignite R used in the different submodels and their origin

Parameter	Value	Origin
Pyrolysis parameters	see Table 7.6	PWMR, BabiTER, PiTER
Intrinsic reactivity		
n_{CO_2}	0.41	PRETA (PiTER chars)
E_{AL1,CO_2}	200 kJ/mol	PRETA (PiTER chars)
k_{OL1,CO_2}	$7516 \left[\frac{g}{m^2 \cdot s \cdot MPa^{n_{CO_2}}} \right]$	PRETA (PiTER chars)
n_{H_2O}	0.41	equal to n_{CO_2}
E_{AL1,H_2O}	212 kJ/mol	PRETA (PiTER chars)
k_{OL1,H_2O}	$1.45 \cdot 10^5 \left[\frac{g}{m^2 \cdot s \cdot MPa^{n_{H_2O}}} \right]$	PRETA (PiTER chars)
Surface area		
S_{ini}	$(475+37 \cdot p_{total} [MPa]) \text{ m}^2/\text{g}$	PiTER data
$\Psi_{1200^\circ C}$	5.4	PiTER data
$\Psi_{1400^\circ C}$	3.5	PiTER data
$\Psi_{1600^\circ C}$	2.7	PiTER data
Char deactivation		
A_{max}	23.4	ATGA (PiTER/PWMR chars)
F_0	21000 s^{-1}	ATGA (PiTER/PWMR chars)
$E_{A,F}$	117.2 kJ/mol	ATGA (PiTER/PWMR chars)
Particle size and density		
Swelling index	1	PSD (PiTER char)
α	0.95	[Liu2004b]
Fuel particle diameter	50 μm	d_{mean} pyrolysis char
Initial char density	1.04 g/cm ³	measurement (Table 5.7)
Pore diffusion		
Molecular diffusivity	binary coefficients	[Baerns2002]
ϵ	0.54	from char density (Table 5.7)
τ	3	[Baerns2002]
Pore diameter	1 nm	assumption (micropore range)

are also shown in the diagram. As shown in Figure 7.17, the simulation underestimates char and overall conversion.

Due to the relatively low reactant gas concentrations in the PiTER, the reaction rate even at 1600°C is relatively slow and mass transport limitations in the boundary layer do not occur⁶.

The reaction rate in the simulation is limited by pore diffusion as the effectiveness factor is calculated to be 0.22 to 0.52 (char-CO₂ reaction) and 0.12 to 0.29 (char-H₂O reaction), both at the lowest temperature of 1200°C. The effective diffusion coefficient is calculated from char porosity, tortuosity, molecular, and Knudsen diffusivity and has an important influence on the limitation by pore diffusion. Figure 7.18 shows molecular, Knudsen,

⁶As the reaction rate is far from the maximum boundary diffusion rate, the film diffusion model is not important and a limitation by film diffusion is not considered in the data evaluation.

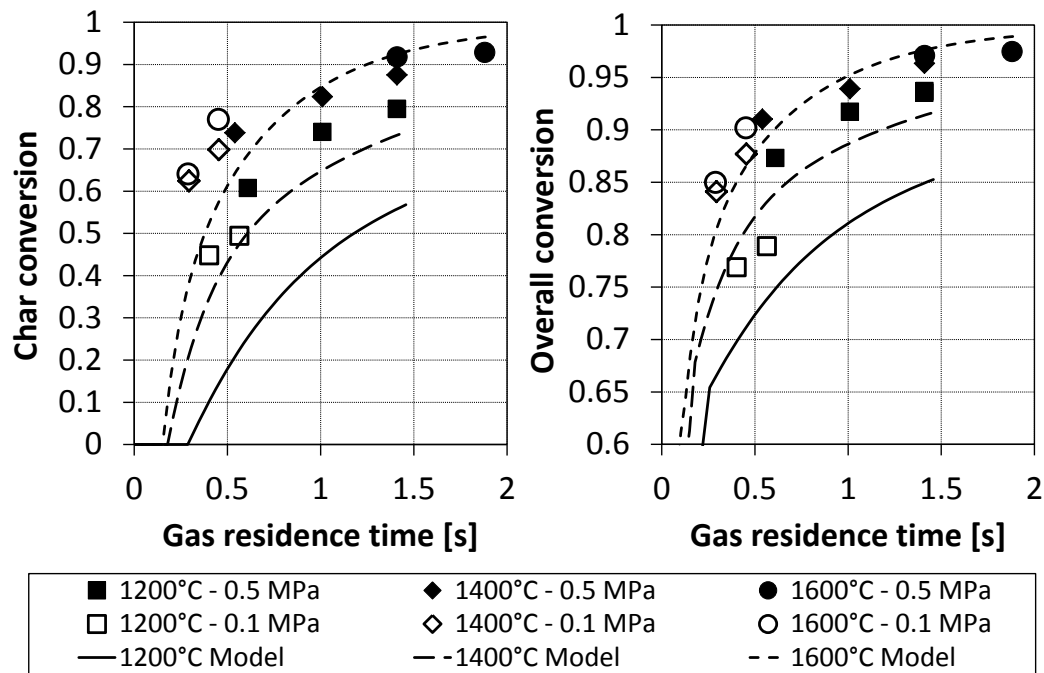


Figure 7.17: Prediction of the combined submodel simulation of lignite R gasification compared with experimental entrained flow data (PiTER and BabiTER; experimental data shown in Figure 5.27)(average pore diameter 10 Å)

and effective diffusivity as a function of the pore diameter at temperatures of 1200°C and 1600°C. In porous structures with a small pore diameter, the effective diffusivity is determined by Knudsen diffusion. With increasing pore diameter the importance of molecular diffusion grows, and at pore diameters above 150 nm the molecular diffusion dominates the mass transport within the porous structure. Compared to pore size, the temperature has only a minor influence on diffusion, especially for small pore diameters. At a larger pore size, the effective diffusivity increases and mass transport limitations within the char structure are reduced. In the pore diffusion submodel a pore diameter of 1 nm (10 Å) is implemented as the gasification reactions occur mainly within the micropores [Feng2003b]. However, during char conversion, the reaction will also occur in the mesopores and the average pore size will be shifted to larger diameters. The contribution of larger pores to the total pore volume depends on carbon type [Jagiello2004] and conversion [Feng2003b]. A certain part of the pore volume can be in the range of 10 Å to 50 Å [Feng2003b] or even in pores with diameters up to 350 Å [Jagiello2004]. As the pore size distribution of the lignite R char is not known, the pore diameter in the simulation is used as an adjustable parameter to minimise the deviation between the experimental data and the model prediction. This procedure leads to an average pore diameter of 47.3 Å which is in the expected range. The comparison of simulation and experimental data after the pore size adjustment is shown in Figure 7.19. The deviation between simulation and experimental data is small and the fuel conversion can be predicted by the numerical calculation based on different submodels. As the simulation predicts the complete gasification process and considers changes in the gas phase as well as particle properties, further simulation results can be compared with experimental data. Figure 7.20(a) compares the model predictions of the CO₂ concentration in the PiTER reaction

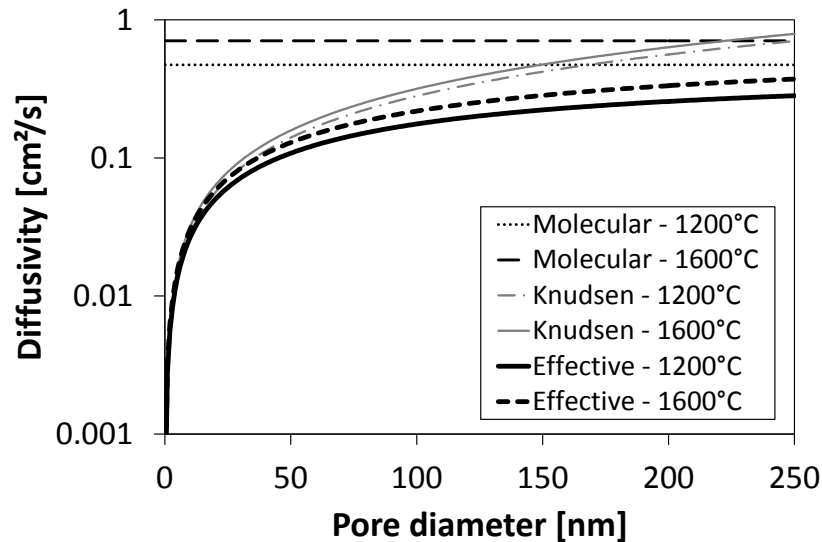


Figure 7.18: Influence of pore diameter, temperature, and of molecular and Knudsen diffusivity on the effective diffusivity in an ideal porous structure ($\epsilon = 1$, $\tau = 1$)

tube to gas measurements using the mass spectroscopy⁷. Despite the large uncertainty in the gas analysis there is a good correlation of the CO_2 quantity and there is a trend between simulation and measurement. Pyrolysis and volatiles combustion lead to a maximum in CO_2 concentration. In the subsequent heterogeneous reactions, CO_2 is consumed and the concentration continuously decreases. The evolution of specific surface area during char gasification is shown in Figure 7.20(b). The measurement uncertainty of the surface area (CO_2 -DFT) is low and there is a very good predictability of the simulation. The small increase in surface area that is observed in BabiTER experiments and also expected in the PiTER at shorter residence time is predicted by the simulation. At longer residence times (higher conversion) the surface area continuously decreases. The deviation of the 1600°C data is caused by the overestimation of char conversion in the simulation.

In conclusion, a good correlation of the model predictions with different experimental data is found. The combination of submodels describes the gasification behaviour of lignite R well under entrained flow operation conditions. A good predictability is also assumed for other fuels when the required experimental data are available.

⁷As the PiTER is operated with a lower gas flow rate at 1600°C compared to 1200°C and 1400°C, the CO_2 concentration after the volatiles combustion is considerably higher. The reactant gas concentrations in the PiTER experiments are usually low in integral experiments because the oxygen amount is adjusted to the stoichiometric requirements to convert the low fuel flow rate of 1.25 kg/h. Moreover, the nitrogen gas flow rate is high to achieve short residence times.

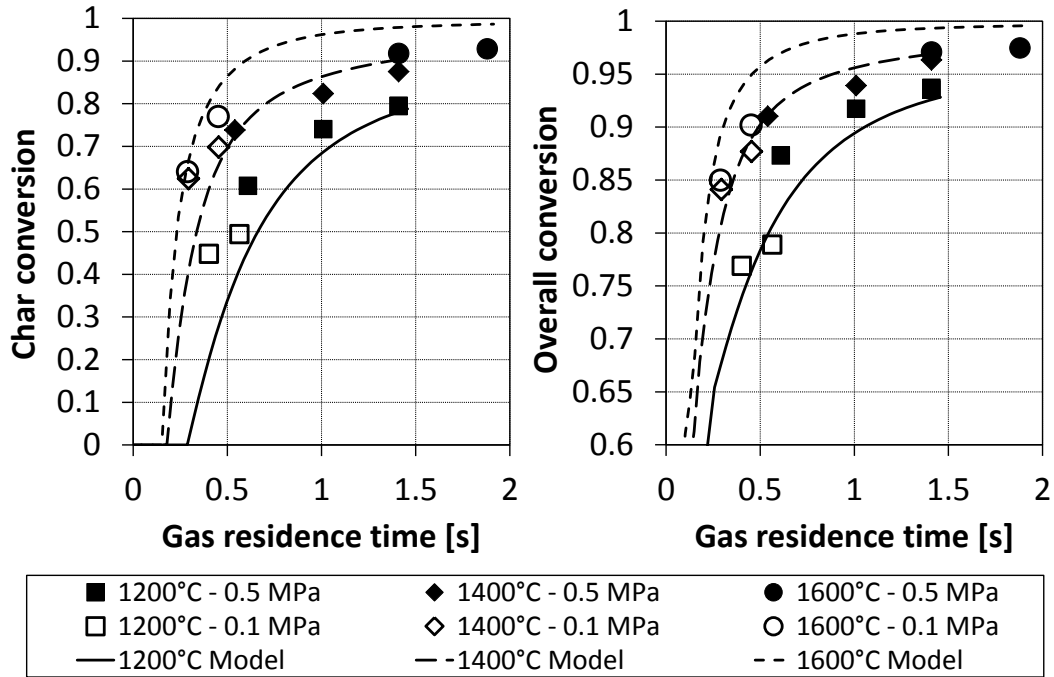


Figure 7.19: Prediction of the combined submodel simulation of lignite R gasification compared with experimental entrained flow data (PiTER and BabiTER; experimental data shown in Figure 5.27) after the adjustment of the average pore diameter (47.3 \AA)

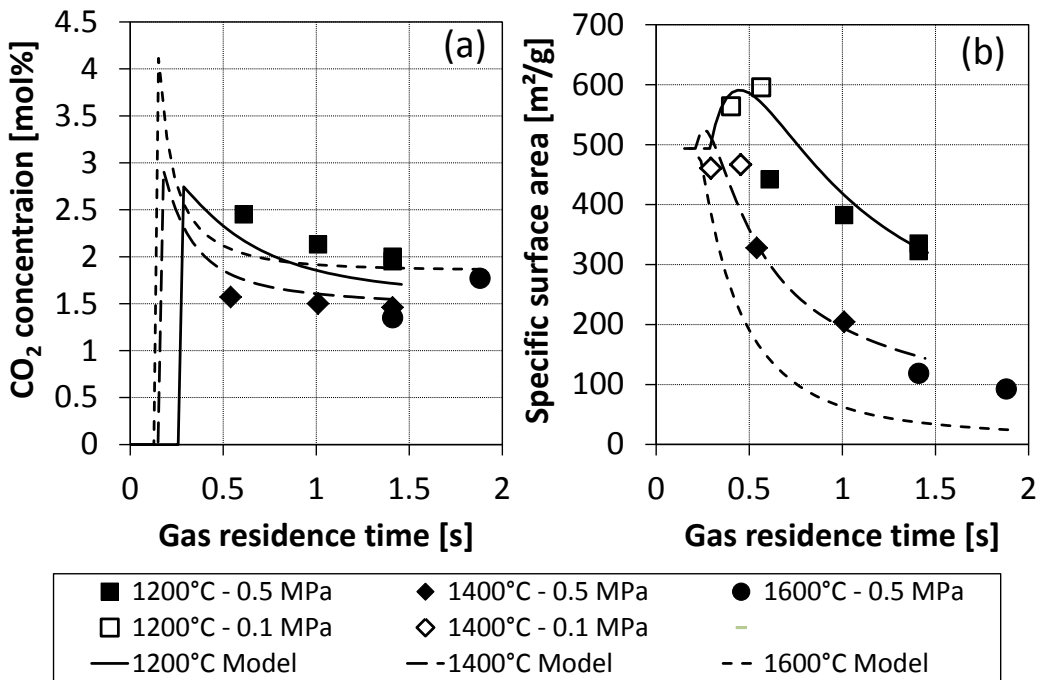


Figure 7.20: Simulation of lignite R gasification in the PiTER at 0.5 MPa compared with experimental data: (a) CO₂ concentration measured by mass spectroscopy; (b) Specific surface area (CO₂-DFT)

Chapter 8

Simulation of Industrial Scale Entrained Flow Gasifiers

This dissertation tries to improve the transferability of lab-scale and pilot-scale data to industrial entrained flow gasifiers. The experiments carried out in bench-scale setups like the PWMR, the ATGA, and the PRETA and in the entrained flow reactors BabiTER and PiTER show the fuel behaviour at high pressure and/or high temperatures. The experimental data are used to develop and validate submodels that describe pyrolysis and char gasification. As the combination of the submodels enables the prediction of the conversion rate in the PiTER, the application at a larger scale is the next step. The reaction rate submodels are integrated in a numerical simulation of an industrial scale entrained flow reactor.

8.1 Description of the Simulation Approach

8.1.1 Gasifier Geometry and Boundary Conditions

The industrial scale gasifier is simulated as a one dimensional plug flow reactor. The geometry is similar to the simulation of the PiTER in Section 7.2 and is shown in Figure 8.1. Fuel and a defined gas mixture (oxygen, fuel carrier gas, steam, CO_2) enters the reactor at the top. The inlet temperature is 90°C and steam is added at its saturation temperature. The reactor chamber is a cylinder with a defined diameter and a defined height. In the first cell the input streams are mixed and ignited. The temperature is increased according to a pre-defined heating rate. Devolatilisation occurs in five consecutive cells. The total length of the devolatilisation zone is variable and can be adjusted to the devolatilisation rates of the solid fuel. As the combustion reactions are very fast and combustion kinetics are not implemented, the combustion of volatiles and char is modelled as a one-step mechanism that occurs in cell 7. After this cell, a mixture of char and reaction gas is further converted in 40 cells. As the reaction rate is

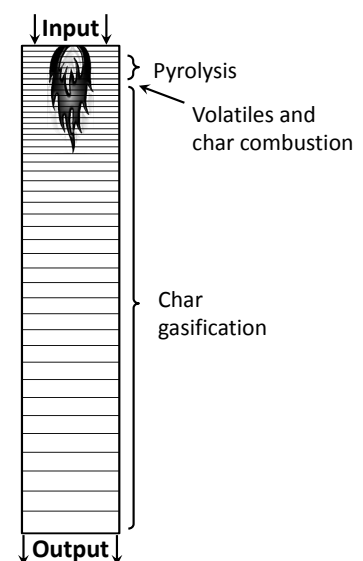


Figure 8.1: Geometry of the industrial scale one-dimensional entrained flow reactor

initially high and then decreases towards the gasifier outlet, the cell height is not constant. The height of the first 10 cells is 1/160 of the total gasifier height to enable a high resolution and to reduce the numerical error in the calculation. Then, the cell size continuously increases and the height of the last cell is 1/12 of the gasifier height.

Plug flow is assumed in each cell and the mass and energy balance of each cell is shown in Figure 8.2. The cell inlet flow rate and composition are identical to the outlet of the next upper cell. Mass transport across the outer cell walls does not occur, but heat transfer is implemented to account for thermal losses across the reactor wall (membrane type or refractory type) of an industrial gasifier.

8.1.2 Calculation of Reaction Rate, Temperature, and Gas Composition

The reaction rate in each cell is calculated using the submodels described in Section 7.2.2. In the devolatilisation zone, the single first order rate equation is implemented. The char gasification rates are calculated from the combination of the intrinsic reactivity, thermal deactivation, specific surface area evolution, and pore diffusion submodels. The concentration gradient in the boundary layer is calculated from the interaction of boundary layer diffusion and char reaction. At very high temperature, the concentrations of CO_2 and H_2O at the external char particle surface are significantly lower than in the bulk phase, and the reaction rate is additionally limited by film diffusion. In this case the reaction occurs in the transition zone between Regime II and III or completely under Regime III conditions. At lower temperatures, the bulk phase and surface concentrations are equal and the reaction rate is limited by pore diffusion and chemical reaction.

The temperature in each cell is calculated by a heat balance. The enthalpy of reaction in each cell and heat capacities of gas and solids are used to calculate the temperature. Values of the heat capacities of gases at reaction temperature are taken from the NIST database [NIST2011]. The heat capacity of char is approached by the heat capacity of graphite [Butland1973] and the heat capacity of ash is estimated to be $1000 \text{ J}/(\text{kg} \cdot \text{K})$. In the devolatilisation stage the heat capacities are taken at a temperature of 1500 K . Standard enthalpies of formation of H_2O , CO_2 and CO [Riedel2004] and the lower heating value of the solid fuel are used to calculate the reaction enthalpy. The enthalpy of vaporisation of water is $2256 \text{ kJ}/\text{kg}$ [Straub1994] and the ash melting enthalpy is assumed to be $1000 \text{ kJ}/\text{kg}$. The temperature is first increased by the exothermic volatiles and char combustion and then continuously decreases due to the endothermic char- $\text{H}_2\text{O}/\text{CO}_2$ reactions.

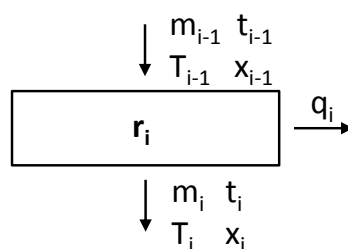


Figure 8.2: Mass and energy balance of each cell during the calculation of industrial scale gasifiers (m: mass, t: time, T: temperature, x: conversion, q: heat flux, r: reaction rate)

The gas composition after devolatilisation and volatiles combustion is approached by a complete conversion to the combustion products CO_2 and H_2O . The fuel nitrogen is converted to N_2 . If there is remaining oxygen in the gas phase, also char is partially converted to CO_2 . If the oxygen amount is too low to completely burn the volatiles, the volatiles are converted to a mixture of $\text{H}_2/\text{CO}/\text{CO}_2/\text{H}_2\text{O}$ assuming the chemical equilibrium. The procedure for the calculation of chemical equilibrium at the reaction temperature is described in the Appendix C. This procedure is also used to calculate the gas composition during the heterogeneous char gasification. In each cell, the amount of carbon in the gas phase is calculated from the char reaction kinetics. As the other main gas elements hydrogen, oxygen, and nitrogen are already in the gas phase after the devolatilisation, the local concentrations of H_2 , CO , CO_2 , H_2O , and N_2 can be calculated. Trace elements in the fuel (e.g. S, Cl) and also trace compounds in the gas phase (e.g. H_2S , NH_3 , COS) are not considered in the gasifier simulation.

8.1.3 Limitations of the Simulation

Due to the simplicity of the simulation, there are several limitations and inaccuracies:

- As the model is a one-dimensional plug flow reactor, back mixing effects and turbulence are not considered. The cells are assumed to be radially mixed and mass transport only occurs top down.
- The particles are assumed to be completely entrained in the gas flow. The particle residence time equals the gas residence time. The particle buoyancy and particle inertia are not considered.
- Pyrolysis, combustion and char gasification are assumed to be consecutive reactions. In reality these reactions occur partially in parallel.
- The assumption of chemical equilibrium in the gas phase at high temperature is a good approximation. However, only the main gas components are considered. The very high temperatures after the volatiles combustion enable further reactions like the formation of radicals and ions which would lower the enthalpy of reaction and also the maximum temperature.
- During char conversion, the fragmentation of particles is expected. For lack of experimental data, fragmentation is not considered in the simulation.
- The simulation focuses on the reaction of the organic fuel matter. Ash reactions are only considered by an ash melting enthalpy and a heat capacity. Chemical reactions of mineral compounds or the limitations of the gasifier operation by slag properties are not considered.

The limitations result in an overestimation of reaction temperature in the flame zone. Due to the absence of turbulence, the locally very limited release of the combustion heat in a single cell, and the non-consideration of high temperature gas reactions, the temperature in the combustion zone and in the first stages of char conversion is overestimated. As the reaction rates are temperature dependent, an over-prediction of fuel conversion is expected. However, the char conversion approaches Regime III conditions at the highest

temperatures and the temperature has only a minor influence on reaction rate. Therefore, the overestimation of temperature does not significantly increase the char conversion. This was proved by several test calculations. In the medium and later stages of conversion, a good predictability of temperature is expected.

8.2 Simulation of a 500 MW Entrained Flow Gasifier for the Conversion of Lignite R

The numerical model is used to obtain the basic geometry of a 500 MW entrained flow gasifier and to optimise its operation.

8.2.1 Design of the Lignite R Gasifier

The gasifier diameter and its length are the size parameters in the simulation. Both can be adapted to the thermal fuel input, to the operation pressure, and to the fuel properties. The design aims at the complete fuel conversion and a minimisation of the reactor size. Only if the fuel conversion is high, the gasifier has an optimum cold gas efficiency and the ash/slag is free from organic matter. The input parameters for the simulation are summarised in Table 8.1.

In order to analyse the influence of the gasifier design on its operation performance, first a base case is defined. Schingnitz and Mehlhose [Schingnitz2005] give basic geometries of the GSP entrained flow gasifier (2.5 MPa) for 150 MW, 500 MW, and 1000 MW thermal input. The height of the 500 MW gasifier is 5.25 m and its diameter is 2.9 m. Both dimensions are used for the base case simulation. The stoichiometry is defined by an O/C ratio of 0.95 which corresponds to an oxygen mass flow rate of 65.8 t/h (fuel feed rate 90.3 t/h). Heat losses along the gasifier wall are neglected.

The simulation yields a fuel conversion of 99.8 %, a cold gas efficiency of 78.4 %, and a gasifier outlet temperature of 1420°C. The ash melting temperature of lignite R is 1260°C to 1280°C¹. The outlet temperature is expected to enable a smooth drain of slag. Due to the absence of heat losses and the almost complete fuel conversion, the cold gas efficiency is very high. The conversion and temperature distribution along the gasifier are shown in Figure 8.3.

The temperature after the volatiles combustion reaches a maximum of 2430°C which might be slightly overestimated, but then decreases rapidly. The conversion occurs in the transition zone from Regime II to Regime III as the concentrations of CO₂ and H₂O at the outer char particle surface are significantly lower than the bulk phase concentrations. The initial effectiveness factors are 0.08 for the char-CO₂ reaction and 0.02 for the faster char-H₂O reaction. The gas concentrations and the effectiveness factor of the char-H₂O reaction are shown in Figure 8.4. Despite the mass transport limitations, the reaction rate is initially very high and most of the conversion occurs in the first metre of the gasifier length. The thermal annealing is very fast at the highest temperatures and the char is

¹The measurements slightly depends on ash preparation conditions in laboratory. Due to different slag formation conditions in a gasifier, the true melting temperature might deviate.

Table 8.1: Summary of input parameters for the simulation of an industrial scale entrained flow gasifier for the conversion of lignite R

Parameter	Value	Origin
Fuel		
Type	lignite R	composition see Table 5.2
LHV (dry basis)	22.7 MJ/kg	measurement (DIN 51900-1)
Moisture content	11 wt%	comparable to PiTER runs
Operation parameters		
Thermal Input	500 MW	assumption
Pressure	2.5 MPa	assumption
O/C ratio	0.95	assumption
Oxygen purity	0.99	[Higman2003]
Input temperature	90°C	assumption
Carrier gas (N ₂)	0.07 m _N ³ /kg(fuel)	conservative value [Higman2003] ^a
Devolatilisation		
Pyrolysis parameters	see Table 7.6	
Particle heating rate	5 · 10 ⁴ K/s	assumption
Pyrolysis time	50 ms	[Kobayashi1977]
Intrinsic reactivity		
Parameters	see Table 7.8	
Surface area		
S_{ini}	$(475+37 \cdot p_{total} [MPa]) \text{ m}^2/\text{g}$	PiTER data
Ψ	2.7	PiTER data at 1600°C
Char deactivation		
Parameters	see Table 7.8	
Particle size and density		
Swelling index	1	PSD (PiTER char)
α	0.5	Regime II [Monson1995]
Fuel particle diameter	100 μm	assumption
Initial char density	1.04 g/cm ³	measurement (Table 5.7)
Pore diffusion		
Molecular diffusivity	binary coefficients	[Baerns2002]
ϵ	0.54	char density (Table 5.7)
τ	3	[Baerns2002]
Pore diameter	4.7 nm	see Section 7.2.2

^aFuel particle loading during dense phase transport is 300-400 kg/actual m³.

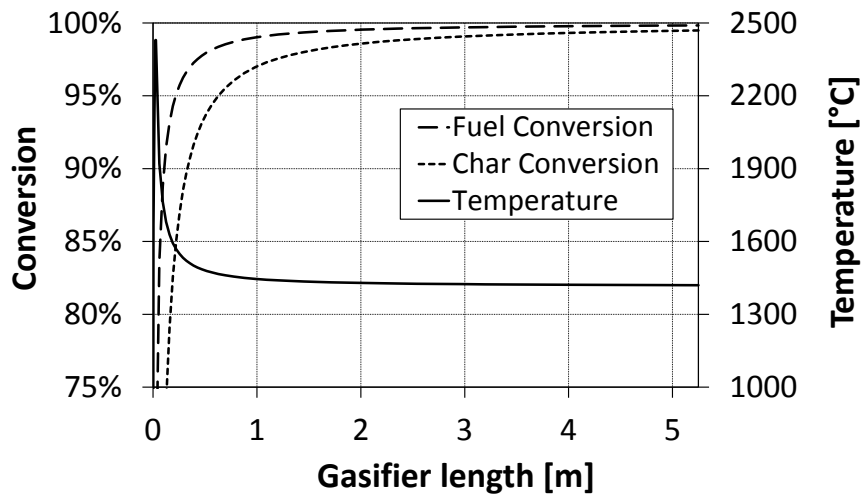


Figure 8.3: Conversion and temperature distribution along the gasifier length of the base case simulation of a 500 MW entrained flow gasifier (lignite R, gasifier length 5.25 m, diameter 2.9 m)

completely deactivated after about 0.5 s of the total residence time of 3.1 s. The thermal deactivation, the loss of surface area, and the continuously decreasing temperature with conversion cause the strong decline of reaction rate towards the gasifier outlet. The conversion almost remains constant after a gasifier length of 3 m. As the effectiveness factor rapidly increases, the char reaction approaches Regime I conditions in the later stages of conversion. Also char surface concentrations equal the bulk phase concentration after about 2 m of reaction length. The concentration of H_2 initially rapidly increases and then almost remains constant as no significant further char conversion occurs. For the char- CO_2 reaction a similar behaviour with reaction length is observed. The gas outlet concentrations are: 22.2 % H_2 , 50.9 % CO , 13.2 % H_2O , 9.1 % CO_2 , and 4.6 % N_2 . These are in the expected range for entrained flow gasification of lignite [Schingnitz2005b].

The geometry of the gasifier is designed for the conversion of several fuels ranging from hard coal and pet coke to sewage sludge [Schingnitz2005b]. The gasifier has to convert the fuel with the lowest reactivity in the given residence time. Therefore, the layout seems to be very conservative for a highly reactive fuel like lignite. As the lignite R conversion is almost completed shortly after the gasifier inlet, a reduction of gasifier diameter or length is possible. Both would decrease the residence time, and would also decrease investment costs for the gasifier layout. The ratio of length to diameter of an industrial scale gasifier is almost constant when the thermal input is changed [Schingnitz2005]. For the scaling of the gasifier dimensions a length to diameter ratio of 1.8 is assumed. In the simulation, the gasifier diameter is reduced and the length is adapted. The cold gas efficiency and the fuel conversion are shown in Figure 8.5.

A reduction of the gasifier size reduces the reaction time and therefore the fuel conversion. The cold gas efficiency is hardly influenced down to a gasifier diameter of 2.25 m (length 4.05 m, residence time 1.45 s). A further decrease in the diameter results in considerable losses due to incomplete conversion. As a lower amount of thermal energy is required for the endothermic char reaction if the conversion is incomplete, the gasifier outlet temperature increases when the diameter is decreased. If heat losses were implemented and these

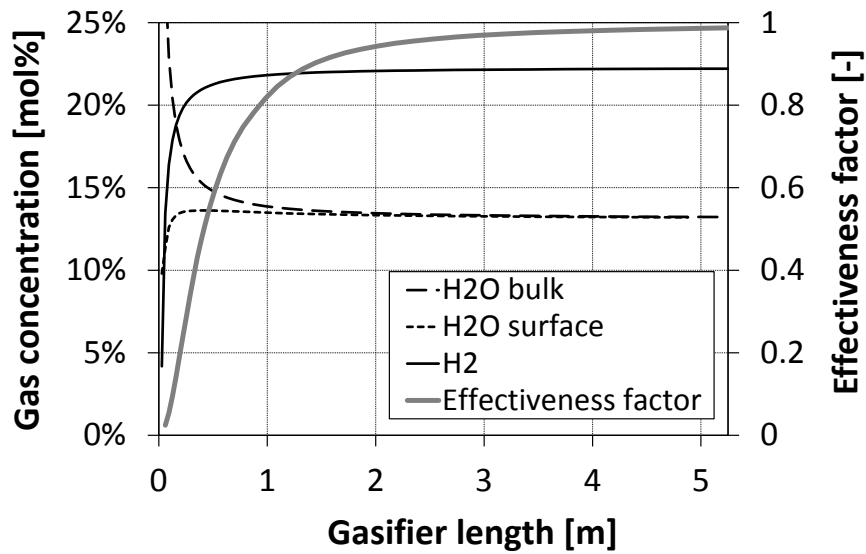


Figure 8.4: Gas concentrations and effectiveness factor for the char-H₂O reaction in the base case simulation of a 500 MW entrained flow gasifier (lignite R, gasifier length 5.25 m, diameter 2.9 m)

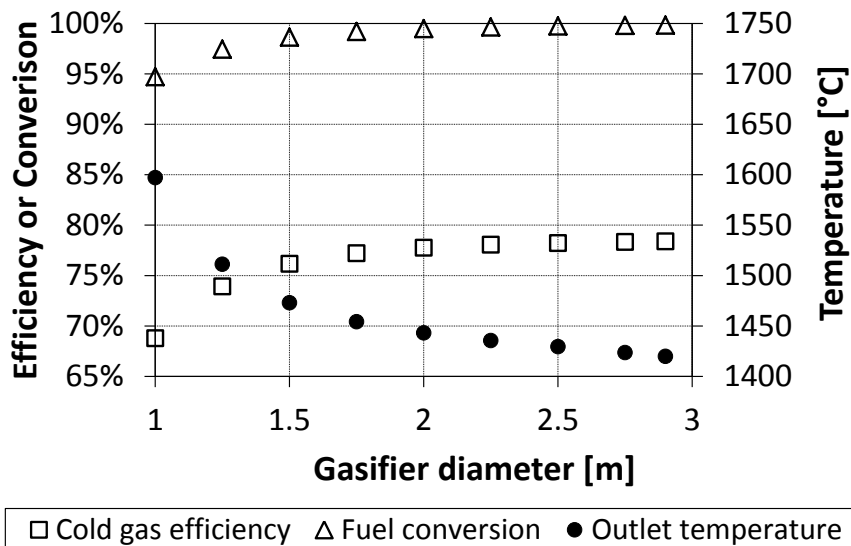


Figure 8.5: Influence of the gasifier geometry (diameter) on the operation performance (cold gas efficiency and fuel conversion) and outlet temperature of a 500 MW entrained flow gasifier (lignite R, gasifier length to diameter ratio 1.8)

were dependent on the gasifier outer surface area, the average gasification temperature would decrease for a larger gasifier size. The lower temperature would then lead to a lower conversion and the gasifier performance is expected to decrease with increasing gasifier size. Therefore, an optimum of cold gas efficiency might occur if heat losses are considered. As heat losses are dependent on a variety of parameters like gasifier type (membrane wall or refractory lined), slag layer thickness, thermal insulation, and gasification temperature, a calculation is not made.

As the gasifier layout is only defined by length and diameter, only a simple dimensioning is possible. The gasifier length of 4.05 m and a diameter of 2.25 m results in an acceptable fuel conversion of 99.6 %. In comparison to the base case size, the gasifier volume is significantly reduced leading to lower investment costs and in reality to lower heat losses. A more detailed dimensioning and a more complex layout is only possible using sophisticated mathematical simulation tools like CFD. Then, the burner design and arrangement and also a variation of diameter with length is possible.

8.2.2 Optimisation of the Lignite R Gasifier

The simple gasifier layout is used to analyse the influence of operation parameters and boundary conditions on the gasifier performance. The gasifier operation aims at an optimisation of cold gas efficiency and fuel conversion. The evaluated operation parameters are:

- Stoichiometry: The influence of the O/C ratio on the gasifier performance is studied.
- Steam/CO₂ addition: Steam or CO₂ can be added to the burner to lower the maximum flame temperature and to achieve a more homogeneous reaction temperature.
- Carrier gas: The amount of carrier gas is dependent on the dense flow transportation requirements of the fuel particles.
- Particle size: A larger particle size reduces the energy consumption for pulverisation, but will increase mass transport limitations during reaction.
- Heat losses: Heat losses will decrease the gasifier performance.

The effects of a variation of these operation parameters on cold gas efficiency and fuel conversion are shown in Figure 8.6. The stoichiometry has the largest influence on the cold gas efficiency (CGE) of the gasifier. There is an optimum O/C ratio around 0.875, and the CGE drops rapidly at both sides of this value. However, an increase in oxygen addition improves the fuel conversion due to the higher temperature in the gasifier. If the complete conversion is required or heat losses occur, the practical O/C ratio has to be higher than the CGE optimum. Furthermore, the gasifier outlet temperature is decreased by the reduction of the stoichiometry. At an O/C ratio of 0.875 the outlet temperature is only 1215°C which is probably too low to achieve a steady slag flow. If more information about the slag viscosity at a certain temperature are available, the O/C ratio can also be adapted to the slag requirements.

Variations of the moisture content and the particle size have almost the same influence on CGE and fuel conversion, but - relatively to stoichiometry - their influences are small.

The effect of an increase in particle size is caused by mass transport limitations in the pore structure and the boundary layer. The average particle effectiveness factor is an indicator for the severity of the mass transport limitations. It is 0.81 for 60 μm particles, 0.62 in the standard case (100 μm particles), but decreases down to 0.01 for 500 μm particles. In Figure 8.6 the particle size is only increased up to 140 μm and almost no effect on CGE and fuel conversion is observed. A considerable larger particle size would cause a drop of gasifier performance. The CGE decreases to 77.5 % (200 μm), 71.9 % (400 μm), and 65.9 % (500 μm). Using the initial gasifier diameter of 2.9 m, the gasifier performance is higher and CGE is 78.3 % (200 μm), 77.4 % (400 μm), and 75.7 % (500 μm). However, fuel conversion decreases (99.8 % (200 μm), 99.3 % (400 μm), and 98.4 % (500 μm)) and it is likely that the organic matter content causes difficulties during the slag use and disposal.

The addition of steam and CO_2 lowers the gasifier performance as both CGE and fuel conversion decrease. The amount of carrier gas that is required for fuel feeding only slightly influences the performance, but its effect on the gas composition is considerable. The gas concentration (dry basis) of N_2 is 3.3 mol% if the carrier gas demand is only $0.04 \text{ m}_N^3/\text{kg}_{\text{coal}}$, but increases to 7.1 mol% for a demand of $0.1 \text{ m}_N^3/\text{kg}_{\text{coal}}$. If lower N_2 concentrations are required (e.g. for a chemical synthesis), the feeding system has to be operated with CO_2 .

The addition of steam and CO_2 can be applied to reduce the flame temperature and to provide a gaseous reactant that might be required for higher rank coals. The maximum temperature after volatiles combustion and the gasifier outlet temperature are shown in Figure 8.7. Although the maximum temperatures are probably overestimated, the qualitative effects of steam and CO_2 addition can be discussed. Steam is the better temperature moderator as the temperature drops by almost 400°C if 0.25 kg of steam are added per kg of coal. An identical addition of CO_2 reduces the maximum temperature by only 220°C as the mass specific heat capacity of CO_2 is lower at the high temperatures. Both additives influence the gasifier outlet temperature in the same way. The heat losses are assumed to occur continuously along the gasifier outer wall. Therefore, the effect on the maximum temperature is low, but heat losses reduce the gasifier outlet temperature. If the outlet temperature is below the ash melting temperature, slag flow difficulties are likely. Therefore, the decrease in the outlet temperature has probably to be balanced by an increase in stoichiometry which, however, would then lower the CGE.

A variety of boundary conditions has to be considered during the optimisation of the gasifier performance. The main operation parameter is the stoichiometry (O/C ratio) which is adjusted by the addition of oxygen to the burner. First, the CGE and the fuel conversion are improved by an increase in O/C ratio, but then CGE rapidly decreases as more fuel is burned and the heating value of the product gas decreases. The optimum O/C ratio for lignite R gasification is approximately 0.9, but in practical applications higher values might be applied due to thermal losses and slagging issues.

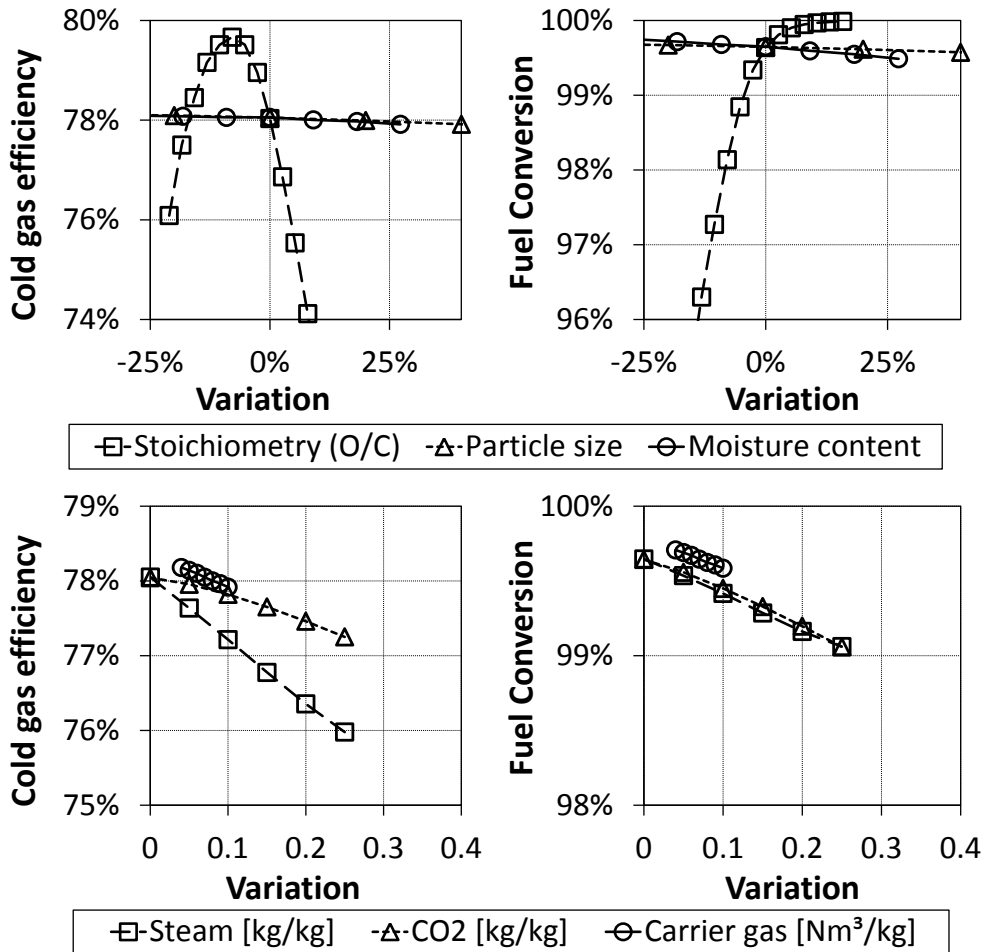


Figure 8.6: Sensitivity analysis of operation parameters in the simulation of a 500 MW entrained flow gasifier (0% values in the upper two diagrams: O/C = 0.95; particle size 100 μm ; moisture content 11 wt%; steam and CO₂ additions are in kg per kg of coal; carrier gas is in m³ (273K, 0.1013 MPa) per kg of coal)(gasifier length: 4.05 m, diameter: 2.25 m)

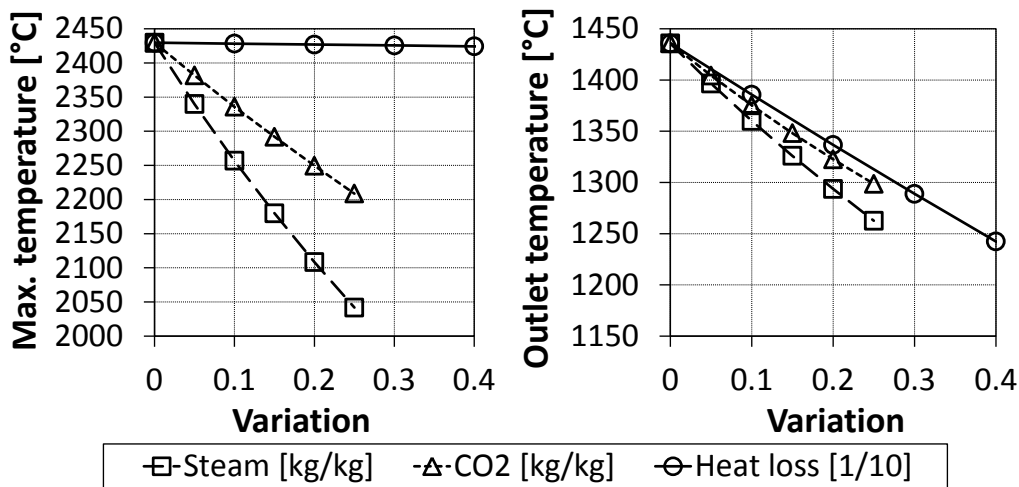


Figure 8.7: Effect of heat losses, steam and CO₂ addition on maximum and outlet temperature of a 500 MW entrained flow gasifier (steam and CO₂ additions are in kg per kg of coal; heat loss is in percent (e.g. 0.3 \equiv 3% of the thermal fuel input))(lignite R, gasifier length: 4.05 m, diameter: 2.25 m)

8.3 Fuel Specific Adaption of Gasifier Layout and Operation

The model of the industrial scale gasifier is also applied to other fuels to analyse their suitability for entrained flow gasification. The proximate and ultimate analysis of the fuels is given in Table 5.2. The devolatilisation parameters are taken from Table 7.6. They are shown together with the char gasification parameters in Table 8.2. The simulation is based on the simple empirical char gasification model as further data of the fuels are not available. The simple model does not consider thermal annealing, intrinsic reactivity, surface area evolution, and pore diffusion. The limitation by boundary layer diffusion is implemented and the reaction rate is limited by diffusion if the mass transport rate in the boundary layer is slower than the char reaction rate. The surface concentrations of CO_2 and H_2O are assumed to be zero in the mass transport equation. Therefore, the maximum possible gas concentration gradient is used in the model which leads to a slight overestimation of reaction rate by boundary layer diffusion. The simulation is run for a constant particle diameter of $100\ \mu\text{m}$.

The simple model is first tested for the lignite R and the results are compared with the detailed calculations for a 500 MW gasifier with a diameter of 2.25 m. As there is a large difference in the profoundness of the models, the simulation results deviate. The simple model predicts faster reaction rates. Therefore, the temperature required for complete conversion is lower and a lower oxygen feed rate is needed. As a result the CGE is higher. The optimum O/C ratio of 0.825 in the simulation results in a CGE of 83.6 %. However, the temperature at the gasifier outlet is only 1010°C . As the comprehensive model is available for lignite R, further calculation with the simple model are not made. Due to the better correlation of the advanced model to PiTER data, a reliable application of the model on a larger scale is expected. The simple model is able to estimate gasifier layout and operation, but the uncertainty is higher. As an advanced model is not available for the other fuels, the gasifier layout and optimisation for bituminous coal A, lignite V, and biocoal are briefly described using the simple empirical model.

Lignite V As the coal properties and model parameters of the two lignites are similar, no significant deviations are expected in the simulation. The gasifier geometry and boundary conditions are taken from the lignite R simulation: the gasifier has a length of 4.05 m and a diameter of 2.25 m, the thermal input is 500 MW, and the coal moisture content is 11 wt%. Lignite V has a LHV of 22.4 MJ/kg on a dry basis. Similar to lignite R, the reaction rate at high temperature in the simple model is very fast. As the gasifier is operated in a slagging-mode, the minimum outlet temperature is assumed to be 1400°C . The variation of the O/C ratio results in a minimum value of 0.96 to achieve the required gasifier outlet temperature. Fuel conversion is predicted to be 100 % and the cold gas efficiency is 78.7 %. The product gas concentrations are: 22.3 % H_2 , 50.1 % CO , 13.7 % H_2O , 9.4 % CO_2 , and 4.5 % N_2 .

Bituminous Coal A A thermal input of 500 MW, a pressure of 2.5 MPa, and the modified gasifier geometry (length 4.05 m, diameter 2.25 m) are used in the simulation. The

Table 8.2: Summary of devolatilisation and char gasification parameters of the simple empirical model used in the simulation of industrial scale gasifiers

Fuel	Bituminous coal A	Lignite V	Biocoal
Particle heating rate [K/s]	$5 \cdot 10^4$	$5 \cdot 10^4$	$5 \cdot 10^4$
Pyrolysis time	50 ms	50 ms	50 ms
p_{set} [MPa]	0.5	0.5	0.5
T_{set} [°C]	1000	1000	1000
$Y_{V,pset,Tset}$ [-]	0.48	0.559	0.746
$Y_{V,pset,Tmax}$ [-]	0.55^a	0.655	0.746^b
ϑ [-]	0.01^c	0.0141	0.01^d
ρ [-]	63.8	207.6	41.1
A_V [s ⁻¹]	293^e	293	293
$E_{A,V}$ [kJ/mol]	51	51	51
$k_{0,obs}$ [s ⁻¹]	5860	510	10
$E_{A,obs}$ [kJ/mol]	129	66	20

^aAssumption: volatile yield is increased by a factor of 1.15 at high temperature

^bA further increase in volatile yield is not assumed

^cAssumption

^dAssumption

^eAssumption: All fuels have identical devolatilisation kinetics

LHV of bituminous coal A is 27.4 MJ/kg (dry basis) and the coal is fed to the gasifier with a moisture content of 2 wt%. The carrier gas demand is defined to be 0.07 m_N³/h N₂ per kg coal. Due to the high heating value and the low moisture content, the flame temperatures in the simulation are very high. In practical applications, steam is used as a moderator in the burner zone. Stoichiometry and steam addition are varied to optimise the cold gas efficiency. The effect of both parameters on CGE and fuel conversion is shown in Figure 8.8.

The maximum CGE of 80.1 % is achieved at an O/C ratio of 0.825 and for an addition of 0.1 kg steam per kg coal. If no steam is added, the concentrations of the gasification agents are too low to achieve complete conversion and some carbon cannot be converted to the gas phase. Even at the optimum CGE the conversion is only 98.5 %. The fuel conversion is complete at a higher O/C ratio of 0.85 and for low to medium steam addition. In the optimum simulation, the maximum temperature is calculated to be 2843°C that is very high and not possible in practical terms. The gasifier outlet temperature is still 1510°C. A further addition of steam might be required to reduce the reaction temperatures.

The simulation is run using the smaller gasifier diameter that is derived from the requirements of lignite R conversion. As bituminous coal A has a lower reactivity, the simulation is also applied to the initial gasifier diameter of 2.9 m and the length of 5.25 m. Due to the higher residence time, the optimum operation point changes. An O/C ratio of 0.8 and the addition of 0.1 kg steam per kg coal results in the optimum CGE of 82.5 % at a conversion of 99.2 %. The maximum temperature in the combustion zone is 2760°C and the gasifier outlet temperature is reduced to 1380°C. The product gas concentrations are: 30.4 % H₂, 60.9 % CO, 2.7 % H₂O, 1.7 % CO₂, and 4.3 % N₂.

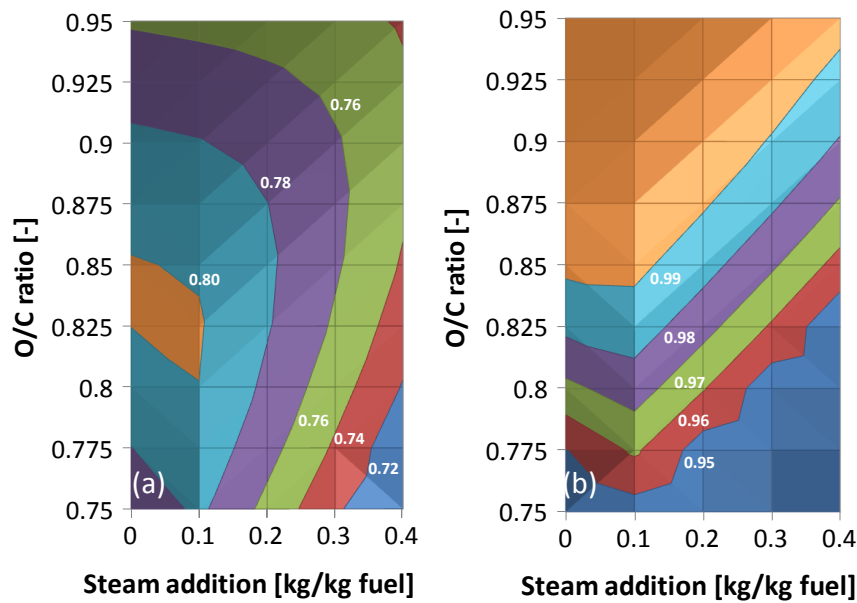


Figure 8.8: Effect of stoichiometry and steam addition in the simulation of a 500 MW gasifier for bituminous coal A (gasifier length: 4.05 m, diameter: 2.25 m): (a) Effect on cold gas efficiency; (b) Effect on fuel conversion (contour lines and areas of the same colour indicate the same range of values)

The larger gasifier volume seems to be better suited for the entrained flow gasification of bituminous coal A. The better gasifier performance compared with lignite R is mainly caused by the higher coal quality (LHV).

The simulation shows that the reactivity of a solid fuel has a strong influence on the gasifier layout. The gasifier layout and the operation conditions have to be adapted to fuel specific properties to optimize the performance.

Biocoal Due to the lower energy density of biomass and biocoal, the logistics of a larger scale gasifier may be difficult. The adaption of entrained flow gasification to biomass is still under development [Drift2004]. The conversion of biomass to biocoal via a hydrothermal carbonisation (HTC) is a promising technology to increase the energy density and allow the conversion of biomass on a larger scale [Erlach2010]. However, the HTC technology as well as other pre-treatment processes (e.g. torrefaction [Bergman2004]) are in the research and development stage. Due to the biomass logistics and uncertain technological requirements that impose a high financial risk for large scale installation, the application of entrained flow gasification on a smaller scale is an interesting possibility.

The biocoal gasifier is designed for a thermal input of 10 MW (1900 kg/h). Possible product gas applications at a smaller scale are gas engines, small turbines or a simple chemical synthesis (e.g. SNG), which all require lower pressures than in the larger scale facilities. Therefore, the biocoal gasifier is operated at a pressure of 0.5 MPa. The LHV of biocoal on a dry basis is 21.6 MJ/kg [Tremel2011] and moisture content is chosen to be equal to the lignite R (11 wt%). The feeding requirements are expected to be similar to lignite, but the fuel density is lower. Therefore, a lower fuel particle loading of 120 kg per actual m³ of N₂ during the dense phase transport is assumed. As the volatile yield and the char reactivity of biocoal are high and the ash content is low, the operation of

the gasifier below the ash melting temperature is a viable option. The non-slugging mode would possibly reduce ash related problems and would increase the CGE. As the operation mode (slugging or non-slugging) is strongly dependent on ash properties, both options are considered for the gasifier design.

The ash fusion temperature of biocoal (flow temperature) is 1276°C to 1326°C depending on the standard procedure for the ash fusion measurement [Tremel2011]. A slugging mode operation of the gasifier is expected to be feasible above 1400°C. As ash deformation begins at 1175°C, the gasifier outlet temperature in a non-slugging operation should be below this value and higher temperatures are only acceptable in a narrow region around the burner zone.

The lower thermal input requires a reduced gasifier size. A length of 1.8 m and a diameter of 1.0 m are assumed. In the slugging mode the O/C ratio is increased until the outlet temperature reaches 1400°C. The addition of steam is not considered. Due to the relatively high LHV of biocoal, the optimum O/C ratio is only 0.76 which requires an oxygen feed rate of 860 kg/h. The maximum temperature in the combustion zone is calculated to be 2243°C. The cold gas efficiency is 78.9 % and a fuel conversion of 99.3 % is achieved. If the LHV of biocoal is decreased due to the use of another feedstock or a change of preparation conditions, the oxygen feed rate has to be increased. For example, the O/C ratio has to be increased to 1.08 if the LHV is 18.0 MJ/kg, a typical value for dry biomass. As a result, the fuel conversion remains high, but the CGE drops to 71.2 %.

In order to operate the gasifier in a non-slugging mode, steam is added to the combustion zone to lower the maximum temperature. The outlet temperature is kept above 900°C to enable an acceptable char conversion rate also in the later stages of conversion. The ratio of steam and oxygen addition defines the temperature distribution within the reaction zone. The addition of more steam homogenises the temperature profile, but reduces the gasifier performance as more heat is required to heat up the steam. A possible trade-off is the addition of 0.2 kg steam per kg of biocoal and the operation with an O/C ratio of 0.64 which causes an oxygen demand of 820 kg/h. The peak temperature is then 1600°C, but the reaction temperature is rapidly decreased and is below the ash melting temperature after 320 ms. The temperature profile of both operation modes is shown in Figure 8.9. The total residence time is 1.5 s and a CGE of 82.0 % is achieved. The losses are partly caused by incomplete burn-off as the fuel conversion is only 98.1 % due to the lower reaction temperature. However, the CGE is higher than in the slugging gasifier and the potential of the conversion of highly reactive fuels below their ash fusion temperature is shown.

The product gas compositions for both operation strategies are summarised in Table 8.3. The addition of steam and the lower temperature in the non-slugging gasifier leads to a change of the water gas shift equilibrium and all product gas species except N₂ are affected.

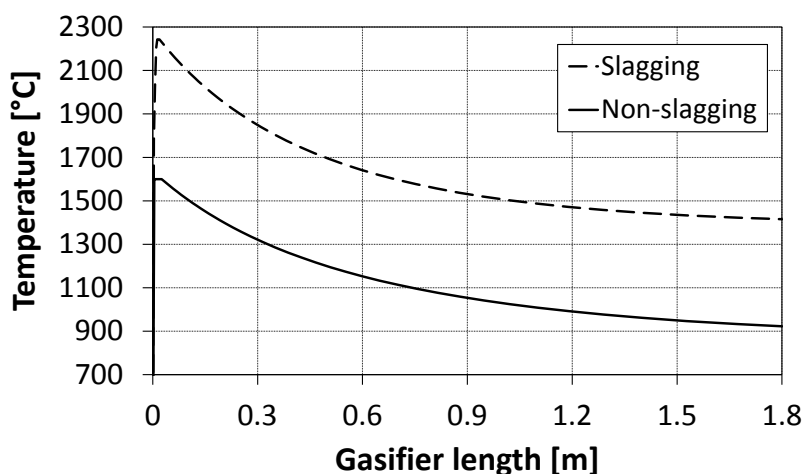


Figure 8.9: Temperature distribution along the reactor length of a 10 MW gasifier for biocoal in a slagging and non-slagging operation mode (gasifier length 1.8 m, diameter 1 m)

Table 8.3: Product gas composition (mol%, wet basis) in the simulation of a 10 MW entrained flow gasifier for biocoal

Operation mode	H ₂	CO	H ₂ O	CO ₂	N ₂
Slagging	27.2	48.0	14.8	7.9	2.1
Non-slagging	34.1	35.9	16.0	12.1	1.9

8.4 Analysis of the Reaction Regime in Entrained Flow Gasifiers

Due to the low amount of data from high temperature entrained flow reactors and the limitation of these data by an upper temperature of 1500°C in literature, the reaction regime of char gasification at high temperature is not known. In a recent PhD thesis [Hodge2009], the char-CO₂ reaction is studied at high temperature and the transition from Regime I to Regime II occurred at or around 1000°C to 1100°C. The author safely assumes that in entrained flow gasifiers at a temperature above 1200°C the char-CO₂ reaction will occur under Regime II conditions. In other experimental studies [Ahn2001, Kajitani2002, Kajitani2006] the transition temperatures to Regime II conditions are between 1000°C and 1400°C for the CO₂ and H₂O gasification. In contrast to solid fuel combustion, the transition to Regime III conditions is expected to occur at very high temperature for entrained flow gasifiers.

The model framework derived on the basis of experimental data can be used to analyse the reaction regime of entrained flow gasification. The model framework consists of the SFOR devolatilisation model and the char conversion submodels shown in Figure 7.1. The model parameters are summarised in Table 8.1. The gasifier diameter is 2.25 m and a stoichiometry of 0.875 is applied. In the simulation of a larger scale gasifier the temperature decreases continuously during char gasification because thermal energy is consumed by the endothermic reactions. Furthermore, the reaction rate changes along the reaction pathway. A diagram similar to the classical Arrhenius plot can be derived from the temperature profile and the local reaction rate. The logarithm of the apparent reaction

rate [g/(g·s)] is plotted versus the inverse temperature in Figure 8.10 for the 500 MW gasifier of lignite R. Reaction rate is plotted up to a fuel conversion of 95 wt% because at higher conversion the reaction temperature is not the main influencing parameter and other effects (e.g. loss of surface area) are important.

At low temperatures near the gasifier outlet ($\sim 1330^{\circ}\text{C}$) the temperature influence is described by an activation energy of 210 kJ/mol. This is in the range of the activation energy for the intrinsic char- CO_2 and char- H_2O reactions². The effectiveness factors at the gasifier outlet are 0.89 for the char- CO_2 reaction and 0.52 for the faster char- H_2O reaction which indicates conditions close to Regime I.

The slope of the curve continuously decreases at higher temperatures and a defined transition temperature to Regime II conditions is not observed. In ideal Regime II conditions the observed activation energy is half the activation energy under Regime I conditions. This is the case in the medium region of the gasifier. Directly after the combustion zone, the maximum temperature during char conversion occurs and the observed activation energy is only 64 kJ/mol. As this value is lower than half the activation energy under Regime I conditions, the reaction occurs in the transition zone to Regime III. This is also confirmed by the initial deviation between the bulk gas concentration and the concentration at the outer particle surface that is for instance shown in Figure 8.4. The effectiveness factors in the burner zone are 0.05 (char- CO_2) and 0.02 (char- H_2O), i.e. only 5 % of the internal surface area of the char is accessible for CO_2 and only 2 % for H_2O .

Only the effect of temperature is shown in the Arrhenius plot. As other parameters like particle size and density, conversion, and surface area also vary along the reaction path, the variation of observed activation energy cannot only be attributed to the temperature effect. But, as temperature has a very significant influence on the reaction rate, the qualitative trend of the Arrhenius plot is expressive.

The particle size is another important parameter that determines the reaction regime. At a larger particle size the reaction shifts further to Regime III conditions. In the evaluation so far a particle size of 100 μm is used. If the diameter is increased to 200 μm , the initial activation energy is 50 kJ/mol, and at a particle size of 500 μm it is only 30 kJ/mol indicating the further approach of pure Regime III conditions.

The simulation shows that all three reaction regimes are important during entrained flow gasification. In order to predict reaction behaviour under entrained flow conditions, it is required to evaluate the effects of operation parameters and boundary conditions in all three regimes and include intrinsic reactivities as well as mass transport limitations.

The model framework developed in this dissertation considers the influence of operation conditions and fuel properties in all three reaction regimes and is able to quantitatively predict solid fuel conversion in larger scale entrained flow gasifiers.

²As the gasification rate is not only influenced by the intrinsic reactivity the activation energy slightly deviates.

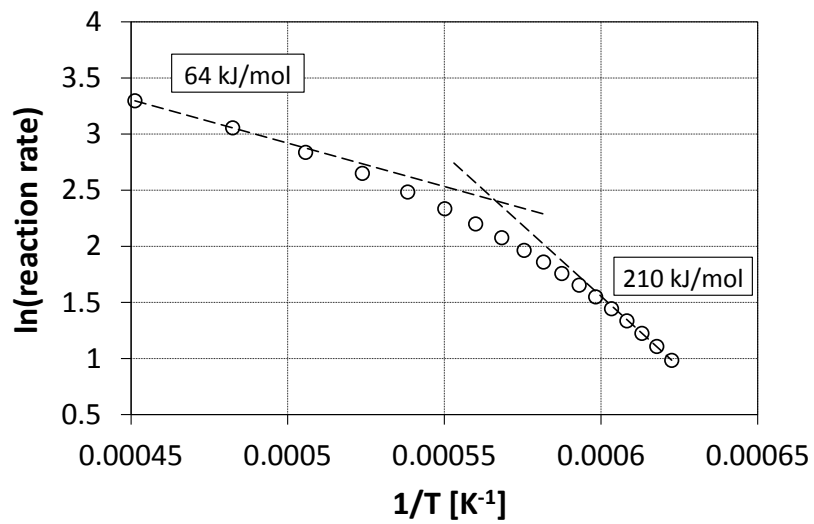


Figure 8.10: Arrhenius plot (observed reaction rate vs. inverse temperature) extracted from the simulation of a 500 MW entrained flow gasifier for lignite R

Chapter 9

Development of a Fuel Test Procedure for Entrained Flow Gasification

Experimental data are very important to evaluate the applicability of conventional and alternative fuels in entrained flow gasifiers. The data are used to develop mathematical formulations that quantify the fuel behaviour at high temperature and high pressure. These models can then be implemented in sophisticated simulation tools to predict the reaction behaviour of a fuel in an industrial scale gasifier. The theoretical and experimental framework developed in this dissertation is used to suggest a test procedure that enables the measurement of a fuel specific data set. The data should characterise fuel specific reaction behaviour and should readily be applicable to derive the unknown parameters in the model equations.

The amount of data required depends on the range of operation parameters that are of interest in the industrial application and on the desired quality and reliability of the models. Entrained flow gasifiers are operated from atmospheric pressure up to about 5.0 MPa. In state of the art coal gasifiers, the outlet temperature is around 1400°C, but higher temperatures are achieved in the burner zone. In multi-stage designs, fuel is injected after the primary burner in order to use the sensible heat of the reaction gas by a chemical quench. The average reaction temperature of the fuel is then lower and fuel chars are not exposed to the initially high temperatures in the burner zone. Furthermore, high reactive fuels like lignite or biomass have the potential to operate the gasifier below the ash melting temperature and thereby increase the cold gas efficiency. As the reaction temperature in a non-slugging gasifier is considerably lower, kinetic data are also required below 1400°C. To characterise a fuel for several entrained flow conversion options (slugging, non-slugging, multi-stag) the desired temperature range is about 1000°C to 2000°C.

A pressurised flow reactor and a wire mesh reactor are required for the test procedure. These could be facilities like the Pressurised High Temperature Entrained Flow Reactor (PiTER) and a Pressurised Wire Mesh Reactor (PWMR) that were used in this dissertation. An atmospheric entrained flow reactor (like the BabiTER) can be used to derive important high temperature data, but effects of pressure on devolatilisation and char structure cannot be studied. Furthermore, a commercially available thermogravimetric analyser is required that can be operated under increased pressure and in the temperature range up to 1000°C. The test procedure is graphically summarised in Figure 9.1.

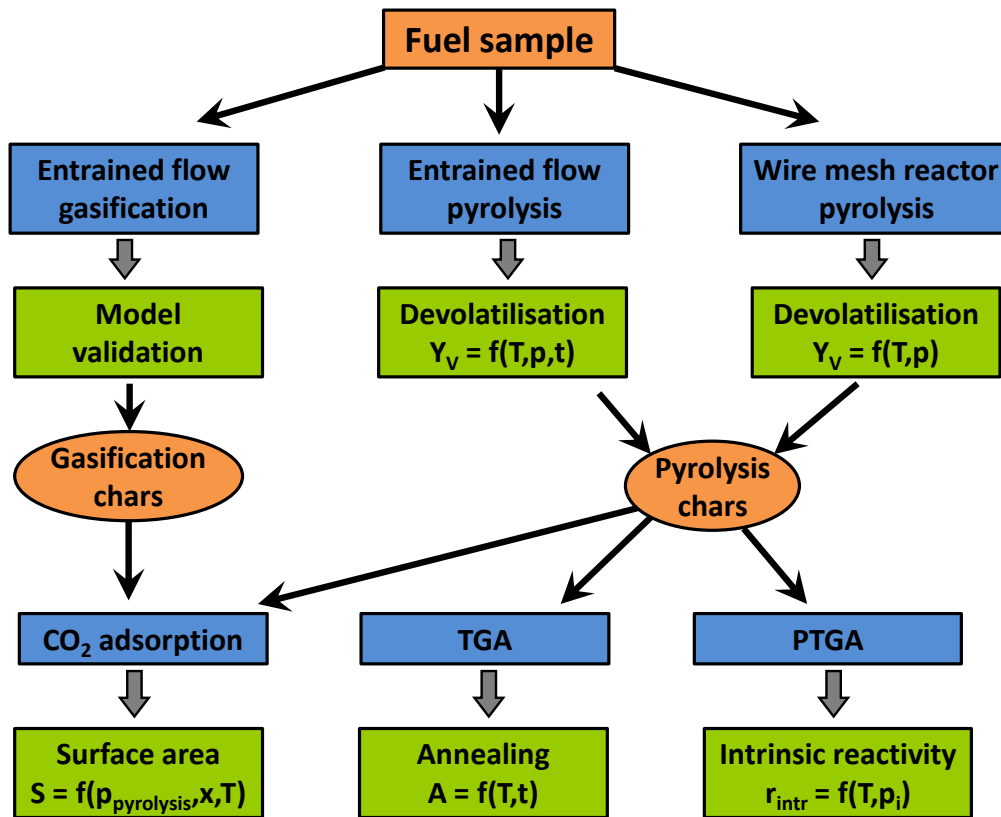


Figure 9.1: Test procedure for the evaluation of entrained flow gasification behaviour of a unknown or novel fuel

9.1 Entrained Flow Gasification Experiments

Very important information about the reaction behaviour at high temperature and high pressure are directly derived from experiments in a pressurised entrained flow reactor. First, integral experiments with a defined oxygen to fuel stoichiometry are recommended. As the temperature range should be similar to the later industrial application, experiments should begin at 1000°C or 1200°C and should range up to 1600°C/1800°C (or even higher if technically feasible). If the pressure of the later industrial application is known, it is sufficient to work only at this pressure. As the char properties like particle size and structure are influenced by devolatilisation pressure, it is important to simulate realistic conditions. If a pressurised entrained flow reactor is not available, experiments at atmospheric pressure are an alternative, but an inherent deviation from the industrial application may exist. The residence time adjusted in the entrained flow experiments is dependent on the fuel reactivity. Fuels with a high content of volatile matter and/or fuels that produce a highly reactive char are almost converted in a time interval of less than 1 s, especially at the highest temperatures. In contrast, several seconds are required to measure significant char conversion of fuels with low reactivity. For a fuel with a unknown reactivity, the residence time should be varied from the lowest possible value up to about 3 s. To measure char conversion in the early stages, it may be required to adjust a fuel residence time of only 100 ms or 200 ms.

In entrained flow experiments soot formation may occur at particular conditions, especially

for bituminous coals. To reduce the tendency of soot formation, water steam can be added in the integral experiments. Furthermore, low volatile coals require a gasification medium in addition to oxygen to achieve complete conversion. In industrial gasifiers, steam is also added to lower the temperature in the combustion zone, especially for coals with a high heating value and a low moisture content. The operation of the research entrained flow reactor with a gas mixture containing oxygen and water steam is relevant to larger scale conditions. Integral experiments for lower rank fuels (lignite, biomass) can be carried out using oxygen as the gasification medium because the hydrogen and oxygen content of the fuel usually enables complete conversion. Higher rank fuels require a reactive gas mixture containing oxygen and steam.

The entrained flow experiments provide a data set that describes fuel conversion at different temperatures and residence times. If a pyrolysis experiment in an inert gas atmosphere is carried out at each temperature and at a medium residence time¹, volatile yield at high temperature is known. Char conversion can be calculated by subtracting the fuel conversion in the pyrolysis experiment from fuel conversion in the gasification experiment at the same temperature. Then, the time dependent char conversion data are used to derive the pre-exponential factor and the activation energy in a simple Arrhenius type rate equation. The simple model can predict fuel and char conversion in the experimental data range and for the particle size used in the experiments. A simple extrapolation to higher or lower temperatures leads to an unknown uncertainty. However, the simple kinetic model is useful for the direct comparison of different fuels, for a first estimation of gasifier layout on an industrial scale, and for the rough prediction of suitable industrial operation conditions. Furthermore, the entrained flow data set allows a validation of the model framework that is later derived in the laboratory and bench-scale analysis. Only if the model framework can correctly predict the gasification rates in the research entrained flow reactor, an application at the industrial scale is recommended.

To derive the desired data set, at least experiments at 3 to 4 temperatures (1200°C/ 1400°C/ 1600°C/ (1800°C)) and at least at 3 residence times at each temperature are required. The operation pressure is constant and equals the industrial application. Including the 3 to 4 pyrolysis experiments, a total number of 12 to 16 experimental runs for each fuel is required. Further experiments can be useful to analyse the influence of particle size and stoichiometry. If the fuel reaction behaviour at different operation pressures is required, the experimental procedure is carried out at each pressure of interest.

9.2 Pyrolysis Experiments

In the entrained flow test trials a limited number of pyrolysis experiments is required to measure volatile yield at each operation temperature and calculate char conversion. A kinetic pyrolysis model cannot be derived from the data and the char amount and range collected during these experiments may be too low for further char investigations.

¹If devolatilisation is complete, the volatile yield is not dependent on residence time. As the devolatilisation rate is fuel and temperature dependent, the residence time to reach the maximum volatile yield is not known a priori. PiTER experiments have shown that a residence time of 1.5 s is sufficient even at low temperature to measure the final volatile yield.

Therefore, a larger number of pyrolysis experiments is suggested as the next step. To simulate conditions relevant to larger scale gasifiers, it is required to study pyrolysis at a high heating rate, at high temperature and under pressure. The experimental facilities that can achieve these operation conditions are the pressurised entrained flow reactor and a wire mesh reactor operated under pressure.

9.2.1 Entrained Flow Pyrolysis Experiments

The derivation of a kinetic pyrolysis model requires experimental data at different temperatures and different residence times. As pyrolysis is a very fast process, the range of measurements should be at low time scales that are considerably shorter than in the gasification experiments. At high temperature, experimental data at a residence time of < 100 ms is required. At lower temperature, experiments have shown that a time interval of 1 s to 1.5 s may be needed to achieve the final volatile yield. In industrial applications the devolatilisation temperature is very high as the release of volatiles occurs in the burner zone where the highest temperatures of the process exist. Hence, the entrained flow experiments should aim at the highest possible temperatures ($1600^{\circ}\text{C}/1800^{\circ}\text{C}$). As devolatilisation is much slower at lower temperature and therefore easier to measure, experiments at lower temperature ($1000^{\circ}\text{C}/1200^{\circ}\text{C}$) can be an useful supplement.

The operation pressure can have a significant influence on the volatile yield. If the operation pressure of the industrial gasifier is known, a variation of pressure in the experiments is not needed. If the fuel should be characterised for several applications that have various pressures, the variation of pressure is required in the experiments. As the pressure has the largest influence at lower pressures and the pressure effect diminishes at higher pressures, the pressure interval between two measurements can be continuously increased towards higher pressures. In the experiments of this dissertation the following pressure stages were used: 0.1 MPa, 0.5 MPa, 2.5 MPa, and 5.0 MPa. If the pressure stages of the industrial applications are known, these should be used instead.

Besides the analysis of devolatilisation rates, the pyrolysis experiments are required to produce char that is similar to char produced in larger scale applications. The char collected during the entrained flow experiments can further be analysed in laboratory and bench-scale rigs. As only an entrained flow reactor provides the highest heating rate, char samples can hardly be produced in smaller scale facilities. It is recommended to collect at least 5 g of char to provide enough sample mass for several subsequent analysis procedures.

The fuel mass flow rate in the pyrolysis experiments should be low to achieve a high heating rate of each particle. If the mass flow rate is too high, particles influence their neighbours and delay the heat-up. Furthermore, the volatiles should be removed from the particle surface to reduce the possibility of secondary tar reactions. A high mass flow rate might increase the concentration of volatiles in the surrounding of the particles and might favour undesired reactions like condensation.

A test procedure that enables the analysis of devolatilisation rates and the collection of realistic char samples could be composed of experiments at 3 to 4 temperatures ($1200^{\circ}\text{C}/1400^{\circ}\text{C}/1600^{\circ}\text{C}/(1800^{\circ}\text{C})$) and each 3 residence times at very short time scales. For the analysis of the final volatile yield the pyrolysis experiments from the initial gasifi-

cation tests (Section 9.1) can be used. As the simultaneous variation of temperature and pressure would multiply the number of runs, it is recommended to vary pressure at one temperature (e.g. 1400°C). The measurement set comprises 12 to 15 experimental runs per fuel. Further experiments can focus on the effect of particle size on the devolatilisation kinetics, and on the influence of moisture content that could lead to partial fuel gasification. For further char reactivity studies, it is required to produce a highly deactivated char. This can be done by a pyrolysis experiment at the highest possible temperature and a residence time of 2s to 3 s.

9.2.2 Pyrolysis Experiments in the Wire Mesh Reactor

A wire mesh reactor is an ideal tool to analyse fuel devolatilisation behaviour at high heating rate in a bench-scale apparatus. If the mesh is situated in a pressure vessel, experiments at an increased pressure are feasible. The range of experiments strongly depends on the technical possibilities of the reactor. The PWMR used in this dissertation can only be operated at up to 1100°C because a stainless steel mesh is used. Experiments are carried out that analyse the effect of pressure on volatile yield. If it is assumed that this effect is independent from the operation temperature, experiments can be carried out using the stainless steel mesh. These experiments could substitute the pressure variations in the entrained flow reactor. The highest possible heating rate should be applied and the holding time at temperature should be 2 s to ensure a complete devolatilisation. As the experimental effort is very low, pressure can be varied in smaller intervals.

To analyse the effect of pressure on volatile yield, experiments at the following pressure stages are recommended: 0.1 MPa, 0.5 MPa, 1.0 MPa, 2.5 MPa, and 5.0 MPa. At each pressure it is required to carry out at least three independent runs to reduce the measurement uncertainty and to quantify the measurement errors. For each fuel, a total number of 15 runs is required.

The char from the experiments can be used in subsequent analysis methods. As the amount of char that is produced in each experiment is only about 5 mg, several runs are required to produce enough sample mass. If entrained flow pyrolysis experiments are carried out, the char should be taken from these experiments.

In contrast to the entrained flow reactor, the PWMR can be used to produce a very reactive char sample. The mesh temperature can be set to 700°C where no thermal deactivation of char is expected. The holding time in the PWMR is arbitrary and can be adjusted to the fuel devolatilisation time. In the entrained flow reactor the residence time is only a few seconds and it is uncertain whether devolatilisation would be completed at this low temperature. The 700°C char from the PWMR is expected to represent char with the highest possible reactivity. About 10 experimental runs at 700°C are required to produce a significant char mass. The sample is required in further char reactivity studies.

The test procedure at the PWMR is limited because of the technical limitations of the reactor. If experiments at higher temperature were feasible, the effect of temperature on volatile yield could be studied. Furthermore, the wire mesh reactor could be equipped with a quench system that enables the instant termination of the reaction. In this case, it would be possible to do pyrolysis experiments at various residence times and derive the

reaction rate of devolatilisation. Further possibilities of a wire mesh reactor (e.g. reactive gas atmosphere) are not considered here.

9.3 Char Analysis

Several char samples are collected in the entrained flow pyrolysis and gasification experiments and from the PWMR. These can be used to analyse the char properties during entrained flow gasification and derive submodels that explain certain phenomena during the high temperature char conversion. The char properties that are considered are the thermal char deactivation, the evolution of surface area with conversion, and the intrinsic char reactivity. The test procedures that can be used to derive the parameters of these submodels from the char samples in different laboratory and bench-scale rigs are presented in the following sections.

9.3.1 Char Specific Surface Area Evolution during Conversion

The char-gas reactions occur at the char surface. Therefore, the specific surface area of char is an important parameter. If the specific char surface [m^2/g] is large, the char is expected to have a large number of reaction sites and also a high porosity. Both are important parameters for the reaction rate of char in the heterogeneous gasification reactions. Surface area is measured by adsorption of CO_2 at 273 K and the adsorption isotherm is analysed by the DFT or DR method. To analyse the development of the specific surface area with conversion the determination of the surface areas of all gasification chars and the 4 pyrolysis chars from the entrained flow gasification tests is required. These are about 20 adsorption measurements that enable the development of a surface area submodel that describes the evolution of char surface with conversion at different temperatures. As the devolatilisation pressure has an influence on char structure and therefore surface area, also the analysis of the pyrolysis chars is recommended. The surface measurements of the chars produced at one temperature and at 0.1 MPa, 0.5 MPa, 2.5 MPa, and 5.0 MPa are implemented in the surface area submodel to predict the effect of pressure on surface area evolution. The measurement of surface area of the other pyrolysis chars (entrained flow reactor and PWMR) is required for the thermal deactivation submodel. In total, about 40 measurements are required in the test procedure of one fuel.

9.3.2 Quantification of Thermal Char Deactivation

The severity of the char heat treatment strongly influences its reactivity. In the experiments, a decline of char reactivity is observed at higher temperature and longer time scales at temperature. This loss of reactivity is correlated to a loss of active sites on the char surface. It is found during the analysis of pyrolysis and gasification chars that the decrease in reactivity can be measured by thermogravimetric analysis at lower temperature. The char reaction rate is measured at around 400°C in an atmosphere containing 5 % O_2 in N_2 at atmospheric pressure, and at 750°C in pure CO_2 at 0.5 MPa. In both setups, the weight loss rate declines if the char preparation temperature is increased. A thermal deactivation

submodel is developed from the reactivity data at atmospheric pressure and it is observed that the implementation of this submodel in numerical simulations of entrained flow data at higher temperature improves the model quality. Therefore, the loss of reactivity that is measured at low temperature can be correlated to the loss of reactivity under entrained flow conditions. The quantitative trend of standard reactivity that is measured in a TGA can directly be used for the modelling of high temperature reactions.

Due to the simpler experimental procedure of the atmospheric TGA, the standard reactivity should be measured at atmospheric pressure in an oxygen containing atmosphere. The measurement temperature is dependent on the char reactivity. If the temperature is too high, mass transport limitations might arise for the most reactive chars. If the temperature is too low, the weight loss rate could be close to or below the detection limit. A suitable temperature is found if the reactivity of all chars of the fuel can be measured and the sample mass has no influence on the observed reaction rate. Good results have been achieved at a temperature of 375°C for high reactive lignite chars and at 400°C for bituminous coal chars. A low concentration of oxygen (5% O₂ in N₂) is chosen to further limit the reaction rate and reduce the effect of the exothermic char-O₂ reaction.

As the char deactivation depends on temperature and time at temperature, the standard reactivity of char samples collected in the entrained flow pyrolysis experiments should be measured. For each char preparation temperature, there are char samples for 4 different residence times available. Additionally, the char reactivity of the highly deactivated char (highest possible experimental temperature, long residence time) and of the fresh char prepared in the PWMR (700°C, relatively long residence time) is measured. The submodel for thermal deactivation can be directly derived from the standard reactivity data if the submodel is implemented in a reaction rate model on a mass basis (observed reactivity [g/(g·s)]). If the combination with an intrinsic reaction rate model is desired the standard reactivity needs to be related to the specific surface area of the char (g/(m²·s)).

The measurement set in the TGA comprises a maximum of 21 experiments which enable the derivation of a very reliable thermal deactivation submodel. The chars prepared at very short residence time could still hold significant amounts of volatile matter. It may be necessary to exclude these chars from the standard reactivity analysis. In further experiments the chars from the entrained flow gasification tests could be used. However, the degree of conversion of these chars differs and char reactivity could also be influenced by conversion. As the influence of conversion is already considered in the specific surface area measurements, it seems to be sufficient to base the char deactivation submodel on pyrolysis chars that have similar conversion.

9.3.3 Measurement of Intrinsic Char Reactivity

Intrinsic char reactivity can be derived from specific surface area and observed reaction rate in TGA experiments. TGA experiments are designed to exclude any influences of mass transport limitations on the reaction rate. Therefore the complete internal char surface is involved in the reaction. As the surface area of each char is known from adsorption measurements, the observed reaction rate [g/(g·s)] can be transformed to the intrinsic reaction rate [g/(m²·s)].

The reactions with CO_2 and H_2O lead to significant char conversion. As the methanation reaction (char-H_2) is very slow, it is not considered in this test procedure. The combustion rate (char-O_2) is very fast and the assumption of a very fast reaction rate is a good approximation in entrained flow gasification. As the test procedure focuses on the heterogeneous char reactions with CO_2 and H_2O , only these are considered in the intrinsic char reactivity measurements. To further reduce the measurement programme only one char is used in the thermogravimetric analysis. Since the effects of conversion and thermal deactivation are already considered in other submodels, the highly deactivated char from the entrained flow pyrolysis experiments is the best choice. The char should be produced at the pressure of interest. The intrinsic reactivity of this char can be assigned to other stages of conversion and less annealed chars.

To investigate the influence of reactant gas concentration on reactivity, the partial pressures of CO_2 and H_2O should be varied over a wide range. In the simulation of the industrial scale gasifiers the maximum concentrations of both gases are in the range 30 mol% to 50 mol%. At a gasifier pressure of 2.5 MPa this corresponds to a partial pressure of 0.75 MPa to 1.25 MPa, but can even be higher if the gasifier is operated at a higher total pressure. At the gasifier outlet, both concentrations may be as low as 2 mol% 3 mol% (~ 0.1 MPa partial pressure). To enable this partial pressure range in the experiment, measurements in a pressurised TGA are required. The TGA should be operated at the same total pressure as the industrial gasifier to exclude any influences of total pressure.

The number of experiments is dependent on the model equation that is used to describe the influences of partial pressure and temperature. If an n th order rate equation is used, at least 3 experiments at a constant temperature and at different reactant partial pressures are required. As an n th order rate equation is able to predict the influence of partial pressure within a limited range, the experiments should be carried out at partial pressures that are expected in the industrial gasifier. In case of a 2.5 MPa gasifier, experiments could be carried out at a total pressure of 2.5 MPa and at partial pressures of 0.25 MPa, 0.75 MPa, and 1.25 MPa. If CO_2 and H_2O gasification is considered, a total number of 6 experiments is required.

Additionally, the influence of temperature needs to be evaluated. At a medium partial pressure (e.g. 0.75 MPa) reaction rate measurements at 3 different temperatures are required for a classical Arrhenius plot. Alternatively, the temperature could be continuously increased in one experiment and the activation energy could be derived by the comparison to an experiment at a constant temperature. The characterisation of intrinsic reactivity using the n th order rate equation requires in total 10 to 12 experiments to describe CO_2 and H_2O gasification.

If a LH rate equation is used to model the influences of temperature and reactant gas partial pressure, the number of experiments increases. The model equation is able to describe the partial pressure influence over wider ranges. Again, a minimum of 3 experiments is required for each reactant gas. As the influence of temperature is not only considered in the reaction but also in the adsorption/desorption process of the reactant gases, the experiments at different partial pressures also have to be carried out at different temperatures. As at least 3 temperature stages are required for an Arrhenius plot; in total 18 experiments are needed to analyse the influence of temperature and partial pressure of the

char-CO₂ and char-H₂O reactions. If the adsorption/inhibition of further gases (e.g. CO, H₂) should be implemented more experiments are required. Further experiments could also address the interaction of the CO₂ and H₂O reactions.

However, the intrinsic model based on nth order rate equations in combination with other submodels has been able to predict entrained flow data of the PiTER reasonably well. Therefore, it is expected that nth order rate equations are able to describe the reaction behaviour of char under the desired operation conditions. If extrapolations of the experimental data are needed, LH rate equations are better suited and the error is probably lower.

In all TGA experiments it is important to analyse only the initial stages of char conversion. As the specific surface area of the char sample will change during conversion, the reaction rate is not constant in the experiment. The change of surface area differs from the surface area evolution under entrained flow conditions. As only the initial specific surface area of the char sample is known from the CO₂ adsorption measurements, the initial reaction rate (e.g. up to 20 % conversion) should be used to calculate intrinsic reactivity.

The test procedure described here is an efficient way to analyse the reaction behaviour of solid fuels in high temperature and high pressure gasification systems. If the test procedure is carried out for an unknown or novel fuel, a data set is generated that enables the derivation of several submodels for devolatilisation and char conversion. The role of mass transfer limitations is addressed by the calculation of pore and boundary layer diffusion. In a final step, the model framework is compared with the entrained flow gasification experiments. The simulation can be validated and the diffusion model can be adjusted.

If there is a good correlation to the pilot scale data, the models can then be used to design or optimise gasifiers on larger scales and to address reaction specific issues during gasifier operation.

As the focus of the model development is on the heterogeneous char gasification, further important reactions are not considered in detail. More experiments are required to describe the devolatilisation kinetics and to derive a more comprehensive devolatilisation model. Moreover, the reaction rates of volatiles and char combustion are not considered. These are important reactions if the burner zone of an industrial gasifier is modelled and they should be addressed by further studies.

Chapter 10

Summary, Conclusions, and Recommendations

In this dissertation, measurements from pilot-scale and bench-scale facilities have provided a data set that describes the reaction behaviour of solid fuels at high temperature and high pressure. The experimental data have been used for the development of a model framework that enables the prediction of fuel conversion rate and gasifier performance on larger scales. The results of the dissertation are now addressed to summarise major findings and recommend areas that require further research activities.

10.1 Summary of the Dissertation

10.1.1 Provision of a Data Set for Fuel Conversion under Entrained Flow Conditions

The behaviour of solid fuels at high temperature and high pressure is analysed in several measurement sets using laboratory procedures, bench-scale, and pilot-scale facilities. The range of solid fuels includes anthracite, bituminous coal, lignite, biocoal, and biomass. Entrained flow gasification reactions are studied in the Pressurised High Temperature Entrained Flow Reactor (PiTER). The design, built-up and operation of this novel pilot-scale research reactor is a main achievement of this dissertation. The pyrolysis of several fuels is analysed at temperatures of up to 1600°C and pressures of up to 4.0 MPa. In gasification experiments, a defined oxygen to fuel stoichiometry is applied and the fuel conversion is measured at up to 1600°C, 2.5 MPa and at a particle residence time from 0.5 s to 3 s. The high temperature data set is extended by measurements with the atmospheric Baby High Temperature Entrained Flow Reactor (BabiTER). The pyrolysis of solid fuels is further studied in a pressurised wire mesh reactor at high heating rate (1000 K/s) and at pressures of up to 5.0 MPa.

Chars samples collected from all three reactors are analysed in laboratory procedures and bench-scale setups. The surface area of the entrained flow chars is measured by CO₂ adsorption at 273 K and DFT analysis. A decline of the mass specific surface area [m²/g] is observed at higher conversion and also at higher temperature. The melting of mineral matter might block the micropore structure at the highest temperatures and reduce the specific surface area. When different pyrolysis chars are compared, an influence of the devolatilisation pressure on char surface area is found.

The intrinsic char reactivity is calculated from the observed reaction rate and from specific surface area. The observed reaction rate at low temperature and in the absence of mass transport limitations is measured in the Pressurised Thermogravimetric Analyser (PRETA). As the devolatilisation conditions strongly influence char reactivity, chars that are produced in the PiTER at a high heating rate, at high temperature and under pressure are used for the analysis. The rate of the char-CO₂ reaction is measured in the temperature range 650°C to 850°C and at CO₂ partial pressures between 0.1 MPa and 2.5 MPa. The rate of the char-H₂O reaction is measured at 650°C to 850°C and 0.5 MPa partial pressure. In some test experiments CO is added to the reaction gas and a significant decrease in the reaction rate is observed.

In the PRETA experiments a significant influence of the char preparation conditions on char reactivity is observed. This correlation is further analysed in an atmospheric TGA at 375°C to 400°C and in an oxygen containing atmosphere (5% O₂ in N₂). The so called standard reactivity is measured under these defined conditions. A loss of reactivity is observed if the char is exposed to a higher temperature and longer time scales at temperature. It is expected that the loss of active sites on the char surface occurs during the heat treatment. As the thermal deactivation is measured at low temperatures in the TGA, at medium temperatures in the PRETA, and the quantitative trend is the same, it is expected that the loss of active sites also influences the intrinsic reaction rate at higher temperatures in an entrained flow gasifier.

10.1.2 Model Development for Entrained Flow Gasification

The experimental data and the theoretical derivations are used to develop a model framework that describes the reaction behaviour of solid fuels in entrained flow gasifiers. A pyrolysis submodel is derived that describes the influences of pressure and temperature on volatile yield and the effects of temperature and reaction time on the devolatilisation rates. The heterogeneous char gasification is described by a combination of submodels for intrinsic reactivity, surface area evolution during conversion, thermal char deactivation, mass transport limitation by pore diffusion, and mass transport limitation by boundary layer diffusion.

The intrinsic reactivity of the char-CO₂ and char-H₂O reactions is described by an nth order Arrhenius type rate equation. The model parameters are derived from the reaction rate measurements in the PRETA. Furthermore, Langmuir-Hinshelwood (LH) and Langmuir-Hinshelwood-Hougen-Watson (LHHW) type model equations are developed that describe the influence of reactant gas and product gas adsorption at the char surface. The Random Pore Model that was developed to describe the variation of volume specific surface area [m²/m³] during char conversion is applied to the measurements of mass specific surface area [m²/g] of entrained flow chars. The original model is extended to describe the influences of devolatilisation pressure and conversion temperature on the char surface area. The standard reactivity of the TGA analysis is used to derive a submodel for thermal char deactivation. The model is based on the idea of a continuous transformation of active sites on the char surface to deactivated sites. The process is dependent on temperature and reaction time. Since mass transport limitations cannot be measured directly, a the-

oretical framework is derived that predicts the evolution of reactant gas concentrations within the boundary layer and the pore structure. The limitation by pore diffusion is based on an effectiveness factor approach. As the mathematical formulation is dependent on the intrinsic rate equation, specific submodels are derived for n th order, LH, and LHHW rate equations. The mass transport limitation in the particle boundary layer is calculated via a mass transfer coefficient and a Sherwood Number correlation for a sphere.

Since the mass transport limitation within the porous structure is strongly affected by the average pore size, the pore diameter is an important model parameter. The assumption of a pore diameter of 10 \AA is initially used to reflect the microporous char structure. However, the simulation then underestimates the experimental fuel conversion data of Rhenish lignite. If the simulation is adjusted to the experimental data by a variation of the average pore diameter, this results in a diameter of 47.3 \AA which is a reasonable value as it indicates the involvement of mesopores in the conversion process. After the adjustment a good correlation is achieved between the simulation and the experimental high temperature conversion data.

As the model framework is able to predict conversion data from research entrained flow reactors (PiTER and BabiTER) based on low-temperature reactivity data, it is also expected to predict conversion rates in industrial scale gasifiers where similar operation conditions occur.

10.1.3 Layout and Optimisation of Larger Scale Entrained Flow Gasifiers

The comprehensive devolatilisation and char gasification model is applied to the layout and optimisation of entrained flow gasifiers on an industrial scale. The gasifier model can predict the influence of fuel reactivity and operation parameters on the gasifier efficiency, the fuel conversion, and the distribution of temperature and gas concentration within the reaction zone. The gasifier is modelled as a one-dimensional plug flow reactor.

As all model parameters are only available for the Rhenish lignite, the gasifier dimensioning is based on this fuel. A reduction of the gasifier volume reduces the particle residence time and possibly the fuel conversion if the reaction rate is too slow. A 500 MW entrained flow gasifier (2.5 MPa) is simulated using a geometry derived from literature [Schingnitz2005]. Due to the high reactivity of the lignite it is possible to reduce the gasifier volume and to downsize the reactor by up to 50 % and still achieve a high conversion and a high cold gas efficiency (CGE). At the optimum stoichiometry the CGE is 79.7 % and the fuel conversion is 98.1 wt%. Due to the need for a higher conversion and the potential requirement of higher temperatures at the gasifier outlet, it might be required to increase the oxygen mass flow rate to the gasifier. The variation of several process parameters and boundary conditions shows the sensitivity of the gasifier performance. For example, the addition of water steam to the burner zone reduces the maximum flame temperature, but also reduces the average conversion temperature which may lead to a decrease in gasifier performance.

A simple empirical reaction rate equation is derived from the entrained flow experiments of Lusatian lignite, a bituminous coal, and biocoal. A comparison of the simple model with the

more comprehensive simulation of Rhenish lignite indicates that the simple purely empirical model slightly overestimates the gasification rates which might lead to an optimistic fuel conversion. Nevertheless, the simple model based on experimental data is a good method to estimate gasification behaviour at a larger scale. The simulation of Lusatian lignite gasification on the 500 MW scale results in a similar performance as for Rhenish lignite. The optimum CGE is 78.7 % when a gasifier outlet temperature of 1400°C is required. Due to the higher heating value the optimum CGE of the bituminous coal is 82.5 %, but a larger gasifier volume compared with the lignites and the addition of water steam to reduce the maximum flame temperature might be required. The entrained flow gasification of biocoal is simulated for a thermal input of 10 MW and a operation pressure of 0.5 MPa. In a slagging-operation mode (above the ash melting temperature) the CGE is 78.9 %. Due to the high reactivity of biocoal, also the conversion at lower temperature below the ash melting temperature is considered. For a non-slagging operation the injection of water steam may be required, but the CGE is possibly increased to 82.0 %.

The model framework and the numerical simulation provide the possibility to transfer experimental data from bench-scale and pilot-scale setups to the design and optimisation of larger scale entrained flow gasifiers. The gasification rate can be calculated in all three reaction regimes and the influences of pressure and gas atmosphere are implemented. It is possible to design the gasification technology according to the needs and properties of the solid fuel and to support the optimisation and operation procedure by simulations.

10.1.4 The Reaction Regime during Entrained Flow Gasification

In entrained flow gasifiers, the reaction regime is dependent on operation and fuel parameters like reaction temperature and char particle diameter. In the PiTER experiments the reaction regime depends on temperature and conversion. Experiments are evaluated for the Rhenish lignite. At 1200°C the effectiveness factor is initially 0.2 to 0.4 indicating Regime II conditions. In the later stages of conversion the char reactivity is reduced and the effectiveness factor approaches unity indicating the conversion under Regime I conditions. At 1400°C and 1600°C the average effectiveness factor is always below unity indicating Regime II conditions. Up to 1600°C Regime III conditions are not observed, as the reaction rate remains far below the film diffusion limitation.

The reaction regime in an industrial scale gasifier is evaluated using the simulation of a 500 MW gasifier for Rhenish lignite. Directly after the combustion zone the activation energy is only 64 kJ/mol and in the later stages of conversion an activation energy of 210 kJ/mol is calculated. The initial low activation energy is decreased further if for example the average particle diameter is increased. The wide range of activation energies indicates that the reaction occurs in all three reaction regimes. Initially at high temperature the char conversion occurs in the transition to Regime III conditions and it is partly limited by boundary layer diffusion. In the later stages of conversion the temperature and char reactivity¹ are significantly lower and the reaction approaches Regime I conditions as the observed activation energy is in the range of the intrinsic reactivity and the effectiveness

¹Char reactivity decreases at higher conversion due to thermal deactivation and the loss of specific surface area.

factor is close to unity.

The PiTER experiments and the simulations of a larger scale gasifier show that mass transport limitations as well as the intrinsic reaction rate are important in entrained flow gasification. The reaction rate in all three regimes has to be considered in order to study or reliably predict entrained flow gasification reactions.

10.1.5 Development of a Test Procedure for Solid Fuels

The experience obtained during the measurement sets and during developing the theoretical model framework is used to suggest a test procedure for the entrained flow gasification of solid fuels. The test procedure consists of 20 to 30 pilot-scale entrained flow experiments and about 25 measurements in the pressurised wire mesh reactor. The chars from both reactor types are then analysed in laboratory and bench-scale setups. Surface area of all chars needs to be measured and char reactivity measurements are required in a thermogravimetric analyser. The data set can then be used to derive the fuel specific parameters in the submodels and evaluate the suitability of the fuel for entrained flow gasification.

10.2 Recommendations for Future Work

As an inherent property of experimental research, this work answered some questions, but raises many others. This dissertation offers an extensive data set of gasification reactions at high temperature and high pressure, but the general knowledge about the rates of these reactions is still low. More experimental work is required to confirm the findings of this dissertation, to develop new ideas, and to fully understand the reaction processes in entrained flow gasifiers.

10.2.1 Recommendations for Future Experimental Work

- The entrained flow experiments in this dissertation address pyrolysis and gasification at a defined oxygen to fuel stoichiometry. Future measurements should divide the gasification process into single reactions to understand the reaction processes in more detail. In differential experiments, the influence of operation parameters on the char-CO₂ and char-H₂O reactions needs to be analysed. From the low-temperature measurements in this dissertation it is expected that product gas inhibition plays only a minor role under entrained flow operation conditions. Experimental evidence from entrained flow reactors is required to support or reject this assumption.
- In high temperature conversion systems, the particle size required to achieve complete conversion in a given reaction time is an important fuel parameter. The energy demand for pulverisation is strongly dependent on the particle size requirements. The particle size is especially an issue of highly reactive fuels (lignite, biomass) as they offer the potential of conversion in short reaction time and at low temperature. If the particle diameter is too big, mass transport limitations prevent the conversion despite the high intrinsic reactivity. Experiments with selected particle size classes

in entrained flow reactors are required to confirm the model prediction of this thesis or develop new formulations that include the effect of fuel particle size.

- In this work, an influence of ash melting properties on the specific surface area of char is found. Future experiments and char analysis methods should focus on this effect in more detail as ash melting occurs in industrial scale entrained flow gasifiers and could significantly influence the reaction rate.
- The fuel conversion in entrained flow experiments can be calculated by an ash tracer method or by product gas analysis. The ash tracer method can reliably measure conversion using a char sample that is collected from the hot reaction zone. As the calculation of conversion is only based on the char sample and a standard laboratory analysis, the number of error sources is low. However, as the potential devolatilisation of ash components may lead to a measurement error, the accuracy of the ash tracer method is limited and an uncertainty will always exist. The alternative is the determination of fuel conversion from the gas analysis if gas concentrations of the main components are measured. The product gas flow rate is either directly measured or can be calculated using an inert gas like N_2 or Ar that is added to the initial gas flow. The calculation of conversion is dependent on several input parameters like gas flow rate, fuel mass flow rate, and concentration measurement of each gas. The error in conversion is only low if all these parameters are precisely measured. Therefore, an uncertainty in one of these parameters leads to an uncertainty in fuel conversion. If the precise measurement of all parameters is possible, the fuel conversion calculated from the gas analysis can be more accurate than from the ash tracer method. The applicability of both methods depends on the specific measurement capabilities. The ideal approach is the application of ash tracer method and gas analysis in the experiment and the direct comparison of the results.
- In the thermogravimetric analysis a possible effect of N_2 partial pressure and/or total pressure on the char gasification reactions is found. The knowledge about total pressure effects on the intrinsic reactivity is low and only a few studies are available. As the number of experiments in this dissertation is too low to reliably quantify the influence, future experiments should address the effect of N_2 partial and total pressure on the reaction rate.
- The wire mesh reactor is operated at up to 1100°C due to the use of a stainless steel mesh. The application of a high temperature mesh material or a carbon strip would enable experiments at temperatures similar to the entrained flow reactors. It is then possible to evaluate if chars from the wire mesh reactor are identical to entrained flow chars and more experiments could be carried out in the wire mesh reactor.

10.2.2 Recommendations for Future Model and Simulation Approaches

- The model development in this dissertation is mainly based on experimental data from the conversion of Rhenish lignite. The complete model framework should also

be tested for further fuels. The required data could be derived by applying the test procedure developed in this dissertation.

- In the theoretical part of the dissertation, model equations are derived that enable the combination of an effectiveness factor approach and LH/LHHW kinetics. If more experimental data were available to reliably derive the model parameters, the model equations could be implemented in the numerical simulations.
- Recent research activities in Australia (e.g. [Benfell2001, Yu2007, Hodge2009]) have focused on the role of char morphology in entrained flow gasification. In this dissertation char morphology is only considered in terms of char density and effective diffusivity. In future developments, the effect of devolatilisation pressure on char morphology and the influence of char morphology on gasification rates should be addressed in more detail.
- In the simulation of industrial scale entrained flow gasifiers, the reactor is assumed to be a one-dimensional plug flow reactor. Turbulence and temperature/concentration gradients in three dimensions are not considered. More sophisticated numerical methods like Computational Fluid Dynamics (CFD) should be used to implement the model framework and simulate industrial scale gasifiers in more detail.
- The gasifier layout and operation optimisation are based on the reaction kinetics of the fuel. State of the art entrained flow gasifiers are operated above the ash melting temperature and a liquid slag is formed. The operation of the gasifier is also determined by the ash melting and slag viscosity properties. These parameters need to be considered in the modelling of entrained flow gasification of a certain fuel. In a simple approach threshold temperatures could be defined at certain locations within the gasifier. If the temperature within the gasifier had to be high to meet slag issues, this would decrease the cold gas efficiency as a higher oxygen feed rate would be required. A further step could then be the implementation of measured slag properties to determine the threshold temperatures.
- The model framework is validated using pilot-scale experimental data from the PiTER and is then used for the simulation of industrial scale gasifiers. A direct comparison of the model predictions with realistic operation parameters from a larger scale reactor is required to determine the accuracy and reliability of the model.

Bibliography

- [Ahn2001] D. H. Ahn, B. M. Gibbs, K. H. Ko, and J. J. Kim. Gasification kinetics of an Indonesian sub-bituminous coal-char with CO₂ at elevated pressure. *Fuel*, 80(11):1651–1658, 2001.
- [Alonso2001] M. J. G. Alonso, A. G. Borrego, D. Alvarez, W. Kalkreuth, and R. Menendez. Physicochemical transformations of coal particles during pyrolysis and combustion. *Fuel*, 80(13):1857–1870, 2001.
- [Alonso2001b] M. J. G. Alonso, A. G. Borrego, D. Alvarez, J. B. Parra, and R. Menendez. Influence of pyrolysis temperature on char optical texture and reactivity. *Journal of Analytical and Applied Pyrolysis*, 58-59:887–909, 2001.
- [Alonso2001c] M. J. G. Alonso, A. G. Borrego, D. Alvarez, and R. Menendez. A reactivity study of chars obtained at different temperatures in relation to their petrographic characteristics. *Fuel Processing Technology*, 69(3):257–272, 2001.
- [Anthony1976] D. B. Anthony and J. B. Howard. Coal devolatilization and hydrogasification. *AIChE Journal*, 22(4):625–656, 1976.
- [Aris1957] R. Aris. On shape factors for irregular particles—I: The steady state problem. Diffusion and reaction. *Chemical Engineering Science*, 6(6):262–268, 1957.
- [Atkins1996] P. W. Atkins. *Physikalische Chemie*. Wiley-Vch Verlag GmbH, ISBN 9783527292752, Weinheim, Second edition, 1996.
- [Baerns2002] M. Baerns, H. Hofmann, and A. Renken. *Chemische Reaktionstechnik - Lehrbuch der Technischen Chemie*. Wiley-Vch Verlag GmbH, ISBN 3-527-30841-5, Third edition, 2002.
- [Bailey1990] J. G. Bailey, A. Tate, C. F. K. Diessel, and T. F. Wall. A char morphology system with applications to coal combustion. *Fuel*, 69(2):225–239, 1990.
- [Barrio2000] M. Barrio, B. Gbel, H. Rimes, U. Henriksen, J.E. Hustad, and L.H. Srensen. Steam Gasification of Wood Char and the Effect of Hydrogen Inhibition on the Chemical Kinetics. In A.V. Bridgewater, editor, *Progress in Thermochemical Biomass Conversion*, pages 32–46. Tyrol, Austria, ISBN 0-632-05533-2, 2000.
- [Bautista1986] J. R. Bautista, W. B. Russel, and D. A. Saville. Time-resolved pyrolysis product distributions of softening coals. *Industrial & Engineering Chemistry Fundamentals*, 25(4):536–544, 1986.

- [Beath1996] Andrew Charles Beath. *Mathematical Modelling of Entrained Flow Coal Gasification*. PhD thesis, University of Newcastle, Newcastle, Australia, 1996.
- [Beeley1996] T. Beeley, J. Crelling, J. Gibbins, R. Hurt, M. Lunden, C. Man, J. Williamson, and N. Yang. Transient high-temperature thermal deactivation of monomaceral-rich coal chars. *Symposium (International) on Combustion*, 26(2):3103–3110, 1996.
- [Belfiore2003] L. A. Belfiore. *Transport phenomena for chemical reactor design*. J. Wiley, ISBN 0471202754, New York, 2003.
- [Benfell2000] K. E. Benfell, G.-S. Liu, D. G. Roberts, D. J. Harris, J. A. Lucas, J. G. Bailey, and T. F. Wall. Modeling char combustion: The influence of parent coal petrography and pyrolysis pressure on the structure and intrinsic reactivity of its char. *Proceedings of the Combustion Institute*, 28(2):2233–2241, 2000.
- [Benfell2001] Kathy E. Benfell. *Assessment of Char Morphology in High Pressure Pyrolysis and Combustion*. PhD thesis, University of Newcastle, Newcastle, Australia, 2001.
- [Bergman2004] P. Bergman, A. Boersma, J. Kiel, M. Prins, K. Ptasinski, and F. Janssen. Torrefaction for entrained-flow gasification of biomass. In *Second World Conference and Technology Exhibition on Biomass for Energy, Industry and Climate Protection*, Rome, Italy, 2004.
- [Bhatia1980] S. K. Bhatia and D. D. Perlmutter. A random pore model for fluid-solid reactions: I. Isothermal, kinetic control. *AIChE Journal*, 26(3):379–386, 1980.
- [Bhatia1981] S. K. Bhatia and D. D. Perlmutter. A random pore model for fluid-solid reactions: II. Diffusion and transport effects. *AIChE Journal*, 27(2):247–254, 1981.
- [Bhatia1996] S. K. Bhatia and B. J. Vartak. Reaction of microporous solids: The discrete random pore model. *Carbon*, 34(11):1383–1391, 1996.
- [Bird2007] R. B. Bird, W. E. Stewart, and E. N. Lightfoot. *Transport phenomena*. J. Wiley, ISBN 0470115394, New York, rev. 2nd edition, 2007.
- [Bischoff1965] Kenneth B. Bischoff. Effectiveness factors for general reaction rate forms. *AIChE Journal*, 11(2):351–355, 1965.
- [Blackwood1960] J. D. Blackwood and A. J. Ingeme. The Reaction of Carbon with Carbon Dioxide at High Pressure. *Australian Journal of Chemistry*, 13(2):194, 1960.

-
- [Bockelie2002] M. J. Bockelie, M. K. Denison, Z. Chen, T. Linjewile, C. L. Senior, and A. F. Sarofim. CFD Modeling For Entrained Flow Gasifiers in Vision 21 Systems. In *19th Annual International Pittsburgh Coal Conference*. Pittsburgh, USA, 2002.
- [Bockelie2002b] M. J. Bockelie, M. K. Denison, Z. Chen, T. Linjewile, C. L. Senior, A. F. Sarofim, and N. Holt. CFD Modeling For Entrained Flow Gasifiers. In *Gasification Technologies Conference*. San Francisco, 2002.
- [Brix2010] J. Brix, P. A. Jensen, and A. D. Jensen. Coal devolatilization and char conversion under suspension fired conditions in O₂/N₂ and O₂/CO₂ atmospheres. *Fuel*, 89(11):3373–3380, 2010.
- [Brown1988] B. W. Brown, L. D. Smoot, P. J. Smith, and P. O. Hedman. Measurement and prediction of entrained-flow gasification processes. *AIChE Journal*, 34(3):435–446, 1988.
- [Brown2001] A. L. Brown, D. C. Dayton, M. R. Nimlos, and J. W. Daily. Design and Characterization of an Entrained Flow Reactor for the Study of Biomass Pyrolysis Chemistry at High Heating Rates. *Energy & Fuels*, 15(5):1276–1285, 2001.
- [Butland1973] A. T. D. Butland and R. J. Maddison. The specific heat of graphite: An evaluation of measurements. *Journal of Nuclear Materials*, 49(1):45–56, 1973.
- [Cai1993] H. Cai, A. Güell, D. Dugwell, and R. Kandiyoti. Heteroatom distribution in pyrolysis products as a function of heating rate and pressure. *Fuel*, 72(3):321–327, 1993.
- [Cai1996] H. Cai, A.J. Güell, I.N. Chatzakis, J.-Y. Lim, D.R. Dugwell, and R. Kandiyoti. Combustion reactivity and morphological change in coal chars: Effect of pyrolysis temperature, heating rate and pressure. *Fuel*, 75(1):15–24, 1996.
- [Carberry1976] J. J. Carberry. *Chemical and catalytic reaction engineering*. McGraw-Hill, ISBN 0070097909, New York, 1976.
- [Cetin2005] E. Cetin, R. Gupta, and B. Moghtaderi. Effect of pyrolysis pressure and heating rate on radiata pine char structure and apparent gasification reactivity. *Fuel*, 84(10):1328–1334, 2005.
- [Couhert2009] C. Couhert, S. Salvador, and J.-M. Commandre. Impact of torrefaction on syngas production from wood. *Fuel*, 88(11):2286–2290, 2009.
- [Cramer2010] B. Cramer and H. Andruleit. Reserven, Ressourcen und Verfügbarkeit von Energierohstoffen. Technical report, Bundesanstalt für Geowissenschaften und Rohstoffe (BGR), Hannover, Germany, 2010.
-

- [Crnomarkovic2007] N. Crnomarkovic, B. Repic, R. Mladenovic, O. Neskovic, and M. Veljkovic. Experimental investigation of role of steam in entrained flow coal gasification. *Fuel*, 86(1-2):194–202, 2007.
- [DIN1319-4] Deutsches Institut für Normung. DIN1319-4, Grundlagen der Messtechnik - Auswertung von Messungen, Meßunsicherheiten, 1999.
- [DOE2010] Department of Energy. Worldwide Gasification Database 2010, 2010. www.netl.doe.gov/technologies/coalpower/gasification/worlddatabase/index.html, accessed 04/07/2011.
- [DiBlasi2008] C. Di Blasi. Modeling chemical and physical processes of wood and biomass pyrolysis. *Progress in Energy and Combustion Science*, 34(1):47–90, 2008.
- [DiBlasi2009] C. Di Blasi. Combustion and gasification rates of lignocellulosic chars. *Progress in Energy and Combustion Science*, 35(2):121–140, 2009.
- [Dongen2006] A. van Dongen and M. Kanaar. Co-gasification at the Buggenum IGCC power plant. In W. Adlhoch, editor, *Beiträge zur DGMK-Fachbereichstagung "Energetische Nutzung von Biomassen"*. DGMK, ISBN 3-936418-49-7, Hamburg, 2006.
- [Drift2004] A. van der Drift, H. Boerrigter, B. Coda, M.K. Cieplik, and K. Hemmes. Entrained Flow Gasification of Biomass: Ash behaviour, feeding issues, and system analysis. Technical Report ECN-C–04-039, ECN, 2004.
- [Ergun1961] S. Ergun. Kinetics of the reactions of carbon dioxide and steam with coke. *US Bureau of Mines Bulletin*, 1961(598), 1961.
- [Erlach2010] B. Erlach and G. Tsatsaronis. Upgrading of biomass by hydrothermal carbonisation: Analysis of an industrial-scale plant design. In *Proceedings of the 23rd International ECOS Conference*, Lausanne, Switzerland, 2010.
- [Essenhigh1994] Robert H. Essenhigh. Influence of initial particle density on the reaction mode of porous carbon particles. *Combustion and Flame*, 99(2):269–279, 1994.
- [Fedoseev1986] D. V. Fedoseev, S. P. Vnukov, V. L. Bukhovets, and B. A. Anikin. Surface graphitization of diamond at high temperatures. *Surface and Coatings Technology*, 28(2):207–214, 1986.
- [Feng2003] B. Feng and S. K. Bhatia. Variation of the pore structure of coal chars during gasification. *Carbon*, 41(3):507–523, 2003.
- [Feng2003b] B. Feng, A. Jensen, S. K. Bhatia, and K. Dam-Johansen. Activation Energy Distribution of Thermal Annealing of a Bituminous Coal. *Energy & Fuels*, 17(2):399–404, 2003.

-
- [Fermoso2009] J. Fermoso, C. Stevanov, B. Moghtaderi, B. Arias, C. Pevida, M.G Plaza, F. Rubiera, and J.J Pis. High-pressure gasification reactivity of biomass chars produced at different temperatures. *Journal of Analytical and Applied Pyrolysis*, 85(1-2):287–293, 2009.
- [Gmehling1992] J. Gmehling and B. Kolbe. *Thermodynamik*. Wiley, ISBN 9783527285471, Weinheim, Second edition, 1992.
- [Goettlicher1999] G. Göttlicher. *Energetik der Kohlendioxidrückhaltung in Kraftwerken*. VDI-Verlag, ISBN 9783183421060, Düsseldorf, 1999.
- [Goto1990] S. Goto and H. Ito. Approximate solutions of effectiveness factor based on bulk conditions. *The Canadian Journal of Chemical Engineering*, 68(1):167–170, 1990.
- [Goyal1989] A. Goyal, R. F. Zabransky, and A. Rehmat. Gasification kinetics of Western Kentucky bituminous coal char. *Industrial & Engineering Chemistry Research*, 28(12):1767–1778, 1989.
- [Gupta2000] J. S. Gupta and S. K. Bhatia. A modified discrete random pore model allowing for different initial surface reactivity. *Carbon*, 38(1):47–58, 2000.
- [Hampartsoumian1993] E. Hampartsoumian, P. L. Murdoch, M. Pourkashanian, D. T. Trangmar, and A. Williams. The Reactivity of Coal Chars Gasified in a Carbon Dioxide Environment. *Combustion Science and Technology*, 92(1):105–121, 1993.
- [Hansen1997] L.K. Hansen, O. Rathmann, A. Olsen, and K. Poulsen. Steam Gasification of Wheat Straw, Barley Straw, Willow and Giganteus. Technical Report Riso-R-944(EN), RISO National Laboratory, 1997.
- [Harris1991] D. J. Harris and I. W. Smith. Intrinsic reactivity of petroleum coke and brown coal char to carbon dioxide, steam and oxygen. *Symposium (International) on Combustion*, 23(1):1185–1190, 1991.
- [Harris2006] D. J Harris, D. G Roberts, and D. G. Henderson. Gasification behaviour of Australian coals at high temperature and pressure: Presented at The 21st Annual International Pittsburgh Coal Conference. *Fuel*, 85(2):134–142, 2006.
- [Higman2003] C. Higman and M. van der Burgt. *Gasification*. Elsevier/Gulf Professional Pub., ISBN 978-0-7506-7707-3, Boston, USA, 2003.
- [Hindmarsh1995] C. J. Hindmarsh, K. M. Thomas, W. X. Wang, H. Y. Cai, A. J. Güell, D. R. Dugwell, and R. Kandiyoti. A comparison of the pyrolysis of coal in wire-mesh and entrained-flow reactors: Presented at the 1993 Eastern Oil Shale Symposium. *Fuel*, 74(8):1185–1190, 1995.
- [Hinshelwood1940] C. N. Hinshelwood. *The Kinetics of Chemical Change*. Clarendon Press, ASIN B0007JEABO, Oxford, GB, 1940.
-

- [Hla2006] S. S. Hla, D. J. Harris, and D. G. Roberts. CFD Modelling for an Entrained Flow Gasification Reactor Using Measured "Intrinsic" Kinetic Data. In *Fifth International Conference on CFD in the Process Industries, CSIRO*. Melbourne, Australia, 2006.
- [Hla2007] San Shwe Hla, D. J. Harris, and D. G. Roberts. Gasification Conversion Model - PEFR: Research Report 80. Technical Report 80, CSIRO, 2007.
- [Hodge2009] Elizabeth M. Hodge. *The Coal Char-CO₂ Reaction at High Temperature and High Pressure*. PhD thesis, University of New South Wales, 2009.
- [Hodge2010] E. M. Hodge, D. G. Roberts, D. J. Harris, and J. F. Stubington. The Significance of Char Morphology to the Analysis of High-Temperature Char–CO₂ Reaction Rates. *Energy & Fuels*, 24(1):100–107, 2010.
- [Hong2000] Jianhui Hong. *Modeling Char Oxidation as a Function of Pressure Using an Intrinsic Langmuir Rate Equation*. PhD thesis, Brigham Young University, Provo, 2000.
- [Hong2000b] J. Hong, W. C. Hecker, and T. H. Fletcher. Improving the Accuracy of Predicting Effectiveness Factors for mth Order and Langmuir Rate Equations in Spherical Coordinates. *Energy & Fuels*, 14(3):663–670, 2000.
- [Hougen1943] O. A. Hougen and K. M. Watson. *Chemical process principles*. Wiley, ISBN 047141283X, New York, 1943.
- [IEA2010] International Energy Agency. 2010 Key World Energy Statistics, 2010. http://www.iea.org/textbase/nppdf/free/2010/key_stats_2010.pdf, accessed 08/07/2011.
- [IEA2010b] International Energy Agency. *World Energy Outlook 2010*. ISBN 9264086242, 2010.
- [Ito2007] K. Ito, Y. Morita, K. Koyama, Z. Shen, A. Yanagisawa, and S. Suehiro. Asia/World Energy Outlook 2007: Results of the energy supply and demand forecast for Asia and the World. Technical report, The Institute of Energy Economics Japan, 2007.
- [Jagiello2004] J. Jagiello and M. Thommes. Comparison of DFT characterization methods based on N₂, Ar, CO₂, and H₂ adsorption applied to carbons with various pore size distributions. *Carbon*, 42(7):1227–1232, 2004.
- [Jakobs2011] T. Jakobs, N. Djordjevic, S. Fleck, M. Mancini, R. Weber, and T. Kolb. Gasification of high viscous slurry R&D on atomization and numerical simulation: Presented at the 36th International Technical Conference on Clean Coal & Fuel System, 2011, Clearwater, FL, USA. *Applied Energy*, 93:449–456, 2012.

-
- [Jensen1975] G. A. Jensen. The Kinetics of Gasification of Carbon Contained in Coal Minerals at Atmospheric Pressure. *Industrial & Engineering Chemistry Process Design and Development*, 14(3):308–314, 1975.
- [Jupudi2009] R. S. Jupudi, V. Zamansky, and T. H. Fletcher. Prediction of Light Gas Composition in Coal Devolatilization. *Energy & Fuels*, 23(6):3063–3067, 2009.
- [Kajitani2002] S. Kajitani, S. Hara, and H. Matsuda. Gasification rate analysis of coal char with a pressurized drop tube furnace. *Fuel*, 81(5):539–546, 2002.
- [Kajitani2006] S. Kajitani, N. Suzuki, M. Ashizawa, and S. Hara. CO₂ gasification rate analysis of coal char in entrained flow coal gasifier: Presented at The 21st Annual International Pittsburgh Coal Conference. *Fuel*, 85(2):163–169, 2006.
- [Khan1986] M. R. Khan and R. G. Jenkins. Swelling and plastic properties of coal devolatilized at elevated pressures: an examination of the influences of coal type. *Fuel*, 65(5):725–731, 1986.
- [Kimber1967] G.M Kimber and M.D Gray. Rapid devolatilization of small coal particles. *Combustion and Flame*, 11(4):360–362, 1967.
- [Kinoshita1988] K. Kinoshita. *Carbon: electrochemical and physicochemical properties*. John Wiley & Sons, ISBN 978-0-471-84802-8, New York, USA, 1988.
- [Kobayashi1977] H. Kobayashi, J.B. Howard, and A.F. Sarofim. Coal devolatilization at high temperatures. *Symposium (International) on Combustion*, 16(1):411–425, 1977.
- [Kolb2009] T. Kolb, T. Jakobs, E. Pantouflas, and N. Zarzalis. Production of syngas from biomass-based slurry in an entrained-flow gasifier. In *24. Deutscher Flammentag, Bochum, Germany*, 2009.
- [Lahaye1991] J. Lahaye and P. Ehrburger. *Fundamental issues in control of carbon gasification reactivity*. Kluwer Academic Publishers, ISBN 9780792310808, 1991.
- [Laurendeau1978] N. M. Laurendeau. Heterogeneous kinetics of coal char gasification and combustion. *Progress in Energy and Combustion Science*, 4(4):221–270, 1978.
- [Lee1991] C. W. Lee, A. W. Scaroni, and R. G. Jenkins. Effect of pressure on the devolatilization and swelling behaviour of a softening coal during rapid heating. *Fuel*, 70(8):957–965, 1991.
- [Lee1996] J. G. Lee, J. H. Kim, H. J. Lee, T. J. Park, and S. D. Kim. Characteristics of entrained flow coal gasification in a drop tube reactor. *Fuel*, 75(9):1035–1042, 1996.
-

- [Li2007] C.-Z. Li. Some recent advances in the understanding of the pyrolysis and gasification behaviour of Victorian brown coal. *Fuel*, 86(12-13):1664–1683, 2007.
- [Lim1997] J. Lim, I. Chatzakis, A. Megaritis, H.-Y. Cai, D.R. Dugwell, and R. Kandiyoti. Gasification and char combustion reactivities of Daw Mill coal in wire-mesh and 'hot-rod' reactors. *Fuel*, 76(13):1327–1335, 1997.
- [Liu1999] G. Liu, H. Wu, K.E Benfell, J.A Lucas, and T.F Wall. The effect of char structure on burnout during pulverized coal combustion at pressure. In *16th Annual International Pittsburgh Coal Conference, Pittsburgh, Pennsylvania, USA*, 1999.
- [Liu1999b] G.S Liu, A.G Tate, H.R Rezaei, A.C Beath, and T.F Wall. Modeling of Infra-Particle C-CO₂ Reaction: An Application of the Random Pore Model. *Developments in Chemical Engineering and Mineral Processing*, 7(5-6):525–536, 1999.
- [Liu2000] G. Liu, P. Benyon, K. E. Benfell, G. W. Bryant, A. G. Tate, R. K. Boyd, D. J. Harris, and T. F. Wall. The porous structure of bituminous coal chars and its influence on combustion and gasification under chemically controlled conditions. *Fuel*, 79(6):617–626, 2000.
- [Liu2000b] Gui-Su Liu, A. G. Tate, G. W. Bryant, and T. F. Wall. Mathematical modeling of coal char reactivity with CO₂ at high pressures and temperatures. *Fuel*, 79(10):1145–1154, 2000.
- [Liu2004] G.-S. Liu and S. Niksa. Coal conversion submodels for design applications at elevated pressures. Part II. Char gasification. *Progress in Energy and Combustion Science*, 30(6):679–717, 2004.
- [Liu2004b] H. Liu, M. Kaneko, C. Luo, S. Kato, and T. Kojima. Effect of pyrolysis time on the gasification reactivity of char with CO₂ at elevated temperatures. *Fuel*, 83(7-8):1055–1061, 2004.
- [Liu2004c] Y.-L. Liu, R. Malhotra, and S. Niksa. Impact of Pressure Variations on Coal Devolatilization Products. 1. Detailed Product Distributions from 0.1 MPa. *Energy & Fuels*, 18(2):508–519, 2004.
- [Liu2006] H. Liu, C. Luo, S. Kato, S. Uemiya, M. Kaneko, and T. Kojima. Kinetics of CO₂/Char gasification at elevated temperatures: Part I: Experimental results. *Fuel Processing Technology*, 87(9):775–781, 2006.
- [Liu2006b] H. Liu, C. Luo, M. Toyota, S. Uemiya, and T. Kojima. Kinetics of CO₂/char gasification at elevated temperatures. Part II: Clarification of mechanism through modelling and char characterization. *Fuel Processing Technology*, 87(9):769–774, 2006.

-
- [Lowell2006] S. Lowell, E. Shield, M. Thomas, and M. Thommes. *Characterization of porous solids and powders: Surface area, pore size and density*. Springer, ISBN 9789048166336, New York, USA, 2006.
- [Ma2006] Liqiang Ma. *Combustion and Gasification of Chars in Oxygen and Carbon Dioxide at Elevated Pressure*. PhD thesis, Stanford University, Stanford, 2006.
- [Mancini2011] M. Mancini, R. Buczynski, R. Weber, S. Fleck, P. Stoesser, and T. Kolb. Gasification of Glycol: Measurements and Mathematical Modelling. In *25. Deutscher Flammentag – Verbrennung und Feuerung, Karlsruhe, VDI-Bericht 2119*, pages 221–226, 2011.
- [Manton2004] N. Manton, J. Cor, G. Mul, D. Eckstrom, R. Malhotra, and S. Niksa. Impact of Pressure Variations on Coal Devolatilization Products. 2. Detailed Product Distributions from 1.0 MPa. *Energy & Fuels*, 18(2):520–530, 2004.
- [Matsumoto2009] K. Matsumoto, K. Takeno, T. Ichinose, T. Ogi, and M. Nakanishi. Gasification reaction kinetics on biomass char obtained as a by-product of gasification in an entrained-flow gasifier with steam and oxygen at 900–1000°C. *Fuel*, 88(3):519–527, 2009.
- [Matsuoka2005] K. Matsuoka, H. Akiho, W.-C. Xu, R. Gupta, T. F. Wall, and A. Tomita. The physical character of coal char formed during rapid pyrolysis at high pressure. *Fuel*, 84(1):63–69, 2005.
- [Mentser1973] M. Mentser and S. Ergun. A study of the carbon dioxide-carbon reaction by oxygen exchange. *US Bureau of Mines Bulletin*, 1973(664), 1973.
- [Messenboeck1999] R. C. Messenböck, D. R. Dugwell, and R. Kandiyoti. Coal Gasification in CO₂ and Steam: Development of a Steam Injection Facility for High-Pressure Wire-Mesh Reactors. *Energy & Fuels*, 13(1):122–129, 1999.
- [Messenboeck2000] R. C. Messenböck, N. P. Paterson, D. R. Dugwell, and R. Kandiyoti. Factors governing reactivity in low temperature coal gasification. Part 1. An attempt to correlate results from a suite of coals with experiments on maceral concentrates. *Fuel*, 79(2):109–121, 2000.
- [Molina1998] A. Molina and F. Mondragon. Reactivity of coal gasification with steam and CO₂. *Fuel*, 77(15):1831–1839, 1998.
- [Monson1995] C. R. Monson, G. J. Germane, A. U. Blackham, and L. Douglas Smoot. Char oxidation at elevated pressures. *Combustion and Flame*, 100(4):669–683, 1995.
- [Muehlen1985] H.-J. Mühlen, K. H. van Heek, and H. Jüntgen. Kinetic studies of steam gasification of char in the presence of H₂, CO₂ and CO. *Fuel*, 64(7):944–949, 1985.
-

- [NIST2011] National Institute of Standards and Technology. Chemistry WebBook, 2011. <http://webbook.nist.gov/chemistry/> accessed 03/04/2011.
- [Niksa1995] S. Niksa. Predicting the devolatilization behavior of any coal from its ultimate analysis. *Combustion and Flame*, 100(3):384–394, 1995.
- [Niksa2003] S. Niksa, G.S. Liu, and R. H. Hurt. Coal conversion submodels for design applications at elevated pressures. Part I. devolatilization and char oxidation. *Progress in Energy and Combustion Science*, 29(5):425–477, 2003.
- [Ollero2003] P. Ollero, A. Serrera, R. Arjona, and S. Alcantarilla. The CO₂ gasification kinetics of olive residue. *Biomass and Bioenergy*, 24(2):151–161, 2003.
- [Omega2011] Omega. Revised Thermocouple Reference Tables, 2011. <http://www.omega.com/temperature/Z/pdf/z212-213.pdf> accessed 03/05/2011.
- [Osafune1988] K. Osafune and H. Marsh. Gasification kinetics of coal chars in carbon dioxide. *Fuel*, 67(3):384–388, 1988.
- [Ouyang1998] S. Ouyang, H. Yeasmin, and J. Mathews. A pressurized drop-tube furnace for coal reactivity studies. *Review of Scientific Instruments*, 69(8):3036, 1998.
- [Park2007] H. Y. Park and D. H. Ahn. Gasification kinetics of five coal chars with CO₂ at elevated pressure. *Korean Journal of Chemical Engineering*, 24(1):24–30, 2007.
- [Peng1995] F. F. Peng, I. C. Lee, and R. Y. K. Yang. Reactivities of in situ and ex situ coal chars during gasification in steam at 1000–1400°C. *Fuel Processing Technology*, 41(3):233–251, 1995.
- [Penner1957] S.S. Penner. *Chemistry problems in jet propulsion*. Pergamon Press, ISBN 1124019995, London, GB, 1957.
- [Polifke2005] W. Polifke and J. Kopitz. *Wärmeübertragung: Grundlagen, analytische und numerische Methoden*. Pearson Studium, ISBN 382737104X, München and Boston, 2005.
- [Riede1975] B. E. Riede and D. Hanesian. Kinetic Study of Carbon-Steam Reaction. *Industrial & Engineering Chemistry Process Design and Development*, 14(1):70–74, 1975.
- [Riedel2004] E. Riedel. *Anorganische Chemie*. W. de Gruyter, ISBN 3110181681, Berlin and New York, Sixth edition, 2004.
- [Roberts2000] D. G. Roberts, D. J. Harris, and T. F. Wall. Total pressure effects on chemical reaction rates of chars with O₂, CO₂ and H₂O. *Fuel*, 79(15):1997–1998, 2000.

-
- [Roberts2000c] Daniel Geoffrey Roberts. *Intrinsic Reaction Kinetics of Coal Chars with Oxygen, Carbon Dioxide and Steam at Elevated Pressures*. PhD thesis, University of Newcastle, Newcastle, 2000.
- [Roberts2003] D. G. Roberts, D. J. Harris, and T. F. Wall. On the Effects of High Pressure and Heating Rate during Coal Pyrolysis on Char Gasification Reactivity. *Energy & Fuels*, 17(4):887–895, 2003.
- [Roberts2007] D. G. Roberts and D. J. Harris. Char gasification in mixtures of CO₂ and H₂O: Competition and inhibition. *Fuel*, 86(17-18):2672–2678, 2007.
- [Rosenberg1996] P. Rosenberg, H. I. Petersen, and E. Thomsen. Combustion char morphology related to combustion temperature and coal petrography. *Fuel*, 75(9):1071–1082, 1996.
- [Russell1999] N. V. Russell, J. R. Gibbins, and J. Williamson. Structural ordering in high temperature coal chars and the effect on reactivity. *Fuel*, 78(7):803–807, 1999.
- [Salatino1998] P. Salatino, O. Senneca, and S. Masi. Gasification of a coal char by oxygen and carbon dioxide. *Carbon*, 36(4):443–452, 1998.
- [Salatino1999] P. Salatino, O. Senneca, and S. Masi. Assessment of Thermodeactivation during Gasification of a Bituminous Coal Char. *Energy & Fuels*, 13(6):1154–1159, 1999.
- [Santo2007] U. Santo, H. Seifert, T. Kolb, L. Krebs, D. Kuhn, H.-J Wiemer, E. Pantouflas, and N. Zarzalis. Conversion of Biomass Based Slurry in an Entrained Flow Gasifier. *Chemical Engineering & Technology*, 30(7):967–969, 2007.
- [Satterfield1981] C. Satterfield. *Mass transfer in heterogeneous catalysis*. Robert E. Krieger Publishing Company, ISBN 0262190621, New York, USA, 1981.
- [Schingnitz2005] M. Schingnitz and F. Mehlhose. MEGA-GSP Process: Entrained-Flow Gasification of Coal, Biomass and Waste. In *First International Freiberg Conference on IGCC&XtL Technologies*, Freiberg, Germany, 2005.
- [Schingnitz2005b] M. Schingnitz and F. Mehlhose. The GSP-Process: Entrained-Flow Gasification of different Types of Coal. In *Proceedings of the Second International Conference on Clean Coal Technologies, Sardinia, Italy*, 2005.
- [Schmal1982] M. Schmal, J. L. F. Monteiro, and J. L. Castellan. Kinetics of coal gasification. *Industrial & Engineering Chemistry Process Design and Development*, 21(2):256–266, 1982.
- [Senneca1997] O. Senneca, P. Russo, P. Salatino, and S. Masi. The relevance of thermal annealing to the evolution of coal char gasification reactivity. *Carbon*, 35(1):141–151, 1997.
-

- [Senneca2007] O. Senneca, P. Salatino, and D. Menghini. The influence of thermal annealing on oxygen uptake and combustion rates of a bituminous coal char. *Proceedings of the Combustion Institute*, 31(2):1889–1895, 2007.
- [Sha1990] X.-Z. Sha, Y.-G. Chen, J. Cao, Y.-M. Yang, and D.-Q. Ren. Effects of operating pressure on coal gasification. *Fuel*, 69(5):656–659, 1990.
- [Shields1985] J. E. Shields and S. Lowell. A method for the determination of ambient temperature adsorption of gases on porous materials. *Journal of Colloid and Interface Science*, 103(1):226–229, 1985.
- [Shim2000] H.-S. Shim and R. H. Hurt. Thermal Annealing of Chars from Diverse Organic Precursors under Combustion-like Conditions. *Energy & Fuels*, 14(2):340–348, 2000.
- [Silaen2010] A. Silaen and T. Wang. Effect of turbulence and devolatilization models on coal gasification simulation in an entrained-flow gasifier. *International Journal of Heat and Mass Transfer*, 53(9-10):2074–2091, 2010.
- [Simone2009] M. Simone, E. Biagini, C. Galletti, and L. Tognotti. Evaluation of global biomass devolatilization kinetics in a drop tube reactor with CFD aided experiments. *Fuel*, 88(10):1818–1827, 2009.
- [Slezak2010] A. Slezak, J. M. Kuhlman, L. J. Shadle, J. Spenik, and S. Shi. CFD simulation of entrained-flow coal gasification: Coal particle density/sizefraction effects, Selected Papers from the 2009 NETL Multiphase Flow Workshop. *Powder Technology*, 203(1):98–108, 2010.
- [Smith1994] K. L. Smith. *The structure and reaction processes of coal*. Plenum Press, ISBN 9780306446023, New York, USA, 1994.
- [Solomon1991] P. R. Solomon, M. A. Serio, R. M. Carangelo, R. Bassilakis, Z. Z. Yu, S. Charpenay, and J. Whelan. Analysis of coal by thermogravimetry–fourier transform infrared spectroscopy and pyrolysis modeling. *Journal of Analytical and Applied Pyrolysis*, 19:1–14, 1991.
- [Solomon1993] P. R. Solomon, T. H. Fletcher, and R. J. Pugmire. Progress in coal pyrolysis. *Fuel*, 72(5):587–597, 1993.
- [Sonobe2008] T. Sonobe and N. Worasuwanarak. Kinetic analyses of biomass pyrolysis using the distributed activation energy model. *Fuel*, 87(3):414–421, 2008.
- [Spliethoff2010] H. Spliethoff. Investigations on high temperature gasification and gas cleaning. In *8th International Symposium of High Temperature Air Combustion and Gasification*, Poznan, Poland, 2010.
- [Spliethoff2010b] H. Spliethoff. *Power generation from solid fuels*. Springer, ISBN 3642028551, Heidelberg and New York, 2010.

-
- [Stanmore2001] B. R. Stanmore, J. F. Brilhac, and P. Gilot. The oxidation of soot: a review of experiments, mechanisms and models. *Carbon*, 39(15):2247–2268, 2001.
- [Stetka2011] M. Stetka, S. Gleis, and H. Spliethoff. Entwicklung einer Hochdruck-Thermowaage und Untersuchung zum Alkaliverhalten: Forschungsbericht an die Bayerische Forschungstiftung, 2011.
- [Straub1994] J. Straub. Stoffwerte von Wasser. In Verband Deutscher Ingenieure, editor, *VDI-Wärmeatlas*, pages Db2–Db15. VDI-Verlag, Düsseldorf, Seventh edition, 1994.
- [Sun1997] Chen L. Sun, Yuan Q. Xiong, Qian X. Liu, and Ming Y. Zhang. Thermogravimetric study of the pyrolysis of two Chinese coals under pressure. *Fuel*, 76(7):639–644, 1997.
- [Suuberg1978] Eric Michael Suuberg. *Rapid Pyrolysis and Hydrolyrolysis of Coal*. PhD thesis, Massachusetts Institute of Technology, 1978.
- [Suuberg1979] E. M. Suuberg, W. A. Peters, and J. B. Howard. Product compositions and formation kinetics in rapid pyrolysis of pulverized coal—Implications for combustion: Presented at the Seventeenth Symposium (International) on Combustion. *Symposium (International) on Combustion*, 17(1):117–130, 1979.
- [Suuberg1991] E. M. Suuberg. Thermally Induced Changes in Reactivity of Carbons. In J. Lahaye and P. Ehrburger, editors, *Fundamental issues in control of carbon gasification reactivity*. Kluwer Academic Publishers, ISBN 0792310802, 1991.
- [Thiele1939] E. W. Thiele. Relation between Catalytic Activity and Size of Particle. *Industrial & Engineering Chemistry*, 31(7):916–920, 1939.
- [Tremel2011] A. Tremel, J. Stemann, M. Herrmann, B. Erlach, and H. Spliethoff. Entrained Flow Gasification of Biocoal from Hydrothermal Carbonization. *Fuel*, 102:396–403, 2012.
- [UN2011] United Nations. Word Population to reach 10 billion by 2100 if Fertility in all Countries Converges to Replacement Level, Press Release, May 2011. http://esa.un.org/unpd/wpp/Other-Information/Press_Release_WPP2010.pdf accessed 05/06/2011.
- [Wall2002] T. F. Wall, G.-S. Liu, H.-W. Wu, D. G. Roberts, K. E. Benfell, S. Gupta, J. A. Lucas, and D. J. Harris. The effects of pressure on coal reactions during pulverised coal combustion and gasification. *Progress in Energy and Combustion Science*, 28(5):405–433, 2002.
- [Watanabe2006] H. Watanabe and M. Otaka. Numerical simulation of coal gasification in entrained flow coal gasifier. *Fuel*, 85(12-13):1935–1943, 2006.
-

- [Weeda1990] M. Weeda, P. J. J. Tromp, B. van der Linden, and J. A. Moulijn. High temperature gasification of coal under severely product inhibited conditions. *Fuel*, 69(7):846–850, 1990.
- [Weeda1993] M. Weeda, H. H. Abcouwer, F. Kapteijn, and J. A. Moulijn. Steam gasification kinetics and burn-off behaviour for a bituminous coal derived char in the presence of H₂: Presentend at Third International Rolduc Symposium on Coal Science and Technology and Related Processes. *Fuel Processing Technology*, 36(1-3):235–242, 1993.
- [White1991] W.E. White, C.H. Bartholomew, W.C. Hecker, and D.M. Smith. Changes in Surface Area, Pore Structure and Density During Formation of High-Temperature Chars from Representative U.S. Coals. *Adsorption Science & Technology*, 1991(4):180–209, 1991.
- [Wu2000] H. Wu, G. Bryant, K. Benfell, and T. Wall. An Experimental Study on the Effect of System Pressure on Char Structure of an Australian Bituminous Coal. *Energy & Fuels*, 14(2):282–290, 2000.
- [Ye1998] D. P. Ye, J. B. Agnew, and D. K. Zhang. Gasification of a South Australian low-rank coal with carbon dioxide and steam: kinetics and reactivity studies. *Fuel*, 77(11):1209–1219, 1998.
- [Yeasmin1999] H. Yeasmin, J. F. Mathews, and S. Ouyang. Rapid devolatilisation of Yallourn brown coal at high pressures and temperatures. *Fuel*, 78(1):11–24, 1999.
- [Yoshiie2011] R. Yoshiie, Y. Taya, T. Ichiyanagi, Y. Ueki, and I. Naruse. Emissions of particles and trace elements from coal gasification. *Fuel*, In Press, Corrected Proof, <http://dx.doi.org/10.1016/j.fuel.2011.06.011>, 2011.
- [Yu2007] J. Yu, J. A. Lucas, and T. F. Wall. Formation of the structure of chars during devolatilization of pulverized coal and its thermoproperties: A review. *Progress in Energy and Combustion Science*, 33(2):135–170, 2007.
- [Zeng2005] D. Zeng, M. Clark, T. Gunderson, W. C. Hecker, and T. H. Fletcher. Swelling properties and intrinsic reactivities of coal chars produced at elevated pressures and high heating rates. *Proceedings of the Combustion Institute*, 30(2):2213–2221, 2005.
- [Zhuo2000] Y. Zhuo, R. Messenböck, A.-G. Collot, A. Megaritis, N. Paterson, D. R. Dugwell, and R. Kandiyoti. Conversion of coal particles in pyrolysis and gasification: comparison of conversions in a pilot-scale gasifier and bench-scale test equipment. *Fuel*, 79(7):793–802, 2000.
- [Zolin2001] A. Zolin, A. Jensen, and K. Dam-Johansen. Coupling thermal deactivation with oxidation for predicting the combustion of a solid fuel. *Combustion and Flame*, 125(4):1341–1360, 2001.

Appendix A

Calculation of Conversion - Ash Tracer Method

The fuel conversion after the entrained flow experiments (PiTER and BabiTER) is calculated by coal and char analysis. The composition of each fuel and each char after the experiments is known from the laboratory measurements. In a standard analysis, ash content and elemental compositions (CHNS) are determined. The schematic composition of a fuel and a char sample is shown in Figure A.1. If not indicated otherwise, ash and elemental composition are on a water free (wf) basis. Due to devolatilisation and char conversion the amounts of carbon, hydrogen, nitrogen, sulphur, and oxygen within the sample decrease. However, it is assumed that the mass of ash remains constant. Any potential effect of ash devolatilisation is neglected.

Elemental Conversion From the concentration of carbon in the coal sample $x_{0,C}$ and the sample mass m_0 , the initial mass of carbon $m_{0,C}$ is calculated:

$$x_{0,C} \cdot m_0 = m_{0,C} \quad (\text{A.1})$$

During the experiment carbon is converted to the gas phase and the remaining mass of carbon is

$$m_C = x_C \cdot m \quad (\text{A.2})$$

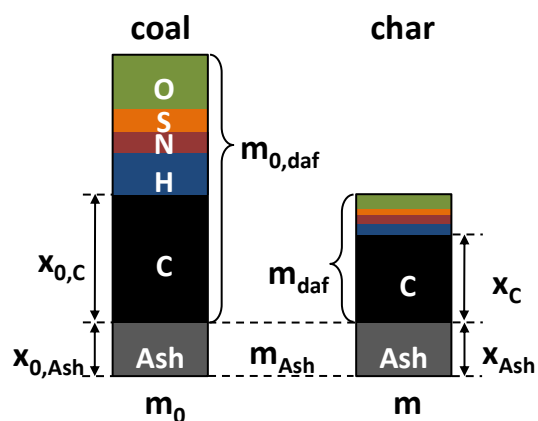


Figure A.1: Composition of a fuel sample before the experiments and a char sample after an entrained flow experiment

Carbon conversion is then

$$C_C = 1 - \frac{m_C}{m_{0,C}} = 1 - \frac{x_C \cdot m}{x_{0,C} \cdot m_0} \quad (\text{A.3})$$

The mass of ash does not change during conversion and is equal in both samples:

$$m_{Ash} = m_0 \cdot x_{0,Ash} = m \cdot x_{Ash} \quad (\text{A.4})$$

$$\frac{m}{m_0} = \frac{x_{0,Ash}}{x_{Ash}} \quad (\text{A.5})$$

By combining Equations A.5 and A.3 carbon conversion C_C is calculated from the ash and carbon content

$$C_C = 1 - \frac{x_C \cdot x_{0,Ash}}{x_{0,C} \cdot x_{Ash}} \quad (\text{A.6})$$

Analogous to carbon conversion, the conversions of other elements are calculated:

$$C_i = 1 - \frac{x_i \cdot x_{0,Ash}}{x_{0,i} \cdot x_{Ash}} \quad \text{for } i = H, N, S, O \quad (\text{A.7})$$

Overall Conversion Overall conversion is calculated on a dry ash free (daf) basis and is defined as follows

$$C_{Ov} = \frac{m_{0,daf} - m_{daf}}{m_{0,daf}} \quad (\text{A.8})$$

Again, it is assumed that the mass of ash remains constant during conversion. In the fuel and in the char samples, the ash content is defined as follows

$$x_{0,Ash} = \frac{m_{Ash}}{m_{Ash} + m_{0,daf}} \quad (\text{A.9})$$

$$x_{Ash} = \frac{m_{Ash}}{m_{Ash} + m_{daf}} \quad (\text{A.10})$$

The Equations A.9 and A.10 are solved for $m_{0,daf}$ and m_{daf} , and then applied to Equation A.8. Finally, overall conversion is calculated:

$$C_{Ov} = \frac{1 - \frac{x_{0,Ash}}{x_{Ash}}}{1 - x_{0,Ash}} \quad (\text{A.11})$$

Appendix B

Error Calculation

The conversion of fuel in the entrained flow reactors is influenced by several operation parameters. Deviations of these parameters from the setpoints can affect conversion. For example, if the real temperature within the reaction tube is above the setpoint, the conversion measured is likely to be high. Furthermore, an error in the char analysis also influences the conversion that is calculated after the experiment. In the following section, operation parameters and laboratory procedures are discussed in terms of their accuracy.

PiTER Operation Parameters

Temperature The gasification reactions occur within the reaction tube that is heated by four cylindrical heating elements. The temperature in each heating zone is measured by thermocouples (Type C, Tungsten-5% Rhenium vs. Tungsten-26% Rhenium) at the outer surface of the reaction tube. Therefore, the temperature within the reaction zone is not measured directly.

Due to the cylindrical shape of the heating elements, a uniform radial temperature distribution is achieved. The nominal deviations of different heating zones are minimized by a temperature controller for each zone. By using a PID algorithm the nominal deviation between each heating zone and the setpoint is less than $\pm 5^\circ\text{C}$, even at very high temperature.

Type C thermocouples are not precise at low temperature. The standard error is 4.5°C up to 425°C [Omega2011]. At higher temperature, the temperature measurement is more precise and the standard error is only 1.0 % up to the maximum temperature of 2320°C [Omega2011]. For the typical PiTER operation temperatures the maximum thermocouple errors are summarised in Table B.1.

Table B.1: Thermocouple (Type C) errors for typical PiTER operation temperatures

Temperature	Standard Error
1000°C	$\pm 10^\circ\text{C}$
1200°C	$\pm 12^\circ\text{C}$
1400°C	$\pm 14^\circ\text{C}$
1600°C	$\pm 16^\circ\text{C}$
1800°C	$\pm 18^\circ\text{C}$

Due to thermal radiation at high temperature, a homogenous temperature distribution is

expected within each heating zone. Therefore, the temperature within the reaction tube approaches the external surface temperature. The deviation is assumed to be less than 5°C and is lower at higher temperature. The increase in standard thermocouple error at high temperature is therefore compensated by thermal radiation.

The total uncertainty in reaction temperature is in the worst case the sum of the controller deviation ($\pm 5^\circ\text{C}$), the standard thermocouple error (approximately $\pm 15^\circ\text{C}$), and temperature inhomogeneity within the heating zone (approximately $\pm 5^\circ\text{C}$). In total, the accuracy of the temperature within the reaction tube is estimated to be $\pm 25^\circ\text{C}$.

Pressure The reactor pressure is monitored by a pressure indicator (Rosemount 3051, 10.5-55VDC) at the reactor outlet and is controlled by a PI controller (Simatic S7). The accuracy of the pressure indicator ($\pm 0.065\%$ of span) and control algorithm is very high resulting in a measurement accuracy of reactor pressure of ± 52 mbar.

Gas Flow Rate and Residence Time The gas flow rate within the reaction tube is controlled by mass flow controllers (Bronkhorst). The measurement error of each MFC is given in Table B.2. The residence time of fuel particles within the reaction tube is adjusted

Table B.2: Standard errors for mass flow controller used in the PiTER experiments

Gas	Range	Accuracy
Nitrogen	2...100 Nm ³ /h	0.8 % of Rd plus 0.2 % of FS
Hydrogen	1...50 Nm ³ /h	0.8 % of Rd plus 0.2 % of FS
Oxygen	0.2...10 Nm ³ /h	1.0 % of FS
Carbon Dioxide	0.8...40 kg/h	0.5 % of Rd plus FS uncertainty
Water	0.04...20 kg/h	0.5 % of Rd plus FS uncertainty

by the gas flow rate. The standard errors directly influence the deviation of residence time from the setpoint. The main gas component in most of the experiments is nitrogen. A typically average gas flow rate of nitrogen is 10 Nm³/h. The error at this setpoint is ± 0.3 Nm³/h, resulting in a relative error of $\pm 3\%$. The residence time within the reaction tube is inverse proportional to the volumetric gas flow rate. Therefore, the relative error of the MFCs is also valid for residence time. The uncertainty in residence time is $\pm 3\%$. For a typical residence time of 2 s, the error is ± 0.06 s. As this range is much smaller than the uncertainties from the particle free fall velocity, the increase in the gas amount, and the gas flow profile within the reaction tube, the MFC error is neglected in the error calculation.

BabiTER Operation Parameters

Temperature The reaction zone of the BabiTER is heated by two heating zones. The temperature in each zone is measured by Type B thermocouples (Platinum-30% Rhodium vs. Platinum-6% Rhodium) at the outer surface of the reaction tube. The nominal deviation of each heating zone from the setpoint temperature is minimised by a PID controller.

The observed deviation between setpoint temperature and measured temperature is less than $\pm 5^{\circ}\text{C}$.

Type B thermocouples are not precise at low temperatures, but their accuracy is improved at higher temperatures. Above a temperature of 800°C the standard error is only 0.5°C [Omega2011].

Due to the radiation influence at higher temperature, the temperature within the reaction tube approaches the external surface temperature. A deviation of less than 5°C is assumed. The total uncertainty of the reaction temperature is assumed to be the sum of the controller deviation, the standard thermocouple error, and the temperature inhomogeneity. In total the temperature deviation from the setpoint is in the range $\pm 10^{\circ}\text{C}$.

Gas Flow Rate and Residence Time During the operation of the BabiTER different mass flow controllers are used. All mass flow controllers are calibrated manually within their individual operation range. From the calibration an average relative standard deviation of $\pm 5\%$ can be estimated. As the uncertainty of residence time is strongly influenced by the effects of particle free fall velocity, the increase in the gas amount, and the flow profile within the reaction tube, the estimated error from the calibration is not considered in the error calculation.

Coal and Char Analysis in Laboratory

Measurement Uncertainty in the Laboratory Analysis After each entrained flow experiment, a char sample is analysed in laboratory and ash and ultimate (CHNS) content are determined. The uncertainty of the analysis is estimated by repeated measurements and is summarised in Table B.3. For the error analysis the lignite R, its reference char, and a char sample (sample ID: 20101220_PiTER_c) were used. For fuels with a high

Table B.3: Absolute measurement uncertainties of the laboratory analysis of fuel and char samples (on a wf basis)

Coal Analysis	Ash content	$\pm 0.14 \text{ wt}\%$
	Carbon content	$\pm 0.30 \text{ wt}\%$
	Sulphur content	$\pm 0.15 \text{ wt}\%$
	Nitrogen content	$\pm 0.02 \text{ wt}\%$
Char Analysis	Ash content	$\pm 0.15 \text{ wt}\%$
	Carbon content	$\pm 0.41 \text{ wt}\%$
	Sulphur content	$\pm 0.13 \text{ wt}\%$
	Nitrogen content	$\pm 0.05 \text{ wt}\%$

reactivity the mass of the char sample - especially in the BabiTER experiments - is very low and a direct measurement of the ash content was not always possible. However, the oxygen concentration in a char sample after devolatilisation is very low. Therefore, the ash content can be calculated directly from the CHNS analysis assuming an oxygen concentration of $0 \text{ wt}\%$. This results in a higher uncertainty of $\pm 0.47 \text{ wt}\%$ of the ash content which is significantly higher than the result from the standard error analysis in Table B.3.

Uncertainty in Conversion from Fuel and Char Analysis

The uncertainties from the laboratory analysis are used to calculate uncertainties in the conversion data. Following the procedure in DIN 1319-4 the uncertainty of an output quantity (e.g. conversion) is related to the uncertainties of input quantities (e.g. char analysis).

$$y = f(x_1, x_2, \dots, x_m) \quad (\text{B.1})$$

$$u(y) = \sqrt{\sum_{k=1}^m \left(\frac{\partial G}{\partial x_k} \right)^2 \cdot u^2(x_k)} \quad (\text{B.2})$$

$$y = y \pm u(y) \quad (\text{B.3})$$

where y is the output quantity, x_k the input quantities, and u the uncertainty of each quantity.

Using the uncertainty a confidence interval is defined. The confidence interval is defined as follows

$$y - e \cdot u(y) \leq y \leq y + e \cdot u(y) \quad (\text{B.4})$$

where $e \cdot u(y)$ is the extended uncertainty.

The confidence interval is used to quantify the reliability of the data. Using $e = 1$, the real value of y lies with a confidence level of 68.3 % in the confidence interval. When a value of 2 is used for e the real value of y lies in the confidence interval with a confidence level of 95 %. The $e = 2$ criterion is often used in industrial metrology [DIN1319-4].

The uncertainty of overall conversion and elemental conversion for each data point is calculated using Equation B.2 in combination with Equations A.7 and A.11. The average extended uncertainties for two confidence levels for PiTER experiments are summarized in Table 5.6.

Appendix C

Calculation of Chemical Equilibrium

The calculation of gas concentrations in the gas phase at high temperature is based on the assumption of chemical equilibrium of the water gas shift reaction:



The position of the equilibrium is described by the equilibrium constant

$$K_{eq} = \frac{p_{CO_2} \cdot p_{H_2}}{p_{CO} \cdot p_{H_2O}} = \frac{n_{CO_2} \cdot n_{H_2}}{n_{CO} \cdot n_{H_2O}} \quad (C.2)$$

where p_i are the partial pressures of the gases and n_i are the molar amounts within a certain gas volume.

The equilibrium constant of the water gas shift reaction can be calculated from the equilibrium constants of the following reactions [Penner1957]:



The equilibrium constants of these reactions are tabulated in the temperature range 298 K to 5000 K by Penner [Penner1957]. To derive a continuous function from these tables the following empirical formulation is used:

$$\ln K_{eq} = A + \frac{B}{T} \quad (C.6)$$

where A and B are empirical constants and T is the temperature in K.

A least squares fitting procedure is applied for the temperature range 1000 K to 2750 K. A is determined to be -3.276 and B is 3512. The empirical function (Equation C.6) compared to the tabulated equilibrium constants is shown in Figure C.1.

To calculate the equilibrium gas concentrations a molar balance of the reaction volume is required. The elemental composition in the gas phase is derived from the gas flow rates, the fuel mass flow rate, and the fuel conversion. The molar amounts of carbon n_C , hydrogen n_H , oxygen n_O , and nitrogen n_N are known. The calculation of the molar

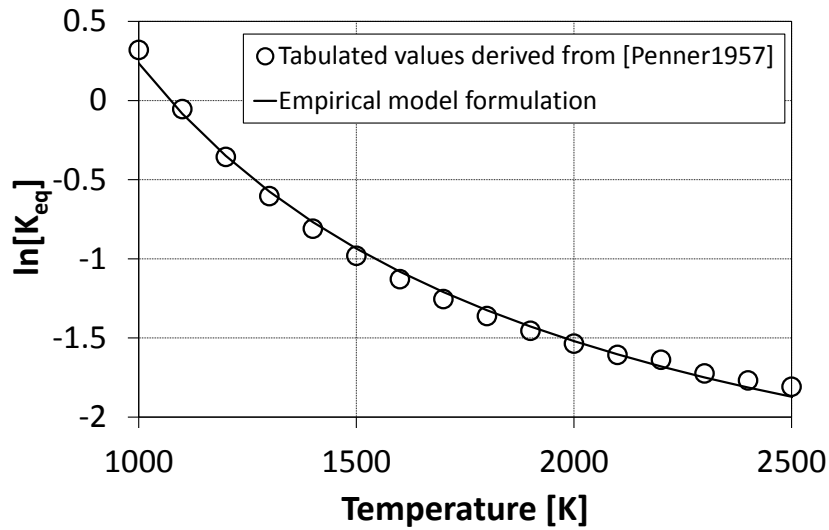


Figure C.1: Comparison of the empirical function for the chemical equilibrium constant of the water gas shift reaction compared to tabulated values from [Penner1957]

amounts of gases is based on the following molar balances:

$$n_{CO_2} + n_{CO} = n_C \quad (C.7)$$

$$n_{H_2} + n_{H_2O} = 0.5n_H \quad (C.8)$$

$$2n_{CO_2} + n_{CO} + n_{H_2O} = n_O \quad (C.9)$$

$$n_{N_2} = 0.5n_N \quad (C.10)$$

The 4 molar balances together with the water gas shift equilibrium (Equation C.2) are used to derive the 5 unknown molar amounts of the gases CO_2 , CO , H_2 , H_2O , and N_2 . The molar gas amounts are then used to calculate the molar gas concentrations x_i :

$$x_i = \frac{n_i}{\sum n_i} \quad (C.11)$$